

Nonlinear Optics

Christian Koos¹

Institute of Photonics and Quantum Electronics (IPQ)

Institute of Microstructure Technology (IMT)

<http://www.ipq.kit.edu>

Karlsruhe Institute of Technology (KIT)

Summer Term 2018

April 10, 2018

¹Not to be published. All rights reserved. No part of this compuscript may be reproduced or utilized in any form by any means without permission in writing from the author.
<mailto:christian.koos@kit.edu>

Contents

Preface	1
1 Linear and nonlinear optics	2
1.1 Maxwell's equations and nonlinear optics	2
1.1.1 Maxwell's equations	2
1.1.2 Electric polarization and nonlinear optics	2
1.1.3 Phenomena and applications of nonlinear optics	3
1.2 Linear media and wave propagation	4
1.2.1 The linear optical susceptibility for different types of media	4
1.2.2 Frequency-domain representation of Maxwell's equations and complex dielectric	6
1.2.3 Kramers-Kronig relation	6
1.2.4 Maxwell's equations for analytic time-domain signals of monochromatic waves	8
1.2.5 Wave propagation in linear isotropic media	10
1.3 Harmonic and anharmonic oscillator model of optical media	11
1.3.1 The Lorentz oscillator model of linear dielectric media	12
1.3.2 Anharmonic oscillator model of electronic nonlinearities	14
1.4 Wave propagation in nonlinear media	14
1.4.1 Nonlinear wave equation	16
1.4.2 Representation of the nonlinear polarization	17
1.4.3 Plane waves and slowly-varying envelope approximation (SVEA)	17
1.5 Survey of nonlinear optical processes	19
1.5.1 Second-order nonlinearities	19
1.5.2 Third-order nonlinearities	20
1.5.3 Intensity-dependent refractive index and Kerr effect	25
1.6 Parametric versus nonparametric processes	26
2 The nonlinear optical susceptibility	29
2.1 Formal definition of the nonlinear optical susceptibility tensor	29
2.1.1 Time-domain representation	29
2.1.2 Short-form tensor notation	30
2.1.3 Frequency-domain representation	31
2.1.4 Representation by complex time-domain amplitudes for positive nonzero frequencies	31
2.1.5 Examples for second and third-order nonlinearities	34
2.2 Properties of the nonlinear optical susceptibility tensor	35
2.2.1 Causality	35
2.2.2 Intrinsic symmetries	35
2.2.3 Spatial symmetry of the nonlinear medium	37
2.3 Influence of spatial symmetry on the second-order nonlinear susceptibility	41
2.3.1 Contracted notation for second-order nonlinear susceptibility	41
2.3.2 Nonlinear susceptibility tensors for different spatial symmetries	42

2.4	Influence of spatial symmetry on the third-order nonlinear susceptibility	42
3	Second-order nonlinear effects	49
3.1	Wave propagation in linear anisotropic media	49
3.1.1	Permeability and impermeability tensors of anisotropic media	49
3.1.2	Wave propagation along a principal axis	50
3.1.3	Wave propagation in arbitrary direction	52
3.2	Linear electro-optic effect (Pockels effect)	56
3.2.1	Mathematical description	56
3.2.2	Electro-optic modulators	57
3.3	Phase matching for second-order nonlinear processes	67
3.3.1	Impact of phase mismatch on sum-frequency and second-harmonic generation	69
3.3.2	Phase matching by exploiting birefringence	71
3.3.3	Quasi-phase-matching (QPM)	77
3.4	Difference-frequency generation and parametric amplification	81
3.4.1	The Manley-Rowe relations	82
3.4.2	Parametric amplification and parametric oscillators	83
4	Acousto-optics and photon-phonon interactions	85
4.1	Elasto-optic effect	85
4.2	Acousto-optics	86
4.2.1	Acousto-optic light deflector	86
4.2.2	Coupled-wave analysis	88
4.2.3	Acousto-optic devices	91
4.3	Interaction of photons and phonons	97
4.3.1	Brillouin scattering	97
4.3.2	Raman scattering	100
5	Third-order nonlinear effects	103
5.1	Signal propagation in linear waveguides	103
5.1.1	Waveguide modes for monochromatic waves	103
5.1.2	Propagation of time-dependent signals in linear dispersive waveguides	104
5.2	Signal propagation in third-order nonlinear waveguides	107
5.2.1	Maxwell's equations and mode expansion for nonlinear propagation	107
5.2.2	The nonlinear Schrödinger equation (NLSE)	110
5.3	Applications and phenomena related to third-order nonlinear waveguides	111
5.3.1	Nonlinear phase shift and spectral broadening	111
5.3.2	Optical solitons	113
5.3.3	Modulation instability	114
A	Mathematical Definitions and Conventions	122
A.1	Time- and Frequency-Domain Quantities	122
A.1.1	Fourier Transformation	122
A.2	Vector calculus	122
A.2.1	The Nabla operator	122
A.2.2	Basic formulae of vector differential operators	123
	Bibliography	124

Preface

This lecture is an introduction to the field of nonlinear optics. The lecture notes are in parts based on lectures held by Prof. Franz X. Kärtner, Prof. Uwe Morgner, and Prof. Juerg Leuthold at the University of Karlsruhe and at Karlsruhe Institute of Technology (KIT) between 1999 and 2012. The lectures of Prof. Kärtner are in turn based on the lectures of Prof. Herman A. Haus, Prof. Erich Ippen and Prof. Jim Fujimoto at Massachusetts Institute of Technology (MIT), on a lecture of Dr. Christian Bosshard at Swiss Federal Institute of Technology (ETH) Zurich, and on a series of textbooks [10, 3, 11, 28, 27, 7].

Understanding of the of the lecture contents requires mathematical skills along with basic knowledge of electromagnetic wave theory and photonics. The lecture aims at providing a self-contained introduction into the field on nonlinear optics. Nevertheless, the lecture notes cannot reproduce the wealth of educational material that can be found in various textbooks and that is referenced in the following chapters. The following books are recommended as accompanying literature:

- R. W. Boyd. *Nonlinear Optics*. Academic Press, San Diego, 2003.
- G. P. Agrawal. *Nonlinear Fiber Optics*. Academic Press, 2013.
- B. E. A. Saleh and M. C. Teich. *Fundamentals of Photonics*. John Wiley and Sons, 2007.
- Y. R. Shen. *Nonlinear Optics*. John Wiley and Sons, New York, 1984.

Christian Koos, April 2018

Chapter 1

Linear and nonlinear optics

Nonlinear optics describes the behavior of light in nonlinear media, that feature a nonlinear relationship between the electric polarization \mathbf{P} and the electric field \mathbf{E} . In this chapter, we will shortly review the fundamentals of linear optics and wave propagation in linear media. Based on this, we will introduce basic concepts of wave propagation in nonlinear media and discuss selected nonlinear-optical phenomena of second and third order. A formal and more general definition of the nonlinear optical susceptibility will be given in Chapter 2.

1.1 Maxwell's equations and nonlinear optics

1.1.1 Maxwell's equations

In the absence of any free carriers and currents, Maxwell's equations take the following form [19]:

$$\nabla \cdot \mathbf{D}(\mathbf{r}, t) = 0 \quad (1.1)$$

$$\nabla \times \mathbf{E}(\mathbf{r}, t) = -\frac{\partial \mathbf{B}(\mathbf{r}, t)}{\partial t} \quad (1.2)$$

$$\nabla \cdot \mathbf{B}(\mathbf{r}, t) = 0 \quad (1.3)$$

$$\nabla \times \mathbf{H}(\mathbf{r}, t) = \frac{\partial \mathbf{D}(\mathbf{r}, t)}{\partial t} \quad (1.4)$$

Note that in this lecture we use SI units rather than, e.g., Gaussian units that may be found in some older textbooks [10]. The vector $\mathbf{r} = (x, y, z)^T$ defines a point in three-dimensional space. In optics, media are generally assumed to be nonmagnetic. The magnetic flux density \mathbf{B} is then related to the magnetic field \mathbf{H} by

$$\mathbf{B}(\mathbf{r}, t) = \mu_0 \mathbf{H}(\mathbf{r}, t), \quad (1.5)$$

where $\mu_0 = 1.25664 \times 10^{-6} \text{ Vs}/(\text{A m})$ is the magnetic permeability of vacuum. The relation between the electric field \mathbf{E} and the electric displacement \mathbf{D} can be expressed as

$$\mathbf{D}(\mathbf{r}, t) = \epsilon_0 \mathbf{E}(\mathbf{r}, t) + \mathbf{P}(\mathbf{r}, t), \quad (1.6)$$

where $\epsilon_0 = 8.85419 \times 10^{-12} \text{ As}/(\text{V m})$ is the electric permittivity of vacuum, and where \mathbf{P} denotes the electric polarization. These equations are also referred to as constitutive relations.

1.1.2 Electric polarization and nonlinear optics

The presence of an electric field \mathbf{E} within an optical medium leads to a displacement of positive and negative charges, thereby inducing an electric polarization \mathbf{P} . The optical properties of the medium depend on the relationship between \mathbf{E} and \mathbf{P} , and optical media are often classified by the nature of

this relationship. In linear media, \mathbf{P} depends linearly on \mathbf{E} , i.e., a linear superposition $a_1\mathbf{E}_1 + a_2\mathbf{E}_2$ of different electric fields \mathbf{E}_1 and \mathbf{E}_2 leads to a polarization profile $\mathbf{P} = a_1\mathbf{P}_1 + a_2\mathbf{P}_2$ that is given by the corresponding linear superposition of the polarizations \mathbf{P}_1 and \mathbf{P}_2 invoked individually by the respective electric fields. In many cases of practical interest, a linear relationship is a sufficiently good approximation, and it is therefore used throughout classical optics. For high field strengths, however, the relationship becomes nonlinear. In this case, the superposition principle no longer holds, and novel optical phenomena can occur, such as the formation of new spectral components within the nonlinear medium. We may hence define the field of nonlinear optics as follows:

Nonlinear Optics: The field of nonlinear optics (often abbreviated as NLO) comprises the branch of optics that describes the behavior of light in nonlinear media, in which the electric polarization \mathbf{P} responds nonlinearly to the electric field \mathbf{E} of the light.

The nonlinearity in the relationship between \mathbf{E} and \mathbf{P} is typically only observed at very high light intensities, featuring electric fields that are comparable to interatomic electric fields (typically of the order of 10^8 V/m). Such field strengths can be generated by using pulsed lasers and/or focussing the light to a very small cross section. The nonlinear relationship between polarization and electric field can also be interpreted by means of intensity-dependent optical material properties. A less formal definition of nonlinear optics is therefore based on the statement that nonlinear optical materials change their optical properties by the presence of light. In many cases of practical interest, these definitions are equivalent.

1.1.3 Phenomena and applications of nonlinear optics

An illustration of different nonlinear optical phenomena is given in Figure 1.1. Launching a monochromatic wave with angular frequency ω into a nonlinear optical material can produce new waves oscillating at, e.g., 2ω or 3ω , Fig. 1.1 (a). These processes are referred to as second-harmonic generation (SHG) and third-harmonic generation (THG). In a similar way, launching a superposition of two plane waves at frequencies ω_1 and ω_2 into a nonlinear material will lead to the formation of intermodulation products of the two frequencies. In another class of materials, the absorption can be subject to nonlinear effects, Fig. 1.1 (b). In this context, absorption bleaching refers to the case where the absorption coefficient decreases with intensity and hence the transmission increases. Conversely, a decrease of transmission with increasing intensity is referred to by the term “saturation”. Moreover, nonlinear effects can lead to an intensity-dependent refractive index. In interference experiments, this can lead to intensity-dependent shifts of the interference patterns, 1.1 (c). The underlying nonlinear-optic phenomenon is referred to as self-phase modulation (SPM): The intensity of the beam changes the refractive index and hence modulates the phase. SPM can also lead to intensity-dependent beam profiles, 1.1 (d): If a focussed beam of light propagates through a nonlinear optic medium, the high-intensity center of the beam will experience a different (usually higher) refractive index than the low-intensity periphery. At high intensities, this can lead to so-called self-focussing of the beam. Inset (1) of 1.1 (d) depicts the beam profile at low intensities, and Inset (2) indicates self-focussing at higher intensities. At very high intensity, the beam profile becomes unstable and breaks up in multiple filaments, Inset (3).

Nonlinear optical phenomena can be exploited for a wide range of applications. SHG, THG or related processes such as parametric amplification can be used to realize optical sources and amplifiers that can be tuned over a wide range of wavelengths, see Chapter 3 for a more detailed discussion. Second-order nonlinearities lend themselves to electro-optic modulators, which are key elements of high-speed optical communications. Nonlinear absorption can be used for multi-photon microscopy and lithography. Phonon-assisted nonlinear interactions are the basis of acousto-optic modulators and broadband Raman amplifiers, see Chapter 4. SPM and related third-order nonlinear processes such as cross-phase modulation (XPM) and four-wave mixing (FWM) allow for ultra-fast all-optical signal processing or supercontinuum generation, see Chapter 5. With the availability of low-cost pulsed laser sources with high peak powers, the importance of nonlinear optics is steadily increasing.

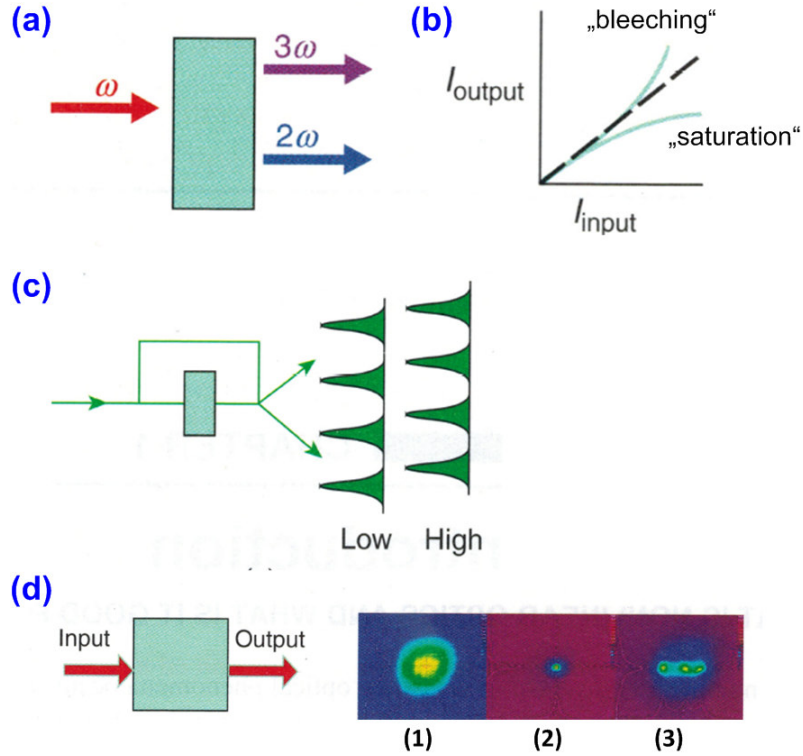


Figure 1.1: Illustration of nonlinear optical phenomena. (a) Generation of new frequency components: A monochromatic wave oscillating at angular frequency ω can produce new waves oscillating at, e.g., 2ω (second-harmonic generation, SHG) or 3ω (third-harmonic generation, THG). (b) Power-dependent transmission, e.g., nonlinear absorption or absorption bleaching. (c) Intensity-dependent interference patterns, caused by, e.g., self-phase modulation (SPM). (d) Intensity-dependent beam profiles caused by, e.g., self-focussing. (Figure adapted from [29])

1.2 Linear media and wave propagation

In the following sections we will first review the mathematical description of a linear relationship between \mathbf{E} and \mathbf{P} and derive the respective wave equation for the case of homogeneous media. This will then serve as a starting point for the analysis of wave propagation in nonlinear media, where the effect of nonlinear optical interaction can be considered as a small perturbation of linear wave propagation in the framework of the so-called slowly varying envelope approximation, see Section 1.4. Using this approach, we will derive a simplified differential equation for wave propagation in nonlinear media that allows to study a wide range of nonlinear optical effects.

1.2.1 The linear optical susceptibility for different types of media

The linear optical susceptibility in the general case

In the case of linear media, the electric polarization $\mathbf{P}(\mathbf{r}_0, t_0)$ at time t_0 and position \mathbf{r}_0 depends linearly on the electric field $\mathbf{E}(\mathbf{r}, t)$ in the vicinity of \mathbf{r}_0 as well as on the history of this field for $t \leq t_0$. In the most general case, this can be represented as

$$\mathbf{P}_L(\mathbf{r}, t) = \epsilon_0 \int_{-\infty}^{\infty} \iiint_{-\infty}^{\infty} \chi^{(1)}(\mathbf{r}, \mathbf{r}', t, t') \mathbf{E}(\mathbf{r}', t') d\mathbf{r}' dt', \quad (1.7)$$

where $\chi^{(1)}(\mathbf{r}, \mathbf{r}', t, t')$ represents the linear influence function that is non-local both in space and time. The linear influence function can also be considered as a first-order approximation of the more general nonlinear case and is therefore labeled with a superscript (1). Similarly, nonlinear second- or third-order contributions will later be denoted with superscripts (2) and (3). Note that in the general case, $\chi^{(1)}(\mathbf{r}, \mathbf{r}', t, t')$ corresponds to a (3×3) -matrix that links a (3×1) -vector $\mathbf{E}(\mathbf{r}', t')$ to the (3×1) -vector $\mathbf{P}_L(\mathbf{r}, t)$. The subscript “L” relates to the fact we consider the linear contribution of the electric field to the electric polarization.

Classification of linear optical media

In many cases of practical interest, the general relation according to Eq. (1.7) may be simplified if we can assume certain properties of the material and the associated influence function. This leads to the following classification of linear optical materials:

Time-invariant media: If the optical properties of the material do not explicitly depend on time t , we may simplify Eq. (1.7) by replacing the explicit dependence on t and t' by a single parameter $\tau = t - t'$,

$$\mathbf{P}_L(\mathbf{r}, t) = \epsilon_0 \int_{-\infty}^{\infty} \iiint_{-\infty}^{\infty} \chi^{(1)}(\mathbf{r}, \mathbf{r}', \tau) \mathbf{E}(\mathbf{r}', t - \tau) d\mathbf{r}' d\tau. \quad (1.8)$$

This is generally true for materials that are not subject to a time-dependent external influence that changes their optical properties.

Media that are local in space: The electric field \mathbf{E} and the optical polarization \mathbf{P} are mostly considered mean quantities, averaged over a length scale smaller than the optical wavelength, but much larger than the interatomic distance of the optical medium. In most cases of practical interest, the local polarization $\mathbf{P}_L(\mathbf{r}, t)$ at position \mathbf{r} depends only on contributions from dipoles that are in direct vicinity and that are induced by electric fields $\mathbf{E}(\mathbf{r}', t')$ at positions \mathbf{r}' very close to \mathbf{r} . In this case, we may assume that the relationship between \mathbf{E} and \mathbf{P} depends only on the local optical properties of the material. The influence function can then be considered to be local in space. A linear time-invariant material that is local in space can be represented by

$$\mathbf{P}_L(\mathbf{r}, t) = \epsilon_0 \int_{-\infty}^{\infty} \chi^{(1)}(\mathbf{r}, \tau) \mathbf{E}(\mathbf{r}, t - \tau) d\tau. \quad (1.9)$$

For the remainder of these lecture notes, we will assume that media are local in space, unless explicitly otherwise stated.

Isotropic materials: For isotropic materials, the optical properties are independent of the direction along which the electric field is oriented. In this case, the (3×3) -matrix $\chi^{(1)}$ can be replaced by a scalar $\chi^{(1)}$. For an isotropic linear time-invariant material that is local in space, we obtain the relation

$$\mathbf{P}_L(\mathbf{r}, t) = \epsilon_0 \int_{-\infty}^{\infty} \chi^{(1)}(\mathbf{r}, \tau) \mathbf{E}(\mathbf{r}, t - \tau) d\tau. \quad (1.10)$$

Homogeneous materials: In homogeneous materials, the optical properties are completely independent of location \mathbf{r} , and we may drop the explicit dependence of $\chi^{(1)}(\mathbf{r}, \tau)$ on \mathbf{r} . A linear homogeneous material that is time-invariant and local in space can be described by

$$\mathbf{P}_L(\mathbf{r}, t) = \epsilon_0 \int_{-\infty}^{\infty} \chi^{(1)}(\tau) \mathbf{E}(\mathbf{r}, t - \tau) d\tau. \quad (1.11)$$

1.2.2 Frequency-domain representation of Maxwell's equations and complex dielectric

In the case of a linear time-invariant optical medium, Maxwell's equations and the constitutive relations, Eqs. (1.1) to (1.6), can be conveniently expressed in the frequency domain along with the linear relations Eqs. (1.7) to (1.11). In this lecture, we use Fourier transforms $\tilde{\Psi}(\omega)$ with respect to the angular frequency ω ,

$$\tilde{\Psi}(\omega) = \int_{-\infty}^{+\infty} \Psi(t) \exp(-j\omega t) dt \quad (1.12)$$

$$\Psi(t) = \frac{1}{2\pi} \int_{-\infty}^{+\infty} \tilde{\Psi}(\omega) \exp(j\omega t) d\omega \quad (1.13)$$

When applying this transformation to Maxwell's equations, Eqs. (1.1) to (1.4), we obtain

$$\nabla \cdot \tilde{\mathbf{D}}(\mathbf{r}, \omega) = 0 \quad (1.14)$$

$$\nabla \times \tilde{\mathbf{E}}(\mathbf{r}, \omega) = -j\omega \tilde{\mathbf{B}}(\mathbf{r}, \omega) \quad (1.15)$$

$$\nabla \cdot \tilde{\mathbf{B}}(\mathbf{r}, \omega) = 0 \quad (1.16)$$

$$\nabla \times \tilde{\mathbf{H}}(\mathbf{r}, \omega) = j\omega \tilde{\mathbf{D}}(\mathbf{r}, \omega), \quad (1.17)$$

where the tilde ($\tilde{}$) denotes a Fourier transform with respect to time t . The constitutive relations are given by

$$\tilde{\mathbf{B}}(\mathbf{r}, \omega) = \mu_0 \tilde{\mathbf{H}}(\mathbf{r}, \omega), \quad (1.18)$$

$$\tilde{\mathbf{D}}(\mathbf{r}, \omega) = \epsilon_0 \tilde{\mathbf{E}}(\mathbf{r}, \omega) + \tilde{\mathbf{P}}(\mathbf{r}, \omega). \quad (1.19)$$

For linear time-invariant media, the general relation between the electric polarization \mathbf{P} and the electric field \mathbf{E} according to Eq. (1.8) can be written as

$$\tilde{\mathbf{P}}_L(\mathbf{r}, \omega) = \epsilon_0 \iiint_{-\infty}^{\infty} \tilde{\chi}^{(1)}(\mathbf{r}, \mathbf{r}', \omega) \tilde{\mathbf{E}}(\mathbf{r}', \omega) d\mathbf{r}', \quad (1.20)$$

where we have exploited the fact that the time-domain convolution in Eq. (1.8) translates into a simple multiplication in the Fourier domain. For the case of a linear time-invariant material that is local in space, Eq. 1.20 simplifies to

$$\tilde{\mathbf{P}}_L(\mathbf{r}, \omega) = \epsilon_0 \tilde{\chi}^{(1)}(\mathbf{r}, \omega) \tilde{\mathbf{E}}(\mathbf{r}, \omega). \quad (1.21)$$

In these relations, $\tilde{\chi}^{(1)}(\mathbf{r}, \omega)$ represents the Fourier transform of the influence function $\chi^{(1)}(\mathbf{r}, \tau)$ with respect to the time argument τ . The complex quantity $\tilde{\chi}^{(1)}(\mathbf{r}, \omega)$ is also referred to as the electric susceptibility and often denoted as $\chi^{(1)}(\mathbf{r}, \omega)$ without the tilde. We will adhere to this simplified notation whenever it is clear from the context that the (complex) frequency-domain quantity is meant rather than the (real) time-domain influence function.

1.2.3 Kramers-Kronig relation

One important restriction to the frequency dependence of the electric susceptibility $\tilde{\chi}^{(1)}(\mathbf{r}, \omega)$ results from the fact that it represents the Fourier transform of a causal real-valued influence

function. For simplicity of notation, we assume a scalar, space-invariant complex susceptibilities $\tilde{\chi}(\omega)$ and influence functions $\chi(t)$ in the remainder of this section. The influence function $\chi(t)$ can be interpreted as the impulse response of the medium upon a Dirac-like electric-field excitation at $t = 0$. Due to causality of the dielectric response¹, the corresponding time-domain influence function must vanish for negative times, i.e., $\chi(t < 0) = 0$, since no electric polarization can be induced before the electric field penetrates the medium.

We may decompose $\tilde{\chi}(\omega)$ into its real and its imaginary part and write it as a complex function of frequency $f = \omega / (2\pi)$,

$$\tilde{\chi}(\omega) = \chi(\omega) + j\chi_i(\omega). \quad (1.22)$$

Due to causality of the time-domain influence function, the real and the imaginary part of $\tilde{\chi}(\omega)$ are related by the Hilbert transform,

$$\chi(\omega) = -\frac{1}{\pi} \mathcal{P} \int_{-\infty}^{\infty} \frac{\chi_i(\omega_0)}{\omega_0 - \omega} d\omega_0 \quad (1.23)$$

$$\chi_i(\omega) = \frac{1}{\pi} \mathcal{P} \int_{-\infty}^{\infty} \frac{\chi(\omega_0)}{\omega_0 - \omega} d\omega_0 \quad (1.24)$$

In these relations, $\mathcal{P} \int_{-\infty}^{\infty} \dots d\omega_0$ denotes the Cauchy principal value of the integral, i.e., the integral must be interpreted as a limiting value for which the integration limits approach the pole at $\omega_0 = \omega$ symmetrically from both sides,

$$\mathcal{P} \int_{-\infty}^{\infty} \frac{\chi(\omega_0)}{\omega_0 - \omega} d\omega_0 = \lim_{\epsilon \rightarrow 0} \left(\int_{-\infty}^{\omega - \epsilon} \frac{\chi(\omega_0)}{\omega_0 - \omega} d\omega_0 + \int_{\omega + \epsilon}^{\infty} \frac{\chi(\omega_0)}{\omega_0 - \omega} d\omega_0 \right). \quad (1.25)$$

Note that $\chi(t)$ is real and hence $\chi(\omega) = \chi(-\omega)$ and $\chi_i(\omega) = -\chi_i(-\omega)$. Inserting these relations in Eqs. (1.23) and (1.24), the so-called Kramers-Kronig relations can be derived:

$$\chi(\omega) = -\frac{2}{\pi} \mathcal{P} \int_0^{\infty} \frac{\omega_0 \chi_i(\omega_0)}{\omega_0^2 - \omega^2} d\omega_0 \quad (1.26)$$

$$\chi_i(\omega) = \frac{2}{\pi} \mathcal{P} \int_0^{\infty} \frac{\omega \chi(\omega_0)}{\omega_0^2 - \omega^2} d\omega_0 \quad (1.27)$$

These relations allow us to calculate either the imaginary or the real part of the complex susceptibility if the respective other quantity is known. This implies that the absorption or the gain spectrum of a medium, which is related to the imaginary part of the electric susceptibility, is linked to its frequency-dependent refractive index and vice versa. Absorption and dispersion are intimately related.

Kramers-Kronig relations have a few important consequences: For instance, assuming a dispersionless² medium, the frequency-independent real part $\chi(\omega) = \text{const}_\omega$ of the complex susceptibility is constant, we find $\chi_i(\omega) = 0$ from Eq. (1.24), which implies $\chi(\omega) = 0$, Eq. (1.24). There is hence no dispersionless medium with $\chi \neq 0$! Real media with $\chi \neq 0$ always have loss (or gain) in some frequency ranges, and the electric susceptibility is always frequency-dependent. $\chi(\omega) \approx \text{const}_\omega$ and $\chi_i \approx 0$ is only possible in certain frequency ranges.

¹A causal system is a system where the output depends on past and current inputs but not future inputs. Causality is a fundamental principle that applies to any physical system.

²In photonics, the term “dispersion” relates to the frequency dependence of the refractive index and hence of the real part of the electric susceptibility. In a “dispersionless” medium, these quantities do not depend on frequency - at least for a certain range of wavelengths. As a consequence, all spectral components of an optical signal propagate with the same velocity.

1.2.4 Maxwell's equations for analytic time-domain signals of monochromatic waves

As an alternative to the Fourier-domain analysis of Maxwell's equations according to Section (1.2.2), we may use analytic time-domain signals of monochromatic waves, i.e., complex amplitudes $\underline{\psi}(t) = A \exp(j(\omega_0 t + \varphi))$ with single-sided power spectra, the real part of which corresponds to the physical time-domain signal $\psi(\mathbf{r}, t) = A \cos(\omega_0 t + \varphi)$. For linear optics, the two approaches result in mathematically identical relations and are therefore often not clearly distinguished in the literature. For the case of nonlinear optics, however, an understanding of the difference between Fourier transforms and complex time-domain amplitudes of monochromatic signals is important. We will therefore shortly recall the relationships between the Fourier transform and the analytic time-domain representation of a signal.

Analytic time-domain signal

For a real time-domain signal $\psi(t) \in \mathbb{R}$, the Fourier spectrum $\tilde{\psi}(\omega)$ has Hermitian symmetry,

$$\tilde{\psi}(\omega) = \tilde{\psi}^*(-\omega), \quad (1.28)$$

i.e., the spectrum for $\omega < 0$ does not contain any new information and can be completely reconstructed from the spectrum for $\omega \geq 0$. We may hence discard the negative-frequency components without any loss of information by constructing a function $\underline{\tilde{\psi}}(\omega)$ with a single-sided spectrum,

$$\underline{\tilde{\psi}}(\omega) = \tilde{\psi}(\omega) + \text{sgn}(\omega)\tilde{\psi}^*(\omega), \quad (1.29)$$

where the sign function $\text{sgn}(\omega)$ is given by

$$\text{sgn}(\omega) = \begin{cases} 1 & \text{for } \omega > 0 \\ 0 & \text{for } \omega = 0 \\ -1 & \text{for } \omega < 0 \end{cases}. \quad (1.30)$$

$\underline{\tilde{\psi}}(\omega)$ hence contains only the non-negative frequency components of $\tilde{\psi}(\omega)$. Note that the operation is reversible,

$$\tilde{\psi}(\omega) = \frac{1}{2} \left(\underline{\tilde{\psi}}(\omega) + \underline{\tilde{\psi}}^*(-\omega) \right). \quad (1.31)$$

The time-domain analogon of Eq. (1.29) is given by

$$\underline{\psi}(t) = \psi(t) + j \left(\psi(t) \star \frac{1}{\pi t} \right), \quad (1.32)$$

where $\underline{\psi}(t)$ denotes the analytic time-domain signal of $\psi(t)$. Note that the convolution of $\psi(t)$ with $1/(\pi t)$ on the right-hand side of Eq. (1.32) corresponds to a Hilbert transform. For a given real time-domain signal $\psi(t)$, the corresponding analytic signal $\underline{\psi}(t)$ can hence be obtained by constructing the imaginary part by means of the Hilbert transformation. The real time-domain signal $\psi(t)$ can be easily retrieved by just taking the real part,

$$\psi(t) = \text{Re} \{ \underline{\psi}(t) \}, \quad (1.33)$$

which corresponds to the time-domain analogon of Eq. (1.31).

Example: Representation of harmonic oscillations by complex time-domain amplitudes As an example, let us consider analytic time-domain signals which are commonly used to describe monochromatic oscillations. The time-domain representation of such an oscillation is given by $\psi(t) = A \cos(\omega_0 t + \varphi)$, and the Hilbert transform of $\psi(t)$ is given by $A \sin(\omega_0 t + \varphi)$. As an analytic signal, we hence obtain the commonly used complex exponential $\underline{\psi}(t) = A \exp(j(\omega_0 t + \varphi))$ with a single-sided spectrum. The real part of $\underline{\psi}(t)$ corresponds to the original signal. Note, however, that the concept of analytic time-domain signals is much more general and goes far beyond the description of monochromatic oscillations.

Maxwell's equations for complex time-domain amplitudes

Let us now consider a monochromatic electromagnetic wave, oscillating at an angular frequency ω_0 and propagating through a linear time-invariant medium. All real electromagnetic field quantities $\psi(\mathbf{r}, t) = \text{Re} \{ \underline{\psi}(\mathbf{r}, t) \}$ can then be represented as the real parts of equivalent analytic time-domain signals $\underline{\psi}(\mathbf{r}, t)$ having the form

$$\underline{\psi}(\mathbf{r}, t) = \underline{\Psi}(\mathbf{r}, \omega_0) \exp(j\omega_0 t). \quad (1.34)$$

The quantity $\underline{\Psi}(\mathbf{r}, \omega_0)$ represents a complex time-domain amplitude of the analytical time-domain signal $\underline{\psi}(\mathbf{r}, t)$. The Fourier spectrum of the real time-domain function is then given by

$$\tilde{\psi}(\mathbf{r}, \omega) = \underline{\Psi}(\mathbf{r}, \omega_0) \frac{1}{2} (\delta(\omega - \omega_0) + \delta(\omega + \omega_0)), \quad (1.35)$$

i.e., there are only nonzero spectral components at $\omega = \pm\omega_0$. Inserting these relations into Eqs. (1.14) to (1.21), we obtain Maxwell's equations for the complex time-domain amplitudes $\underline{\Psi}(\mathbf{r}, \omega_0)$,

$$\nabla \cdot \underline{\mathbf{D}}(\mathbf{r}, \omega_0) = 0, \quad (1.36)$$

$$\nabla \times \underline{\mathbf{E}}(\mathbf{r}, \omega_0) = -j\omega_0 \underline{\mathbf{B}}(\mathbf{r}, \omega_0), \quad (1.37)$$

$$\nabla \cdot \underline{\mathbf{B}}(\mathbf{r}, \omega_0) = 0, \quad (1.38)$$

$$\nabla \times \underline{\mathbf{H}}(\mathbf{r}, \omega_0) = j\omega_0 \underline{\mathbf{D}}(\mathbf{r}, \omega_0). \quad (1.39)$$

The corresponding constitutive relations are given by

$$\underline{\mathbf{B}}(\mathbf{r}, \omega_0) = \mu_0 \underline{\mathbf{H}}(\mathbf{r}, \omega_0), \quad (1.40)$$

$$\underline{\mathbf{D}}(\mathbf{r}, \omega_0) = \epsilon_0 \underline{\mathbf{E}}(\mathbf{r}, \omega_0) + \underline{\mathbf{P}}(\mathbf{r}, \omega_0). \quad (1.41)$$

For linear time-invariant media, the complex time-domain amplitude $\underline{\mathbf{P}}_L(\mathbf{r}, \omega_0)$ of the electric polarization and the complex amplitude $\underline{\mathbf{E}}(\mathbf{r}, \omega_0)$ of the electric field are related by

$$\underline{\mathbf{P}}_L(\mathbf{r}, \omega_0) = \epsilon_0 \iiint_{-\infty}^{\infty} \underline{\chi}^{(1)}(\mathbf{r}, \mathbf{r}', \omega_0) \underline{\mathbf{E}}(\mathbf{r}', \omega_0) d\mathbf{r}', \quad (1.42)$$

which simplifies to

$$\underline{\mathbf{P}}_L(\mathbf{r}, \omega_0) = \epsilon_0 \underline{\chi}^{(1)}(\mathbf{r}, \omega_0) \underline{\mathbf{E}}(\mathbf{r}, \omega_0) \quad (1.43)$$

for the case of a linear time-invariant material that is local in space. The quantities $\underline{\chi}^{(1)}(\mathbf{r}, \mathbf{r}', \omega_0)$ and $\underline{\chi}^{(1)}(\mathbf{r}, \omega_0)$ are equal to the corresponding Fourier-domain representations of the electric susceptibilities,

$$\underline{\chi}^{(1)}(\mathbf{r}, \mathbf{r}', \omega_0) = \tilde{\chi}^{(1)}(\mathbf{r}, \mathbf{r}', \omega_0) \quad (1.44)$$

$$\underline{\chi}^{(1)}(\mathbf{r}, \omega_0) = \tilde{\chi}^{(1)}(\mathbf{r}, \omega_0) \quad (1.45)$$

The electric susceptibility $\underline{\chi}^{(1)}$ links two vectorial quantities $\underline{\mathbf{P}}$ and $\underline{\mathbf{E}}$ and is therefore a matrix in the general case.

Note that Eqs. (1.36) to (1.43) are mathematically identical to Eqs. (1.14) to (1.21), i.e., the complex time-domain amplitudes of a monochromatic analytic signal with oscillation frequency ω_0 obey the Fourier-domain representation of Maxwell's equations at frequency $\omega = \omega_0$. This is a direct consequence of the linearity of Maxwell's equations. In linear optics, there is hence no need to distinguish between Fourier transforms $\tilde{\Psi}(\mathbf{r}, \omega)$ and complex space-dependent time-domain amplitudes $\underline{\Psi}(\mathbf{r}, \omega_0)$. For nonlinear optics, this discrimination is important: Products of field quantities, that often occur in nonlinear optics, simply correspond to the product of the corresponding time-domain amplitude, whereas the corresponding Fourier transforms would have to be combined by means of more complicated convolutions.

1.2.5 Wave propagation in linear isotropic media

Complex electric susceptibility, dielectric permeability, and complex refractive index

In the following, we assume a linear isotropic time-invariant material that is local in space. Using Eqs. (1.41) and (1.43), we can state a simple linear relationship between the electric field and the electric displacement,

$$\begin{aligned}\underline{\mathbf{D}}(\mathbf{r}, \omega) &= \epsilon_0 \underline{\mathbf{E}}(\mathbf{r}, \omega) + \underline{\mathbf{P}}(\mathbf{r}, \omega) \\ &= \epsilon_0 \left(1 + \underline{\chi}^{(1)}(\mathbf{r}, \omega) \right) \underline{\mathbf{E}}(\mathbf{r}, \omega) \\ &= \epsilon_0 \underline{\epsilon}_r(\mathbf{r}, \omega) \underline{\mathbf{E}}(\mathbf{r}, \omega) \\ &= \epsilon_0 \underline{n}^2(\mathbf{r}, \omega) \underline{\mathbf{E}}(\mathbf{r}, \omega).\end{aligned}\tag{1.46}$$

The complex relative dielectric constant $\underline{\epsilon}_r$ and the complex refractive index \underline{n} are related to the complex electric susceptibility $\underline{\chi}^{(1)}$ by

$$\underline{\epsilon}_r(\mathbf{r}, \omega) = 1 + \underline{\chi}^{(1)}(\mathbf{r}, \omega) = \underline{n}^2(\mathbf{r}, \omega).\tag{1.47}$$

From this relation, we can derive various relationships of the real and imaginary parts of $\underline{\epsilon}_r$ and \underline{n} ,

$$\begin{aligned}\underline{n} &= n - j n_i, & \underline{\epsilon}_r &= \epsilon_r - j \epsilon_{ri}, \\ \epsilon_r &= n^2 - n_i^2, & \epsilon_{ri} &= 2nn_i, \\ n^2 &= \frac{1}{2}\epsilon_r \left(1 + \sqrt{1 + \epsilon_{ri}^2/\epsilon_r^2} \right), & n_i &= \epsilon_{ri}/(2n), \\ n &\approx \sqrt{\epsilon_r} \quad (\text{for } |\epsilon_{ri}| \ll \epsilon_r) & n_i &\approx \epsilon_{ri}/(2\sqrt{\epsilon_r}), \\ n &\approx \sqrt{|\epsilon_{ri}|/2} \quad (\text{for } |\epsilon_{ri}| \gg \epsilon_r) & n_i &\approx \text{sgn}(\epsilon_{ri})\sqrt{|\epsilon_{ri}|/2}.\end{aligned}\tag{1.48}$$

Note the somewhat unusual negative signs for the imaginary parts in Eq. (1.48) result from the convention to assign positive values of n_i to lossy media, whereas negative values of n_i correspond to media with gain.

Wave equations in the general form

By reshaping Eqs. (1.36) to (1.41) and using Eq. (1.46), we obtain the vector wave equations for the electric and the magnetic fields,

$$\nabla^2 \underline{\mathbf{E}}(\mathbf{r}, \omega) + \nabla \left(\frac{\nabla \underline{\epsilon}_r(\mathbf{r}, \omega)}{\underline{\epsilon}_r(\mathbf{r}, \omega)} \cdot \underline{\mathbf{E}}(\mathbf{r}, \omega) \right) + k_0^2 \underline{\epsilon}_r(\mathbf{r}, \omega) \underline{\mathbf{E}}(\mathbf{r}, \omega) = 0\tag{1.49}$$

$$\nabla^2 \underline{\mathbf{H}}(\mathbf{r}, \omega) + \frac{\nabla \underline{\epsilon}_r(\mathbf{r}, \omega)}{\underline{\epsilon}_r(\mathbf{r}, \omega)} \times (\nabla \times \underline{\mathbf{H}}(\mathbf{r}, \omega)) + k_0^2 \underline{\epsilon}_r(\mathbf{r}, \omega) \underline{\mathbf{H}}(\mathbf{r}, \omega) = 0,\tag{1.50}$$

where $k_0 = \omega/c$ represents the free-space wavenumber. For arbitrary media with strong spatial variations of $\underline{\epsilon}_r(\mathbf{r}, \omega)$, these equations cannot be solved analytically, since all vector components of the electric and the magnetic fields are coupled by the expression $(\nabla \underline{\epsilon}_r / \underline{\epsilon}_r)$ on the left-hand sides of Eqs. (1.49) and (1.50). For homogeneous or weakly inhomogeneous media, however, we may simplify these relations considerably. If the dielectric constant $\underline{\epsilon}_r(\mathbf{r}, \omega)$ does not change significantly over an optical wavelength, we find that $|\nabla \underline{\epsilon}_r / \underline{\epsilon}_r| \ll |n k_0|$, and we can neglect the second expressions on the left-hand sides of Eqs. (1.49) and (1.50) in comparison to the first ones. This leads to the so-called Helmholtz equations for the electric and magnetic fields,

$$\nabla^2 \underline{\mathbf{E}}(\mathbf{r}, \omega) + k_0^2 \underline{\epsilon}_r(\mathbf{r}, \omega) \underline{\mathbf{E}}(\mathbf{r}, \omega) = 0\tag{1.51}$$

$$\nabla^2 \underline{\mathbf{H}}(\mathbf{r}, \omega) + k_0^2 \underline{\epsilon}_r(\mathbf{r}, \omega) \underline{\mathbf{H}}(\mathbf{r}, \omega) = 0\tag{1.52}$$

Note that, in contrast to Eqs. (1.49) and (1.50), the vector components of the magnetic and electric fields are now decoupled, i.e., Eqs. (1.51) and (1.52) can each be decomposed into three scalar differential equations for three vector components.

Plane waves in homogeneous media

For homogenous media, $\epsilon_r(\mathbf{r}, \omega) = \epsilon_r(\omega)$ is constant throughout space, and Eqs. (1.51) and (1.52) are solved by so-called plane waves of the form

$$\mathbf{E}(\mathbf{r}, t) = \text{Re} \{ \underline{\mathbf{E}}(\mathbf{r}, \omega) e^{j\omega t} \} = \text{Re} \{ \underline{\mathbf{E}}_0 e^{j(\omega t - \mathbf{k}\mathbf{r})} \}, \quad (1.53)$$

$$\mathbf{H}(\mathbf{r}, t) = \text{Re} \{ \underline{\mathbf{H}}(\mathbf{r}, \omega) e^{j\omega t} \} = \text{Re} \{ \underline{\mathbf{H}}_0 e^{j(\omega t - \mathbf{k}\mathbf{r})} \}, \quad (1.54)$$

where the wave vector \mathbf{k} defines the direction of propagation and obeys the relation

$$\underline{\mathbf{k}}^2 = k_0^2 \epsilon_r(\omega). \quad (1.55)$$

The surfaces of equal phase (“phase fronts”) are planes that are normal to \mathbf{k} . Phase fronts travel with the phase velocity $v_p = c/n(\omega)$.

For a plane wave, the magnetic field can be derived from the electric field and vice versa. Introducing the plane-wave solution for the electric field, Eq. (1.53), into Maxwell’s curl equations (1.2) and (1.4), we find

$$\underline{\mathbf{H}}_0 = \frac{1}{\omega \mu_0} \underline{\mathbf{k}} \times \underline{\mathbf{E}}_0, \quad (1.56)$$

$$\underline{\mathbf{E}}_0 = -\frac{1}{\omega \epsilon_0 \epsilon_r} \underline{\mathbf{k}} \times \underline{\mathbf{H}}_0. \quad (1.57)$$

Maxwell’s divergence equations (1.1) and (1.3) lead to

$$\mathbf{k} \cdot \underline{\mathbf{E}}_0 = 0 \quad (1.58)$$

$$\mathbf{k} \cdot \underline{\mathbf{H}}_0 = 0. \quad (1.59)$$

In other words: The vectors (\mathbf{k} , $\underline{\mathbf{E}}_0$, $\underline{\mathbf{H}}_0$) are mutually orthogonal and form a right-handed system.

Note that the wave vector $\underline{\mathbf{k}}$ is in general a complex number,

$$\underline{\mathbf{k}} = \mathbf{k} - j\mathbf{k}_i = k_0 n \mathbf{e}_k \quad (1.60)$$

where \mathbf{e}_k denotes the unit vector in the direction of propagation. The time-averaged energy flux carried by the wave is obtained from the real part of the complex Poynting vector $\underline{\mathbf{S}}$ [19],

$$\text{Re} \{ \underline{\mathbf{S}} \} = \text{Re} \left\{ \frac{1}{2} \underline{\mathbf{E}}(\mathbf{r}, \omega) \times \underline{\mathbf{H}}^*(\mathbf{r}, \omega) \right\} = \frac{\mathbf{k}}{2\omega \mu_0} |\underline{\mathbf{E}}_0|^2 e^{-2\mathbf{k}_i \mathbf{r}} \quad (1.61)$$

If we assume a plane wave propagating into positive z -direction, then $\mathbf{k} = k_0 n \mathbf{e}_z$ and the power decays as $e^{-\alpha z}$, where the power attenuation coefficient α is linked to the imaginary part of the refractive index by

$$\alpha = 2k_0 n_i. \quad (1.62)$$

Due to the convention to use negative signs for the imaginary parts in Eq. (1.48), a positive value of n_i corresponds to a positive attenuation coefficient α and therefore to optical loss, whereas negative values of n_i and α occur for media that show optical gain.

1.3 Harmonic and anharmonic oscillator model of optical media

In many cases of practical interest, the electric polarization \mathbf{P} is dominated by the contributions of electrons that are bound to atomic nuclei. Under the influence of an external electric field, the

center of each electron cloud is displaced from the center of the corresponding nucleus, which leads to a microscopic electric dipole moment \mathbf{p} and hence to a macroscopic electric polarization \mathbf{P} of the material. For small electric fields, the displacement increases linearly with the applied field. This corresponds to an harmonic oscillator, for which the restoring force depends linearly and the stored energy depends quadratically on the displacement, thereby leading to a linear relationship between electric field and polarization \mathbf{P} . Conversely, for large electric fields, the relationship between electric field and displacement becomes nonlinear, corresponding to an anharmonic oscillator, which leads to a nonlinear relationship between electric field and polarization. The following sections are dedicated to a more detailed study of these phenomena.

1.3.1 The Lorentz oscillator model of linear dielectric media

Let us first consider a simple model for the interaction of an electric field \mathbf{E} with a linear dielectric medium. The external electric field \mathbf{E} leads to a displacement of charges within the individual atoms and molecules, thereby inducing an electric dipole moment \mathbf{p} , Fig. 1.2. The electric polarization \mathbf{P} is then given by the dipole moment that is induced per unit volume,

$$\mathbf{P} = N\mathbf{p}, \quad (1.63)$$

where N is the number of charges per unit volume. Assuming $\mathbf{E} = E_x \mathbf{e}_x$, and denoting the dis-

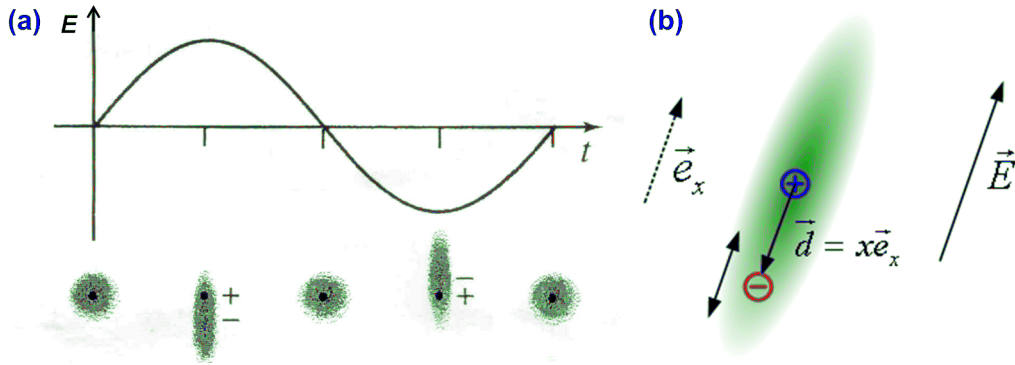


Figure 1.2: Lorentz model of electrons that are bound to a positively charged nucleus. (a) An external electric field E leads to a displacement of a bound electron and hence to a shift \mathbf{d} of the center of negative charges away from the positively charged nucleus. This causes an electric dipole moment that oscillates with the frequency of the external field. (b) For an electric field oriented along the x -direction, the problem can be simplified to a one-dimensional equation of motion for the electron. (Figure adapted from [26]).

placement of a single bound electron with x , the dipole moment $\mathbf{p} = p_x \mathbf{e}_x$ is given by $p_x = -xe$. The dynamic displacement of the electron obeys Newton's second law, which states that the sum of forces (driving plus restoring force) equals electron mass m_e times acceleration,

$$m_e \frac{d^2 x}{dt^2} = -eE_x - m_e \omega_r^2 x - m_e \gamma_r \frac{dx}{dt}, \quad (1.64)$$

where $\gamma_r \ll \omega_r$. In this relation, a linear increase of the restoring force $m_e \omega_r^2 x$ with displacement x was assumed.

Solving Eq. (1.64) for a monochromatic excitation $E_x = \text{Re} \{ \underline{E}_x \exp(j\omega t) \}$, the complex electric polarization is obtained, and the electric susceptibility can be derived,

$$\underline{\chi}(\omega) = \chi_0 \frac{\omega_r^2}{\omega_r^2 - \omega^2 + j\omega\gamma_r}, \quad (1.65)$$

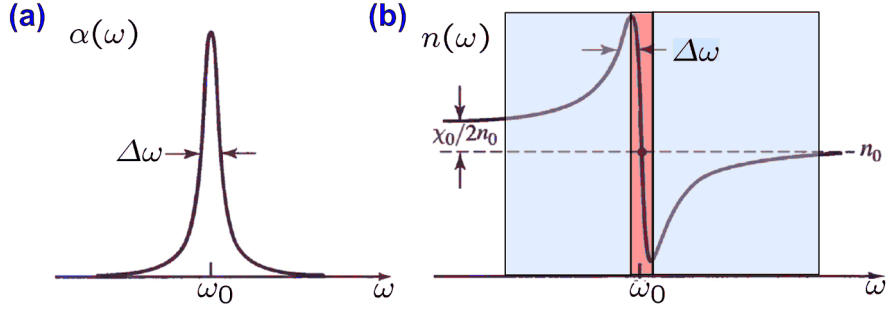


Figure 1.3: (a) Absorption coefficient α , and (b) refractive index n of a dielectric medium near resonance frequency ω_0 . The absorption spectrum assumes the shape of a narrow line, whereas the refractive index undergoes a typical pattern which shows an increased refractive index for frequencies below resonance and a decreased refractive index for frequencies above resonance (Figure adapted from [26]).

where

$$\chi_0 = \frac{Ne^2}{\epsilon_0 m_e \omega_r^2}. \quad (1.66)$$

The real and the imaginary parts of the complex electric susceptibility hence read

$$\chi(\omega) = \frac{(\omega_r^2 - \omega^2) \omega_r^2}{(\omega_r^2 - \omega^2)^2 + \omega^2 \gamma_r^2} \chi_0 \quad (1.67)$$

$$\chi_i(\omega) = -\frac{\omega \gamma_r \omega_r^2}{(\omega_r^2 - \omega^2)^2 + \omega^2 \gamma_r^2} \chi_0. \quad (1.68)$$

From these relations, we may deduce some very general properties of dielectric media:

- Well below resonance, i.e., for $\omega \ll \omega_r$ we find $\chi \approx \chi_0$ and $\chi_i \approx 0$. In the low-frequency limit, dielectric media hence exhibit only refraction, but no absorption.
- Well above resonance, i.e., for $\omega \gg \omega_r$ we find $\chi \approx \chi_i \approx 0$. The medium hence behaves essentially like free space; electrons cannot any more “follow” the electric field because it changes too fast. As a consequence, most materials appear transparent at X-ray frequencies and have a refractive index close to unity.
- Right at resonance, i.e., for $\omega = \omega_r$ we find $\chi \approx 0$ and $\chi_i \approx Q\chi_0$, where $Q = \omega_r/\gamma_r$. This implies strong absorption and a strongly frequency-dependent refractive index.

Equations (1.67) and (1.68) lead to a characteristic behavior of the refractive index near a resonance line, see Fig. (1.3). For real media, different electrons exhibit different resonance frequencies, Fig. (1.4), and the real and imaginary parts of the susceptibility are given by a sum over the various contributions,

$$\chi(\omega) = \sum_{\nu} \frac{(\omega_{r\nu}^2 - \omega^2) \omega_r^2}{(\omega_{r\nu}^2 - \omega^2)^2 + \omega^2 \gamma_{r\nu}^2} \chi_{0\nu}, \quad (1.69)$$

$$\chi_i(\omega) = -\sum_{\nu} \frac{\omega \gamma_{r\nu} \omega_{r\nu}^2}{(\omega_{r\nu}^2 - \omega^2)^2 + \omega^2 \gamma_{r\nu}^2} \chi_{0\nu}. \quad (1.70)$$

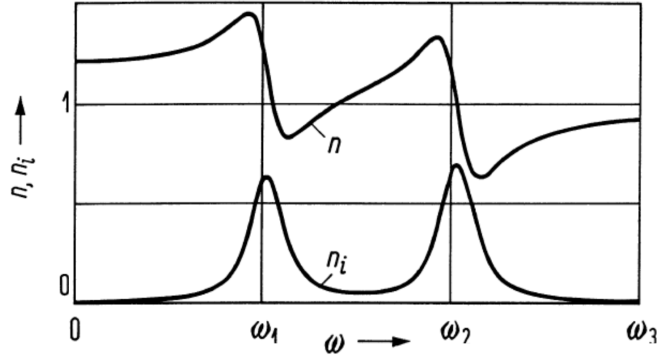


Figure 1.4: In real media, the real and imaginary parts of the susceptibility are given by a sum over the contributions of various electrons (Figure adapted from [14]).

Example: Lenses for X-ray radiation At X-ray frequencies, $\omega \gg \omega_r$, we find $\chi \approx \chi_i \approx 0$ and $\chi < 0$. Hence, materials are in essence transparent for these wavelengths, and X-rays are widely used for tomographic analysis of the interior structures of biological and technical samples. At the same time, the refractive indices at X-ray frequencies are close to unity, and it is therefore challenging to produce refractive optical components. X-ray lenses are therefore composed of arrays of single lens elements, Fig. (1.5). In contrast to normal optics, focusing X-ray lenses must have concave cross sections, since the refractive index is smaller than unity.

1.3.2 Anharmonic oscillator model of electronic nonlinearities

In Eq. (1.64), a linear relationship between the restoring force and the displacement was assumed. This can be represented by a quadratic potential of a harmonic oscillator, see Fig. 1.6, and represents a very good first-order approximation for small electric fields \mathbf{E} . For strong fields, however, the nonlinearity of the relationship between electric polarization and electric field becomes noticeable, and anharmonic correction terms have to be considered. The solid red line in Fig. 1.6 represents an anharmonic potential with a cubic contribution, which leads to a quadratic term $-ax^2$ in the restoring force. Similarly to Eq. (1.64), the equation of motion can now be written as

$$m_e \frac{d^2x}{dt^2} = -eE_x - m_e \gamma_r \frac{dx}{dt} - m_e \omega_r^2 x - ax^2, \quad (1.71)$$

Inserting a monochromatic electric field $E_x = \text{Re} \{ \underline{E}_x \exp(j\omega_0 t) \} = \cos(\omega_0 t - \varphi)$ as an excitation, the displacement x now features frequency components at $\omega = 0$, $\omega = \omega_0$, and $\omega = 2\omega_0$, and the same applies to the polarization, see [29] for a more detailed analysis. This leads to formation of new spectral components at $\omega = 0$, $\omega = \omega_0$, and $\omega = 2\omega_0$ - a typical phenomenon of second-order nonlinearities. Similarly, third-order nonlinearities are associated with a fourth-order term in the potential and a cubic term in the restoring force, thereby generating new spectral components at, e.g., $\omega = 3\omega_0$.

1.4 Wave propagation in nonlinear media

In Section 1.2, we have studied wave propagation in homogeneous media that are linear and isotropic. We will now consider nonlinear media and investigate the impact of optical nonlinearities on wave propagation. To this end, we will first derive the wave equation in homogeneous nonlinear

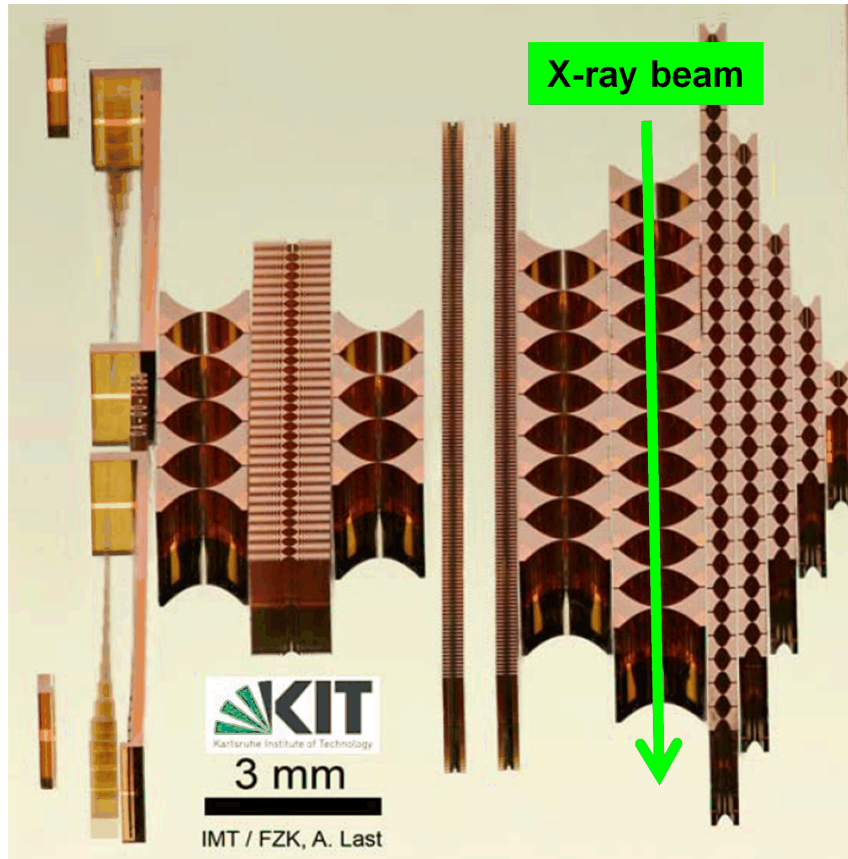


Figure 1.5: To obtain sufficient refractive power despite refractive indices n that are close to unity, X-ray lenses are composed of an array of individual lens elements. Since $n < 1$ for X-ray frequencies, focussing lenses must have concave shapes. (Source: A. Last, KIT-IMT)

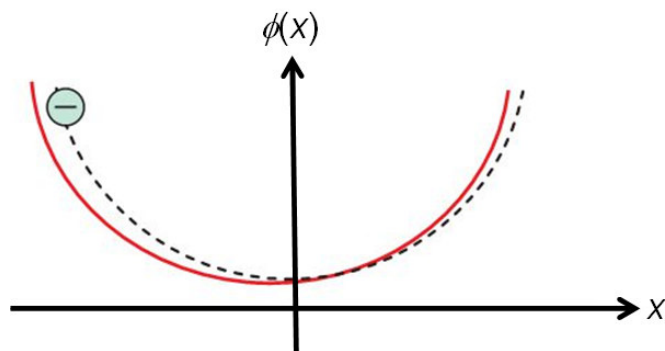


Figure 1.6: Harmonic potential (dashed black line) and anharmonic potential (solid red line) experienced by a bound electron. The harmonic potential has a parabolic shape, and the restoring force is hence proportional to the displacement x . The anharmonic potential contains a cubic component, which contributes quadratically to the restoring force. This leads to a nonlinear relationship between the electric field and the electric polarization and hence to optical nonlinearities. If a sinusoidal excitation field is applied, we observe higher harmonics in the electric polarization. (Figure adapted from [29]).

media, and then solve it by a first-order perturbation approach using the so-called slowly varying envelope approximation (SVEA).

1.4.1 Nonlinear wave equation

Consider a superposition of plane waves, where all electromagnetic field quantities can be represented by an expression of the form

$$\mathbf{E}(\mathbf{r}, t) = \frac{1}{2} \left(\sum_l \underline{\mathbf{E}}(\mathbf{r}, \omega_l) \exp(j\omega_l t) + \text{c.c.} \right). \quad (1.72)$$

In this relation, “c.c.” denotes the complex conjugate of the preceding expression. The linear polarization is then given by

$$\mathbf{P}_L(\mathbf{r}, t) = \frac{1}{2} \left(\sum_l \underline{\mathbf{P}}(\mathbf{r}, \omega_l) \exp(j\omega_l t) + \text{c.c.} \right), \quad (1.73)$$

where the complex amplitudes of the polarization $\underline{\mathbf{P}}(\mathbf{r}, \omega_l)$ are linked to the corresponding complex amplitudes of the field $\underline{\mathbf{E}}(\mathbf{r}, \omega_l)$ by Eq. (1.43),

$$\underline{\mathbf{P}}_L(\mathbf{r}, \omega_l) = \epsilon_0 \underline{\chi}^{(1)}(\mathbf{r}, \omega_l) \underline{\mathbf{E}}(\mathbf{r}, \omega_l) \quad (1.74)$$

If the medium is operated far away from any electronic resonances, then the first-order susceptibilities $\underline{\chi}^{(1)}(\mathbf{r}, \omega_l)$ can be assumed to be real and independent of frequency ω_l ,

$$\underline{\chi}^{(1)}(\mathbf{r}, \omega_l) \approx \chi^{(1)}(\mathbf{r}) \in \mathbb{R}. \quad (1.75)$$

In this case, we can relate the instantaneous linear polarization $\mathbf{P}_L(\mathbf{r}, t)$ directly to the electric field, neglecting any memory of the medium,

$$\mathbf{P}_L(\mathbf{r}, t) = \epsilon_0 \chi^{(1)}(\mathbf{r}) \mathbf{E}(\mathbf{r}, t) \quad (1.76)$$

In a nonlinear medium, the total polarization is given by the sum of the linear and the nonlinear contributions,

$$\mathbf{P}(\mathbf{r}, t) = \mathbf{P}_L(\mathbf{r}, t) + \mathbf{P}_{NL}(\mathbf{r}, t), \quad (1.77)$$

where the nonlinear contribution is usually much smaller than the linear one,

$$|\mathbf{P}_{NL}(\mathbf{r}, t)| \ll |\mathbf{P}_L(\mathbf{r}, t)|. \quad (1.78)$$

Inserting Eq. (1.77) in Maxwell’s equations, Eqs. (1.36) to (1.43), we can derive the wave equation for nonlinear media,

$$\nabla \times \nabla \times \mathbf{E}(\mathbf{r}, t) + \mu_0 \epsilon_0 \epsilon_r \frac{\partial^2 \mathbf{E}(\mathbf{r}, t)}{\partial t^2} = -\mu_0 \frac{\partial^2 \mathbf{P}_{NL}(\mathbf{r}, t)}{\partial t^2} \quad (1.79)$$

For small nonlinearities, we may simplify this relation to

$$\nabla^2 \mathbf{E}(\mathbf{r}, t) - \frac{n^2}{c^2} \frac{\partial^2 \mathbf{E}(\mathbf{r}, t)}{\partial t^2} = \mu_0 \frac{\partial^2 \mathbf{P}_{NL}(\mathbf{r}, t)}{\partial t^2}. \quad (1.80)$$

For linear media, the right-hand side vanishes, and the relation is solved by plane waves. For nonlinear media, we may assume that the solutions are similar to plane waves, but with amplitudes that vary slowly in time and space. This approach is also referred to as the slowly varying envelope approximation (SVEA) and shall be considered further in the next section.

1.4.2 Representation of the nonlinear polarization

For the sake of simplicity, we assume a homogeneous isotropic medium and reduce the representation to plane waves that are polarized along the x -direction,

$$\mathbf{E}(\mathbf{r}, t) = E(z, t) \mathbf{e}_x, \quad (1.81)$$

$$\mathbf{P}(\mathbf{r}, t) = P(z, t) \mathbf{e}_x, \quad (1.82)$$

where \mathbf{e}_x denotes the unit vector along the x -direction, and where the scalar electric field $E(z, t)$ is given by

$$E(z, t) = \frac{1}{2} \left(\sum_l \underline{E}(\omega_l) \exp(j(\omega_l t - k_l z)) + \text{c.c.} \right). \quad (1.83)$$

In this relation, $k_l = n\omega_l/c$ denotes the propagation constant of the plane wave. For representation of the nonlinear polarization, we also assume a memory-less instantaneous response to the electric field. We can then expand $P(z, t)$ into a power series of $E(z, t)$,

$$P(z, t) = \epsilon_0 \chi^{(1)} E(z, t) + \epsilon_0 \chi^{(2)} E^2(z, t) + \epsilon_0 \chi^{(3)} E^3(z, t) + \dots \quad (1.84)$$

As explained in the last section, we can now decompose the polarization into a linear contribution $P_L(z, t)$ and a nonlinear contribution $P_{NL}(z, t)$,

$$P(z, t) = P_L(z, t) + P_{NL}(z, t) \quad (1.85)$$

$$P_L(z, t) = \epsilon_0 \chi^{(1)} E(z, t) \quad (1.86)$$

$$P_{NL}(z, t) = \epsilon_0 \chi^{(2)} E^2(z, t) + \epsilon_0 \chi^{(3)} E^3(z, t) + \dots \quad (1.87)$$

As an example, let us consider the second-order nonlinear polarization for a superposition of two plane waves, oscillating at frequencies ω_1 and ω_2 ,

$$E(z, t) = \frac{1}{2} \left(\underline{E}(\omega_1) \exp(j(\omega_1 t - k_1 z)) + \underline{E}(\omega_2) \exp(j(\omega_2 t - k_2 z)) + \text{c.c.} \right). \quad (1.88)$$

Using the abbreviation $\underline{E}_l = \underline{E}(\omega_l)$, the corresponding second-order nonlinear polarization can be written as

$$P_{NL}(z, t) = \frac{1}{4} \epsilon_0 \chi^{(2)} \left(\underline{E}_1^2 e^{j2(\omega_1 t - k_1 z)} + \underline{E}_2^2 e^{j2(\omega_2 t - k_2 z)} + 2|\underline{E}_1|^2 + 2|\underline{E}_2|^2 + 2\underline{E}_1 \underline{E}_2 e^{j((\omega_1 + \omega_2)t - (k_1 + k_2)z)} + 2\underline{E}_1 \underline{E}_2^* e^{j((\omega_1 - \omega_2)t - (k_1 - k_2)z)} + \text{c.c.} \right) \quad (1.89)$$

Note that $|\underline{E}_1|^2 \in \mathbb{R}$, i.e., $|\underline{E}_1|^2 + \text{c.c.} = 2|\underline{E}_1|^2$ on the right-hand side of Eq. (1.89). The physical meaning of the various contributions are discussed in more detail in Section 1.5. Note that the individual expressions exhibit a plane wave-like space and time dependence such that the nonlinear polarization can be written as

$$P_{NL}(z, t) = \frac{1}{2} \left(\sum_l \underline{P}_{NL}(\omega_l) \exp(j(\omega_l t - k_{p,l} z)) + \text{c.c.} \right), \quad (1.90)$$

where $\omega_l \in \{2\omega_1, 2\omega_2, \omega_1 + \omega_2, \omega_1 - \omega_2, 0\}$ and $k_{p,l} \in \{2k_1, 2k_2, k_1 + k_2, k_1 - k_2, 0\}$.

1.4.3 Plane waves and slowly-varying envelope approximation (SVEA)

The nonlinear polarization on the right-hand side of Eq. (1.80) acts as a source for new frequency components. For a simplified analysis, let us again consider a superposition of plane waves that

are polarized along the x -direction and propagate along the z -direction. The effects of optical nonlinearities shall be taken into account by allowing for a weak space and time dependence of the scalar plane-wave amplitudes $\underline{E}(z, t, \omega_l)$,

$$E(z, t) = \frac{1}{2} \left(\sum_l \underline{E}(z, t, \omega_l) \exp(j(\omega_l t - k_l z)) + \text{c.c.} \right). \quad (1.91)$$

We use the same set of frequencies ω_l to expand the second-order nonlinear polarization,

$$P_{\text{NL}}(z, t) = \frac{1}{2} \left(\sum_l \underline{P}_{\text{NL}}(z, t, \omega_l) \exp(j(\omega_l t - k_{p,l} z)) + \text{c.c.} \right). \quad (1.92)$$

We insert Eq. (1.91) and (1.92) into Eq. (1.80), and consider the various frequency components individually. We further exploit the fact that $\underline{E}(z, t, \omega_l)$ varies only slowly with space and time and hence

$$\left| \frac{\partial^2 \underline{E}(z, t, \omega_l)}{\partial t^2} \right| \ll \omega_l \left| \frac{\partial \underline{E}(z, t, \omega_l)}{\partial t} \right|, \quad (1.93)$$

$$\left| \frac{\partial^2 \underline{E}(z, t, \omega_l)}{\partial z^2} \right| \ll k_l \left| \frac{\partial \underline{E}(z, t, \omega_l)}{\partial z} \right|. \quad (1.94)$$

This leads to a relation of the form

$$\frac{\partial \underline{E}(z, t, \omega_l)}{\partial z} + \frac{n}{c} \frac{\partial \underline{E}(z, t, \omega_l)}{\partial t} = -j \frac{\omega_l}{2\epsilon_0 c n} \underline{P}_{\text{NL}}(z, t, \omega_l) e^{-j(k_{p,l} - k_l)z}. \quad (1.95)$$

The expression on the left-hand side can be simplified by introducing a retarded time frame,

$$t' = t - \frac{nz}{c}, \quad (1.96)$$

$$z' = z, \quad (1.97)$$

$$\underline{E}(z, t, \omega_l) = \underline{E}'(z, t - \frac{nz}{c}, \omega_l). \quad (1.98)$$

This leads finally to the relation

$$\frac{\partial \underline{E}'(z', t', \omega_l)}{\partial z'} = -j \frac{\omega_l}{2\epsilon_0 c n} \underline{P}'_{\text{NL}}(z', t', \omega_l) e^{-j(k_{p,l} - k_l)z'}. \quad (1.99)$$

Note that the primes are sometimes omitted in the literature without explicit mentioning that the time dependence refers to a retarded reference frame.

By using the SVEA, we could hence reduce the second-order differential equation (1.80) to a first-order equation (1.99) which describes the evolution of the complex field amplitudes during propagation through a nonlinear medium. The nonlinear polarization $\underline{P}'_{\text{NL}}(z', t', \omega_l)$ on the right-hand side of Eq. (1.99) can be interpreted as a source for the electric field component $\underline{E}'(z', t', \omega_l)$ that is oscillating at the same frequency ω_l . Depending of the relative phase between $\underline{P}'_{\text{NL}}(z', t', \omega_l)$ and $\underline{E}'(z', t', \omega_l)$, the nonlinear polarization can cause amplification, absorption or phase shifts. Proper phase matching is an aspect of prime importance for efficient nonlinear interaction: If $(k_{p,l} - k_l) \neq 0$ and if the evolution according to Eq. (1.99) is considered over a length L for which $(k_{p,l} - k_l) L \gg 1$, then the effects of optical nonlinearities average out due to a constantly changing phase relation between the existing electric field $\underline{E}'(z', t', \omega_l)$ and the newly generated contribution $\partial \underline{E}'(z', t', \omega_l) / \partial z'$.

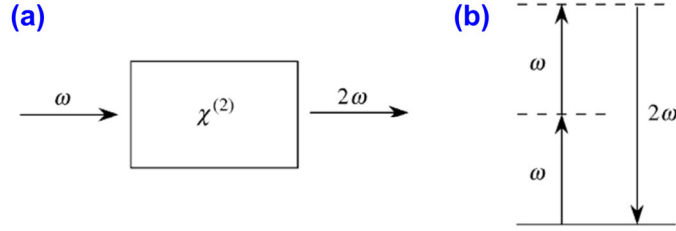


Figure 1.7: Second-harmonic generation (SHG). (a) Interaction scheme. (b) Energy-level description (Figure adapted from [9]).

1.5 Survey of nonlinear optical processes

In this section we give a short overview on the nonlinear optical processes that occur as a consequence of Eq. (1.99). For better understanding let us recall that Eq. (1.99) only describes the evolution of a single frequency component centered at ω_l as a consequence of nonlinear interaction. If we launch a superposition of monochromatic waves with different frequencies into a nonlinear medium, we will generate a multitude of new frequency components, see, e.g., Eq. (1.89) for the case of a superposition of two waves in a second-order nonlinear medium. Eq. (1.99) has then to be applied to each of these frequency components separately. In general, for a nonlinearity of order n , we will see newly generated frequency components that correspond to the sum of any n positive or negative frequency components of the incident wave. Each combination of input frequencies that leads to a certain new frequency component can be associated with a specific nonlinear optical process. We will give an overview on these processes in the following sections. To simplify the analysis, we will operate in the retarded time frame defined by Eqs. (1.96) - (1.98), but we will omit the primes for the sake of readability.

1.5.1 Second-order nonlinearities

For a superposition of monochromatic plane waves at frequencies ω_1 and ω_2 in a second-order nonlinear medium, the nonlinear optical polarization is given by Eq. (1.89). Comparing Eqs. (1.89) and (1.90), we can identify the complex amplitude of the nonlinear polarization at frequency ω_p , which is associated with a wave vector k_p . These amplitudes can be associated with the following second-order nonlinear processes:

Second-harmonic generation (SHG)

The second harmonic of a monochromatic wave at frequency ω_1 oscillates at $\omega_p = 2\omega_1$ and features a wave vector $k_p = 2k_1$. The nonlinear polarization leading to this process is given by

$$\underline{P}_{\text{SHG}}(z, t, 2\omega_1) = \frac{1}{2} \epsilon_0 \chi^{(2)} \underline{E}^2(z, t, \omega_1) \quad (1.100)$$

The interaction scheme and the energy-level diagram of second-harmonic generation are shown in Fig. 1.7. In SHG, two photons interact to generate a new photon with twice the energy.

Optical rectification (OR)

For optical rectification, nonlinear interaction of a monochromatic wave with itself leads to a DC field at $\omega_p = 0$, which is associated with a wave vector of $k_p = 0$. Note that the amplitude for $\omega_p = 0$ is real and hence identical to the corresponding “+cc”-term. Taking this into account, the nonlinear polarization responsible for optical rectification is given by

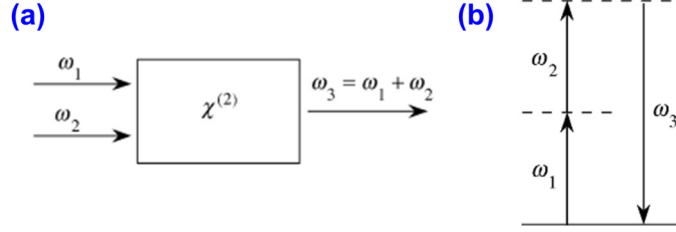


Figure 1.8: Sum-frequency generation (SFG). (a) Interaction scheme. (b) Energy-level description (Figure adapted from [9]).

$$\underline{P}_{\text{OR}}(z, t, 0) = \frac{1}{2} \epsilon_0 \chi^{(2)} \underline{E}(z, t, \omega_1) \underline{E}(z, t, -\omega_1) \quad (1.101)$$

Note that $\underline{E}(z, t, -\omega_1) = -\underline{E}^*(z, t, \omega_1)$, ensuring that $\underline{P}_{\text{NL}}(z, t, 0)$ is a real-valued quantity.

Sum-frequency generation (SFG)

For sum frequency generation, the frequency of the newly generated wave is given by $\omega_p = \omega_3 = \omega_1 + \omega_2$. Accordingly, the wave vector associated with the nonlinear optical polarization corresponds to $k_p = k_1 + k_2$. Taking into account the degeneracy factor of 2 in Eq. (1.89), the nonlinear optical polarization can be written as

$$\underline{P}_{\text{SFG}}(z, t, \omega_1 + \omega_2) = \epsilon_0 \chi^{(2)} \underline{E}(z, t, \omega_1) \underline{E}(z, t, \omega_2) \quad (1.102)$$

The geometry and the energy-level diagram of sum-frequency generation is shown in Fig. 1.8. In SFG, a new photon of energy $\hbar\omega_3$ is generated by interaction of two photons with energies $\hbar\omega_1$ and $\hbar\omega_2$.

Difference-frequency generation (DFG)

Likewise, we have $\omega_p = \omega_3 = \omega_1 - \omega_2$ and $k_p = k_1 - k_2$ for difference-frequency generation, and the nonlinear optical polarization is given by

$$\underline{P}_{\text{DFG}}(z, t, \omega_1 - \omega_2) = \epsilon_0 \chi^{(2)} \underline{E}(z, t, \omega_1) \underline{E}(z, t, -\omega_2) \quad (1.103)$$

The geometry and the energy-level diagram of difference-frequency generation is shown in Fig. 1.9. A photon of energy $\hbar\omega_3$ and a photon of energy $\hbar\omega_2$ are generated from a photon with energy $\hbar\omega_1$.

Note that in the simplified consideration that we use here, the nonlinear optical element $\chi^{(2)}$ is the same in all relations (1.100)–(1.103). This is a direct consequence of assuming an instantaneous response of the polarization to the electric field in the time-domain Taylor expansion, in Eq. (1.84). We will later introduce frequency-dependent susceptibilities to account for a non-instantaneous time-domain response.

1.5.2 Third-order nonlinearities

To understand the various nonlinear processes that can occur in a third-order nonlinear medium, let us consider a superposition of three plane waves, oscillating at frequencies ω_1 , ω_2 and ω_3 ,

$$E(z, t) = \frac{1}{2} \left(\underline{E}_1 e^{j(\omega_1 t - k_1 z)} + \underline{E}_2 e^{j(\omega_2 t - k_2 z)} + \underline{E}_3 e^{j(\omega_3 t - k_3 z)} + \text{c.c.} \right), \quad (1.104)$$

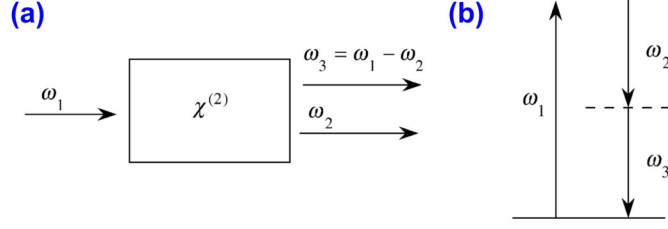


Figure 1.9: Difference-frequency generation (DFG). (a) Interaction scheme. (b) Energy-level description (Figure adapted from [9]).

where $\underline{E}_l = \underline{E}(z, t, \omega_l)$ denotes the slowly varying envelope of the wave oscillating frequency ω_l . Assuming again an instantaneous response of the nonlinear polarization to the electric field, we can follow Eq. (1.84), and write the corresponding third-order nonlinear polarization as

$$\begin{aligned}
 P_{\text{NL}}(z, t) &= \epsilon_0 \chi^{(3)} E^3(z, t) \\
 &= \frac{1}{8} \epsilon_0 \chi^{(3)} \left(\underline{E}_1 e^{j(\omega_1 t - k_1 z)} + \underline{E}_2 e^{j(\omega_2 t - k_2 z)} + \underline{E}_3 e^{j(\omega_3 t - k_3 z)} \right. \\
 &\quad \left. + \underline{E}_1^* e^{-j(\omega_1 t - k_1 z)} + \underline{E}_2^* e^{-j(\omega_2 t - k_2 z)} + \underline{E}_3^* e^{-j(\omega_3 t - k_3 z)} \right)^3
 \end{aligned} \tag{1.105}$$

When expanding the cubic expression on the right-hand side, we obtain terms of the form $\exp(j(\omega_p t - k_p z))$, where $\omega_p = \omega_m + \omega_n + \omega_o$, $k_p = k_m + k_n + k_o$, and where for each of the variables ω_m , ω_n , and ω_o we can assume any of the values $\pm\omega_1$, $\pm\omega_2$, or $\pm\omega_3$. Each term features a degeneracy factor D that corresponds to the number of distinct permutations of the frequency triad $(\omega_1, \omega_2, \omega_3)$, leading to a relation of the form

$$\begin{aligned}
 P_{\text{NL}}(z, t) &= \frac{1}{2} \epsilon_0 \chi^{(3)} \left(\underbrace{\frac{1}{4} \underline{E}_1^3 e^{j(3\omega_1 t - 3k_1 z)} + \dots + \text{c.c.}}_{\text{THG}} \right. \\
 &\quad + \underbrace{\frac{3}{4} \underline{E}_1^2 \underline{E}_2 e^{j((2\omega_1 + \omega_2)t - (2k_1 + k_2)z)} + \dots + \text{c.c.}}_{\text{degenerate FWM / third-order SFG}} \\
 &\quad + \underbrace{\frac{6}{4} \underline{E}_1 \underline{E}_2 \underline{E}_3 e^{j((\omega_1 + \omega_2 + \omega_3)t - (k_1 + k_2 + k_3)z)} + \text{c.c.}}_{\text{non-degenerate FWM / third-order SFG}} \\
 &\quad + \underbrace{\frac{3}{4} |\underline{E}_1|^2 \underline{E}_1 e^{j(\omega_1 t - k_1 z)} + \dots + \text{c.c.}}_{\text{SPM}} \\
 &\quad + \underbrace{\frac{6}{4} |\underline{E}_2|^2 \underline{E}_1 e^{j(\omega_1 t - k_1 z)} + \dots + \text{c.c.}}_{\text{XPM}} \\
 &\quad + \underbrace{\frac{3}{4} \underline{E}_1^2 \underline{E}_2^* e^{j((2\omega_1 - \omega_2)t - (2k_1 - k_2)z)} + \dots + \text{c.c.}}_{\text{degenerate FWM}} \\
 &\quad \left. + \underbrace{\frac{6}{4} \underline{E}_1 \underline{E}_2 \underline{E}_3^* e^{j((\omega_1 + \omega_2 - \omega_3)t - (k_1 + k_2 - k_3)z)} + \dots + \text{c.c.}}_{\text{non-degenerate FWM}} \right).
 \end{aligned} \tag{1.106}$$

Process	Abbreviation	Involved frequencies	Degeneracy factor D
Third-harmonic generation	THG	$(+\omega_1, +\omega_1, +\omega_1)$	1
Self-phase modulation	SPM	$(+\omega_1, -\omega_1, +\omega_1)$	3
Cross-phase modulation	XPM	$(+\omega_2, -\omega_2, +\omega_1)$	6
Non-degenerate four-wave mixing	(non-degenerate) FWM	$(+\omega_1, +\omega_2, +\omega_3)$	6
		$(+\omega_1, +\omega_2, -\omega_3)$	6
Degenerate four-wave mixing	(degenerate) FWM	$(+\omega_1, +\omega_1, +\omega_2)$	3
		$(+\omega_1, +\omega_1, -\omega_2)$	3

Table 1.1: Summary of third-order nonlinear processes. Non-degenerate four-wave mixing with frequencies $(\omega_1, \omega_2, \omega_3)$ is also referred to as third-order sum frequency generation.

In this equation, “+c.c.” denotes the complex conjugate of the preceding expression in the same line, and “+ . . .” represents the ensemble of all expressions that are obtained from the first expression in the line by considering all distinct combinations of subscripts, i.e.,

$$\begin{aligned}
\frac{3}{4} \underline{E}_1^2 \underline{E}_2 e^{j((2\omega_1 + \omega_2)t - (2k_1 + k_2)z)} + \dots = & \frac{3}{4} \underline{E}_1^2 \underline{E}_2 e^{j((2\omega_1 + \omega_2)t - (2k_1 + k_2)z)} \\
& + \frac{3}{4} \underline{E}_2^2 \underline{E}_1 e^{j((2\omega_2 + \omega_1)t - (2k_2 + k_1)z)} \\
& + \frac{3}{4} \underline{E}_1^2 \underline{E}_3 e^{j((2\omega_1 + \omega_3)t - (2k_1 + k_3)z)} \\
& + \frac{3}{4} \underline{E}_2^2 \underline{E}_3 e^{j((2\omega_2 + \omega_3)t - (2k_2 + k_3)z)} \\
& + \frac{3}{4} \underline{E}_3^2 \underline{E}_1 e^{j((2\omega_3 + \omega_1)t - (2k_3 + k_1)z)} \\
& + \frac{3}{4} \underline{E}_3^2 \underline{E}_2 e^{j((2\omega_3 + \omega_2)t - (2k_3 + k_2)z)}
\end{aligned} \tag{1.107}$$

The different expressions in Eq. (1.106) can be associated with distinct third-order nonlinear processes, the abbreviations of which are indicated under the underbraces. A summary of third-order nonlinear processes is given in Table (1.1). These processes shall be investigated in more detail in the following sections. Note that the individual frequency components of Eq. (1.106) exhibit again a space and time dependence that corresponds to that of a plane wave. The nonlinear polarization can hence be written as

$$P_{\text{NL}}(z, t) = \frac{1}{2} \left(\sum_l \underline{P}_{\text{NL}}(z, t, \omega_l) \exp(j(\omega_l t - k_{p,l} z)) + \text{c.c.} \right), \tag{1.108}$$

By comparing Eqs. (1.106) and (1.108), we can identify the complex amplitude of the nonlinear polarization $\underline{P}_{\text{NL}}(z, t, \omega_l)$ that is associated with a certain third-order nonlinear process.

Third-harmonic generation (THG)

The third harmonic of a monochromatic wave at frequency ω_1 oscillates at $\omega_p = 3\omega_1$ and features a wave vector $k_p = 3k_1$. The nonlinear polarization leading to this process is given by

$$\underline{P}_{\text{THG}}(z, t, 3\omega_1) = \frac{1}{4} \epsilon_0 \chi^{(3)} \underline{E}^3(z, t, \omega_1) \tag{1.109}$$

The energy-level diagram of third-harmonic generation is shown in Fig. 1.10 (a). In THG, three photons interact to generate a new photon with three times the energy.

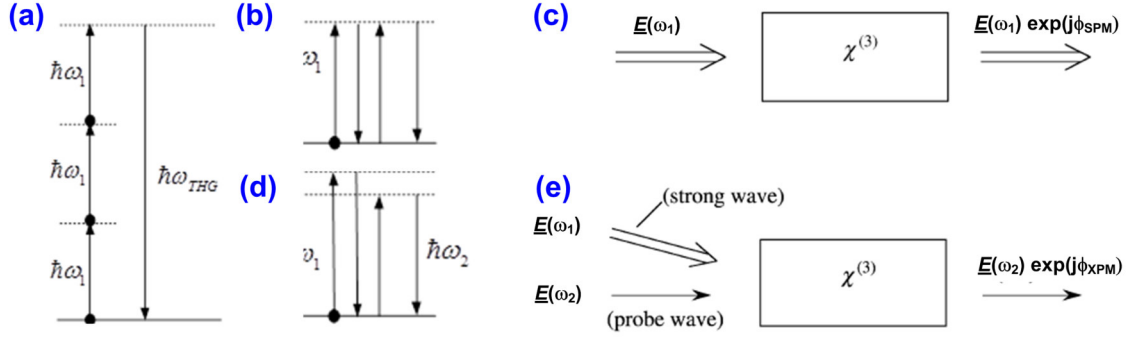


Figure 1.10: Third-order nonlinear processes. (a) Energy-level description of third-harmonic generation (THG): Three photons interact and generate a new photon having three times the energy. (b) Energy-level description and (c) interaction scheme of self-phase modulation (SPM): The presence of a strong wave leads to an increase in refractive index and hence to a negative nonlinear phase shift $\phi_{\text{SPM}} < 0$ that the wave imposes on itself. (d) Energy-level description and (e) interaction scheme of cross-phase modulation (XPM): A strong wave at frequency ω_1 imposes a nonlinear phase shift $\phi_{\text{XPM}} < 0$ on a co-propagating wave at frequency ω_2 . Note that for a given intensity of the strong wave, the phase shift for XPM is twice as high as the phase shift for SPM, $\phi_{\text{XPM}} = 2\phi_{\text{SPM}}$. (Figures adapted from [9]).

Self-phase modulation (SPM)

Self-phase modulation (SPM) describes a third-order nonlinear optical process by which the field of the incident wave modulates its own phase. The nonlinear polarization of SPM oscillates at the same frequency $\omega_p = \omega_1$ as the incident wave and is given by

$$\underline{P}_{\text{SPM}}(z, t, \omega_1) = \frac{3}{4} \epsilon_0 \chi^{(3)} |\underline{E}(z, t, \omega_1)|^2 \underline{E}(z, t, \omega_1). \quad (1.110)$$

Inserting Eq. (1.110) into Eq. (1.99), omitting the primes, and assuming a real-value third-order susceptibility $\chi^{(3)} \in \mathbb{R}$, we find that the change of the complex electric field amplitude $\partial \underline{E}(z, t, \omega_1) / \partial z$ (left-hand side) features a phase shift of $-\pi/2$ compared to the electric field $\underline{E}(z, t, \omega_1)$. As a consequence, the superposition of the nonlinear and linear polarization at frequency ω_1 results in a phase shift that can be represented by an intensity-dependent refractive index, see Section 1.5.3 for a more detailed description. The energy-level diagram and interaction scheme of SPM is depicted in Fig. 1.10 (b) and (c).

Cross-phase modulation (XPM)

In cross-phase modulation (XPM), the presence of a strong wave oscillating at frequency ω_1 imposes a phase onto a second wave, oscillating at ω_2 . The nonlinear polarization of XPM oscillates at the same frequency $\omega_p = \omega_2$ as the modulated wave and is given by

$$\underline{P}_{\text{XPM}}(z, t, \omega_2) = \frac{6}{4} \epsilon_0 \chi^{(3)} |\underline{E}(z, t, \omega_1)|^2 \underline{E}(z, t, \omega_2). \quad (1.111)$$

Also here, the superposition of the nonlinear and the linear polarization at frequency ω_1 results in a phase shift that can again be represented by an intensity-dependent refractive index. Note that for a given intensity of the strong wave at frequency ω_1 , the phase shift for XPM (multiplier 6/4) is twice as high as the phase shift for SPM (multiplier 3/4). The energy-level diagram and the interaction scheme of XPM are shown in Fig. 1.10 (d) and (e). Note that for SPM and XPM, the phase factor $e^{j(k_p, l - k_l)z'}$ on the right-hand side of Eq. (1.99) vanishes, i.e., these processes are

intrinsically phase-matched. All other processes rely on dedicated phase matching techniques for efficient nonlinear interaction.

Four-wave mixing (FWM)

In four-wave mixing (FWM), new frequency components are generated by third-order nonlinear interaction of two or three waves. In the case of non-degenerate four-wave mixing, three waves oscillating at frequencies ω_1 , ω_2 , and ω_3 interact and generate a fourth wave at frequency $\omega_p = \omega_1 + \omega_2 + \omega_3$ or $\omega_p = \omega_1 + \omega_2 - \omega_3$. Non-degenerate four-wave mixing with frequencies $(\omega_1, \omega_2, \omega_3)$ is also referred to as third-order sum frequency generation. In theory, both frequency components can be generated simultaneously, but phase matching is usually fulfilled for only one of these processes in practice. For non-degenerate FWM, the nonlinear polarization is given by

$$\underline{P}_{\text{FWM}}(z, t, \omega_p = \omega_1 + \omega_2 + \omega_3) = \frac{6}{4} \epsilon_0 \chi^{(3)} \underline{E}(z, t, \omega_1) \underline{E}(z, t, \omega_2) \underline{E}(z, t, \omega_3). \quad (1.112)$$

$$\underline{P}_{\text{FWM}}(z, t, \omega_p = \omega_1 + \omega_2 - \omega_3) = \frac{6}{4} \epsilon_0 \chi^{(3)} \underline{E}(z, t, \omega_1) \underline{E}(z, t, \omega_2) \underline{E}^*(z, t, \omega_3) \quad (1.113)$$

In the case of degenerate four-wave mixing, two of the three frequencies are identical, and the degeneracy factor is reduced by a factor of 2,

$$\underline{P}_{\text{FWM}}(z, t, \omega_p = 2\omega_1 + \omega_2) = \frac{3}{4} \epsilon_0 \chi^{(3)} \underline{E}^2(z, t, \omega_1) \underline{E}(z, t, \omega_2). \quad (1.114)$$

$$\underline{P}_{\text{FWM}}(z, t, \omega_p = 2\omega_1 - \omega_2) = \frac{3}{4} \epsilon_0 \chi^{(3)} \underline{E}^2(z, t, \omega_1) \underline{E}^*(z, t, \omega_2) \quad (1.115)$$

The interaction schemes and energy-level diagrams of degenerate and non-degenerate FWM is shown in Fig. (1.11).

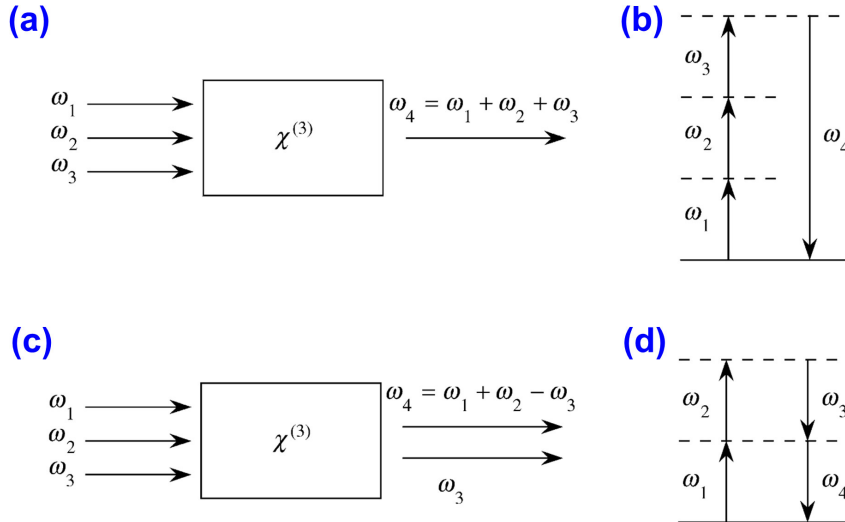


Figure 1.11: Interaction schemes and energy-level descriptions of non-degenerate third-order nonlinear interactions (“four-wave mixing”). (a) Interaction scheme and (b) energy-level description of four-wave mixing that generates one photon, also referred to as third-order sum frequency generation. (c) Interaction scheme and (d) energy-level description of non-degenerate four-wave mixing that generates two photons. For degenerate four-wave mixing, at least two of the involved frequency components are identical (Figure adapted from [9]).

1.5.3 Intensity-dependent refractive index and Kerr effect

For the case of a single wave of frequency ω_1 , only third-harmonic generation (THG) and self-phase modulation (SPM) remain as third-order nonlinear effects. Inserting Eqs. (1.109) and (1.110) in Eq. (1.99), we obtain two partial differential equations describing the evolution of the field amplitudes at ω_1 and $3\omega_1$,

$$\frac{\partial \underline{E}(z, t, 3\omega_1)}{\partial z} = -j \frac{3\omega_1 \chi^{(3)}}{8cn(3\omega_1)} \underline{E}^3(z, t, \omega_1) e^{-j(3k(\omega_1) - k(3\omega_1))z}, \quad (1.116)$$

$$\frac{\partial \underline{E}(z, t, \omega_1)}{\partial z} = -j \frac{3\omega_1 \chi^{(3)}}{8cn(\omega_1)} |\underline{E}(z, t, \omega_1)|^2 \underline{E}(z, t, \omega_1), \quad (1.117)$$

where the frequency-dependent propagation constant is given by $k(\omega) = \frac{\omega}{c}n(\omega)$. Note that the refractive indices $n(\omega_1)$ and $n(3\omega_1)$ usually differ strongly due to unavoidable material dispersion, see Section 1.2.3. For this reason, $3k(\omega_1) - k(3\omega_1) \neq 0$, i.e., THG is generally impaired by phase mismatch unless special phase matching techniques are used. Hence, for many cases of practical interest, only SPM remains as the dominant third-order nonlinear effect. According to Eq. (1.117) SPM causes a negative phase shift that is proportional to the square of the field magnitude, i.e., proportional to the intensity. This corresponds to an intensity-dependent increase Δn of the refractive index. To understand this, let us use Eqs. (1.85) – (1.87) and (1.110) to find an expression for the complex time-domain amplitude of the electric displacement $\underline{D}(z, t, \omega_1)$ for a material that features only linear refraction and third-order nonlinearities,

$$\underline{D}(z, t, \omega_1) = \epsilon_0 \left(1 + \chi^{(1)} + \frac{3}{4}\chi^{(3)} |\underline{E}(z, t, \omega_1)|^2 \right) \underline{E}(z, t, \omega_1) \quad (1.118)$$

From the right-hand side of Eq. (1.118), we can derive the relation $(n_0 + \Delta n)^2 = 1 + \chi^{(1)} + \frac{3}{4}\chi^{(3)} |\underline{E}(z, t, \omega_1)|^2$, where n_0 denotes the linear refractive index of the device. For $\Delta n \ll n_0$, we find

$$\Delta n = \frac{3}{8n_0} \chi^{(3)} |\underline{E}(z, t, \omega_1)|^2 \quad (1.119)$$

For a plane wave propagating along the z -direction, the intensity is related to the electric field by

$$I(z, t, \omega_1) = n_0 \frac{|\underline{E}(z, t, \omega_1)|^2}{2Z_0}, \quad (1.120)$$

where $Z_0 = \sqrt{(\mu_0/\epsilon_0)} \approx 376.73 \Omega$ denotes the free-space wave impedance. We can hence introduce the intensity-dependent refractive index $n = n_0 + \Delta n$,

$$n(z, t, \omega_1) = n_0(\omega_1) + n_2 I(z, t, \omega_1), \quad (1.121)$$

where the so-called Kerr coefficient n_2 is given by

$$n_2 = \frac{3Z_0}{4n_0^2} \chi^{(3)}. \quad (1.122)$$

For a superposition of two waves oscillating at frequencies ω_1 and ω_2 , the refractive index seen by wave 2 will also be influenced by cross-phase modulation (XPM) due to wave 1. Note that XPM has twice the degeneracy factor of SPM. Equation (1.121) can then be rewritten as

$$n(z, t, \omega_2) = n_0(\omega_2) + n_2 (I(z, t, \omega_2) + 2I(z, t, \omega_1)). \quad (1.123)$$

A table with third-order nonlinear optical coefficients of various materials is also given in Fig. 1.12. Note that there are different conventions on how to define complex electromagnetic field amplitudes, and hence the definition of the nonlinear optical susceptibility $\chi^{(3)}$ and the Kerr coefficient n_2 differ. The table in Fig. 1.12 is based on the definition according to Eq. (1.84) and is consistent with the definition³ used in Boyd's textbook [9].

³Note that the definition of complex electromagnetic field amplitudes used by Boyd (Eq. 1.2.1 in [9]) differs by a factor of 2 from the convention we use in this lecture, Eq. (1.72). As a consequence, the corresponding relationships

Material	n_0	$\chi^{(3)}$ (m ² /V ²)	n_2 (cm ² /W)
<i>Crystals</i>			
Al ₂ O ₃	1.8	3.1×10^{-22}	2.9×10^{-16}
CdS	2.34	9.8×10^{-20}	5.1×10^{-14}
Diamond	2.42	2.5×10^{-21}	1.3×10^{-15}
GaAs	3.47	1.4×10^{-18}	3.3×10^{-13}
Ge	4.0	5.6×10^{-19}	9.9×10^{-14}
LiF	1.4	6.2×10^{-23}	9.0×10^{-17}
Si	3.4	2.8×10^{-18}	2.7×10^{-14}
TiO ₂	2.48	2.1×10^{-20}	9.4×10^{-15}
ZnSe	2.7	6.2×10^{-20}	3.0×10^{-14}
<i>Glasses</i>			
Fused silica	1.47	2.5×10^{-22}	3.2×10^{-16}
As ₂ S ₃ glass	2.4	4.1×10^{-19}	2.0×10^{-13}
BK-7	1.52	2.8×10^{-22}	3.4×10^{-16}
BSC	1.51	5.0×10^{-22}	6.4×10^{-16}
Pb Bi gallate	2.3	2.2×10^{-20}	1.3×10^{-14}
SF-55	1.73	2.1×10^{-21}	2.0×10^{-15}
SF-59	1.953	4.3×10^{-21}	3.3×10^{-15}
<i>Nanoparticles</i>			
CdSe in glass	1.5	1.4×10^{-20}	1.8×10^{-14}
CS 3-68 glass	1.5	1.8×10^{-16}	2.3×10^{-10}
Gold in glass	1.5	2.1×10^{-16}	2.6×10^{-10}

Material	n_0	$\chi^{(3)}$ (m ² /V ²)	n_2 (cm ² /W)
<i>Polymers</i>			
Polydiacetylenes			
PTS		8.4×10^{-18}	3.0×10^{-12}
PTS		-5.6×10^{-16}	-2.0×10^{-10}
9BCM U			2.7×10^{-18}
4BCM U	1.56	-1.3×10^{-19}	-1.5×10^{-13}
<i>Liquids</i>			
Acetone	1.36	1.5×10^{-21}	2.4×10^{-15}
Benzene	1.5	9.5×10^{-22}	1.2×10^{-15}
Carbon disulfide	1.63	3.1×10^{-20}	3.2×10^{-14}
CCl ₄	1.45	1.1×10^{-21}	1.5×10^{-15}
Diiodomethane	1.69	1.5×10^{-20}	1.5×10^{-14}
Ethanol	1.36	5.0×10^{-22}	7.7×10^{-16}
Methanol	1.33	4.3×10^{-22}	6.9×10^{-16}
Nitrobenzene	1.56	5.7×10^{-20}	6.7×10^{-14}
Water	1.33	2.5×10^{-22}	4.1×10^{-16}
<i>Other materials</i>			
Air	1.0003	1.7×10^{-25}	5.0×10^{-19}
Ag		2.8×10^{-19}	
Au		7.6×10^{-19}	

Figure 1.12: Third-order nonlinear coefficients of various materials. (Figure adapted from [9]). The numbers are based on the definition of the nonlinear optical susceptibility $\chi^{(3)}$ according to Eq. (1.84) and are consistent with the definition used in Boyd’s textbook [9]. The differences in the relationships for the complex amplitude of the third-order nonlinear polarization, Eq. (2.22) and Eq. (1.3.20) in Boyd, are due to different definitions of the underlying complex field amplitudes³. The numbers provided by [9] can be safely used with the relations given in this lecture notes.

1.6 Parametric versus nonparametric processes

The processes described so far in this section are examples of so-called parametric processes. The origin of the terminology is obscure, but the term “parametric process” refers to interactions of light with matter in which the quantum state of the material remains unchanged. That means that there can be no transfer of energy, momentum, or angular momentum between the optical field and the material. As a consequence, momentum and energy conservation have to be fulfilled for the initial and the final photon population in parametric processes,

$$\sum_i \omega_i = \sum_f \omega_f, \quad (1.124)$$

$$\sum_i k_i = \sum_f k_f, \quad (1.125)$$

where \sum_i (\sum_f) denotes the sum over all photons in the initial (final) state. In a parametric process, the quantum system can hence be removed from the ground state only for those brief intervals of time when it resides in a so-called virtual energy level. According to Heisenberg’s uncertainty principle, a quantum system can reside in a virtual energy level for a time interval of the order of $\Delta t = \hbar/\Delta E$, where ΔE is the energy difference between the virtual level and the nearest real level. Virtual levels are depicted as dotted lines in the energy-level diagrams for

between the complex amplitudes of the third-order nonlinear polarization and of the electric field take different forms when comparing Eq. (2.22) of the lecture notes to Eq. (1.3.20) in Boyd, even though they rely on the very same definition of the nonlinear optical susceptibility $\chi^{(3)}$, according to Eq. (1.84) in this lecture notes a Eq. (1.3.20) in [9]. The numbers provided by [9] and listed in Fig. 1.12 can hence be safely used with the relations given in this lecture notes. When using numbers from other sources, it is important to check for the consistency of the underlying definitions of electromagnetic field quantities.

second- and third-order nonlinearities, Figs. 1.7, 1.8, 1.9, 1.10, and 1.11. Since the “lifetime” Δt of the virtual state is small, parametric processes are among the fastest interaction mechanisms between light and matter.

Conversely, processes that do involve the transfer of a quantum system from one real level to another are known as non-parametric processes. Usually the material relaxes to its initial state, but the process is linked with a time constant that is much larger than for parametric processes. In non-parametric processes photon energy is not constant. The energy transfer between matter and light can happen via phonons (oscillations of the material’s lattice) or via electronic transitions. Non-parametric processes are described by a complex susceptibility, see Section 2. As an example of a non-parametric process, let us consider two-photon absorption.

Two-photon absorption

Two-photon absorption is associated with the imaginary part of the complex third-order nonlinear susceptibility $\underline{\chi}^{(3)}$. Note that in the previous sections, we have assumed a purely real third-order nonlinear susceptibility $\chi^{(3)}$, Eq. (1.75), to enable a simplified model of an instantaneous response in the time domain and hence a Taylor expansion of the relationship between the electric field and the polarization, Eq. (1.84). The formal definition of the complex electric susceptibility will be given in the next section along with its tensor properties. For now, let us consider the simplified case of third-order nonlinear susceptibility, which is represented by a complex scalar $\underline{\chi}^{(3)}$. We consider the interaction of two waves oscillating at frequencies ω_1 and ω_2 . Inserting Eqs. (1.110) and (1.111) in Eq. (1.99), we can state two relations that govern the influence of the waves 1 and 2 on wave 1,

$$\frac{\partial \underline{E}(z, t, \omega_1)}{\partial z} = -j \frac{3\omega_1}{8cn} \underline{\chi}^{(3)} |\underline{E}(z, t, \omega_1)|^2 \underline{E}(z, t, \omega_1), \quad (1.126)$$

$$\frac{\partial \underline{E}(z, t, \omega_1)}{\partial z} = -j \frac{3\omega_1}{4cn} \underline{\chi}^{(3)} |\underline{E}(z, t, \omega_2)|^2 \underline{E}(z, t, \omega_1). \quad (1.127)$$

Note that t corresponds to a retarded time frame even though the primes have been omitted for the sake of readability. The real part of the nonlinear susceptibility $\underline{\chi}^{(3)}$ causes a change $\partial \underline{E}(z, t, \omega_1) / \partial z$ that is perpendicular to the phasor of the complex amplitude $\underline{E}(z, t, \omega_1)$ in the complex plane and oriented to the negative azimuthal direction. This corresponds to an intensity-dependent phase shift and is therefore referred to as self-phase modulation and cross-phase modulation. Likewise, the imaginary part of $\underline{\chi}^{(3)}$ changes the magnitude of $\underline{E}(z, t, \omega_1)$ and hence corresponds to intensity-dependent loss or gain. In most practical cases, the imaginary part of $\underline{\chi}^{(3)}$ is negative, and Eq. (1.126) leads to a decrease of the optical amplitude $\underline{E}(z, t, \omega_1)$. This corresponds to the case of two-photon absorption (TPA), where two photons of the same frequency are absorbed simultaneously, thereby causing a transition of the absorbing quantum system between two energy states that are separated by twice the photon energy, see Fig. 1.13 (a). Similarly, for a negative imaginary part of $\underline{\chi}^{(3)}$, Eq. (1.127) describes a process, in which two photons at frequencies ω_1 and ω_2 are absorbed simultaneously, leading to a transition between quantum states that are separated by the energy $\hbar\omega_1 + \hbar\omega_2$, see Fig. 1.13 (b). This is also referred to as cross-two-photon absorption (XTPA). Similarly to the cases of cross-phase modulation (XPM) and self-phase modulation (SPM), XTPA, Eq. 1.127, has an additional degeneracy factor of 2 compared to regular TPA, Eq. 1.126. In analogy to negative imaginary parts of $\underline{\chi}^{(3)}$ leading to (X)TPA, positive imaginary parts of $\underline{\chi}^{(3)}$ can lead to two-photon emission (TPE). However, evidence of TPE has so far only been observed under specific experimental conditions [15].

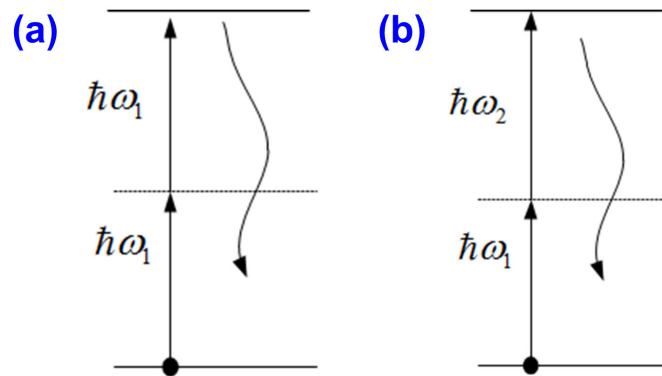


Figure 1.13: Energy-level diagrams of two-photon absorption (TPA). (a) Regular TPA, where two photons of the same frequency are absorbed simultaneously, thereby causing a transition of the absorbing system between two energy states that are separated by twice the photon energy. Note that the energy states here are depicted by solid lines and hence represent real energy eigenstates of the absorbing systems. In contrast to that, the dashed energy levels used in Figs. 1.7, 1.8, 1.9, 1.10, and 1.11 represent so-called virtual energy levels, in which the quantum system can reside for very short time intervals only, as postulated by Heisenberg's uncertainty principle. (b) Cross two-photon absorption (XTPA), in which two photons at frequencies ω_1 and ω_2 are absorbed simultaneously, leading to an energetic transition between quantum states that are separated by $\hbar\omega_1 + \hbar\omega_2$. After excitation by TPA or XTPA, the quantum system usually relaxes to its initial state by a non-radiative transition, thereby dissipating the absorbed energy. This is illustrated by the wiggled array.

Chapter 2

The nonlinear optical susceptibility

In the previous chapter, we have considered optical nonlinearities for linearly polarized plane waves that can be represented by a single scalar field quantity, see Eqs. (1.81) and (1.82). In addition, we have assumed that the polarization reacts instantaneously to the electric field and hence treated optical nonlinearities by a Taylor expansion in the time domain with the nonlinear optical susceptibility as expansion coefficients, see Eq. (1.84). We will now extend this model, taking into account both the vectorial nature of the electric field $\mathbf{E}(\mathbf{r}, t)$ and the polarization $\mathbf{P}(\mathbf{r}, t)$ as well as the non-instantaneous time-domain response of the material.

2.1 Formal definition of the nonlinear optical susceptibility tensor

2.1.1 Time-domain representation

Assuming a dielectric material which is local in space, the polarization $\mathbf{P}(\mathbf{r}, t)$ at time t depends only on the history of the local value of the electric field $\mathbf{E}(\mathbf{r}, \tau)$ for $\tau < t$. To take into account the 'memory' of the nonlinear material, the time-domain multiplications and ascending powers of E are replaced by a series of convolutions. This results in a so-called Volterra series. In general, Volterra series represent an extension of Taylor series for the case of non-linear relationships that are affected by memory effects. In Volterra series, the output of the nonlinear system depends on the input to the system at all other times, which is mathematically expressed by a series of convolutions rather than simple multiplications. As an example, a nonlinear relationship between scalar quantities $P(t)$ and $E(t)$ can be expressed by a Volterra series of the form

$$P(t) = \epsilon_0 \left(\int_{\tau_1} \chi^{(1)}(\tau_1) E(t - \tau_1) d\tau_1 + \iint_{\tau_1, \tau_2} \chi^{(2)}(\tau_1, \tau_2) E(t - \tau_1) E(t - \tau_2) d\tau_1 d\tau_2 + \iiint_{\tau_1, \tau_2, \tau_3} \chi^{(3)}(\tau_1, \tau_2, \tau_3) E(t - \tau_1) E(t - \tau_2) E(t - \tau_3) d\tau_1 d\tau_2 d\tau_3 + \dots \right), \quad (2.1)$$

where $\chi^{(n)}(\tau_1, \tau_2, \dots, \tau_n)$ is called the n -th order Volterra kernel and can be regarded as a higher-order impulse response of the system. The space argument \mathbf{r} has been omitted in Eq. (2.1) for the sake of readability.

Additionally, we have to take into account the vectorial nature of both the electric field $\mathbf{E}(\mathbf{r}, t)$ and the polarization $\mathbf{P}(\mathbf{r}, t)$. Let us consider a single component of the n -th order nonlinear polarization $P_{q_0}^{(n)}(t)$, where $q_0 \in \{x, y, z\}$ denotes the vector component under consideration. In the

most general case, this vector component is influenced by the history of all n -th order products that can be constructed from any set of n electric field components $E_{q_1}(t - \tau_1), E_{q_2}(t - \tau_2), \dots, E_{q_n}(t - \tau_n)$, where $q_1, q_2, \dots, q_n \in \{x, y, z\}$ denote the various vector components under consideration. This can be described by replacing the scalar n -th order Volterra kernel in Eq. (2.1) by a tensor $\chi_{q_0:q_1q_2\dots q_n}^{(n)}(\tau_1, \tau_2, \dots, \tau_n)$ of rank $n + 1$, the elements of which represent the n -th order impulse response to the product $E_{q_1}(t - \tau_1) E_{q_2}(t - \tau_2) \dots E_{q_n}(t - \tau_n)$,

$$P_q^{(n)}(t) = \epsilon_0 \sum_{q_1, \dots, q_n} \int_{-\infty}^{+\infty} \dots \int_{-\infty}^{+\infty} \chi_{q_0:q_1\dots q_n}^{(n)}(\tau_1, \dots, \tau_n) E_{q_1}(t - \tau_1) \dots E_{q_n}(t - \tau_n) d\tau_1 \dots d\tau_n. \quad (2.2)$$

The sum on the right-hand side of Eq. (2.2) extends over all ordered n -tuples $(q_1, q_2 \dots q_n)$ that can be constructed from the involved electric fields. For the simple case of linear polarization, the tensor $\chi_{q_0:q_1}^{(1)}$ is of rank 2 and can be written as a matrix.

Note that in some cases, the sum \sum_{q_1, \dots, q_n} is not explicitly stated on the right-hand side of Eq. (2.2) for the sake of notation brevity. In this case, the relationship has to be interpreted in the sense of the Einstein summation convention or ‘‘Einstein notation’’, that implies summation over all index variables that appear twice in a single term. Since the polarization response of the medium is causal, the tensor component $\chi_{q_0:q_1q_2\dots q_n}^{(n)}(\tau_1, \tau_2 \dots, \tau_n)$ vanishes if any of the time arguments $(\tau_1, \tau_2 \dots, \tau_n)$ becomes negative.

2.1.2 Short-form tensor notation

To express the nonlinear relationship between the vectorial quantities $\mathbf{E}(t)$ and $\mathbf{P}(t)$, we hence have to go back to the level of individual vector components, which are linked by a scalar relationship according to Eq. (2.2). In some cases, however, it is useful to state the fully vectorial relationship in a single expression. To this end, we use a short-form tensor notation that relates vectorial quantities and implies summation over all involved vector components without explicit notation. Let us first consider the simple case of second order nonlinearities,

$$P_q^{(2)}(t) = \epsilon_0 \sum_{r,s} \iint_{\tau_1, \tau_2} \chi_{q:r,s}^{(2)}(\tau_1, \tau_2) E_r(t - \tau_1) E_s(t - \tau_2) d\tau_1 d\tau_2, \quad (2.3)$$

where $q, r, s \in \{x, y, z\}$. In short-form notation, this relation is written as

$$\mathbf{P}^{(2)}(t) = \epsilon_0 \iint_{\tau_1, \tau_2} \chi^{(2)}(\tau_1, \tau_2) : \mathbf{E}(t - \tau_1) \mathbf{E}(t - \tau_2) d\tau_1 d\tau_2, \quad (2.4)$$

where the double multiplication sign ‘‘:’’ comprises the component-by-component multiplication and summation according to Eq. (2.3), i.e.,

$$\chi^{(2)} : \mathbf{E}\mathbf{E} = \sum_{q,r,s} \mathbf{e}_q \chi_{q:r,s}^{(2)} E_r E_s, \quad (2.5)$$

where \mathbf{e}_q denotes the unit vector along the q -direction. This notation can be extended to higher-order nonlinear susceptibilities,

$$\chi^{(n)} : \mathbf{E}(\tau_1) \mathbf{E}(\tau_2) \dots \mathbf{E}(\tau_n) = \sum_{q_0, q_1, \dots, q_n} \mathbf{e}_{q_0} \chi_{q_0:q_1q_2\dots q_n}^{(n)} E_{q_1}(\tau_1) E_{q_2}(\tau_2) \dots E_{q_n}(\tau_n), \quad (2.6)$$

where $q_0, q_1, \dots, q_n \in \{x, y, z\}$, and where the triple multiplication sign ‘‘:’’ denotes the component-by-component multiplication and summation according to Eq. (2.2).

2.1.3 Frequency-domain representation

The time-domain relationship according to Eq. (2.2) can be transformed to the frequency domain. For simplicity, let us first consider the simplified case of second-order nonlinear polarization,

$$P_q^{(2)}(t) = \epsilon_0 \sum_{r,s} \iint_{\tau_1, \tau_2} \chi_{q;r,s}^{(2)}(\tau_1, \tau_2) E_r(t - \tau_1) E_s(t - \tau_2) d\tau_1 d\tau_2, \quad (2.7)$$

where $q, r, s \in \{x, y, z\}$. By using Eqs. (1.12) and (1.13), we can derive the corresponding frequency-domain relationship,

$$\tilde{P}_q^{(2)}(\omega) = \frac{1}{2\pi} \epsilon_0 \sum_{r,s} \int_{\omega_1} \tilde{\chi}_{q;r,s}^{(2)}(\omega_1, \omega - \omega_1) \tilde{E}_r(\omega_1) \tilde{E}_s(\omega - \omega_1) d\omega_1 \quad (2.8)$$

where the frequency-dependent nonlinear optical susceptibility $\tilde{\chi}_{q;r,s}^{(2)}(\omega_1, \omega_2)$ is given by the two-stage Fourier transform of the corresponding time-domain Volterra kernel $\chi_{q;r,s}^{(2)}(\tau_1, \tau_2)$,

$$\tilde{\chi}_{q;r,s}^{(2)}(\omega_1, \omega_2) = \iint_{\tau_1, \tau_2} \chi_{q;r,s}^{(2)}(\tau_1, \tau_2) e^{-j\omega_1\tau_1} e^{-j\omega_2\tau_2} d\tau_1 d\tau_2 \quad (2.9)$$

The basic meaning of Eq. (2.8) can be stated in words: The nonlinear polarization $\tilde{P}_q^{(2)}(\omega)$ at frequency ω is given by an integral which extends over all combined contributions $\tilde{\chi}_{q;r,s}^{(2)}(\omega_1, \omega - \omega_1) \tilde{E}_r(\omega_1) \tilde{E}_s(\omega - \omega_1)$ from components at frequencies ω_1 and $\omega - \omega_1$, which sum up to ω . Note that ω and ω_1 can have both positive and negative signs and that Eq. (2.8) can hence describe the full range of second-order nonlinear processes such as sum-frequency generation, difference-frequency generation, second-harmonic generation and optical rectification.

Eq. (2.8) can be extended to the general case of n -th order nonlinear polarization. The polarization at frequency ω is then given by an $(n-1)$ -fold integral that comprises contributions from components at all frequencies which sum up to ω , i.e., from frequency components at $\omega_1, \omega_2, \dots, \omega_{n-1}$ and $\omega - \sum_{m=1}^{n-1} \omega_m$,

$$\begin{aligned} \tilde{P}_{q_0}^{(n)}(\omega) &= \frac{\epsilon_0}{(2\pi)^{n-1}} \sum_{q_1, \dots, q_n} \int_{-\infty}^{+\infty} \dots \int_{-\infty}^{+\infty} \tilde{\chi}_{q_0:q_1, \dots, q_n}^{(n)} \left(\omega : \omega_1, \dots, \omega_{n-1}, \omega - \sum_{m=1}^{n-1} \omega_m \right) \\ &\quad \times \tilde{E}_{q_1}(\omega_1) \dots \tilde{E}_{q_{n-1}}(\omega_{n-1}) \tilde{E}_{q_n} \left(\omega - \sum_{m=1}^{n-1} \omega_m \right) d\omega_1 \dots d\omega_{n-1}. \end{aligned} \quad (2.10)$$

The components $\tilde{\chi}_{q_0:q_1 q_2 \dots q_n}^{(n)}$ of the n -th order susceptibility tensor $\tilde{\chi}^{(n)}$ are given by the n -stage Fourier transform of the corresponding time-domain Volterra kernel,

$$\tilde{\chi}_{q_0:q_1 \dots q_n}^{(n)} \left(\sum_{m=1}^n \omega_m : \omega_1, \dots, \omega_n \right) = \int_{-\infty}^{+\infty} \dots \int_{-\infty}^{+\infty} \chi_{q_0:q_1, \dots, q_n}^{(n)}(\tau_1, \dots, \tau_n) e^{-j\omega_1\tau_1} \dots e^{-j\omega_n\tau_n} d\tau_1 \dots d\tau_n. \quad (2.11)$$

2.1.4 Representation by complex time-domain amplitudes for positive nonzero frequencies

The frequency-domain representation of the nonlinear optical susceptibility according to Eqs. (2.8) and (2.10) involves evaluation of (multiple) convolution integrals in the Fourier domain. This is

a rather complex operation, which complicates the use of the frequency-domain formalism in the general case. In addition, for monochromatic waves, the spectra $\tilde{E}_{q_n}(\omega_n)$ contain Dirac delta functions, for which products and convolutions are not defined. For this reason, complex time-domain amplitudes or slowly varying envelope approximations (SVEA) are often used in nonlinear optics rather than Fourier transforms.

To illustrate the use of complex time-domain amplitudes, let us consider second-order nonlinearity in short-form notation,

$$\mathbf{P}^{(2)}(t) = \epsilon_0 \iint_{\tau_1, \tau_2} \chi^{(2)}(\tau_1, \tau_2) : \mathbf{E}(t - \tau_1) \mathbf{E}(t - \tau_2) d\tau_1 d\tau_2 \quad (2.12)$$

where the electric field is given by a superposition of monochromatic waves at positive nonzero frequencies ω_l that are represented by their complex time-domain amplitudes $\underline{\mathbf{E}}(\omega_l)$,

$$\mathbf{E}(t) = \frac{1}{2} \left(\sum_{m=1}^M \underline{\mathbf{E}}(\omega_m) e^{j\omega_m t} + \text{c.c.} \right) \quad (2.13)$$

In this relation, the frequencies ω_m , $m = 1 \dots M$, are non-negative. Negative-frequency components are contained by the somewhat sloppy “+cc” expression. It is therefore useful to define the relationships between complex time-domain amplitudes in a slightly more rigorous way by including negative-frequency terms explicitly into the sum on the right-hand side of Eq. (2.13). For simplicity, we associate negative frequencies with negative integer subscripts m using the convention

$$\omega_{-m} = -\omega_m, \quad (2.14)$$

$$\omega_0 = 0 \quad (2.15)$$

$$\underline{\mathbf{E}}(\omega_{-m}) = \underline{\mathbf{E}}^*(\omega_m). \quad (2.16)$$

and extend the index range of the sum to $m = -M \dots M$,

$$\mathbf{E}(t) = \frac{1}{2} \sum_{m=-M}^M \underline{\mathbf{E}}(\omega_m) e^{j\omega_m t}. \quad (2.17)$$

Special attention has to be devoted to DC fields, which are represented by subscript $m = 0$ and frequency $\omega_0 = 0$. This will be discussed in more details on p. 33 at the end of this section. For now, let us assume that $\underline{\mathbf{E}}(\omega_0) = 0$, i.e., the signals under consideration do not feature any DC part.

Inserting Eq. (2.17) in Eq. (2.12), we can express the second-order nonlinear polarization as a superposition of monochromatic waves that oscillate at all possible sum (and difference) frequencies $\omega_l + \omega_m$, where $l, m = -M \dots M$ and $l, m \neq 0$,

$$\mathbf{P}^{(2)}(t) = \frac{1}{2} \epsilon_0 \sum_{l, m=-M}^M \chi^{(2)}(\omega_\Sigma : \omega_l, \omega_m) : \underline{\mathbf{E}}(\omega_l) \underline{\mathbf{E}}(\omega_m) e^{j(\omega_l + \omega_m)t}, \quad (2.18)$$

where we have written the nonlinear optical susceptibility as a function of three arguments. The first argument is redundant and corresponds to the sum of the other two, $\omega_\Sigma = \omega_l + \omega_m$. It is only introduced to explicitly specify the sum frequency ω_Σ that is generated by nonlinear interaction of monochromatic waves at ω_l and ω_m . The frequency-dependent nonlinear optical susceptibility $\chi^{(2)}(\omega_\Sigma : \omega_l, \omega_m)$ is again given by the two-stage Fourier transform of the corresponding time-domain Volterra kernel $\chi^{(2)}(\tau_1, \tau_2)$, see Eq. (2.9).

In analogy to Eq. (2.17), the second-order nonlinear polarization can be expressed by complex time-domain amplitudes $\underline{\mathbf{P}}^{(2)}(\omega_p)$ that are associated with the various sum frequencies $\omega_p = \omega_\Sigma$,

$$\mathbf{P}^{(2)}(t) = \frac{1}{2} \sum_{p=-M}^M \underline{\mathbf{P}}^{(2)}(\omega_p) e^{j\omega_p t}. \quad (2.19)$$

Comparing this relation to Eq. (2.18), we have to take into account that several expressions from the sum on the right-hand side of Eq. (2.18) can lead to the same sum frequency $\omega_p = \omega_l + \omega_m$, e.g., $\underline{\mathbf{E}}(\omega_l)\underline{\mathbf{E}}(\omega_m) \exp((\omega_l + \omega_m)t)$ and $\underline{\mathbf{E}}(\omega_m)\underline{\mathbf{E}}(\omega_l) \exp((\omega_m + \omega_l)t)$. To express the time-domain amplitudes $\underline{\mathbf{P}}^{(2)}(\omega_p)$ by the complex time-domain amplitudes of the electric fields, we have to sum up all contributions for which the sum frequency corresponds to ω_p ,

$$\underline{\mathbf{P}}^{(2)}(\omega_p) = \frac{1}{2}\epsilon_0 \sum_{\mathbb{S}(\omega_p)} \chi^{(2)}(\omega_p : \omega_l, \omega_m) : \underline{\mathbf{E}}(\omega_l)\underline{\mathbf{E}}(\omega_m), \quad (2.20)$$

where the summation on the right-hand side extends over the set $\mathbb{S}(\omega_p)$ of all pairs (l, m) which lead to the sum frequency $\omega_p = \omega_l + \omega_m$,

$$\mathbb{S}(\omega_p) = \{(l, m) | \omega_l + \omega_m = \omega_p\}. \quad (2.21)$$

This sum leads to distinct degeneracy factors for the various nonlinear optical processes, see Section 1.5.

This analysis can be extended to third-order nonlinearities, resulting in

$$\underline{\mathbf{P}}^{(3)}(\omega_p) = \frac{1}{4}\epsilon_0 \sum_{\mathbb{S}(\omega_p)} \chi^{(3)}(\omega_p : \omega_l, \omega_m, \omega_o) : \underline{\mathbf{E}}(\omega_l)\underline{\mathbf{E}}(\omega_m)\underline{\mathbf{E}}(\omega_o) \quad (2.22)$$

where

$$\mathbb{S}(\omega_p) = \{(l, m, n) | \omega_l + \omega_m + \omega_o = \omega_p\}. \quad (2.23)$$

For n -th order nonlinearities, the corresponding relations read

$$\underline{\mathbf{P}}^{(n)}(\omega_p) = \frac{1}{2^{n-1}}\epsilon_0 \sum_{\mathbb{S}(\omega_p)} \chi^{(n)}(\omega_p : \omega_{l_1}, \dots, \omega_{l_n}) : \underline{\mathbf{E}}(\omega_{l_1}) \dots \underline{\mathbf{E}}(\omega_{l_n}), \quad (2.24)$$

where

$$\mathbb{S}(\omega_p) = \{(l_1, \dots, l_n) | \omega_{l_1} + \dots + \omega_{l_n} = \omega_p\}. \quad (2.25)$$

Remark on zero frequencies and DC fields

As a representation of the electric field $\mathbf{E}(t)$ and the polarization $\mathbf{P}(t)$, we have chosen the relations

$$\mathbf{E}(t) = \frac{1}{2} \sum_{m=-M}^M \underline{\mathbf{E}}(\omega_m) e^{j\omega_m t}, \quad (2.26)$$

$$\mathbf{P}(t) = \frac{1}{2} \sum_{m=-M}^M \underline{\mathbf{P}}(\omega_m) e^{j\omega_m t}. \quad (2.27)$$

In these relations, DC fields are associated with frequency subscript $m = 0$, $\omega_0 = 0$, see explanation in the context of Eq. (2.17). As a matter of fact, $\underline{\mathbf{E}}(\omega_0 = 0)$ and $\underline{\mathbf{P}}(\omega_0 = 0)$ must be real numbers,

$$\omega_0 = 0, \quad (2.28)$$

$$\underline{\mathbf{E}}(\omega_0) \in \mathbb{R}. \quad (2.29)$$

Using this definition in conjunction with Eq. (2.26) would lead to the strange situation that a DC field with constant field strength $\mathbf{E}(t) = \text{const.}$ is associated with a zero-frequency time-domain

amplitude of $\underline{\mathbf{E}}(\omega_0 = 0) = 2\underline{\mathbf{E}}(t)$. To avoid this, the time-domain amplitudes at $\omega_0 = 0$ in the sums of Eqs. (2.26) and (2.27) are doubled by including a correction factor $(1 + \delta_{l,0})$ into the relations,

$$\underline{\mathbf{E}}(\mathbf{r}, t) = \frac{1}{2} \sum_{l=-N}^N (1 + \delta_{l,0}) \underline{\mathbf{E}}(\mathbf{r}, \omega_l) e^{j\omega_l t}, \quad (2.30)$$

$$\underline{\mathbf{P}}(\mathbf{r}, t) = \frac{1}{2} \sum_{l=-N}^N (1 + \delta_{l,0}) \underline{\mathbf{P}}(\mathbf{r}, \omega_l) e^{j\omega_l t}. \quad (2.31)$$

In these relations, $\delta_{l,0}$ denotes the Kronecker delta, $\delta_{l,0} = 1$ for $l = 0$ and $\delta_{l,0} = 0$ for $l \neq 0$. The correction factors for zero-frequency components show up in the time-domain amplitude $\underline{\mathbf{P}}^{(n)}(\omega_p)$ of the n -th order nonlinear polarization, which can then be written as

$$\underline{\mathbf{P}}^{(n)}(\omega_p) = \frac{1}{2^{n-1}} \epsilon_0 \sum_{\mathbb{S}(\omega_p)} \frac{(1 + \delta_{l_1,0}) \dots (1 + \delta_{l_n,0})}{1 + \delta_{p,0}} \underline{\chi}^{(n)}(\omega_p : \omega_{l_1}, \dots, \omega_{l_n}) : \underline{\mathbf{E}}(\omega_{l_1}) \dots \underline{\mathbf{E}}(\omega_{l_n}). \quad (2.32)$$

2.1.5 Examples for second and third-order nonlinearities

To understand the use of Eq. (2.32), let us consider a few examples for the cases of second- and third-order nonlinearities:

Sum-frequency generation (SFG): For SFG, we consider interaction of waves at frequencies ω_1 and ω_2 in a second-order nonlinear medium, thereby producing a third wave at frequency $\omega_3 = \omega_1 + \omega_2$. None of the involved frequencies is zero, and taking into account the distinct permutations (ω_1, ω_2) and (ω_2, ω_1) , we obtain the complex time-domain amplitude of the second-order nonlinear polarization at ω_3 ,

$$\underline{\mathbf{P}}^{(2)}(\omega_3) = \epsilon_0 \underline{\chi}^{(2)}(\omega_3 : \omega_1, \omega_2) : \underline{\mathbf{E}}(\omega_1) \underline{\mathbf{E}}(\omega_2). \quad (2.33)$$

Optical rectification (OR): For OR, we consider interaction of waves with frequency components ω_1 and $-\omega_1$ in a second-order nonlinear medium, thereby producing DC field at zero output frequency $\omega_p = \omega_0 = 0$. We hence find an additional factor of $1/(1 + \delta_{p,0}) = 1/2$ on the right-hand side of Eq. (2.32). Taking into account the distinct permutations $(\omega_1, -\omega_1)$ and $(-\omega_1, \omega_1)$, we obtain the DC time-domain amplitude of the second-order nonlinear polarization,

$$\underline{\mathbf{P}}^{(2)}(\omega_3 = 0) = \frac{1}{2} \epsilon_0 \underline{\chi}^{(2)}(0 : \omega_1, -\omega_1) : \underline{\mathbf{E}}(\omega_1) \underline{\mathbf{E}}^*(\omega_1). \quad (2.34)$$

Electro-optic Kerr effect: The electro-optic Kerr effect, also referred to as the quadratic electro-optic effect, denotes a third-order nonlinear interaction between a wave at ω_1 and a DC-field $\underline{\mathbf{E}}(0) \in \mathbb{R}$ at $\omega_0 = 0$. This results in a phase shift of the wave at ω_1 which depends quadratically on the external DC field. Formally, the quadratic electro-optic effect can be described as an interaction of the frequencies $(\omega_1, \omega_0, \omega_0)$ two of which are zero. This results in an additional factor of $(1 + \delta_{l_2,0})(1 + \delta_{l_3,0}) = 4$ on the right-hand side of Eq. (2.32). Taking into account the three distinct permutations of the triple $(\omega_1, \omega_0, \omega_0)$, we find the time-domain amplitude of the third-order nonlinear polarization at ω_1 to be,

$$\underline{\mathbf{P}}^{(3)}(\omega_1) = 3\epsilon_0 \underline{\chi}^{(3)}(\omega_1 : \omega_1, 0, 0) : \underline{\mathbf{E}}(\omega_1) \underline{\mathbf{E}}(0) \underline{\mathbf{E}}(0). \quad (2.35)$$

For cases where only nonzero frequency components play a role, Eqs. (2.20), (2.22), and (2.24) are valid and can directly be used. If DC fields are involved, the definitions according to Eqs. (2.30) and (2.31) should be used along with Eq. (2.32).

2.2 Properties of the nonlinear optical susceptibility tensor

In this section we investigate some formal properties of the nonlinear optical susceptibility. This comprises causality of the time-domain response as well as a number of symmetry relations that mutually relate the various frequency-domain tensor elements.

2.2.1 Causality

In linear optics, the causality of the dielectric impulse response can be translated to the frequency domain, resulting in a relation between the real and the imaginary part of the complex optical susceptibility, which is commonly referred to as the Kramers Kronig relation, see Section 1.2.3. Similarly, the time-domain formulation of the nonlinear optical susceptibility must also obey the causality principle, i.e.

$$\chi_{q_0:q_1q_2\dots q_n}^{(n)}(\tau_1, \tau_2, \dots, \tau_n) = 0 \quad \text{for} \quad \tau_1 < 0 \vee \tau_2 < 0 \cdots \vee \tau_n < 0. \quad (2.36)$$

The corresponding frequency-domain formulation is somewhat intricate. For some nonlinear processes, Kramers-Kronig relations similar to the linear case are valid. For some processes such as self-phase modulation, however, it is not possible to formulate a Kramers-Kronig relation. More details on Kramers-Kronig relations in nonlinear optics can be found in [9].

2.2.2 Intrinsic symmetries

Symmetry properties of the nonlinear susceptibility tensor allow to considerably reduce the number of coefficients that are needed to specify nonlinear optical interactions. As an example, let us consider the mutual interaction of three waves of frequencies ω_1 , ω_2 , and $\omega_3 = \omega_1 + \omega_2$. To describe this interaction, we first need to know the nonlinear polarization at the three frequencies, which are given by twelve complex tensors, namely

$$\underline{\chi}^{(2)}(\omega_3 : \omega_1, \omega_2), \quad \underline{\chi}^{(2)}(\omega_1 : \omega_3, -\omega_2), \quad \underline{\chi}^{(2)}(\omega_2 : \omega_3, -\omega_1), \quad (2.37)$$

$$\underline{\chi}^{(2)}(\omega_3 : \omega_2, \omega_1), \quad \underline{\chi}^{(2)}(\omega_1 : -\omega_2, \omega_3), \quad \underline{\chi}^{(2)}(\omega_2 : -\omega_1, \omega_3), \quad (2.38)$$

and six additional tensors in which each of the above-mentioned frequency elements is replaced by its negative counterpart. Moreover, each of these third-rank tensors comprises 27 tensor elements $\underline{\chi}_{q:r,s}^{(2)}$. As a consequence, $12 \times 27 = 324$ complex numbers are needed to specify the interaction of the three waves at frequencies ω_1 , ω_2 , and $\omega_3 = \omega_1 + \omega_2$. Fortunately, the different components of the nonlinear optical susceptibility are not independent from each other, and even without further assumptions, they possess certain symmetry properties that lead to a number of symmetry relations between the various components of $\underline{\chi}^{(2)}$. These relations allow to reduce complexity considerably. These relations will be explained in the next sections. In the following $\omega_\Sigma = \sum_{m=1}^n \omega_m$ denotes the sum of the input frequencies.

Reality of fields

Time-domain field quantities have to be real. From Eq. (2.13) we can conclude that complex time-domain amplitudes at positive frequencies are the complex conjugate of their negative-frequency counterparts, $\underline{\mathbf{E}}(\omega_l) = \underline{\mathbf{E}}^*(-\omega_l)$ and $\underline{\mathbf{P}}(\omega_l) = \underline{\mathbf{P}}^*(-\omega_l)$. As a consequence, the positive- and negative-frequency components of the complex susceptibility tensor are the complex conjugate of each other,

$$\underline{\chi}_{q_0:q_1q_2\dots q_n}^{(n)}(\omega_\Sigma : \omega_1, \omega_2, \dots, \omega_n) = \left[\underline{\chi}_{q_0:q_1q_2\dots q_n}^{(n)}(-\omega_\Sigma : -\omega_1, -\omega_2, \dots, -\omega_n) \right]^*. \quad (2.39)$$

Intrinsic permutation symmetry

To understand intrinsic permutation symmetry, let us consider the simplified case of a second-order nonlinearity in tensor notation,

$$\underline{P}_q^{(2)}(\omega_p) = \frac{1}{2}\epsilon_0 \sum_{r,s} \sum_{(l,m) \in \mathbb{S}(\omega_p)} \underline{\chi}_{q:r,s}^{(2)}(\omega_p : \omega_l, \omega_m) : \underline{E}_r(\omega_l) \underline{E}_s(\omega_m). \quad (2.40)$$

The sum on the right-hand side of this expression contains both the term $\underline{\chi}_{q:r,s}^{(2)}(\omega_p : \omega_l, \omega_m) : \underline{E}_r(\omega_l) \underline{E}_s(\omega_m)$ and $\underline{\chi}_{q:s,r}^{(2)}(\omega_p : \omega_m, \omega_l) : \underline{E}_s(\omega_m) \underline{E}_r(\omega_l)$. Since both terms relate to the same physical quantities, the corresponding tensor elements must be identical as well,

$$\underline{\chi}_{q:r,s}^{(2)}(\omega_p : \omega_l, \omega_m) = \underline{\chi}_{q:s,r}^{(2)}(\omega_p : \omega_m, \omega_l). \quad (2.41)$$

That means that the nonlinear susceptibility tensor element remains unchanged if we simultaneously swap two frequency arguments along with the corresponding Cartesian indices. Note that the intrinsic permutation symmetry is the consequence of a somewhat arbitrary definition. For example, we could have set one of the tensor elements $\underline{\chi}_{q:r,s}^{(2)}(\omega_p : \omega_l, \omega_m)$ and $\underline{\chi}_{q:s,r}^{(2)}(\omega_p : \omega_m, \omega_l)$ to zero while doubling the value of the other one. The result of the physically meaningful sum in Eq. (2.40) would have remained unchanged.

The intrinsic permutation symmetry can be generalized to the elements of the n -th order nonlinear susceptibility tensor,

$$\underline{\chi}_{q_0:q_1 \dots q_i q_j \dots q_n}^{(n)}(\omega_\Sigma : \omega_1, \dots, \omega_i, \omega_j, \dots, \omega_n) = \underline{\chi}_{q_0:q_n \dots q_j q_i \dots q_1}^{(n)}(\omega_\Sigma : \omega_n, \dots, \omega_j, \omega_i, \dots, \omega_1) \quad (2.42)$$

Note that the intrinsic permutation symmetry holds for all pairs of frequencies and the corresponding Cartesian indices except for the resulting frequency ω_Σ and the resulting vector component index q_0 .

Symmetries for lossless media

For lossless media, or, more precisely, for media that are lossless within a certain range of frequencies, two more symmetry properties apply. First, all components of the nonlinear susceptibility tensor are real,

$$\underline{\chi}_{q_0:q_1 \dots q_i q_j \dots q_n}^{(n)}(\omega_\Sigma : \omega_1, \dots, \omega_i, \omega_j, \dots, \omega_n) \in \mathbb{R} \quad (2.43)$$

This is clear for the case of the linear susceptibility, where a nonzero imaginary part of $\underline{\chi}^{(1)}$ leads to attenuation of a propagating plane wave and hence to optical loss, see Section (1.2.5). For higher-order nonlinear susceptibilities, the general proof that $\underline{\chi}^{(1)}$ is real for lossless media can be obtained by a quantum-mechanical consideration of the nonlinear optical susceptibility, see, e.g., [9] and the references therein.

Second, for lossless media, the permutation symmetry according to Eq. (2.42) also holds for the resulting frequency ω_Σ . Since this frequency is always the sum of all other frequency arguments, signs must be changed appropriately when interchanging the first argument with any other argument,

$$\underline{\chi}_{q_0:q_1 \dots q_i \dots q_n}^{(n)}(\omega_\Sigma : \omega_1, \dots, \omega_i, \dots, \omega_n) = \underline{\chi}_{q_i:q_1 \dots q_0 \dots q_n}^{(n)}(\omega_i : -\omega_1, \dots, \omega_\Sigma, \dots, -\omega_n) \quad (2.44)$$

The general proof of this relation is again based on a quantum-mechanical consideration of the nonlinear optical susceptibility [9].

Kleinman's symmetry

In many cases of practical interest, optical media are operated at frequencies far below their lowest resonance frequency. The medium can then not only assumed to be lossless, but the nonlinear susceptibility is essentially independent of frequency within the considered wavelength range. The frequency arguments can then be permuted without permuting the indices, i.e.,

$$\underline{\chi}_{q_0:q_1\dots q_i q_j\dots q_n}^{(n)}(\omega_\Sigma : \omega_1, \dots, \omega_i, \omega_j, \dots, \omega_n) = \underline{\chi}_{q_0:q_1\dots q_i q_j\dots q_n}^{(n)}(\omega_\Sigma : \omega_1, \dots, \omega_j, \omega_i, \dots, \omega_n), \quad (2.45)$$

for any two frequencies ω_i and ω_j . This symmetry property is referred to as Kleinman's symmetry. Note that frequency-independent tensor elements correspond to an instantaneous response of the polarization as was assumed in Eq. (1.84).

Reduction of second-order nonlinear susceptibility tensor elements by symmetry relations

At the beginning of this section, we have stated that 324 complex numbers are needed to fully specify the second-order nonlinear susceptibility tensor $\underline{\chi}_{q:r,s}^{(2)}(\omega_3 : \omega_1, \omega_2)$. Systematic exploitation of the aforementioned symmetry relations allows to greatly reduce this number:

- Because of **reality of electromagnetic fields**, only half, i.e., 162, of these elements are independent.
- **Intrinsic permutation symmetry** allows to simultaneously swap the latter two frequencies and vector indices, leading to another reduction of the number of elements of a factor of 2. This results in 81 independent complex numbers.
- For **lossless media**, all elements are real, and we may freely permute also the resulting frequency. This leads to a reduction of the independent elements by a factor of 3. The entire tensor is then specified by 27 independent real numbers.
- If **Kleinman's symmetry** can be applied, only 10 of these elements are independent. In this case, we may use a contracted notation of the tensor in a (3×6) -matrix, see Section 2.3.1 for more details.

Further reduction of the number of independent nonlinear susceptibility tensor is possible by exploiting spatial symmetries of the medium's crystal lattice, see next section.

2.2.3 Spatial symmetry of the nonlinear medium

The number of independent components of the susceptibility tensor can be further reduced if the material features spatial crystal symmetries. This is a direct consequence of Neumann's principle, which states that, if a crystal is invariant with respect to certain geometric transformations, any of its physical properties must also be invariant with respect to the same transformations. Otherwise stated, the symmetry elements of any physical property of a crystal must include the symmetry elements of the point group of the crystal.

Influence of spatial symmetry on susceptibility tensor elements

To understand this principle let us consider a coordinate transformation from a coordinate system (x, y, z) to a coordinate system (x', y', z') ,

$$\begin{pmatrix} E'_{x'} \\ E'_{y'} \\ E'_{z'} \end{pmatrix} = \begin{pmatrix} T_{x'x} & T_{x'y} & T_{x'z} \\ T_{y'x} & T_{y'y} & T_{y'z} \\ T_{z'x} & T_{z'y} & T_{z'z} \end{pmatrix} \begin{pmatrix} E_x \\ E_y \\ E_z \end{pmatrix}. \quad (2.46)$$

Using Einstein summation convention, we can rewrite this relation in a more compact form,

$$E'_{q'} = T_{q'q} E_q, \quad (2.47)$$

where $q \in \{x, y, z\}$ and $q' \in \{x', y', z'\}$ denote the various vector components, and where the summation over q on the right-hand side implied in the Einstein summation convention. The inverse transformation is then given by

$$E_q = (T^{-1})_{qq'} E'_{q'}. \quad (2.48)$$

For orthogonal transformations such as reflections, inversions, or rotations, the transformation operator corresponds to a unitary matrix,

$$\mathbf{T}^{-1} = \mathbf{T}^T \quad (T^{-1})_{qq'} = T_{q'q}. \quad (2.49)$$

To understand how the tensor elements are transformed, we will now apply this coordinate transform to the relationship between the n -th order nonlinear polarization and the electric field. For notational brevity, we again assume an instantaneous time-domain response, making the multiple convolution integrals in the Volterra series of Eq. (2.1) obsolete. Skipping the time arguments and using Einstein notation, the relationship in the original coordinate system can be written as

$$P_{q_0}^{(n)} = \epsilon_0 \chi_{q_0:q_1 \dots q_n}^{(n)} E_{q_1} \dots E_{q_n}. \quad (2.50)$$

We introduce $E_q = T_{q'q} E'_{q'}$ on the right-hand side and apply the coordinate transformation $T_{q'_0 q_0}$ to the resulting equation to obtain an expression for the nonlinear optical susceptibility in the transformed coordinate system,

$$\chi'_{q'_0:q'_1 \dots q'_n}{}^{(n)} = T_{q'_0 q_0} T_{q'_1 q_1} \dots T_{q'_n q_n} \chi_{q_0:q_1 \dots q_n}^{(n)}. \quad (2.51)$$

As expected, the nonlinear susceptibility tensor of rank $n+1$ transforms as the $(n+1)$ -fold product of the coordinates. We may now apply Neumann's principle by exploiting the fact that crystal lattices remain unchanged under certain geometric transformations, and that this invariance has to hold for the nonlinear susceptibility tensor as well. In general, if a crystal lattice remains unchanged under a symmetry operation \mathbf{T} , then the n -th order nonlinear susceptibility must fulfill the relation

$$\chi'_{q'_0:q'_1 \dots q'_n}{}^{(n)} = T_{q'_0 q_0} T_{q'_1 q_1} \dots T_{q'_n q_n} \chi_{q_0:q_1 \dots q_n}^{(n)}. \quad (2.52)$$

Example: Centro-symmetric media and second-order nonlinear effects

As an example, let us consider a crystal lattice with inversion symmetry, i.e., a lattice which remains unchanged if all coordinates are replaced by their negative counterparts. This inversion transformation is given by

$$T_{q'q} = -\delta_{q'q}, \quad (2.53)$$

where $\delta_{q'q}$ denotes the Kronecker delta, i.e., $\delta_{q'q} = 0$ for $q' \neq q$ and $\delta_{q'q} = 1$ for $q' = q$. Since the inversion operation leaves the crystal lattice essentially unchanged, the nonlinear susceptibility tensor must remain unchanged as well,

$$\chi'_{q'_0:q'_1 \dots q'_n}{}^{(n)} = (-1)^{n+1} \chi_{q_0:q_1 \dots q_n}^{(n)}. \quad (2.54)$$

For even orders n this requires all susceptibility tensor elements to vanish. Centro-symmetric media do hence not exhibit any second-order nonlinearity. Note that the same applies to amorphous materials with randomly oriented molecules such as fused silica glass: Even though the microscopic structure of the material is not centro-symmetric, the macroscopic optical properties are defined by an average over all possible random orientations of molecules and do hence not change upon inversion of coordinates.

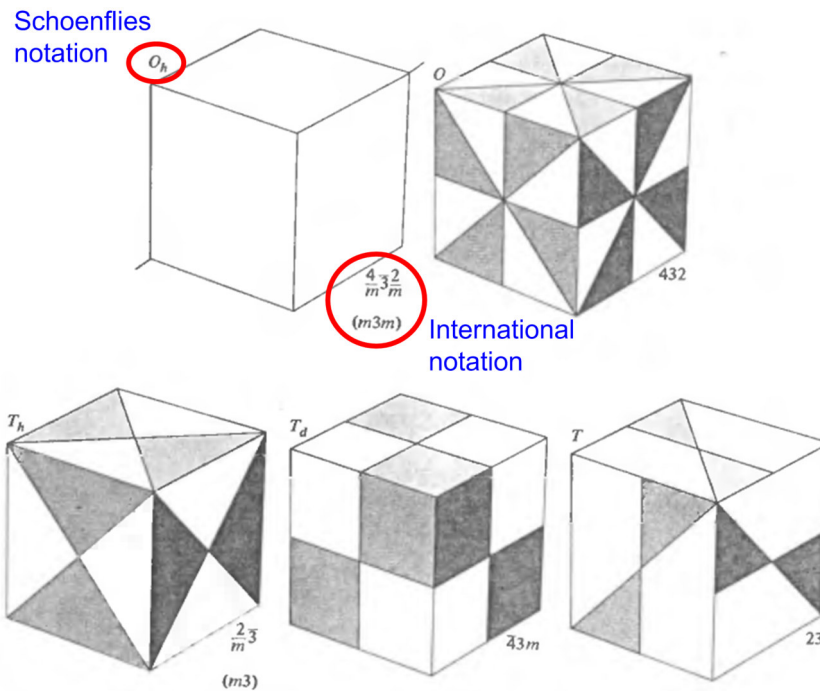


Figure 2.1: Illustration of the five cubic crystallographic point groups. The symmetry groups can be indicated by the so-called Schoenflies notation, indicated on the left of each object, or by the international notation, indicated on the right. (Figure adapted from [6])

Crystal classes, point groups and symmetry operations

To determine the form of the nonlinear susceptibility tensor in the general case, it is important to know the coordinate transformations with respect to which the crystal lattice remains unchanged. In general, crystals can be categorized in 32 crystal classes according to their symmetry properties. Each crystal class is associated with a so-called point group, i.e., a group of symmetry operations with respect to which the crystal lattice is invariant. The 32 crystallographic point groups can be subdivided in 5 cubic point groups and 27 non-cubic point groups, see Figs. 2.1 and 2.2 for graphical illustrations of the symmetry properties. Two nomenclatural conventions, the Schoenflies and the international system, are in use to describe the various point groups, both of which are indicated in the figures. As an example, the point group C_n in Schoenflies notation refers to an n -fold rotation axis and is simply denoted by n in the international system, see first row of Fig. 2.2. Similarly, the point group C_{nv} in Schoenflies notation refers to an object that has an n -fold rotation axis, a mirror plane that contains this axis, plus additional mirror planes as required by the n -fold rotation axis, second row of Fig. 2.2. The point group C_{nh} in Schoenflies notation contains the n -fold rotation axis and a single mirror plane that is perpendicular to this axis, third row of Fig. 2.2. The complete systematic of these nomenclatures goes beyond the scope of this lecture; more information can be found in [6]. In the next sections, we will investigate in more detail which form the second- and the third-order susceptibility tensors assume for the various crystal classes.

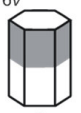
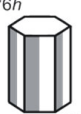
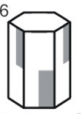
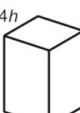
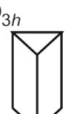
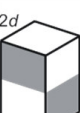
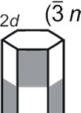
Schoenflies	Hexagonal	Tetragonal	Trigonal	Orthorhombic	Monoclinic	Triclinic	International
C_n	C_6  6	C_4  4	C_3  3		C_2  2	C_1  1	n
C_{nv}	C_{6v}  6 mm	C_{4v}  4 mm	C_{3v}  3 m	C_{2v}  2 mm			
C_{nh}	C_{6h}  6/ m	C_{4h}  4/ m			C_{2h}  2/ m		n/m
	C_{3h}  $\bar{6}$				C_{1h} ($\bar{2}$)  m		\bar{n}
S_n		S_4  $\bar{4}$	S_6  (C_{3i}) $\bar{3}$			S_2  (C_i) $\bar{1}$	
D_n	D_6  622	D_4  422	D_3  32	D_2  (V) 222			$n22$ (n even) $n2$ (n odd)
D_{nh}	D_{6h}  6/ mmm	D_{4h}  4/ mmm		D_{2h} (mmm)  (V_h) 2/ mmm			$\frac{n}{m} \frac{2}{m} \frac{2}{m}$ (n/mmm)
	D_{3h}  $\bar{6}2m$						$\bar{n}2m$ (n even)
D_{nd}		D_{2d}  (V_d) 422	D_{2d} ($\bar{3}m$)  $\bar{3} \frac{2}{m}$				$\bar{n} \frac{2}{m}$ (n odd)

Figure 2.2: Illustration of the 27 non-cubic crystallographic point groups. The symmetry groups can be indicated by the so-called Schoenflies notation, indicated on the left of each object, or by the international notation, indicated on the right. Note that the Schoenflies categories, indicated on the left of each row, are not identical to the categories derived from the international notation, indicated on the right. (Figure adapted from [6])

2.3 Influence of spatial symmetry on the second-order nonlinear susceptibility

2.3.1 Contracted notation for second-order nonlinear susceptibility

In many cases of practical interest, optical media are operated at frequencies far below their lowest resonance frequency such that Kleinman symmetry applies and the frequency arguments can be permuted without permuting the corresponding indices. We may hence assume that the second-order nonlinear susceptibility tensor $\underline{\chi}_{q:r,s}^{(2)}$ is symmetric in its last two vector component indices, i.e. $\underline{\chi}_{q:r,s}^{(2)} = \underline{\chi}_{q:s,r}^{(2)}$. We may then simplify the representation by introducing a contracted notation

$$\underline{\chi}_{q:r,s}^{(2)} \mapsto d_{ql} = \frac{1}{2} \underline{\chi}_{q:r,s}^{(2)} \quad (2.55)$$

where the pair (r, s) is mapped to a single index l according to the following assignment:

$$\begin{array}{cccccc} rs & xx & yy & zz & yz, zy & xz, zx & xy, yx \\ l & 1 & 2 & 3 & 4 & 5 & 6 \end{array} \quad (2.56)$$

The second-order nonlinear susceptibility tensor can then be represented in contracted notation as a (3×6) -matrix,

$$\mathbf{d} = \begin{pmatrix} d_{x1} & d_{x2} & d_{x3} & d_{x4} & d_{x5} & d_{x6} \\ d_{y1} & d_{y2} & d_{y3} & d_{y4} & d_{y5} & d_{y6} \\ d_{z1} & d_{z2} & d_{z3} & d_{z4} & d_{z5} & d_{z6} \end{pmatrix} \quad (2.57)$$

Note that this notation can even be used when Kleinman symmetry is not valid: For second-order susceptibility tensor elements $\underline{\chi}_{q:r,s}^{(2)}(\omega_p : \omega_l, \omega_m)$, for which the last two frequency arguments are nearly identical, $\omega_l \approx \omega_m$, we may also freely exchange the vector indices r and s , thereby fulfilling the conditions for using contracted notation. This applies, e.g., to second-harmonic generation or sum-frequency generation with nearly identical input frequencies.

So far, we have only made use of Kleinman symmetry for the last two indices. Taking into account permutability of all indices, we find that, e.g., $d_{x2} = \frac{1}{2} \underline{\chi}_{x:y,y}^{(2)} = \frac{1}{2} \underline{\chi}_{y:x,y}^{(2)} = d_{y6}$. Exploiting all similar identities, we find that \mathbf{d} has only 10 independent elements,

$$\mathbf{d} = \begin{pmatrix} d_{x1} & d_{x2} & d_{x3} & d_{x4} & d_{x5} & d_{x6} \\ d_{x6} & d_{y2} & d_{y3} & d_{y4} & d_{x4} & d_{x2} \\ d_{x5} & d_{y4} & d_{z3} & d_{y3} & d_{x3} & d_{x4} \end{pmatrix} \quad (2.58)$$

Using the contracted notation, we can express the various second-order nonlinear effects by a matrix equation. For second-harmonic generation, we obtain

$$\begin{pmatrix} \underline{P}_x^{(2)}(2\omega_1) \\ \underline{P}_y^{(2)}(2\omega_1) \\ \underline{P}_z^{(2)}(2\omega_1) \end{pmatrix} = \epsilon_0 \begin{pmatrix} d_{x1} & d_{x2} & d_{x3} & d_{x4} & d_{x5} & d_{x6} \\ d_{x6} & d_{y2} & d_{y3} & d_{y4} & d_{x4} & d_{x2} \\ d_{x5} & d_{y4} & d_{z3} & d_{y3} & d_{x3} & d_{x4} \end{pmatrix} \begin{pmatrix} \underline{E}_x^2(\omega_1) \\ \underline{E}_y^2(\omega_1) \\ \underline{E}_z^2(\omega_1) \\ 2\underline{E}_y(\omega_1) \underline{E}_z(\omega_1) \\ 2\underline{E}_x(\omega_1) \underline{E}_z(\omega_1) \\ 2\underline{E}_x(\omega_1) \underline{E}_y(\omega_1) \end{pmatrix}. \quad (2.59)$$

Similarly, we can describe sum-frequency generation taking into account the additional degeneracy factor of 2 due to the distinct permutations of (ω_1, ω_2) ,

$$\begin{pmatrix} \underline{P}_x^{(2)}(\omega_3) \\ \underline{P}_y^{(2)}(\omega_3) \\ \underline{P}_z^{(2)}(\omega_3) \end{pmatrix} = 2\epsilon_0 \begin{pmatrix} d_{x1} & d_{x2} & d_{x3} & d_{x4} & d_{x5} & d_{x6} \\ d_{x6} & d_{y2} & d_{y3} & d_{y4} & d_{x4} & d_{x2} \\ d_{x5} & d_{y4} & d_{z3} & d_{y3} & d_{x3} & d_{x4} \end{pmatrix} \begin{pmatrix} \underline{E}_x(\omega_1) \underline{E}_x(\omega_2) \\ \underline{E}_y(\omega_1) \underline{E}_y(\omega_2) \\ \underline{E}_z(\omega_1) \underline{E}_z(\omega_2) \\ \underline{E}_y(\omega_1) \underline{E}_z(\omega_2) + \underline{E}_z(\omega_1) \underline{E}_y(\omega_2) \\ \underline{E}_x(\omega_1) \underline{E}_z(\omega_2) + \underline{E}_z(\omega_1) \underline{E}_x(\omega_2) \\ \underline{E}_x(\omega_1) \underline{E}_y(\omega_2) + \underline{E}_y(\omega_1) \underline{E}_x(\omega_2) \end{pmatrix}. \quad (2.60)$$

2.3.2 Nonlinear susceptibility tensors for different spatial symmetries

As a result of Section 2.2.3, we have found that spatial symmetries of various crystal classes may reduce the number of independent susceptibility tensor elements. In particular, the second-order susceptibility vanishes completely for materials that feature inversion symmetry. This applies to 11 out of the 32 crystal classes, see Fig. 2.3. By explicit investigation of the symmetry properties of the remaining 21 crystal classes, one can derive the form of the tensor, i.e., the number of nonzero elements and the relationships among these elements as indicated in Fig. 2.3. For cases where contracted notation can be used, the nonzero tensor elements and the relationships between these elements can be represented graphically, see Fig. 2.4. Numerical values for some of the nonzero tensor elements of selected second-order nonlinear crystals are also given in Fig. 2.5.

Example: Second-order nonlinear susceptibility of silicon (Si) and of gallium arsenide (GaAs) Silicon (Si) and gallium arsenide (GaAs) both possess cubic lattices, see Fig. 2.6. The diamond lattice of silicon belongs to point group $m\bar{3}m = O_h$ and is centrosymmetric, Fig. 2.6 (a). This leads to zero second-order susceptibility, see Fig. 2.3. In contrast to that, the zincblende lattice of GaAs belongs to point group $\bar{4}3m = T_d$ and does not possess centrosymmetry. GaAs hence exhibits nonzero second-order susceptibility tensor elements, see Figs. 2.3 and 2.5.

2.4 Influence of spatial symmetry on the third-order nonlinear susceptibility

As for the second-order nonlinearity, the spatial symmetry of the medium also restricts the form of the third-order nonlinear optical susceptibility. The nonzero tensor elements and the mutual interdependence are specified in Figures 2.7, 2.8, and 2.9 for each of the 32 crystal classes and for isotropic materials.

Crystal System	Crystal Class	Nonvanishing Tensor Elements
Triclinic	$1 = C_1$	All elements are independent and nonzero
	$\bar{1} = S_2$	Each element vanishes
Monoclinic	$2 = C_2$	$xyz, xzy, xxy, xyx, yxx, yyy, yzz, yzx, yxz, zyz,$ zzy, zxy, zyx (twofold axis parallel to \hat{y})
	$m = C_{1h}$	$xxx, xyy, xzz, xzx, xxz, yyz, yzy, yxy, yyx, zxx,$ zyy, zzz, zzx, zxz (mirror plane perpendicular to \hat{y})
	$2/m = C_{2h}$	Each element vanishes
Orthorhombic	$222 = D_2$	$xyz, xzy, yzx, yxz, zxy, zyx$
	$mm2 = C_{2v}$	$xzx, xxz, yyz, yzy, zxx, zyy, zzz$
	$mmm = D_{2h}$	Each element vanishes
Tetragonal	$4 = C_4$	$xyz = -yxz, xzy = -yzx, xzx = yzy, xxz = yyz,$ $zxx = zyy, zzz, zxy = -zyx$
	$\bar{4} = S_4$	$xyz = yxz, xzy = yzx, xzx = -yzy, xxz = -yyz,$ $zxx = -zyy, zxy = zyx$
	$422 = D_4$	$xyz = -yxz, xzy = -yzx, zxy = -zyx$
	$4mm = C_{4v}$	$xzx = yzy, xxz = yyz, zxx = zyy, zzz$
	$\bar{4}2m = D_{2d}$	$xyz = yxz, xzy = yzx, zxy = zyx$
	$4/m = C_{4h}$	Each element vanishes
	$4/mmm = D_{4h}$	Each element vanishes
Cubic	$432 = O$	$xyz = -xzy = yzx = -yxz = zxy = -zyx$
	$\bar{4}3m = T_d$	$xyz = xzy = yzx = yxz = zxy = zyx$
	$23 = T$	$xyz = yzx = zxy, xzy = yxz = zyx$
	$m3 = T_h, m3m = O_h$	Each element vanishes
Trigonal	$3 = C_3$	$xxx = -xyy = -yyz = -yxy, xyz = -yxz, xzy = -yzx,$ $xzx = yzy, xxz = yyz, yyy = -yxx = -xxy = -xyx,$ $zxx = zyy, zzz, zxy = -zyx$
	$32 = D_3$	$xxx = -xyy = -yyz = -yxy, xyz = -yxz,$ $xzy = -yzx, zxy = -zyx$
	$3m = C_{3v}$	$xzx = yzy, xxz = yyz, zxx = zyy, zzz, yyy = -yxx =$ $-xxy = -xyx$ (mirror plane perpendicular to \hat{x})
	$\bar{3} = S_6, \bar{3}m = D_{3d}$	Each element vanishes
Hexagonal	$6 = C_6$	$xyz = -yxz, xzy = -yzx, xzx = yzy, xxz = yyz,$ $zxx = zyy, zzz, zxy = -zyx$
	$\bar{6} = C_{3h}$	$xxx = -xyy = -yxy = -yyx,$ $yyy = -yxx = -xyx = -xxy$
	$622 = D_6$	$xyz = -yxz, xzy = -yzx, zxy = -zyx$
	$6mm = C_{6v}$	$xzx = yzy, xxz = yyz, zxx = zyy, zzz$
	$\bar{6}m2 = D_{3h}$	$yyy = -yxx = -xxy = -xyx$
	$6/m = C_{6h}$	Each element vanishes
	$6/mmm = D_{6h}$	Each element vanishes

Figure 2.3: Form of the second-order susceptibility tensor for each of the 32 crystal classes. For the 11 crystal classes that feature inversion symmetry, the tensor elements vanish. The non-vanishing tensor elements of the remaining 21 crystal classes are denoted by their Cartesian indices. (Figure adapted from [9])

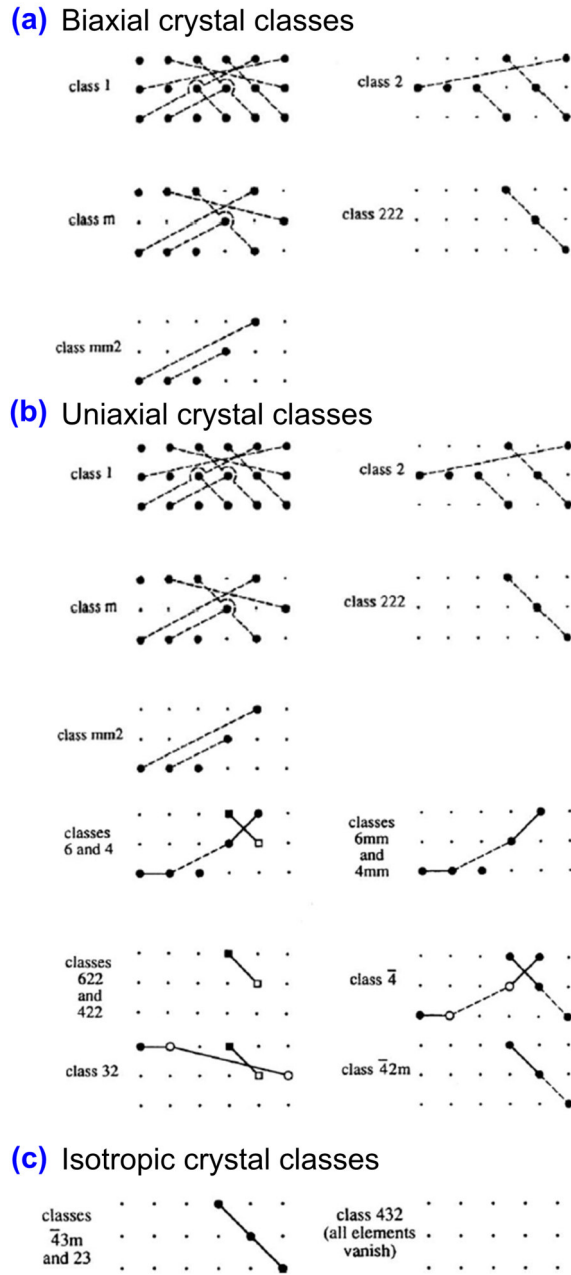


Figure 2.4: Form of the second-order susceptibility tensor in contracted notation for each of the 21 crystal classes that do not feature inversion symmetry. Depending on the symmetry properties of the linear susceptibility tensor, these crystal classes can be subdivided in (a) biaxial crystal classes, (b) uniaxial crystal classes, and (c) isotropic crystal classes, see Section 3.1.1 for a more detailed discussion. Small dots indicate zero coefficients, large dots represent nonzero coefficient. Coefficients indicated by squares are zero if Kleinman symmetry applies. Connected symbols represent numerically equal coefficients; open-symbol coefficients are opposite in sign with respect to the connected closed-symbol coefficient. Dashed connections are valid for the case of Kleinman symmetry only (Figure adapted from [9])

Material	Point Group	d_{il} (pm/V)
Ag ₃ AsS ₃ (proustite)	$3m = C_{3v}$	$d_{22} = 18$ $d_{15} = 11$
AgGaSe ₂	$\bar{4}2m = D_{2d}$	$d_{36} = 33$
AgSbS ₃ (pyrargyrite)	$3m = C_{3v}$	$d_{15} = 8$ $d_{22} = 9$
beta-BaB ₂ O ₄ (BBO) (beta barium borate)	$3m = C_{3v}$	$d_{22} = 2.2$
CdGeAs ₂	$\bar{4}2m = D_{2d}$	$d_{36} = 235$
CdS	$6mm = C_{6v}$	$d_{33} = 78$ $d_{31} = -40$
GaAs	$\bar{4}3m$	$d_{36} = 370$
KH ₂ PO ₄ (KDP)	$2m$	$d_{36} = 0.43$
KD ₂ PO ₄ (KD*P)	$2m$	$d_{36} = 0.42$
LiIO ₃	$6 = C_6$	$d_{15} = -5.5$ $d_{31} = -7$
LiNbO ₃	$3m = C_{3v}$	$d_{22} = 3$ pm/V $d_{31} = -5$ pm/V; $d_{33} = -25$ pm/V
Quartz	$32 = D_3$	$d_{11} = 0.3$ $d_{14} = 0.008$

Figure 2.5: Second-order nonlinear optical susceptibility for several crystals. Additional tensor components may be derived by using the relationships illustrated in Fig. 2.4. (Figure adapted from [9])

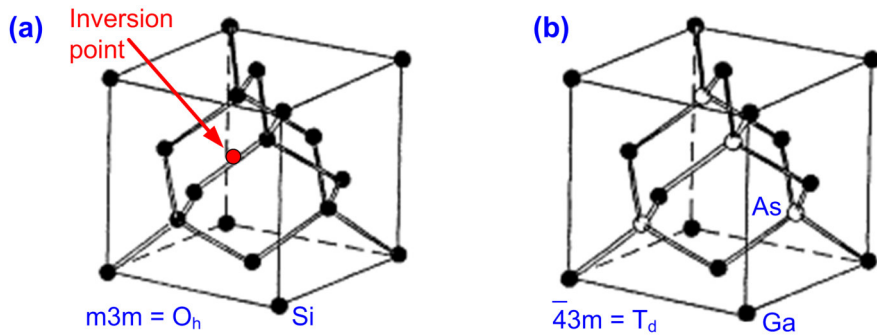


Figure 2.6: Examples of two cubic crystal structures and the associated point groups. (a) Diamond structure of silicon (Si), belonging to point group $m3m = O_h$. This point group features inversion symmetry with inversion points being located in the middle between two neighbouring atoms. As a consequence, all elements of the second-order nonlinear susceptibility must vanish. (b) Zincblende structure of gallium arsenide (GaAs), belonging to point group $\bar{4}3m = T_d$. The structure is non-centrosymmetric and hence features nonzero second-order susceptibility tensor elements ($xyz = xzy = yzx = yxz = zxy = zyx$) (Figure adapted from [9])

Isotropic

There are 21 nonzero elements, of which only 3 are independent. They are:

$$\begin{aligned}yyzz &= zzyy = zzzx = xxzz = xxyy = yyxx, \\yzyz &= zyzy = zxzx = xzxz = xyxy = yxyx, \\yzzz &= zyyz = zxxz = xzzx = xyyx = yxxy;\end{aligned}$$

and

$$xxxx = yyyy = zzzz = xxyy + xyxy + xyyx.$$

Cubic

For the two classes 23 and $m3$, there are 21 nonzero elements, of which only 7 are independent. They are:

$$\begin{aligned}xxxx &= yyyy = zzzz, \\yyzz &= zzzx = xxyy, \\zzyy &= xxzz = yyxx, \\yzyz &= zxzx = xyxy, \\zyzy &= xzxz = yxyx, \\yzzz &= zxxz = xyyx, \\zyyz &= xzzx = yxxy.\end{aligned}$$

For the three classes 432 , $\bar{4}3m$, and $m3m$, there are 21 nonzero elements, of which only 4 are independent. They are:

$$\begin{aligned}xxxx &= yyyy = zzzz, \\yyzz &= zzyy = zzzx = xxzz = xxyy = yyxx, \\yzyz &= zyzy = zxzx = xzxz = xyxy = yxyx, \\yzzz &= zyyz = zxxz = xzzx = xyyx = yxxy.\end{aligned}$$

Hexagonal

For the three classes 6 , $\bar{6}$, and $6/m$, there are 41 nonzero elements, of which only 19 are independent. They are:

$$\begin{aligned}xxxx &= yyyy = zzzz, & \begin{cases} xxyy = yyxx, \\ xyyx = yxxy, \\ xyxy = yxyx, \end{cases} \\yyzz &= xxzz, & xyzz &= -yxzz, \\zzyy &= zzzx, & zzyy &= -zyzx, \\zyyz &= zxxz, & zyyz &= -zyxz, \\yzzz &= xzzx, & xzzz &= -yzzx, \\yzyz &= xzxz, & xzyz &= -yzxz, \\zyzy &= zxzx, & zzyz &= -zyzx, \\xxxy &= -yyyx = yyxy + yxyy + xyyy, & \begin{cases} yyxy = -xxyx, \\ yxyy = -xyxx, \\ xyyy = -yxxx. \end{cases}\end{aligned}$$

(continued)

Figure 2.7: Form of the third-order nonlinear susceptibility tensor for various crystal classes and for isotropic materials. The elements are denoted by their Cartesian coordinates. (Figure adapted from [9])

For the four classes 622 , $6mm$, $6/mmm$, and $\bar{6}m2$, there are 21 nonzero elements, of which only 10 are independent. They are:

$$\begin{aligned}
 & zzzz, \\
 xxxx = yyyy = & xxyy + xyyx + xyxy, \quad \begin{cases} xxyy = yyxx, \\ xyyx = yxxy, \\ xyxy = yxyx, \end{cases} \\
 & yyzz = xxzz, \\
 & zzyy = zzxx, \\
 & zyyz = zxzx, \\
 & yzzz = xzzx, \\
 & yzyz = xzxx, \\
 & zyzzy = zxzx.
 \end{aligned}$$

Trigonal

For the two classes 3 and $\bar{3}$, there are 73 nonzero elements, of which only 27 are independent. They are:

$$\begin{aligned}
 & zzzz, \\
 xxxx = yyyy = & xxyy + xyyx + xyxy, \quad \begin{cases} xxyy = yyxx, \\ xyyx = yxxy, \\ xyxy = yxyx, \end{cases} \\
 & yyzz = xxzz, \quad xyzz = -yxzz, \\
 & zzyy = zzxx, \quad zzyy = -zzyx, \\
 & zyyz = zxzx, \quad zxyy = -zyxz, \\
 & yzzz = xzzx, \quad xzzy = -yzzx, \\
 & yzyz = xzxx, \quad xzyy = -yzxz, \\
 & zyzzy = zxzx, \quad zxyy = -zyxz, \\
 xxxy = -yyyx = & yyxy + yxyy + xyyy, \quad \begin{cases} yyxy = -xxyx, \\ yxyy = -xyxx, \\ xyyy = -yxxx. \end{cases} \\
 & yyyz = -yxxz = -xyxz = -xxyy, \\
 & yyzy = -yxzx = -xyzx = -xxzy, \\
 & yzyy = -yzxx = -xzyx = -xzxy, \\
 & zyyy = -zyxx = -zxyx = -zaxy, \\
 & xxxz = -xyyz = -xyyz = -yyxz, \\
 & xxzx = -xyzy = -yxzy = -yyzx, \\
 & xzxx = -yzxy = -yzxy = -xzyy, \\
 & zxxx = -zxyy = -zyxy = -zyyx.
 \end{aligned}$$

For the three classes $3m$, $\bar{3}m$, and 32 , there are 37 nonzero elements, of which only 14 are independent. They are:

$$\begin{aligned}
 & zzzz, \\
 xxxx = yyyy = & xxyy + xyyx + xyxy, \quad \begin{cases} xxyy = yyxx, \\ xyyx = yxxy, \\ xyxy = yxyx, \end{cases}
 \end{aligned}$$

Figure 2.8: Continued: Form of the third-order nonlinear susceptibility tensor for various crystal classes. The elements are denoted by their Cartesian coordinates. (Figure adapted from [9])

$$\begin{aligned}
yyzz &= xxzz, & xxxz &= -xyyz = -yxyz = -yyxz, \\
zzyy &= zzxx, & xxzx &= -xyzy = -yxzy = -yyzx, \\
zyyz &= zxzx, & xzxx &= -xzyy = -yzxy = -yzyx, \\
yzzy &= xzzx, & zxxx &= -zxyy = -zyxy = -zyyx, \\
& & yzyz &= xzxz, \\
& & zyzy &= zxzx.
\end{aligned}$$

Tetragonal

For the three classes 4 , $\bar{4}$, and $4/m$, there are 41 nonzero elements, of which only 21 are independent. They are:

$$\begin{aligned}
& xxxx = yyyy, \quad zzzz, \\
zzxx &= zzyy, \quad xyzz = -yxzz, \quad xxyy = yyxx, \quad xxyy = -yyyx, \\
xxzz &= zzyy, \quad zzyy = -zzyx, \quad xyxy = yxyx, \quad xxyx = -yyxy, \\
zxzx &= zyzy, \quad xzyz = -yzxz, \quad xyyx = yxxy, \quad xyxx = -yxxy, \\
xzxz &= yzyz, \quad zxzy = -zyzx, \quad yxxx = -xyyy, \\
zxxz &= zyyz, \quad zxyz = -zyxz, \\
xzxx &= yzzx, \quad xzzy = -yzzx.
\end{aligned}$$

For the four classes 422 , $4mm$, $4/mmm$, and $\bar{4}2m$, there are 21 nonzero elements, of which only 11 are independent. They are:

$$\begin{aligned}
& xxxx = yyyy, \quad zzzz, \\
yyzz &= xxzz, \quad yzzy = xzzx \quad xxyy = yyxx, \\
zzyy &= zzxx, \quad yzyz = xzxz \quad xyxy = yxyx, \\
zyyz &= zxzx, \quad zyzy = zxzx \quad xyyx = yxxy.
\end{aligned}$$

Monoclinic

For the three classes 2 , m , and $2/m$, there are 41 independent nonzero elements, consisting of:

- 3 elements with indices all equal,
- 18 elements with indices equal in pairs,
- 12 elements with indices having two y's one x, and one z,
- 4 elements with indices having three x's and one z,
- 4 elements with indices having three z's and one x.

Orthorhombic

For all three classes, 222 , $mm2$, and mmm , there are 21 independent nonzero elements, consisting of:

- 3 elements with indices all equal,
- 18 elements with indices equal in pairs.

Triclinic

For both classes, 1 and $\bar{1}$, there are 81 independent nonzero elements.

Figure 2.9: Continued: Form of the third-order nonlinear susceptibility tensor for various crystal classes. The elements are denoted by their Cartesian coordinates. (Figure adapted from [9])

Chapter 3

Second-order nonlinear effects

In this chapter, we will give a more detailed explanation of second-order nonlinear phenomena such as the the linear electro-optic effect (also referred to as Pockels effect), sum and difference frequency generation, and parametric amplification. Second-order nonlinearities can only exist in non-centrosymmetric materials, which often feature an anisotropic linear susceptibility. We will therefore first introduce a formalism which describes wave propagation in linear anisotropic media. Based on this, we will then investigate the influence of second-order nonlinearities.

3.1 Wave propagation in linear anisotropic media

3.1.1 Permeability and impermeability tensors of anisotropic media

A linear anisotropic medium is characterized by linear permeability tensor $\underline{\epsilon}_r$

$$\underline{\mathbf{D}} = \epsilon_0 \underline{\epsilon}_r \underline{\mathbf{E}}, \quad (3.1)$$

where both $\underline{\mathbf{D}}$ and $\underline{\mathbf{E}}$ denote complex time-domain amplitudes, Eqs. (1.36) to (1.41), and where the arguments (\mathbf{r}, ω_0) have been omitted for better readability. The permeability tensor $\underline{\epsilon}_r$ is represented by a symmetric (3×3) -matrix and can be related to the the susceptibility tensor by

$$\underline{\epsilon}_r = \mathbf{I} + \underline{\chi}, \quad (3.2)$$

where \mathbf{I} denotes the identity matrix. The dielectric tensor is Hermitian such that $\epsilon_{ij} = \epsilon_{ji}^*$. In a lossless material, all elements of $\underline{\epsilon}_r$ are real and the corresponding matrix is symmetric, $\epsilon_{ij} = \epsilon_{ji} \in \mathbb{R}$. The tensor can conveniently be represented in diagonal form by means of a principal axis transformation, i.e., by appropriate rotation of the coordinate axes,

$$\begin{pmatrix} \underline{D}_x \\ \underline{D}_y \\ \underline{D}_z \end{pmatrix} = \epsilon_0 \begin{pmatrix} \epsilon_{xx} & 0 & 0 \\ 0 & \epsilon_{yy} & 0 \\ 0 & 0 & \epsilon_{zz} \end{pmatrix} \begin{pmatrix} \underline{E}_x \\ \underline{E}_y \\ \underline{E}_z \end{pmatrix} = \epsilon_0 \begin{pmatrix} n_1^2 & 0 & 0 \\ 0 & n_2^2 & 0 \\ 0 & 0 & n_3^2 \end{pmatrix} \begin{pmatrix} \underline{E}_x \\ \underline{E}_y \\ \underline{E}_z \end{pmatrix}, \quad (3.3)$$

where n_1 , n_2 , and n_3 denote the refractive indices that are associated with a plane wave that is entirely polarized along the x , y , or z -direction. The coordinate system in which the dielectric tensor assumes diagonal form, defines the principal axes of the of the anisotropic crystal. In many cases, it is convenient to consider the inverse operation, which is represented by the so-called dielectric impermeability tensor $\underline{\eta} = (\epsilon_0 \underline{\epsilon}_r)^{-1}$,

$$\underline{\mathbf{E}} = \frac{1}{\epsilon_0} \underline{\eta} \underline{\mathbf{D}}. \quad (3.4)$$

When using the principal-axes coordinate system, the impermeability tensor can conveniently be represented in diagonal form,

$$\begin{pmatrix} \underline{E}_x \\ \underline{E}_y \\ \underline{E}_z \end{pmatrix} = \frac{1}{\epsilon_0} \begin{pmatrix} \eta_{xx} & 0 & 0 \\ 0 & \eta_{yy} & 0 \\ 0 & 0 & \eta_{zz} \end{pmatrix} \begin{pmatrix} \underline{D}_x \\ \underline{D}_y \\ \underline{D}_z \end{pmatrix} = \frac{1}{\epsilon_0} \begin{pmatrix} \frac{1}{n_1^2} & 0 & 0 \\ 0 & \frac{1}{n_2^2} & 0 \\ 0 & 0 & \frac{1}{n_3^2} \end{pmatrix} \begin{pmatrix} \underline{D}_x \\ \underline{D}_y \\ \underline{D}_z \end{pmatrix}. \quad (3.5)$$

Note that for arbitrary coordinate systems, Eq. (3.5) has to be transformed accordingly. Then the impermeability tensor cannot be represented by a diagonal matrix any more.

Biaxial, uniaxial, and isotropic crystals

Crystals can be classified according to the refractive indices that they exhibit for light polarized along the principal axes.

Biaxial crystals exhibit three different principal refractive indices, $n_1 \neq n_2 \neq n_3$ in Eq. (3.3).

Uniaxial crystals feature two orthogonal directions along which refractive indices are equal. These two indices are usually referred to as ordinary indices $n_o = n_1 = n_2$, whereas the third index is called the extraordinary index $n_e = n_3$. Uniaxial crystals exhibit a single axis with threefold, four-fold, or six-fold symmetry. The z -axis (axis along the extraordinary index) of an uniaxial crystal is called the optical axis. A crystal is said to be positive uniaxial for $n_e > n_o$ and negative uniaxial for $n_e < n_o$.

Isotropic crystals feature higher symmetry, e.g., due to a cubic unit cell. As a consequence, all three indices are equal and the medium is optically isotropic.

The form of the linear permeability tensor for each of the seven crystal classes is depicted in Fig. 3.1.

Index ellipsoid

Optical properties of an anisotropic medium can be described by a mathematical construct called the index ellipsoid or the optical indicatrix. The index ellipsoid is the quadratic representation of the dielectric impermeability tensor $\underline{\eta} = (\epsilon_0 \underline{\epsilon}_r)^{-1}$ and is defined by the relationship

$$\sum_{i,j} \eta_{ij} X_i X_j = 1, \quad (3.6)$$

where $i, j \in \{1, 2, 3\}$ and where X_1 , X_2 , and X_3 are associated with the x , y , and z -direction. When represented with respect to the principal axes of the crystal, the indicatrix assumes the simple representation

$$\frac{X_1^2}{n_1^2} + \frac{X_2^2}{n_2^2} + \frac{X_3^2}{n_3^2} = 1, \quad (3.7)$$

where the main axes of the ellipsoid are oriented along the coordinate axes, and where the principal refractive indices n_1 , n_2 , and n_3 represent the length of the main axes, see Fig. 3.2.

3.1.2 Wave propagation along a principal axis

Propagation of light in anisotropic crystals is complex to describe in the general case. However, things become relatively simple when considering a plane wave propagating along one of the principal axes of the crystal. We will first consider this case and then give an explanation on how to treat the general case in the next section. A more in-depth analysis of wave propagation in anisotropic crystals can be found in [26] and [8].

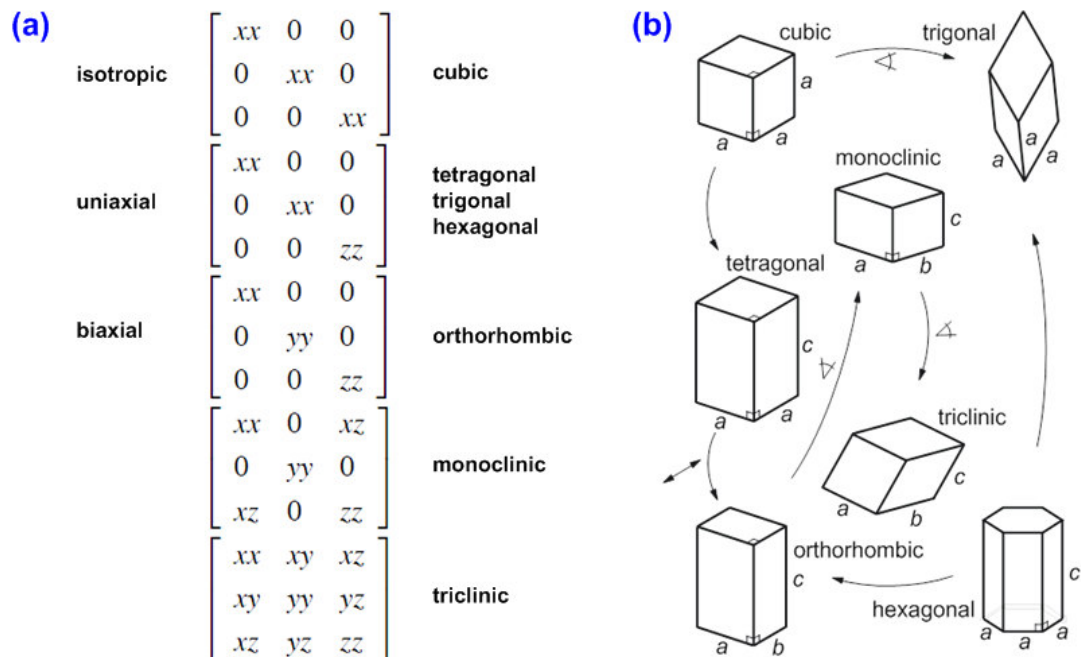


Figure 3.1: (a) General forms of linear permeability tensor ϵ_r for each of the seven crystal classes. Note that a representation of ϵ_r with respect to the coordinates of the unit cell has been chosen. For triclinic and monoclinic crystals, this leads to a non-diagonal representation of the permeability matrix, which can be brought to diagonal form by an appropriate coordinate transformation. (b) Hierarchy and general form of unit cells for the seven crystal classes. (Figure adapted from [6])

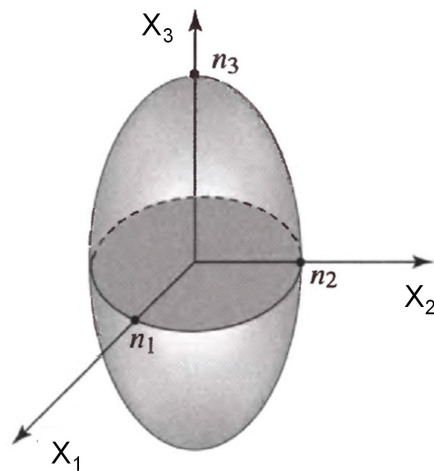


Figure 3.2: The index ellipsoid, also referred to as optical indicatrix of an anisotropic medium is the quadratic representation of the electric impermeability tensor with respect to the principal axes X_1 , X_2 , and X_3 of the crystal. The quantities n_1 , n_2 , and n_3 represent the principal refractive indices of the medium, i.e., the refractive index that is experienced by a plane wave which is linearly polarized along the respective principal axis and which propagates along another principal axis. (Figure adapted from [26])

Normal modes

If the light propagates along a principal axis X_i and if the electric field is oriented along another principal axis X_j , then the wave will propagate like a plane wave in an isotropic medium and experience the refractive index n_j that is associated with the second axis, $k_j = n_j k_0$. These waves are also referred to as normal modes; they maintain their optical polarizations and wavenumbers during propagation. Propagation of normal modes in an anisotropic medium is illustrated in Fig. 3.3 (a).

Polarization along arbitrary direction

Conversely, if a wave propagates along one principal axis, e.g., the z -axis, but is linearly polarized along an arbitrary direction in the (x, y) -plane, then we have to take into account that different components of the wave experience different refractive indices and hence travel at different propagation constants. In particular, the wave can be decomposed into a superposition of two linearly polarized waves, for each of which the electric field is oriented along a principal axis of the crystal. These waves can be considered as normal modes and preserve their optical polarizations and wavenumbers during propagation. However, they will propagate with different wavenumbers $k_1 = k_0 n_1$ and $k_2 = k_0 n_2$, thereby accumulating a steadily increasing phase difference during propagation along z ,

$$\Delta\Phi = -k_0 (n_2 - n_1) z. \quad (3.8)$$

This so-called phase retardation will lead to a continuous change of the state of polarization during propagation along z , converting the wave from linear polarization state to an elliptical, circular or another linear polarization state, see illustration in Fig. 3.3 (b).

3.1.3 Wave propagation in arbitrary direction

We now consider the case of a plane wave traveling in an anisotropic crystal in an arbitrary direction defined by the wave vector \mathbf{k} . In the following, the notion “plane wave” denotes an electromagnetic field configuration, for which the phase fronts are planes. In anisotropic media, that does not imply that the electric field vector lies completely within this plane. To understand this better, let us first revisit some fundamental properties of plane waves in isotropic materials and see how they change due to the anisotropy of the material.

Wavefronts and energy transport vector

In isotropic materials, the vectorial amplitudes of the electric displacement $\underline{\mathbf{D}}$ and the electric field $\underline{\mathbf{E}}$ are parallel, and the same applies to the magnetic flux density $\underline{\mathbf{B}}$ and the magnetic field $\underline{\mathbf{H}}$. The wave vector \mathbf{k} is parallel to the Poynting vector $\underline{\mathbf{S}} = \frac{1}{2}(\underline{\mathbf{E}} \times \underline{\mathbf{H}}^*)$, which denotes the direction of power flux. Moreover, the wave vector \mathbf{k} , the electric field amplitude $\underline{\mathbf{E}}$, and the magnetic field amplitude $\underline{\mathbf{H}}$ are mutually orthogonal and form a right-handed system.

In contrast to that, $\underline{\mathbf{D}}$ and $\underline{\mathbf{E}}$ are related by a matrix equation $\underline{\mathbf{D}} = \epsilon_0 \underline{\epsilon}_r \underline{\mathbf{E}}$, and are therefore not parallel in the general case of anisotropic media. As a consequence, the wave vector \mathbf{k} is only orthogonal to the electric displacement $\underline{\mathbf{D}}$, but generally not to the electric field $\underline{\mathbf{E}}$. Moreover, \mathbf{k} is not anymore parallel to the Poynting vector $\underline{\mathbf{S}} = \frac{1}{2}(\underline{\mathbf{E}} \times \underline{\mathbf{H}}^*)$. In other words: Only the electric displacement $\underline{\mathbf{D}}$ is parallel to the phase fronts of the wave while the electric field $\underline{\mathbf{E}}$ is not, and only the wave vector \mathbf{k} is orthogonal to the phase fronts of the wave, while power flux $\underline{\mathbf{S}}$ is not, see Fig. 3.4. The quantities $(\mathbf{k}, \underline{\mathbf{D}}, \underline{\mathbf{H}})$ are mutually orthogonal and form a right-handed set.

Determining normal modes from the index ellipsoid

To describe propagation of waves with arbitrary polarization in an arbitrary direction, we must again decompose the incoming wave into two normal modes, each of which propagates without changing the associated field amplitudes. The normal modes can be constructed by using the

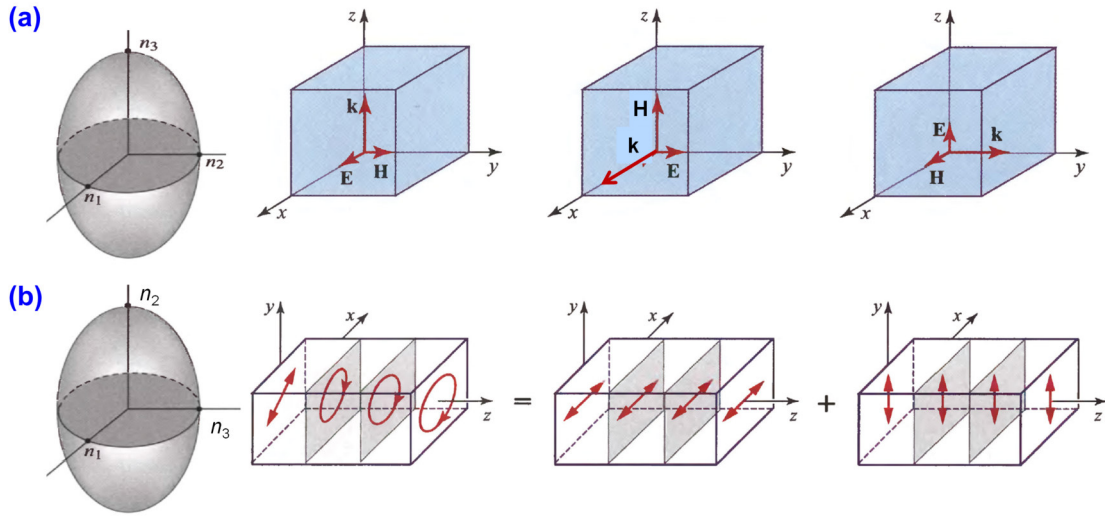


Figure 3.3: Wave propagation in anisotropic crystals. The x -, y -, and z -axis of the laboratory coordinate system are oriented along the main axes X_1 , X_2 , and X_3 of the crystal, respectively. (a) Propagation of normal modes along a principal axis X_i while being linearly polarized along a different principal axis X_j . The waves behave like a plane wave in an isotropic medium and experience the refractive index n_j that is associated with the polarization direction. (b) Propagation along a principal axis that is associated with the z -direction, while initially being linearly polarized along an arbitrary direction in the (x, y) -plane. The wave can be decomposed into a superposition of two linearly polarized normal modes, for each of which the electric field is oriented along a principal axis of the crystal. The normal modes hence propagate with different wavenumbers $k_1 = k_0 n_1$ and $k_2 = k_0 n_2$, thereby accumulating a steadily increasing phase difference which leads to a continuous change of the polarization state. (Figure adapted from [26])

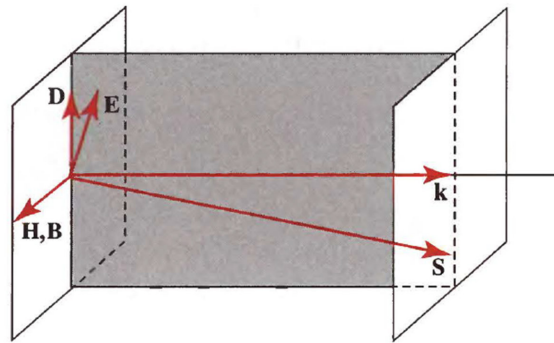


Figure 3.4: In a general anisotropic medium, the electric displacement \mathbf{D} and the electric field \mathbf{E} are not parallel, and the same applies to the wave vector \mathbf{k} and the Poynting vector \mathbf{S} . The electric displacement \mathbf{D} as well as the magnetic flux density \mathbf{B} and the magnetic field \mathbf{H} are parallel to the phase fronts, which are orthogonal to the wave vector \mathbf{k} . The quantities $(\mathbf{k}, \mathbf{D}, \mathbf{H})$ are mutually orthogonal and form a right-handed set. (Figure adapted from [26])

index ellipsoid introduced in Section 3.1.1. To understand this, let us have a short look at the wave equation in anisotropic media.

We start from Maxwell's curl equations for the complex time-domain amplitudes of the electric field $\underline{\mathbf{E}}$, the electric displacement $\underline{\mathbf{D}}$, and the magnetic field $\underline{\mathbf{H}}$ and use a plane-wave ansatz of the form

$$\underline{\mathbf{E}} = \underline{\mathbf{E}}_0 e^{-j\mathbf{k}\mathbf{r}} \quad \underline{\mathbf{H}} = \underline{\mathbf{H}}_0 e^{j\mathbf{k}\mathbf{r}} \quad \underline{\mathbf{D}} = \underline{\mathbf{D}}_0 e^{-j\mathbf{k}\mathbf{r}}. \quad (3.9)$$

This leads to

$$-j\mathbf{k} \times \underline{\mathbf{E}} = -j\omega\mu_0\underline{\mathbf{H}}, \quad (3.10)$$

$$-j\mathbf{k} \times \underline{\mathbf{H}} = j\omega\underline{\mathbf{D}}. \quad (3.11)$$

where $\underline{\mathbf{D}}$ and $\underline{\mathbf{E}}$ are linked by

$$\underline{\mathbf{E}} = \frac{1}{\epsilon_0} \underline{\boldsymbol{\eta}} \underline{\mathbf{D}}. \quad (3.12)$$

Inserting Eq. (3.11) in (3.10) and using Eq. (3.12) we obtain

$$-\mathbf{k} \times (\mathbf{k} \times (\underline{\boldsymbol{\eta}} \underline{\mathbf{D}})) = k_0^2 \underline{\mathbf{D}}. \quad (3.13)$$

Using the identity $\mathbf{A} \times \mathbf{B} \times \mathbf{C} = \mathbf{B} (\mathbf{A}^T \mathbf{C}) - \mathbf{C} (\mathbf{A}^T \mathbf{B})$, multiplying the entire relation with $\underline{\mathbf{D}}^T$ from the right, and exploiting the fact that $\underline{\mathbf{D}}^T \mathbf{k} = \mathbf{k}^T \underline{\mathbf{D}} = 0$, we derive the equation

$$\underline{\mathbf{D}}^T \underline{\boldsymbol{\eta}} \underline{\mathbf{D}} = \frac{k_0^2}{\mathbf{k}^T \mathbf{k}} \underline{\mathbf{D}}^T \underline{\mathbf{D}}. \quad (3.14)$$

We now make use of the principal-axis representation of $\underline{\boldsymbol{\eta}}$ according to Eq. (3.5) to reformulate the relation as

$$\frac{X^2}{n_1^2} + \frac{Y^2}{n_2^2} + \frac{Z^2}{n_3^2} = 1 \quad (3.15)$$

where the quantities X , Y , and Z are given by

$$X = \frac{k}{k_0} \frac{D_x}{D}, \quad Y = \frac{k}{k_0} \frac{D_y}{D}, \quad Z = \frac{k}{k_0} \frac{D_z}{D}, \quad (3.16)$$

and where $k = \sqrt{\mathbf{k}^T \mathbf{k}}$ and $D = \sqrt{\underline{\mathbf{D}}^T \underline{\mathbf{D}}}$ denote the magnitude of the corresponding vector quantities. Equation (3.15) represents the index ellipsoid and can be interpreted as an implicit equation that relates the electric displacement vector $\underline{\mathbf{D}}$ to the corresponding propagation constant $k = nk_0$, where n denotes the effective refractive index that is associated with this wave. However, for a given wave vector \mathbf{k} , only distinct directions of the electric displacement $\underline{\mathbf{D}}$ correspond to plane waves for which definition of an effective refractive index makes sense.

If the direction $\mathbf{u} = \mathbf{k}/|\mathbf{k}|$ of the wave vector \mathbf{k} is known, we may construct the electric field $\underline{\mathbf{E}}$, the electric displacement $\underline{\mathbf{D}}$, the effective refractive index n , and the direction of power flux $\underline{\mathbf{S}}$ from the index ellipsoid, see Fig. 3.5 (a). Starting from the propagation direction \mathbf{u} , draw a plane normal to \mathbf{u} that contains the origin. The intersection of this plane with the index ellipsoid is called the index ellipse. The lengths of the major and minor half-axes of the index ellipse correspond to the effective refractive indices n_a and n_b of the two normal modes; the direction of the half axes are the directions of the associated electric displacement vectors $\underline{\mathbf{D}}_a$ and $\underline{\mathbf{D}}_b$, respectively. The displacement vectors $\underline{\mathbf{D}}_a$ and $\underline{\mathbf{D}}_b$ are orthogonal to each other. The directions of the corresponding magnetic fields $\underline{\mathbf{H}}_a$ and $\underline{\mathbf{H}}_b$ can be obtained by exploiting the fact that $(\mathbf{k}, \underline{\mathbf{D}}, \underline{\mathbf{H}})$ are mutually orthogonal and form a right-handed set even for anisotropic media. More details on the derivation of this method can be found in [8] and [17].

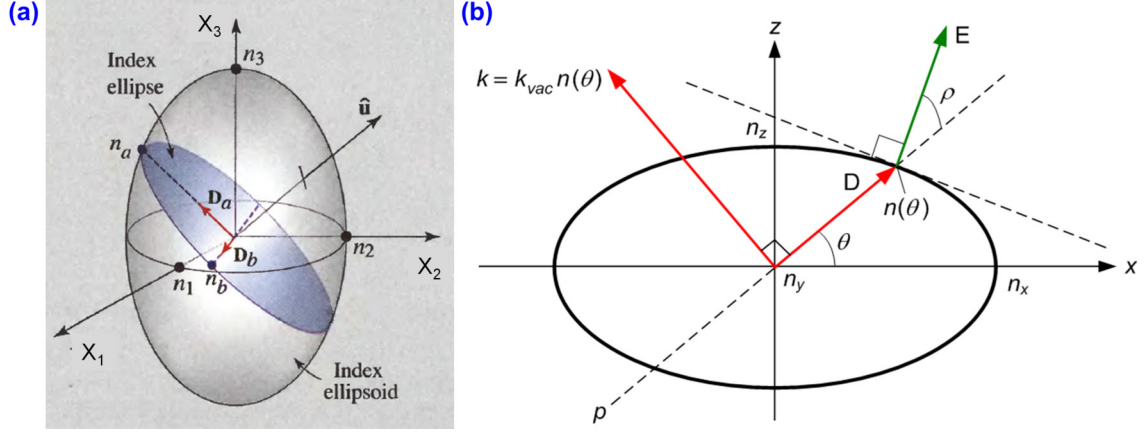


Figure 3.5: Propagation of plane waves in a general anisotropic medium. (a) Construction of the normal modes for a known direction $\mathbf{u} = \mathbf{k}/|\mathbf{k}|$ of the wave vector \mathbf{k} : First we draw a plane normal to \mathbf{u} that contains the origin. The intersection of this plane with the index ellipsoid defines the index ellipse. The major and minor half-axes of the index ellipse define the effective refractive indices n_a and n_b of the two normal modes and the directions of the associated electric displacement vectors \mathbf{D}_a and \mathbf{D}_b . (b) Construction of the electric field vector \mathbf{E} of a normal mode: The direction of the electric field \mathbf{E} is given by the surface normal of the index ellipsoid in the intersection point with the electric displacement \mathbf{D} . (Figure adapted from [26])

We may also derive the directions of the electric field \mathbf{E} from the index ellipsoid. To understand this, let us consider again Eq. (3.15), which represents an implicit equation for the index ellipsoid. The gradient of the left-hand side of Eq. (3.15) with respect to X , Y , and Z is hence associated with the surface-normal direction \mathbf{n} of the index ellipsoid. Using Eq. (3.16) we can show that the direction of the electric field \mathbf{E} is given by the surface normal \mathbf{n} ,

$$\mathbf{n} = \text{grad} \left(\frac{X^2}{n_1^2} + \frac{Y^2}{n_2^2} + \frac{Z^2}{n_3^2} \right) = 2 \begin{pmatrix} \frac{X}{n_1^2} \\ \frac{Y}{n_2^2} \\ \frac{Z}{n_3^2} \end{pmatrix} = \frac{2k}{k_0 D} \begin{pmatrix} \frac{D_x}{n_1^2} \\ \frac{D_y}{n_2^2} \\ \frac{D_z}{n_3^2} \end{pmatrix} = \frac{2k\epsilon_0}{k_0 D} \mathbf{E}. \quad (3.17)$$

In other words: The surface normal of the index ellipsoid is associated with the electric field \mathbf{E} , see Fig. 3.5 (b) for an illustration.

Example: Uniaxial crystal For uniaxial crystals $n_1 = n_2 = n_o$ and $n_3 = n_e$, i.e., the index ellipsoid is rotationally symmetric with respect to the Z -axis. For $n_e < n_o$, the medium is referred to as a negative uniaxial material, for $n_e > n_o$, it is called positive uniaxial. For wave propagation along the optical axis, which is associated with the Z -direction, the two normal modes experience identical refractive indices and the material behaves like an isotropic medium, see Fig. 3.6 (a). For propagation in arbitrary direction, the coordinate system can always be chosen such that the wave vector \mathbf{k} lies in the (Y, Z) -plane and defines an angle θ with the Z -axis, Fig. 3.6 (b). The index ellipse has then one half-axis of length n_o , which is independent of θ , whereas the length $n_e(\theta)$ of the other half axis depends on θ according to the relation

$$\frac{1}{n_e^2(\theta)} = \frac{\cos^2(\theta)}{n_o^2} + \frac{\sin^2(\theta)}{n_e^2}. \quad (3.18)$$

The normal modes hence have effective refractive indices $n_a = n_o$ and $n_b = n_e(\theta)$. The first mode is referred to as the ordinary wave, whereas that the second mode is often referred to as the extraordinary wave even though it does not experience the intrinsic extraordinary index n_e of

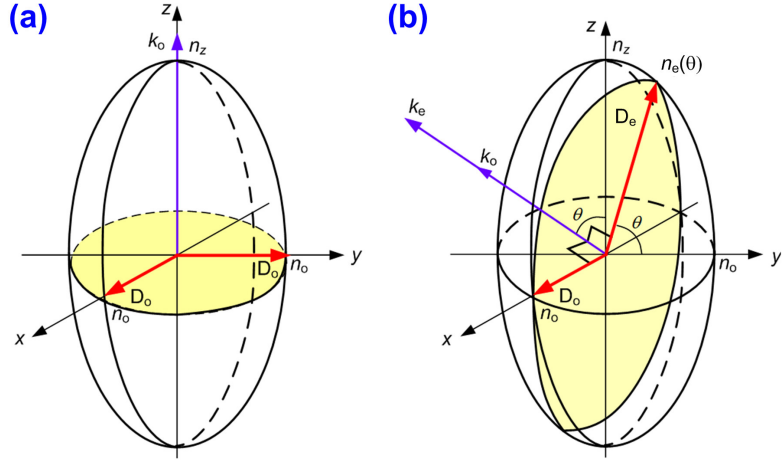


Figure 3.6: Wave propagation in uniaxial crystals. (a) For uniaxial crystals $n_1 = n_2 = n_o$ and $n_3 = n_e$, and the index ellipsoid is rotationally symmetric with respect to the Z -axis (“optical axis”). For wave propagation along the optical axis, the two normal modes experience identical refractive indices and the material behaves like an isotropic medium. (b) For propagation in arbitrary direction, the coordinate system can always be chosen such that the wave vector \mathbf{k} lies in the (Y, Z) -plane and defines an angle θ with the optical axis. Wave propagation can then be described by a superposition of two normal modes, one of which experiences the ordinary refractive index n_o , whereas the other experiences the angle-dependent extraordinary refractive index $n_e(\theta)$. The angle-dependent extraordinary refractive index $n_e(\theta)$ seen by the wave ranges between the ordinary and the extraordinary index of the material, i.e., $n_o < n_e(\theta) < n_e$ for positive uniaxial crystals. (Figure adapted from [26])

the anisotropic material, but rather the angle-dependent extraordinary index $n_e(\theta)$, which ranges between n_e and n_o . The electric displacement $\mathbf{D}_a = \mathbf{D}_o$ of the ordinary mode is parallel to the corresponding electric field vector \mathbf{E}_a and perpendicular to the plane that is defined by the optical axis (Z -axis) and the direction \mathbf{k} of propagation, i.e., the (Y, Z) -plane. For the extraordinary mode, the electric displacement $\mathbf{D}_b = \mathbf{D}_e$ is normal to \mathbf{k} and lies in the (Y, Z) -plane. Note that the corresponding electric field \mathbf{E}_b is not parallel to \mathbf{D}_b .

The walk-off angle ρ between the electric field \mathbf{E}_b and the electric displacement \mathbf{D}_b of the extraordinary mode is identical to the angle between the wave vector \mathbf{k} and the Poynting vector $\mathbf{S}_b = \frac{1}{2}(\mathbf{E}_b \times \mathbf{H}_b^*)$ of the extraordinary mode and can be calculated from the relation

$$\cos(\rho) = \frac{\mathbf{E}_b^T \mathbf{D}_b}{|\mathbf{E}_b| |\mathbf{D}_b|} = \frac{n_e^2 \cos^2(\theta) + n_o^2 \sin^2(\theta)}{\sqrt{n_e^4 \cos^2(\theta) + n_o^4 \sin^2(\theta)}}. \quad (3.19)$$

This relation can be re-written as

$$\rho = \mp \theta \pm \arctan\left(\frac{n_o^2}{n_e^2} \tan(\theta)\right), \quad (3.20)$$

where the upper signs are to be used for negative uniaxial crystals and the lower signs for positive uniaxial crystals.

3.2 Linear electro-optic effect (Pockels effect)

3.2.1 Mathematical description

If an electro-optic material is exposed to a static or low-frequency electric field $\mathbf{E}(t)$, the index ellipsoid is changed by nonlinear interaction. In an arbitrary coordinate system, the index ellipsoid

can be expressed in the form

$$\left(\frac{1}{n^2}\right)_1 X^2 + \left(\frac{1}{n^2}\right)_2 Y^2 + \left(\frac{1}{n^2}\right)_3 Z^2 + 2\left(\frac{1}{n^2}\right)_4 YZ + 2\left(\frac{1}{n^2}\right)_5 XZ + 2\left(\frac{1}{n^2}\right)_6 XY = 1, \quad (3.21)$$

where the elements of the impermeability tensor $\boldsymbol{\eta}$ are denoted as $\eta_{ij} = (1/n^2)_h$ according to the assignment

$$\begin{array}{ccccc} ij & 11 & 22 & 33 & 23, 32 & 13, 31 & 12, 21 \\ h & 1 & 2 & 3 & 4 & 5 & 6 \end{array} . \quad (3.22)$$

In a general approach, the elements η_{ij} of the impermeability tensor can be expressed as a power series in the strength of the components $E_k(t)$ of the modulating low-frequency electric field,

$$\eta_{ij} = \eta_{ij}^{(0)} + \sum_k r_{ijk} E_k + \sum_{k,l} s_{ijkl} E_k E_l + \dots \quad (3.23)$$

In this relation, the tensor r_{ijk} describes the coefficient of linear electro-optic effect, whereas s_{ijkl} represents the coefficient of the so-called quadratic electro-optic effect. For lossless media, the components η_{ij} of the impermeability tensor are real and symmetric, and the electro-optic tensor r_{ijk} must hence be symmetric in its first two indices i and j . The third-rank tensor r_{ijk} may then be expressed as a two-dimensional matrix r_{hk} using contracted notation with the assignment set forward in Eq. (3.22). Neglecting second- and higher-order effects in Eq. (3.23), the change of the impermeability tensor elements can then be written as a matrix equation,

$$\begin{pmatrix} \Delta(1/n^2)_1 \\ \Delta(1/n^2)_2 \\ \Delta(1/n^2)_3 \\ \Delta(1/n^2)_4 \\ \Delta(1/n^2)_5 \\ \Delta(1/n^2)_6 \end{pmatrix} = \begin{pmatrix} r_{11} & r_{12} & r_{13} \\ r_{21} & r_{22} & r_{23} \\ r_{31} & r_{32} & r_{33} \\ r_{41} & r_{42} & r_{43} \\ r_{51} & r_{52} & r_{53} \\ r_{61} & r_{62} & r_{63} \end{pmatrix} \begin{pmatrix} E_1 \\ E_2 \\ E_3 \end{pmatrix}. \quad (3.24)$$

The quantities r_{hk} are hence a measure on how strongly the impermeability tensor elements depend on the externally applied electric field. In analogy to the nonlinear susceptibility tensor, the form of the electro-optic tensor r_{hk} is restricted by the symmetry of the underlying crystal lattice. The forms of the electro-optic tensors for a few selected crystal classes are given in Fig. 3.7 along with numerical values for a selection of electro-optic materials [9]. A complete list of tensor forms for all crystal symmetry classes can be found in [32].

3.2.2 Electro-optic modulators

Electro-optic modulators exploit second-order nonlinearities to modulate a beam of light by means of an electric signal. A voltage $u(t)$ applied to the device leads to a modulating electric field \mathbf{E}_{mod} within the electro-optic material and thereby changes the indicatrix of the medium. For so-called longitudinal modulators, the electric field \mathbf{E}_{mod} is applied parallel to the direction of light propagation, whereas in transverse modulators, \mathbf{E}_{mod} is perpendicular to the direction of light propagation, see Fig. 3.8. In the following sections, we will investigate the two types of modulators in more detail. For simplicity, we consider the modulating electric field to be static unless otherwise stated. This is a valid approximation for low modulation speeds, i.e., if \mathbf{E}_{mod} does not change considerably during the time that the light interacts with the electro-optic material. For high-speed modulators, however, it is necessary to take into vector account the time dependence of the modulating field.

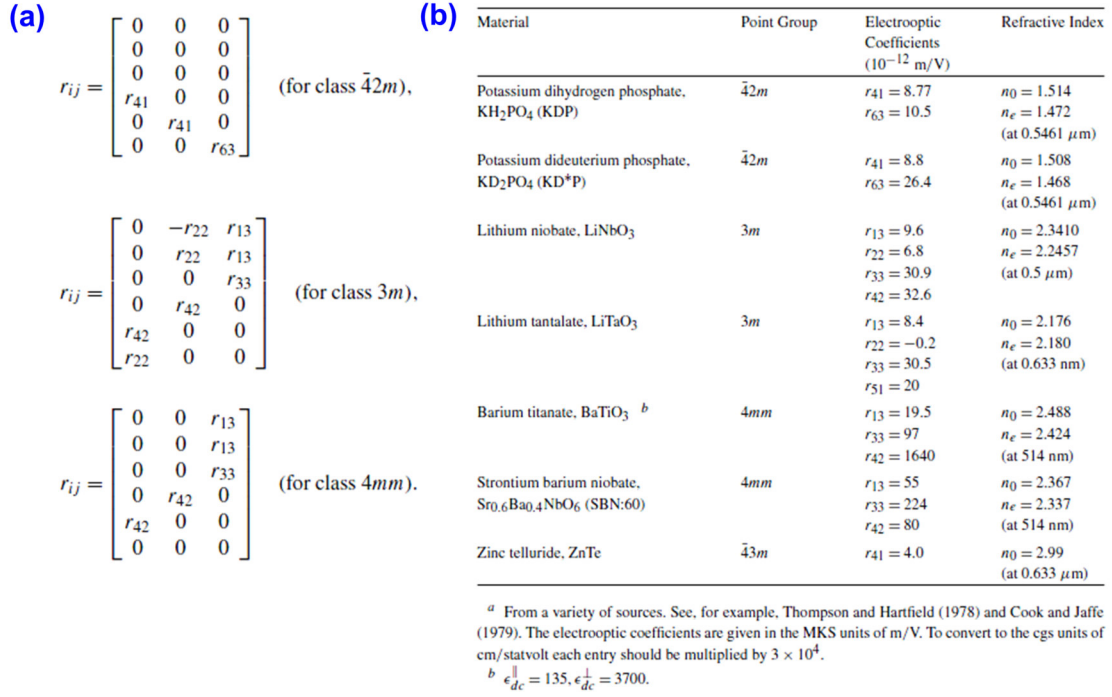


Figure 3.7: (a) Typical form of the electro-optic tensor r_{hk} for different crystal classes. (b) Electro-optic coefficients for selected materials. Note that Zinc telluride (ZnTe) possesses a cubic lattice, which features an isotropic linear permeability tensor, see Fig. 3.1 that corresponds to a refractive index of $n = 2.99$. The corresponding electro-optic tensor has only one degree of freedom, $r_{41} = r_{52} = r_{63}$, whereas all other elements vanish [32]. (Figures adapted from [9])

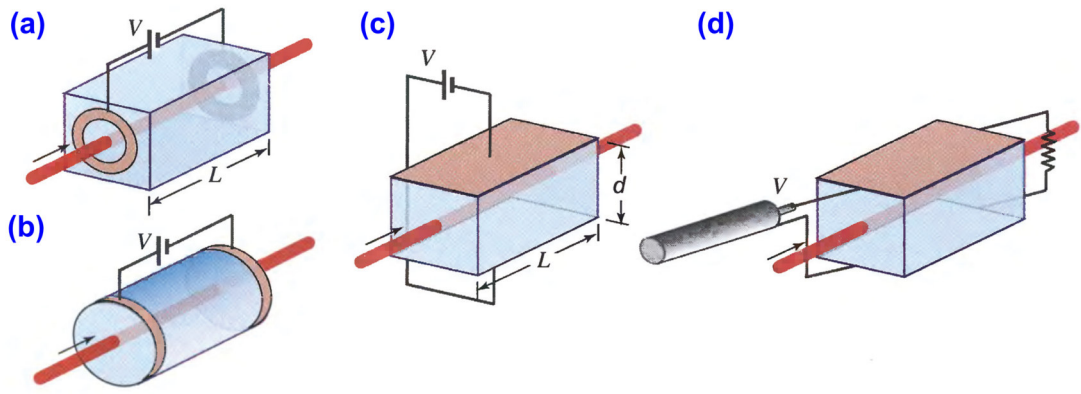


Figure 3.8: Basic concepts of electro-optic modulators (a), (b) Longitudinal modulators: The modulating electric field \mathbf{E}_{mod} is applied parallel to the direction of light propagation. (c), (d) Transverse modulators: \mathbf{E}_{mod} is perpendicular to the direction of light propagation (Figures adapted from [26])

Longitudinal modulators

As an example for a longitudinal modulator, let us assume that potassium dihydrogen phosphate (KH_2PO_4), also referred to as KDP (Kalimudihydrogenphosphat), is used as an electro-optic material. KDP belongs to point group $\bar{4}2m$, and the analysis is formally identical to that of other materials of the same group, such as potassium dideuterium phosphate (KD_2PO_4 ; D denotes deuterium; short name KD^*P) or ammonium dihydrogen phosphate ($\text{NH}_4\text{H}_2\text{PO}_4$; short name ADP). The electro-optic tensor of these materials is given by

$$\mathbf{r} = \begin{pmatrix} 0 & 0 & 0 \\ 0 & 0 & 0 \\ 0 & 0 & 0 \\ r_{41} & 0 & 0 \\ 0 & r_{41} & 0 \\ 0 & 0 & r_{63} \end{pmatrix} \quad (3.25)$$

These materials are uniaxial and the impermeability tensor can be written as

$$\boldsymbol{\eta} = \begin{pmatrix} \frac{1}{n_o^2} & 0 & 0 \\ 0 & \frac{1}{n_o^2} & 0 \\ 0 & 0 & \frac{1}{n_e^2} \end{pmatrix}, \quad (3.26)$$

where n_o denotes the ordinary and n_e the extraordinary refractive index. For an externally applied modulating field \mathbf{E}_{mod} , the optical indicatrix of the material can be written as

$$\frac{X^2 + Y^2}{n_o^2} + \frac{Z^2}{n_e^2} + 2r_{41}E_xYZ + 2r_{41}E_yXZ + 2r_{63}E_zXY = 1, \quad (3.27)$$

where E_x , E_y , and E_z denote the vector components of \mathbf{E}_{mod} ,

$$\mathbf{E}_{\text{mod}} = \begin{pmatrix} E_x \\ E_y \\ E_z \end{pmatrix}. \quad (3.28)$$

In the general case, this indicatrix belongs to a biaxial optical medium, i.e., by applying a modulating field to an uniaxial crystal, we break its symmetry and turn it into a biaxial material.

Let us now consider the case where light propagates in z -direction, and where the modulating field only has a z -component ($E_x = E_y = 0$), Fig. 3.9. The index ellipsoid can then be written as

$$\frac{X^2 + Y^2}{n_o^2} + \frac{Z^2}{n_e^2} + 2r_{63}E_zXY = 1. \quad (3.29)$$

To analyze light propagation, we seek for a transformation of (X, Y, Z) to the coordinate system (X', Y', Z') that corresponds to the principal axes of the index ellipsoid according to Eq. (3.29). The coordinate system (X', Y', Z') is obtained by calculating the eigenvectors of the corresponding impermeability tensor

$$\boldsymbol{\eta}(E_z) = \begin{pmatrix} \frac{1}{n_o^2} & r_{63}E_z & 0 \\ r_{63}E_z & \frac{1}{n_o^2} & 0 \\ 0 & 0 & \frac{1}{n_e^2} \end{pmatrix}, \quad (3.30)$$

and is related to (X, Y, Z) by

$$\begin{aligned} X &= \frac{1}{\sqrt{2}}(X' + Y'), \\ X &= \frac{1}{\sqrt{2}}(-X' + Y'), \\ Z &= Z'. \end{aligned} \quad (3.31)$$

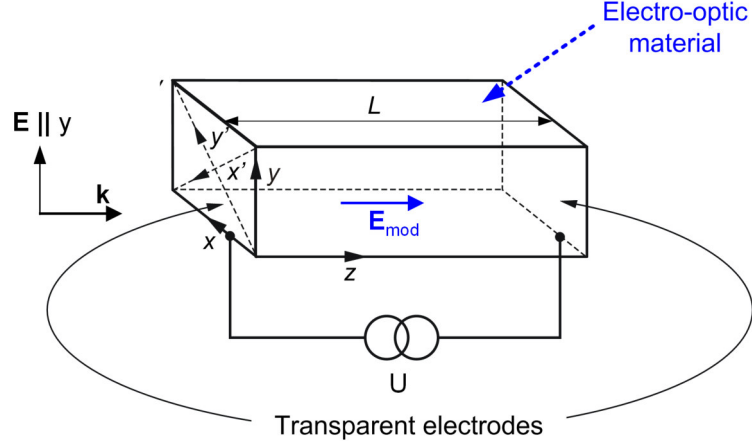


Figure 3.9: Longitudinal modulator, also referred to as Pockels cell: Light propagates in z -direction, and transparent electrodes are used to apply the modulating field in z -direction as well, $\mathbf{E}_{\text{mod}} = E_z \mathbf{e}_z$, where $E_z = U/L$ and where \mathbf{e}_z denotes the unit vector in z -direction. For uniaxial crystals of point group $\bar{4}2m$ such as KDP, KD*P, and ADP, the index ellipsoid is rotationally symmetric about the z -axis for zero modulation voltage U . For nonzero voltage, the rotational symmetry is broken and the material behaves like a biaxial crystal with main axes x' and y' that are rotated by 45° with respect to the axes x and y of the crystal coordinate system.

In other words: (X', Y', Z') is obtained from (X, Y, Z) by a rotation of the coordinate system by 45° about the z -axis, see Fig. 3.10 (a). The refractive indices associated with the principal axes X' , Y' , and Z' are obtained by inserting Eq. (3.31) in Eq. (3.29),

$$n_{x'} = n_o \left(1 + \frac{1}{2} r_{63} n_o^2 E_z \right), \quad (3.32)$$

$$n_{y'} = n_o \left(1 - \frac{1}{2} r_{63} n_o^2 E_z \right), \quad (3.33)$$

$$n_{z'} = n_e. \quad (3.34)$$

In the new coordinate system, the normal modes are simply plane waves polarized along the x' - and y' -direction and propagating in the z' -direction. After propagation through a crystal of length L , the two normal modes experience a relative phase delay of

$$\Delta\Phi = r_{63} n_o^3 E_z k_0 L = r_{63} n_o^3 k_0 U, \quad (3.35)$$

where $U = E_z L$ is the voltage applied to the device along the propagation direction. The crystal hence acts as a wave plate with a voltage-dependent phase delay. Such a device is also referred to as a Pockels cell.

Clearly, the voltage-dependent phase delay leads to a voltage-dependent change of the polarization state at the output of the device. A figure of particular importance is the so-called half-wave-voltage or π -voltage, for which a phase shift of $\Delta\Phi = \pi$ is obtained,

$$U_\pi = \frac{\lambda}{2r_{63}n_o^3}, \quad (3.36)$$

$$\Delta\Phi = \pi \frac{U}{U_\pi} \quad (3.37)$$

For the case of an longitudinal modulator, the π -voltage is independent of the device dimensions. For KDP with $r_{63} = 10.5 \text{ pm/V}$ and for a wavelength of $\lambda = 632.8 \text{ nm}$, a π -voltage of 8750 V

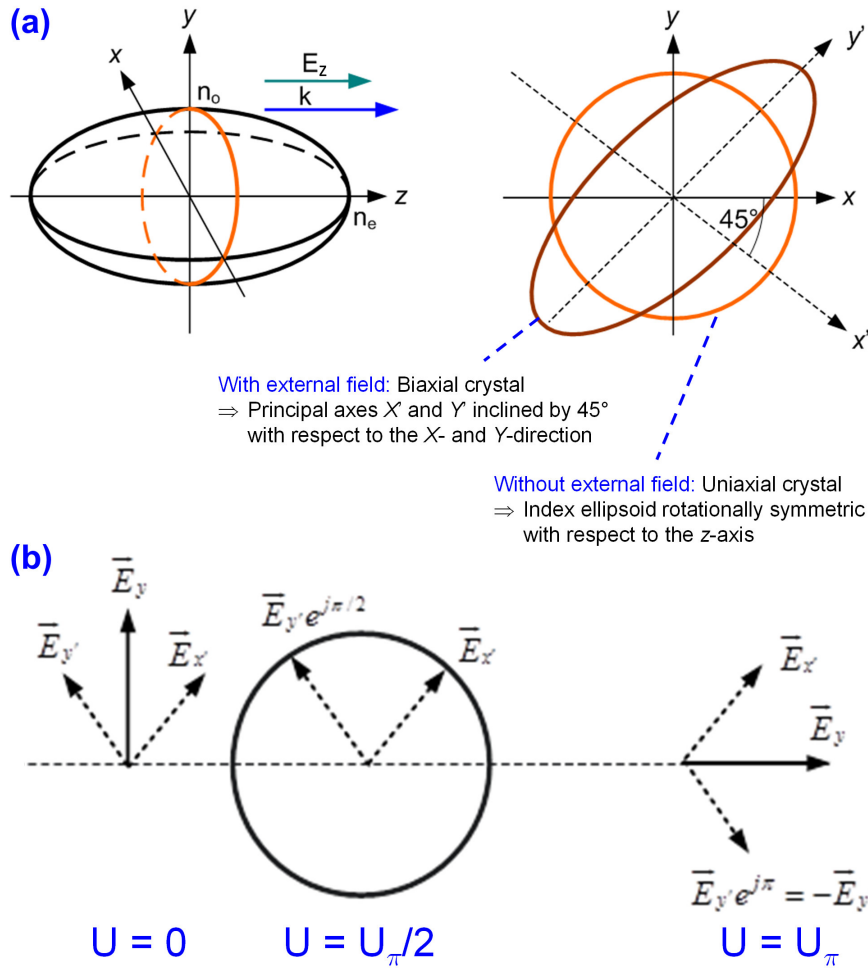


Figure 3.10: (a) Deformation of the index ellipsoid under the influence of an external electric field: For zero modulation voltage U , the index ellipsoid is rotationally symmetric about the z -axis. For nonzero voltage, the rotational symmetry is broken and the material behaves like a biaxial crystal with main axes x' and y' that are rotated by 45° with respect to the axes x and y of the crystal coordinate system. For an incident optical field that is polarized along the y -direction, this leads to a change of the polarization state while propagating along z . (b) Polarization rotation in a Pockels cell for different applied voltages. The incident field is polarized along the z -direction and can be decomposed in two normal modes of equal amplitude, polarized along x' and y' . For zero voltage $U = 0$, the relative phase between the two modes does not change and the polarization state is preserved during propagation. For $U = U_\pi/2$, the two modes accumulate a phase delay of $\pi/2$, which transforms the linear polarization into a circular polarization. For $U = U_\pi$, the phase delay amounts to π , which corresponds to a change in sign for the $E_{y'}$ -component relative to the $E_{x'}$ -component and hence to a rotation of the polarization by 90° .

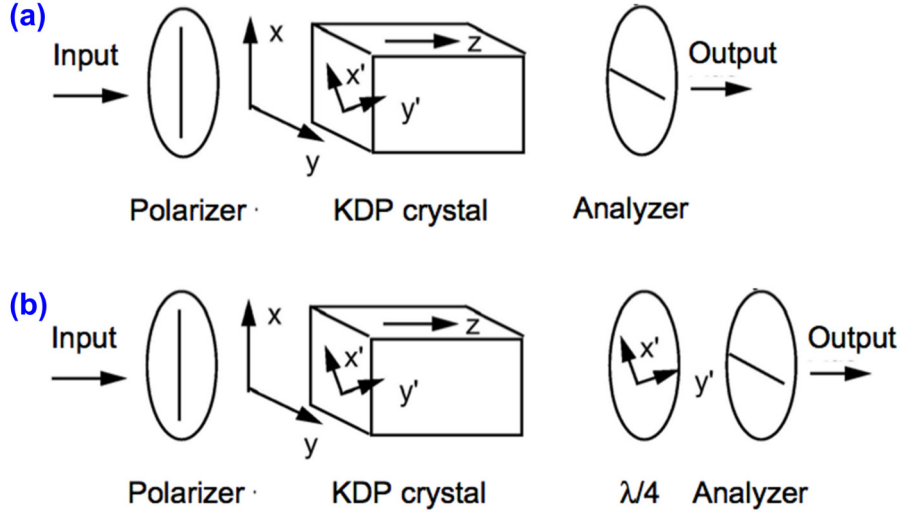


Figure 3.11: Amplitude modulators based on the Pockels cell. (a) Inserting a polarizer before and after the Pockels cell translates the polarization rotation into an amplitude modulation with a sinusoidal dependence of the amplitude transmission on the applied voltage U . (b) Inserting a quarter-wave plate allows to adjust the operation point of the modulator.

is found. Since it is technically demanding to generate broadband signals at such high voltages, Pockels-cell modulators are only used for low-frequency applications.

The phase delay $\Delta\Phi$ leads to a change of the polarization state can be translated into an amplitude modulation, see 3.10 (b). To understand this, let us consider the case where the incident wave is linearly polarized along the y -direction of the original coordinate system and hence rotated by 45° against the principal x' - and the y' -axes, see figure on slides. The incident field vector can be decomposed into x' - and y' - components of equal magnitude and phase. For $\Delta\Phi = 0$, the input polarization state remains unchanged, whereas for $\Delta\Phi = \pi$, the linear polarization is rotated by 90° , Fig. 3.10 (b). If a polarizer is inserted after the Pockels cell, this rotation can be translated into an amplitude modulation, see Fig. 3.11. If the voltage is continuously increased from 0 to U_π then the output wave changes its polarization state beginning from linear, to elliptic, circular, elliptic and finally back to linear. This leads to a sinusoidal dependence of the amplitude transmission function on the applied voltage U . In the configuration depicted in Fig. 3.11 (a), $U = 0$ corresponds to zero transmission, whereas $U = U_\pi$ leads to full transmission. The power transfer function $T(U) = P_{\text{out}}/P_{\text{in}}$ can then be written as

$$T(U) = \sin^2 \left(\frac{\pi U}{2 U_\pi} \right). \quad (3.38)$$

The operating point of the modulator can be changed by inserting an additional wave plate after the electro-optic crystal, see Fig. 3.11 (b). For a quarter-wave plate, the power transfer function can be written as

$$T(U) = \sin^2 \left(\frac{\pi U}{2 U_\pi} + \frac{\pi}{4} \right). \quad (3.39)$$

Transverse modulators

In transverse modulators, the electric field \mathbf{E}_{mod} is applied perpendicular to the direction of light propagation, see Fig. 3.12 (a). This allows partially to decouple the interaction length L from the

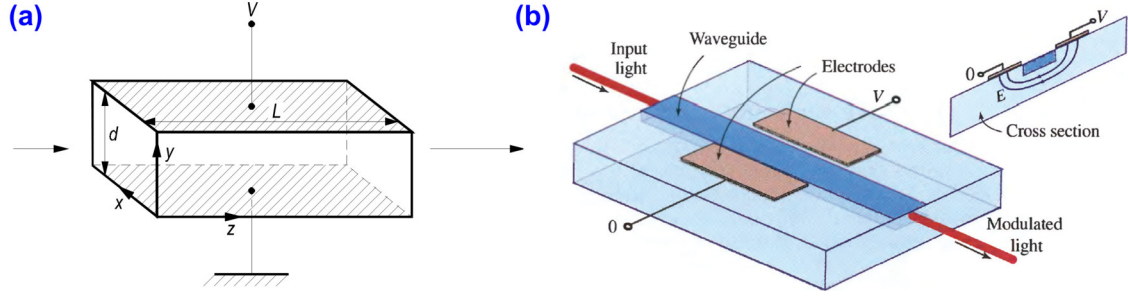


Figure 3.12: Transverse electro-optic modulator (a) Light propagating in the z -direction is modulated by an electric field perpendicular to it (b) Representation of on-chip implementation of a transverse electro-optic modulator (Figures adapted from [26])

spacing d of the electrodes and hence to decrease the modulation voltage that is needed to generate a certain electric field within the electro-optic material. Still, for “bulk” devices that consist of homogeneous electro-optic material, the light propagates through the modulator as a Gaussian beam, and both the minimum electrode spacing d and the maximum interaction length L are hence dictated by the beam parameters, in particular its divergence, which is linked to the beam diameter. To achieve low modulation voltages, it is hence necessary to use a waveguide-based device, where electrode spacings of the order of a few micrometers and interaction lengths of a few centimeters in range become possible, see Fig. 3.12 (b).

One of the most commonly used electro-optic modulator types is based on a lithium niobate (LiNbO_3) substrate and indiffused waveguides, where two fabrication methods are commonly used: Indiffusion of titanium Ti or proton exchange, see Fig. 3.13. For indiffusion of Ti, Fig. 3.13 (a), the metal is deposited on the surface of the wafer and patterned by lithography and etching. A subsequent thermal treatment at around $1000 - 1050^\circ\text{C}$ for several hours leads to indiffusion of Ti into the LiNbO_3 substrate, thereby causing a refractive index increase of around $\Delta n \approx 0.002 \dots 0.01$. Typical waveguide widths are $10 \mu\text{m}$. Due to the anisotropy of the lithium niobate crystal, the behavior of resulting integrated optical components shows a large polarization dependence. For proton exchange, Fig. 3.13 (b), an Al-mask is patterned on the surface of the substrate, and the wafer is then immersed in boiling benzoic acid ($200 - 240^\circ\text{C}$) for 2-4 hours. This leads to a substitution of Li^+ - by H^+ -ions. For the extraordinary polarization, the resulting $\text{Li}_{1-x}\text{H}_x\text{NbO}_3$ has a refractive index n_e which is higher than that of the surrounding LiNbO_3 by $\Delta n \approx 0.02 \dots 0.05$, whereas for the ordinary polarization, the index n_o is decreased, $\Delta n \approx -0.04$. As a consequence, this waveguide is only able to guide modes that are predominantly polarized along the z -direction, i.e., the direction along which the electric field of the optical mode experiences the extraordinary refractive index n_e .

To understand the principle of lithium niobate electro-optic modulators let us first consider the electro-optic tensor of the material in more detail. LiNbO_3 belongs to point group $3m$, and the electro-optic tensor has the form

$$\mathbf{r} = \begin{pmatrix} 0 & -r_{22} & r_{13} \\ 0 & r_{22} & r_{13} \\ 0 & 0 & r_{33} \\ 0 & r_{42} & 0 \\ r_{42} & 0 & 0 \\ -r_{22} & 0 & 0 \end{pmatrix}, \quad (3.40)$$

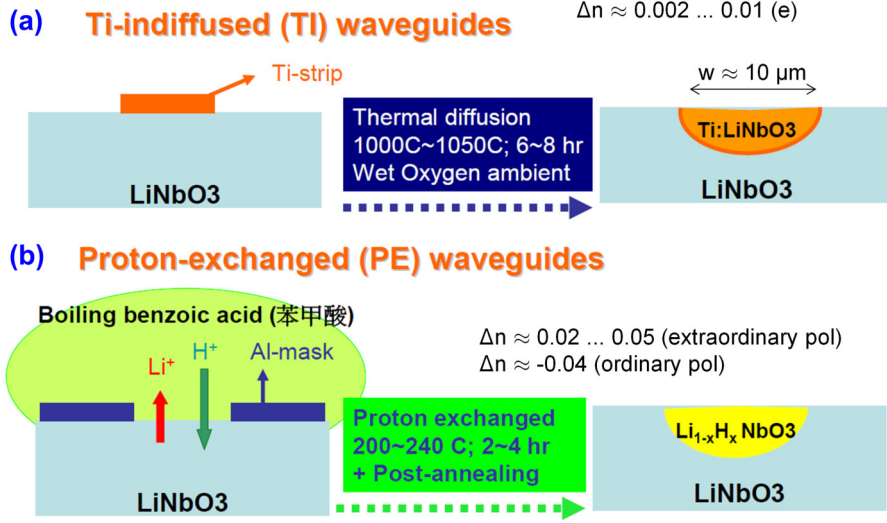


Figure 3.13: Fabrication of lithium niobate waveguides: (a) Indiffusion of titanium (Ti) under high temperatures; (b) “Proton-exchange”, substituting Li^+ by H^+ -ions. This leads to a refractive index increase for one polarization (extraordinary) and to a decrease for the other polarization (ordinary).

where

$$\begin{aligned} r_{13} &= 9.6 \frac{\text{pm}}{\text{V}} \\ r_{22} &= 6.8 \frac{\text{pm}}{\text{V}} \\ r_{33} &= 30.9 \frac{\text{pm}}{\text{V}} \\ r_{42} &= 32.6 \frac{\text{pm}}{\text{V}} \end{aligned}$$

at a wavelength of $0.5 \mu\text{m}$. If no external voltage is applied, the material is uniaxial and the impermeability tensor can be written as

$$\boldsymbol{\eta} = \begin{pmatrix} \frac{1}{n_o^2} & 0 & 0 \\ 0 & \frac{1}{n_o^2} & 0 \\ 0 & 0 & \frac{1}{n_e^2} \end{pmatrix}, \quad (3.41)$$

where $n_o = 2.3410$ is the ordinary and $n_e = 2.2457$ is the extraordinary refractive index, both measured at a wavelength of $0.5 \mu\text{m}$ [9]. At $1.55 \mu\text{m}$, the ordinary and the extraordinary indices are $n_o = 2.2111$ and $n_e = 2.13756$ respectively [33].

In current devices, efficient electro-optic interaction is achieved by orienting the modulating electric field and the electric field of the optical mode along the z -direction, thereby exploiting the large r_{33} coefficient. This is technically preferred to exploiting the r_{42} coefficient, which would change the impermeability tensor element $\eta_{23} = \eta_{32}$ and hence affect the y - and the z -polarization simultaneously. For a simplified quantitative analysis, let us consider a schematic device consisting of a rectangular block of the material, within which both the polarization direction of the optical wave light and the electric modulating field are applied along the z -direction, whereas light propagation is in y -direction, see Fig. 3.14. In the presence of the modulating field $\mathbf{E}_{\text{mod}} = E_z \mathbf{e}_z$, the indicatrix of the material can be written as

$$\left(\frac{1}{n_o^2} + r_{13} E_z \right) X^2 + \left(\frac{1}{n_o^2} + r_{13} E_z \right) Y^2 + \left(\frac{1}{n_e^2} + r_{33} E_z \right) Z^2 = 1. \quad (3.42)$$

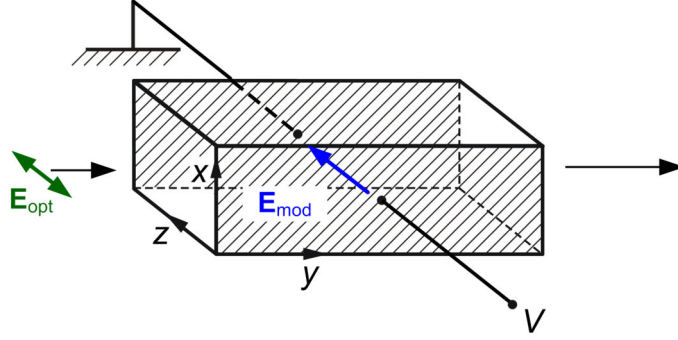


Figure 3.14: Simplified analysis of a transverse lithium niobate (LiNbO_3) modulator: Light propagates in y -direction. The electric field of the optical wave (\mathbf{E}_{opt}) and the electric modulating field (\mathbf{E}_{mod}) are both oriented along the z -direction, thereby exploiting the r_{33} -coefficient of the material.

For a plane wave polarized along the z -direction, the field induced index change is then found to be

$$\Delta n = -\frac{1}{2}n_e^3 r_{33} E_z. \quad (3.43)$$

The corresponding phase shift that a plane wave accumulates along the propagation distance L is given by

$$\Delta\Phi = \frac{1}{2}n_e^3 r_{33} E_z k_0 L, \quad (3.44)$$

where the modulating field E_z depends on the externally applied voltage U and the electrode separation d ,

$$E_z = \frac{U}{d}. \quad (3.45)$$

This leads to a π -voltage of

$$U_\pi = \frac{d}{L} \frac{\lambda_0}{r_{33} n_e^3}. \quad (3.46)$$

In contrast to the longitudinal modulator, the switching voltage can be considerably decreased by using a large device length L and a small electrode spacing d .

Even though these relationships have been derived for a rectangular block of bulk material, they can be qualitatively transferred to waveguide-based devices. Two distinct technical realizations are commonly used for LiNbO_3 modulators, see figures on slides:

z-cut geometry In the so-called z-cut geometry, the wafer surface is normal to the z -direction and the modulating field oriented vertically, i.e., along z -direction. The waveguide is oriented along the y -direction and operated in TM-polarization, i.e., the dominant electric field component of the optical mode is also oriented along z -direction. The phase shift can be estimated by using Eq. (3.44), where E_z denotes the z -component of the modulating field within the optical waveguide. A buffer layer of Al_2O_3 or SiO_2 prevents the optical field from interacting with the metal electrodes which would lead to pronounced optical loss.

x-cut geometry In the x-cut geometry, the wafer surface is normal to the x -direction while the modulating field is oriented horizontally along the z -direction. The waveguide is oriented

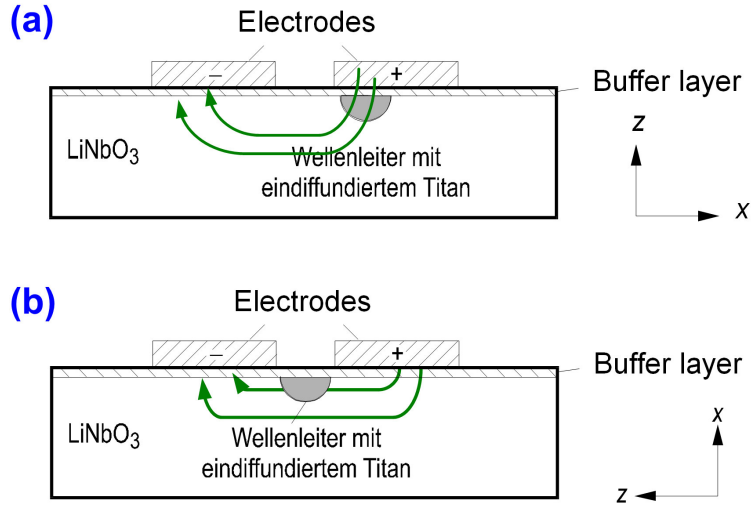


Figure 3.15: Technical realizations of lithium niobate (LiNbO_3) modulators. (a) z -cut geometry: The wafer surface is perpendicular to the z -direction. Within the waveguide core (depicted in grey), both the modulating electric field and the dominant electric field component of the optical mode must be oriented along the z -direction and are hence normal to the wafer surface as well. (b) x -cut geometry: The wafer surface is perpendicular to the x -direction. The modulating electric field and the dominant electric field component of the optical mode are still oriented along the z -direction, which is now parallel to the wafer surface. In both geometries, a buffer layer of Al_2O_3 or SiO_2 prevents the optical field from interacting with the metal electrodes which would lead to pronounced optical loss. (“Wellenleiter mit eindiffundiertem Titan” = Waveguide fabricated by indiffusion of titanium, see Fig. 3.13)

along the y -direction and operated in TE-polarization, i.e., the dominant electric field component of the optical mode is also oriented along the z -direction. The phase shift can again be estimated by using Eq. (3.44), where E_z denotes the z -component of the modulating field within the optical waveguide.

The configurations considered so far can generate a voltage-dependent phase shift in an optical waveguide and hence act as a phase modulator, Fig. 3.16 (a). This phase modulation can be transformed into an amplitude modulation by using an interferometric waveguide structure such as a Mach-Zehnder interferometer, see Fig. 3.16 (b). A Mach-Zehnder Modulator is said to operate in push-pull mode if the phases in both arms of the interferometer are modulated antisymmetrically, i.e., while one arm experiences a phase shift of $\Delta\Phi$, the other arm experiences a phase shift $-\Delta\Phi$ of the same magnitude and opposite sign. This leads to a pure amplitude modulation without any voltage-dependent phase change. The generated signal is then said to be chirp-free. Apart from push-pull devices, there are electro-optic modulators in so-called dual-drive or dual-electrode configuration, which allow individual control of the phase shift in each arm, see Fig. 3.16 (c). These devices allow for more complex signals, which might or might not exhibit a chirp.

Devices in push-pull-configuration can be realized by combining the optical waveguides with coplanar electric transmission lines, see Fig. 3.17. The crystal cut then affects both the modulator efficiency and the modulator chirp. In general, the advantage of a z -cut LiNbO_3 modulator is the high field density which results from the close distance between electrical and optical waveguide. Thus the operation voltages are rather small in comparison to those of x -cut devices. However, the z -cut modulator features an asymmetric structure: The center electrode (“hot electrode”) is placed on top of one waveguide, for which the modulating field is more concentrated, resulting in an improvement of the overlap between the modulating radio-frequency (RF) and the optical field, and hence in a higher modulation efficiency for this waveguide, Fig. 3.17 (a). At

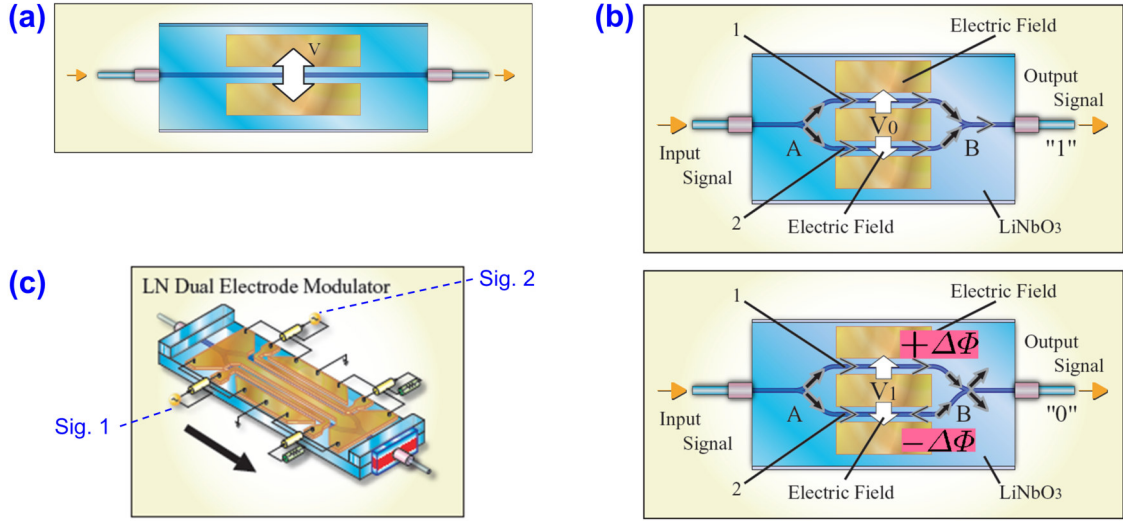


Figure 3.16: Lithium niobate (LiNbO_3) phase and amplitude modulators. (a) Pure phase modulator, consisting of a straight waveguide and two electrodes parallel to the waveguide. The signal at the output of the waveguide experiences a voltage-dependent phase shift. (b) Mach-Zehnder modulator in push-pull configuration: The modulating electric fields in the two interferometer arms are antiparallel, and hence they are modulated antisymmetrically, i.e., while one arm experiences a phase shift of $\Delta\Phi$, the other arm experiences a phase shift $-\Delta\Phi$ of the same magnitude and opposite sign. This leads to a pure amplitude modulation without any voltage-dependent phase change and hence generates a so-called chirp-free signal. (c) Dual-drive Mach-Zehnder modulator: Each arm comprises an individual transmission line, allowing for which allow individual control of the phase shift by two independent signals (Sig. 1, Sig. 2). (Figures adapted from [30])

the same time, the overlap between the modulating field and the optical mode at the ground electrode is reduced. The different overlap between the two waveguides for the z -cut structure results in a nonzero chirp, whereas the x -cut has almost zero chirp due to its symmetric structure, Fig. 3.17 (b). The asymmetry of z -cut push-pull modulators can be overcome by using dual-drive electrode configurations, see Fig. 3.18 (a): For this geometry, the modulating RF field shows very good overlap with the optical mode field, which leads to a small π -voltage of the device. To achieve push-pull-operation in this device, two two RF-signals of identical amplitude but opposite sign are needed. Even though the z -cut device is slightly more complex than the push-pull modulator in x -cut geometry, Fig. 3.18 (b), the better field overlap leads to operation voltages that lower than those of x -cut devices.

Modulation voltages can be decreased by using large interaction lengths in the centimeter range. For high-speed devices, it is then important to ensure that the optical wave and the modulating RF field co-propagate with the same velocity, resulting in so-called travelling-wave devices. Generally the effective refractive index of RF mode is bigger than that of the optical signal due to the large dielectric constant of lithium niobate at microwave frequencies. This can be overcome by, e.g., using thick coplanar electrodes along with a silicon dioxide buffer layer that separates the electrodes from the lithium niobate substrate, see [31] and the references therein for more details.

3.3 Phase matching for second-order nonlinear processes

In Section 1.4.3 we have used the slowly varying envelope approximation (SVEA) to describe the evolution of weakly time- and space-dependent complex field amplitudes during propagation through a nonlinear medium, Eq. (1.99). We found that, depending on the relative phase between

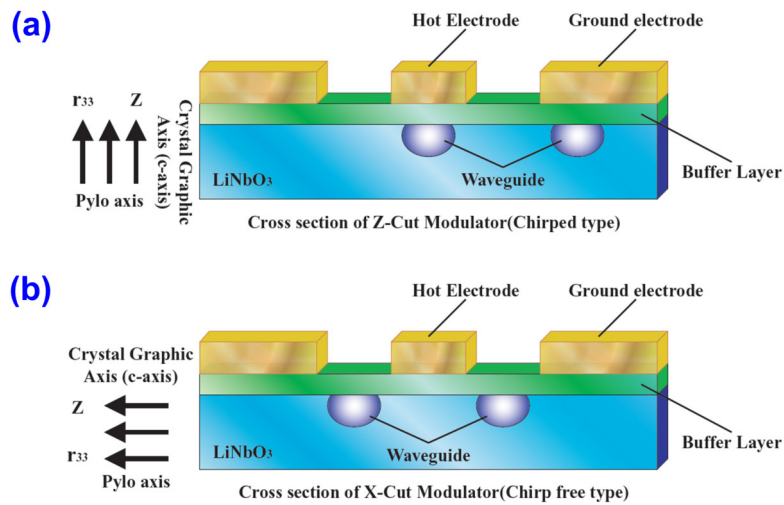


Figure 3.17: Lithium niobate (LiNbO_3) Mach-Zehnder modulators in push-pull configuration. (a) z -cut geometry: Electrodes are placed right above the optical waveguides such that the modulating field is oriented normal to the wafer surface within the waveguide core. For the center electrode (“hot electrode”), the electric field is concentrated to the optical waveguide, which leads to a strong overlap between the optical field and the RF field and hence to high modulation efficiency. For the ground electrodes, the overlap with the optical field is reduced. This leads to a lower modulation efficiency in the right-hand arm of the modulator and hence to asymmetric modulation. As a consequence, the output signal is not chirp-free. (b) x -cut geometry: Optical waveguides are placed in between the electrodes. In comparison with the z -cut geometry, this leads to a slightly decreased overlap of the modulating electric field and the optical mode, and hence to a smaller efficiency. However, since the efficiency is decreased in both arms simultaneously, modulation shows the same amplitude but opposite sign in both arms, thereby leading to perfect push-pull operation and hence unchirped output signals (Figures adapted from[30])

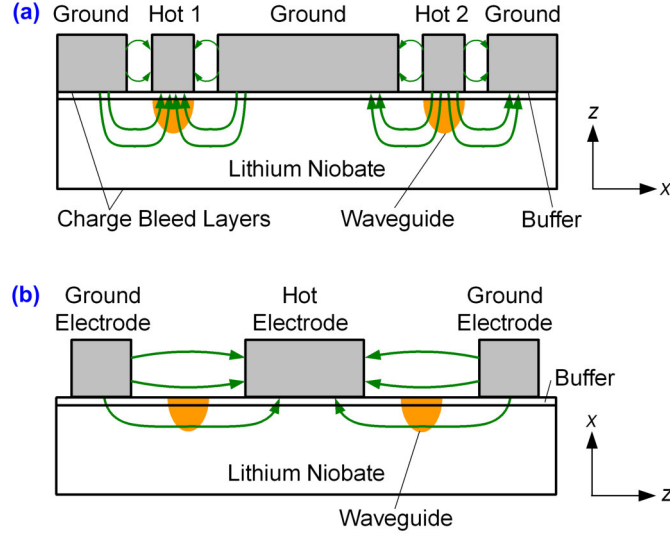


Figure 3.18: Two more examples of lithium niobate (LiNbO_3) Mach-Zehnder modulators. (a) Dual-drive modulator in z -cut geometry: The modulating radio-frequency (RF) field shows very good overlap with the optical mode field, which leads to a small π -voltage of the device. For push-pull-operation, two RF-signals of identical amplitude but opposite sign are needed. (b) Push-pull modulator in x -cut geometry: Due to the symmetry of the device, perfect antisymmetric push-pull operation is achieved with a single RF signal. However, the overlap between the modulation RF field and the optical mode is reduced in comparison with the z -cut geometry, which leads to operation voltages that are approximately 20% higher than those of z -cut devices.

the nonlinear polarization $\underline{P}_{\text{NL}}(z, t, \omega_l)$ and the electric field $\underline{E}(z, t, \omega_l)$, the signal experiences amplification, absorption or a phase shift. Proper phase matching is therefore of prime importance for efficient nonlinear interaction. In this section, we will investigate the impact of phase mismatch for the case of sum frequency generation (SFG) and second harmonic generation (SHG). Based on these investigations, we introduce different techniques to achieve phase matching - either by exploiting birefringence, or by so-called quasi-phase-matching techniques. In the following, we will use the retarded time frame (z', t') introduced by Eqs. (1.96) - (1.98), but omit the primes for the sake of readability.

3.3.1 Impact of phase mismatch on sum-frequency and second-harmonic generation

To understand the impact of phase mismatch on the nonlinear conversion efficiency, let us first consider the case of sum frequency generation. We assume two plane waves, oscillating at frequencies ω_1 and ω_2 , with wave vectors parallel to the z -direction, and consider the evolution of the sum-frequency component $\underline{\mathbf{E}}(z, t, \omega_3)$ along z . The waves do not necessarily need to have the same polarization, i.e., the slowly varying complex amplitude vectors $\underline{\mathbf{E}}(z, t, \omega_1)$ and $\underline{\mathbf{E}}(z, t, \omega_2)$ are in general not parallel. In analogy to Eqs. (1.99) and (1.102), we can describe the evolution of $\underline{\mathbf{E}}(z, t, \omega_3)$ by

$$\frac{\partial \underline{E}_q(z, t, \omega_3)}{\partial z} = -j \frac{\omega_3}{2cn(\omega_3)} \sum_{r,s} \chi_{q:r,s}^{(2)}(\omega_3 : \omega_1, \omega_2) \underline{E}_r(z, t, \omega_1) \underline{E}_s(z, t, \omega_2) e^{-j\Delta k z} \quad (3.47)$$

where $q, r, s \in \{x, y, z\}$ and where

$$\Delta k = k_1 + k_2 - k_3 \quad (3.48)$$

denotes the wave vector mismatch.

Effective value d_{eff} of the nonlinear susceptibility

For a fixed geometry, i.e., for fixed propagation and polarization directions, we can express the complex amplitude vectors $\underline{\mathbf{E}}(z, t, \omega_i)$ by

$$\underline{\mathbf{E}}(z, t, \omega_i) = \underline{E}(z, t, \omega_i) \mathbf{e}_i, \quad (3.49)$$

where \mathbf{e}_i is the unit vector pointing into direction in which the wave oscillating at frequency ω_i is polarized. It is then possible to express the nonlinear polarization by means of a scalar relationship,

$$\frac{\partial \underline{E}(z, t, \omega_3)}{\partial z} = -j \frac{\omega_3}{cn(\omega_3)} d_{\text{eff}} \underline{E}(z, t, \omega_1) \underline{E}(z, t, \omega_2) e^{-j\Delta k z}, \quad (3.50)$$

where, $\mathbf{e}_{i,q}$ denotes the q -th component of the unit vector \mathbf{e}_i , and where, similarly to Eq. (2.55),

$$d_{\text{eff}} = \frac{1}{2} \sum_{q,r,s} \mathbf{e}_{3,q} \chi_{q:r,s}^{(2)}(\omega_3 : \omega_1, \omega_2) \mathbf{e}_{1,r} \mathbf{e}_{2,s} \quad (3.51)$$

denotes the effective value of the dielectric tensor. Following the same procedure, we can derive equations for the wave amplitudes at ω_1 and ω_2 ,

$$\frac{\partial \underline{E}(z, t, \omega_1)}{\partial z} = -j \frac{\omega_1}{cn(\omega_1)} d_{\text{eff}} \underline{E}(z, t, \omega_3) \underline{E}^*(z, t, \omega_2) e^{j\Delta k z}, \quad (3.52)$$

$$\frac{\partial \underline{E}(z, t, \omega_2)}{\partial z} = -j \frac{\omega_2}{cn(\omega_2)} d_{\text{eff}} \underline{E}(z, t, \omega_3) \underline{E}^*(z, t, \omega_1) e^{j\Delta k z}. \quad (3.53)$$

Here we have assumed lossless media with full permutation symmetry, which results in the same value of d_{eff} in each of the three equations.

Phase-matching considerations

To understand the impact of phase mismatch, let us assume that we have two strong waves at frequencies ω_1 and ω_2 at $z = 0$, whereas $\underline{E}(z = 0, t, \omega_3) = 0$. If we consider nonlinear interaction over small length scales only, we can assume that power conversion from the input fields $\underline{E}(z, t, \omega_1)$ and $\underline{E}(z, t, \omega_2)$ to the sum-frequency field $\underline{E}(z, t, \omega_3)$ is small, such that the input fields can be assumed to be constant, and the right-hand side of Eq. (3.50) can be readily integrated. In the literature, this assumption is also referred to as the ‘‘undepleted pump approximation’’, since the conversion of energy from the input (‘‘pump’’) waves to the sum frequency is neglected.

Let us first consider the case of perfect phase matching where $\Delta k = 0$. The amplitude $\underline{E}(z, t, \omega_3)$ of the sum-frequency field increases linearly with interaction length L , and its intensity increases quadratically,

$$\underline{E}(L, t, \omega_3)|_{\Delta k=0} \approx -j \frac{\omega_3}{cn(\omega_3)} d_{\text{eff}} \underline{E}(0, t, \omega_1) \underline{E}(0, t, \omega_2) L. \quad (3.54)$$

Conversely, when $\Delta k \neq 0$, we find that converted power oscillates with interaction length,

$$\underline{E}(L, t, \omega_3)|_{\Delta k \neq 0} = -j \frac{\omega_3}{cn(\omega_3)} d_{\text{eff}} \underline{E}(0, t, \omega_1) \underline{E}(0, t, \omega_2) \frac{2}{\Delta k} \sin\left(\frac{\Delta k L}{2}\right) e^{-j\frac{\Delta k L}{2}}. \quad (3.55)$$

For the case of second harmonic generation (SHG), $\omega_1 = \omega_2$, the evolution of the intensity $I(z, t, 2\omega_1) = |\underline{E}(z, t, 2\omega_1)|^2 / (2Z_0)$ along z is illustrated in Fig. 3.19 (a). Comparing the two cases with and without phase mismatch, we find a considerable decrease of the power conversion efficiency for $\Delta k L \gg 1$,

$$\left| \frac{\underline{E}(L, t, \omega_3)|_{\Delta k \neq 0}}{\underline{E}(L, t, \omega_3)|_{\Delta k=0}} \right|^2 = \frac{\sin^2\left(\frac{\pi}{2} \frac{L}{L_{\text{coh}}}\right)}{\left(\frac{\pi}{2} \frac{L}{L_{\text{coh}}}\right)^2}. \quad (3.56)$$

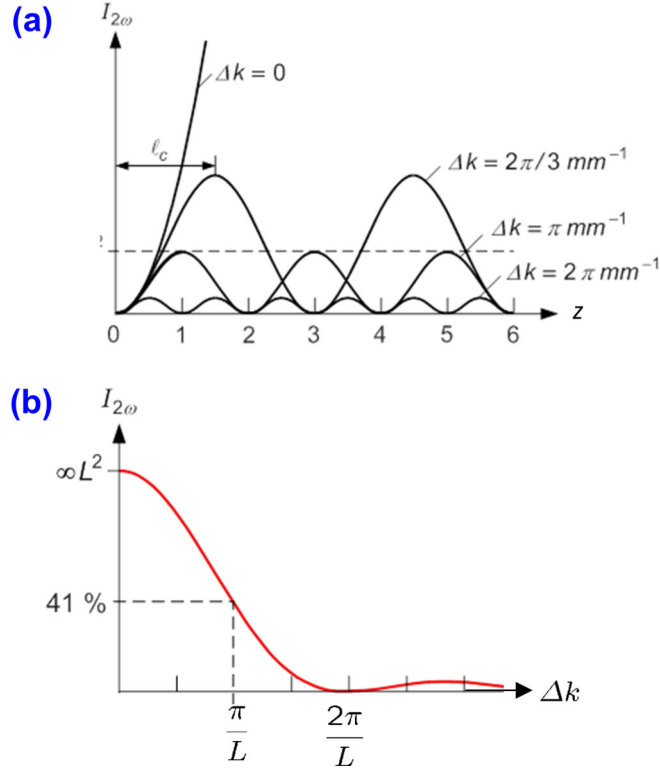


Figure 3.19: Phase matching and conversion efficiency for the case of second-harmonic generation (SHG). (a) Intensity $I(z, t, 2\omega_1)$ at second harmonic for the case of phase matching ($\Delta k = 0$) and for different degrees of phase mismatch, ($\Delta k \neq 0$). For phase mismatch, power oscillates back and forth between the fundamental and the second harmonic. For increasing values of Δk , both the oscillation period decrease and the maximum converted power decrease. (b) Decrease of power conversion efficiency for a given interaction length (crystal thickness) L for different values of Δk . For maximum conversion efficiency, it is important to ensure $\Delta k L \ll 1$.

where L_{coh} denotes the so-called coherent build-up length

$$L_{\text{coh}} = \frac{\pi}{\Delta k}. \quad (3.57)$$

Careful phase matching is therefore of prime importance for efficient nonlinear interaction, see Fig. 3.19 (b).

3.3.2 Phase matching by exploiting birefringence

Phase matching requires that the wave vector mismatch according to Eq. (3.48) vanishes. For sum frequency generation where $\omega_3 = \omega_1 + \omega_2$, this implies

$$\omega_1 n(\omega_1) + \omega_2 n(\omega_2) - \omega_3 n(\omega_3) = 0, \quad (3.58)$$

where we assumed an isotropic material, where the refractive index does not depend on the polarization direction. For the case of second-harmonic generation where $\omega_1 = \omega_2$, this relation can be simplified to

$$n(\omega_1) = n(2\omega_1). \quad (3.59)$$

Since most materials of practical interest are operated below their resonance frequencies, they exhibit normal phase velocity dispersion¹, i.e., a refractive index which increases monotonically with frequency ω . As a consequence, neither Eq. (3.58) nor Eq. (3.59) can be fulfilled, unless combinations of materials with normal and anomalous dispersion would be used.

In practice, another strategy has proven to be viable: The exploitation of birefringence to achieve phase matching of waves propagating in different polarizations. These waves can either be polarized and propagate along one of the principal axes of the index ellipsoid and hence behave just like a plane wave in a bulk medium, or they can propagate under a certain angle with respect to principal axes and hence exhibit a walk-off between the wave vector and the Poynting vector, see Section (3.1.3).

In the following sections, we will discuss different strategies of phase matching for the case of second-harmonic generation and sum-frequency generation. We assume normal dispersion for all materials. The derived phase matching strategies can be readily applied to other cases such as difference-frequency generation.

Type-1 phase matching

For so-called Type-1 phase matching, the lower-frequency components have the same polarization. Let us first consider the case of second-harmonic generation, where we have to fulfill the relation

$$n(2\omega_1) = n(\omega_1). \quad (3.60)$$

In the simplest case, let us assume that all waves are polarized along the principal axes of the index ellipsoid. For normal dispersion, the refractive index increases with frequency. Hence, for the case of a negative-uniaxial crystal where $n_e(\omega) < n_o(\omega)$, we choose the ordinary polarization for the fundamental, and the extraordinary polarization for the second harmonic,

$$n_e(2\omega_1) = n_o(\omega_1) \quad [oo \rightarrow e], \quad (3.61)$$

where $[oo \rightarrow e]$ represents a short-form notation expressing the fact that two photons at the ordinary polarization (oo) interact to generate a photon at the extraordinary (e) polarization. The corresponding dispersion diagrams are illustrated in Fig. 3.20. Conversely, when dealing with a positive-uniaxial crystal, the fundamental propagates as an extraordinary mode, whereas the second harmonic has ordinary polarization

$$n_o(2\omega_1) = n_e(\omega_1) \quad [ee \rightarrow o], \quad (3.62)$$

see Fig. 3.21.

These concepts can be directly transferred to the case of sum-frequency generation, where the relations

$$\omega_3 n_e(\omega_3) = \omega_1 n_o(\omega_1) + \omega_2 n_o(\omega_2) \quad \text{negative-uniaxial, } [oo \rightarrow e] \quad (3.63)$$

$$\omega_3 n_o(\omega_3) = \omega_1 n_e(\omega_1) + \omega_2 n_e(\omega_2) \quad \text{positive-uniaxial, } [ee \rightarrow o] \quad (3.64)$$

have to be fulfilled.

Configurations where all waves are polarized along the principal axes of the index ellipsoid are also referred to as noncritical phase matching, whereas critical phase matching denotes the case where the waves propagate under a certain angle with respect to the principal axes. For noncritical phase matching, all waves propagate through the material as normal modes, see Fig. 3.20 (b) and Fig. 3.21 (b). Noncritical phase matching can be obtained for one specific frequency only. To achieve phase matching for other frequencies as well, we need to tune the wave vectors. Two ways of tuning are commonly used: Temperature tuning and angle tuning. These techniques shall be discussed in more detail in the following sections.

¹Note that in optical communications, the term “dispersion” usually refers to group velocity dispersion, i.e., the wavelength-dependent group refractive index. In contrast to that, here we must consider phase mismatch and hence phase velocity dispersion. In the remainder of these lecture notes, we will omit the term “phase velocity” and just talk about “dispersion” unless otherwise noted.

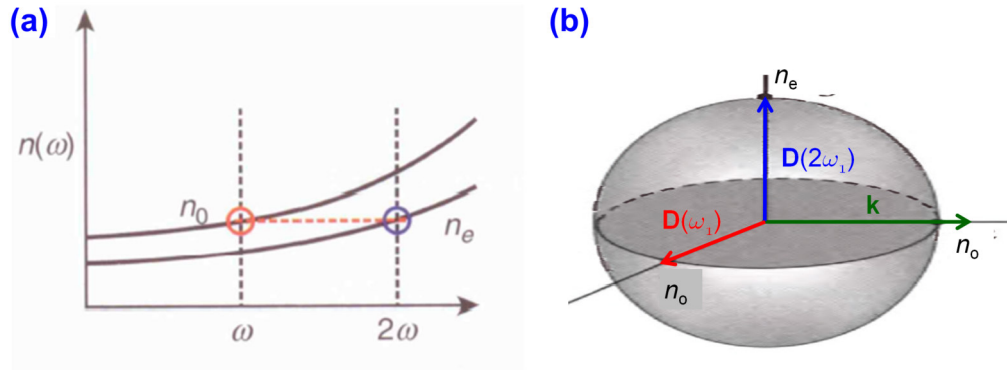


Figure 3.20: Type-1 phase matching in a negative-uniaxial crystal ($n_e(\omega) < n_o(\omega)$) exhibiting normal phase velocity dispersion ($dn_{e,o}/d\omega > 0$). (a) Frequency dependence of the refractive indices and phase matching concept: Phase matching is achieved by choosing the ordinary polarization for the fundamental, and the extraordinary polarization for the second harmonic ($[oo \rightarrow e]$) such that $n_e(2\omega_1) = n_o(\omega_1)$. (b) Both the fundamental and the second harmonic waves represent normal modes of the material, i.e., they are polarized along one main axis of the index ellipsoid and propagate along another main axis. This case is also referred to as noncritical phase matching. (Figure adapted from [29, 26])

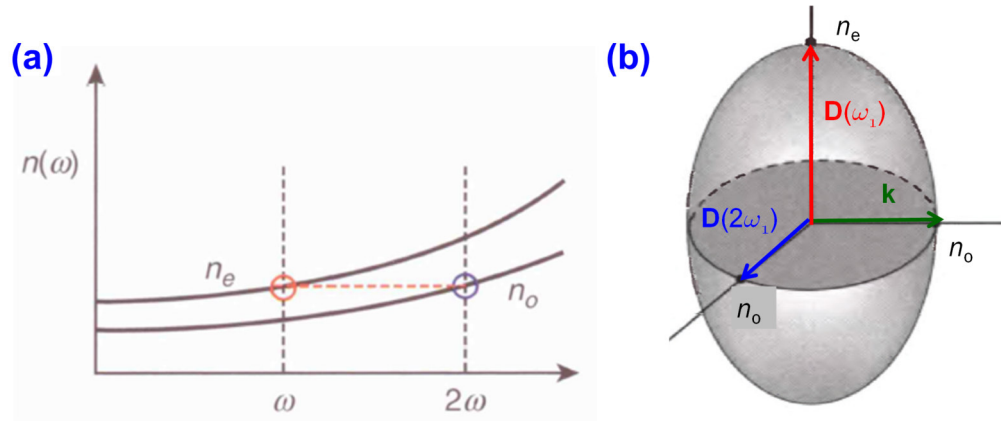


Figure 3.21: Type-1 phase matching in a positive-uniaxial crystal ($n_e(\omega) > n_o(\omega)$) exhibiting normal phase velocity dispersion ($dn_{e,o}/d\omega > 0$). (a) Frequency dependence of the refractive indices and phase matching concept: Phase matching is achieved by choosing the extraordinary polarization for the fundamental, and the ordinary polarization for the second harmonic ($[ee \rightarrow o]$) such that $n_o(2\omega_1) = n_e(\omega_1)$. (b) As in Fig. 3.20, both the fundamental and the second harmonic waves represent normal modes of the material, i.e., they are polarized along one main axis of the index ellipsoid and propagate along another main axis (noncritical phase matching). (Figure adapted from [29, 26])

Temperature tuning

Temperature tuning exploits the fact that for some crystals, the amount of birefringence is strongly temperature-dependent. Phase-matching can hence be achieved by varying the temperature of the crystal. Lithium niobate, for example, exhibits a strong temperature dependence of the birefringence. In contrast to angle tuning, temperature tuning does not have the disadvantage of introducing a walk-off between the Poynting vector and the wave vector of the extraordinary waves, see next section for a more detailed discussion.

Angle tuning

Angle tuning is based on precise adjustment of the propagation direction of the involved rays with respect to the principal axes of the crystal. As an example, let us consider Type-1 phase matching for second-harmonic generation in a negative-uniaxial crystal, see Fig. 3.22. In this configuration, the direction of propagation is defined by the angle Θ between the \mathbf{k} -vector and the optical axis of the crystal. The fundamental wave propagates as an ordinary mode under the influence of a refractive index $n_o(\omega_1)$, whereas the second harmonic experiences an angle-dependent extraordinary refractive index² $n_{e'}(2\omega_1, \Theta)$. To achieve phase matching, the propagation direction Θ is chosen such that both waves experience the same refractive index, $n_{e'}(2\omega_1, \Theta_p) = n_o(\omega_1)$. Similarly, for positive uniaxial crystals, the fundamental wave propagates as an extraordinary mode under the influence of the angle-dependent extraordinary refractive index $n_{e'}(\omega_1, \Theta)$, and the second harmonic propagates as an ordinary mode under the influence of a refractive index $n_o(\omega_1)$, see Fig. 3.22. The angle Θ is again chosen such that both waves experience the same refractive index.

For a quantitative analysis, let us consider the case of a negative uniaxial material. The index ellipse can be constructed from the intersection of the plane normal to the wave vector \mathbf{k} as illustrated in Fig. 3.23 (b) for a positive uniaxial crystal. For the second harmonic in a negative uniaxial crystal, the long half-axis of the index ellipse corresponds to the ordinary refractive index $n_o(2\omega_1)$ and the short half-axis corresponds to the extraordinary index $n_e(2\omega_1)$. In analogy to the derivation of Eq. (3.18), we can derive a relation for the propagation direction Θ_p ,

$$\tan \Theta_p = \frac{n_e(2\omega_1)}{n_o(2\omega_1)} \sqrt{\frac{n_o^2(2\omega_1) - n_o^2(\omega_1)}{n_o^2(\omega_1) - n_e^2(2\omega_1)}}. \quad (3.65)$$

Adjusting phase matching by angle tuning is also referred to as critical phase matching. The attribute “critical” comes from the fact that this technique is very sensitive to misalignment of the beams, i.e., there is only a finite range of beam angles where critical phase matching works, and this range is much smaller than for the case of noncritical phase matching, where all waves propagate as normal modes of the anisotropic crystal, and where, in a first-order approximation, the propagation constant is independent of the propagation direction. The range of possible beam directions is quantified by the so-called acceptance angle, also called angular phase-matching bandwidth. More information on acceptance angles for different configurations can be found in [13].

One drawback of angle tuning is the fact that the Poynting vector and the wave vector are not parallel for the extraordinary ray, whenever the angle Θ has a value other than 0° or 90° . As a consequence, ordinary and extraordinary rays with parallel wave vectors diverge from each other as they propagate through the crystal, see Fig. 3.24. For critical phase matching in a negative uniaxial crystal, the walk-off angle at the second harmonic is obtained in analogy to Eq. (3.19),

$$\cos(\rho) = \frac{n_e^2(2\omega_1) \cos^2(\Theta_p) + n_o^2(2\omega_1) \sin^2(\Theta_p)}{\sqrt{n_e^4(2\omega_1) \cos^2(\Theta_p) + n_o^4(2\omega_1) \sin^2(\Theta_p)}}. \quad (3.66)$$

²Note that the extraordinary refractive index of the crystal is $n_e(\omega)$, whereas $n_{e'}(\omega, \Theta)$ refers to the index seen by an extraordinary mode that propagates under an angle Θ with respect to the z -direction, i.e., $n_e(\omega) = n_{e'}(\omega, \Theta = 90^\circ)$. Often, the prime in the subscript of the angle-dependent refractive index $n_{e'}(\omega, \Theta = 90^\circ)$ is omitted and the quantity is simply referred to as the “angle-dependent extraordinary refractive index”.

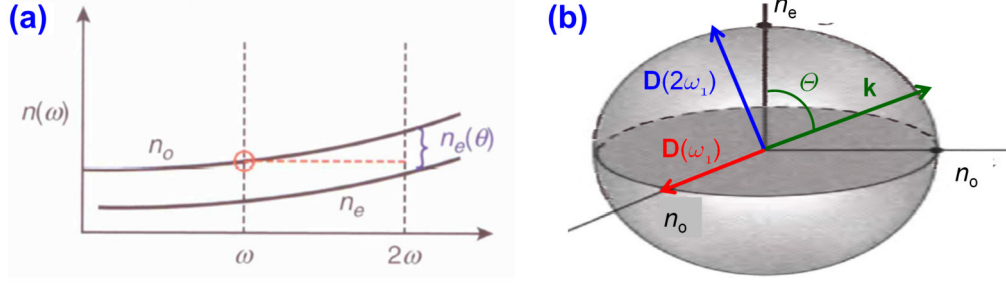


Figure 3.22: Type-1 phase matching and angle tuning in a negative-uniaxial crystal ($n_e(\omega) < n_o(\omega)$) exhibiting normal phase velocity dispersion ($dn_{e,o}/d\omega > 0$). (a) Frequency dependence of the refractive indices and phase matching concept: Phase matching is achieved by adjusting the propagation angle Θ with respect to the crystal axis such that the angle-dependent extraordinary refractive index $n_{e'}(2\omega_1, \Theta_p)$ for the second harmonic is equal to the angle-independent ordinary index $n_o(\omega_1)$ for the fundamental ($[oo \rightarrow e]$). (b) The direction of propagation and the angle-dependent extraordinary refractive index $n_{e'}(2\omega_1, \Theta)$ are defined by the angle Θ between the \mathbf{k} -vector and the optical axis of the crystal. The fundamental wave (illustrated in red) propagates as an ordinary mode under influence of a refractive index $n_o(\omega_1)$, whereas the second harmonic (illustrated in blue) experiences an angle-dependent extraordinary refractive index $n_{e'}(2\omega_1, \Theta)$. The technique is referred to as “critical phase matching” since the conversion efficiency is more sensitive to angular misalignment of the beams than for the case where all waves propagate as normal modes of the anisotropic crystal. (Figure adapted from [29, 26])

For optical beams with finite diameter, this walk-off limits the spatial overlap and decreases the efficiency of nonlinear interaction.

Note that angle tuning can be extended to the case of sum-frequency generation, $\omega_3 = \omega_1 + \omega_2$, where the relations

$$\omega_3 n_e(\omega_3, \Theta_p) = \omega_1 n_o(\omega_1) + \omega_2 n_o(\omega_2) \quad \text{negative-uniaxial, } [oo \rightarrow e] \quad (3.67)$$

$$\omega_3 n_o(\omega_3) = \omega_1 n_e(\omega_1, \Theta_p) + \omega_2 n_e(\omega_2, \Theta_p) \quad \text{positive-uniaxial, } [ee \rightarrow o] \quad (3.68)$$

have to be fulfilled.

Type-2 phase matching

In some cases, the propagation angle Θ_p and hence the walk-off can be reduced by using a different method for phase matching: In so-called Type-2 phase matching, the two waves of lower frequency components propagate with orthogonal polarizations with respect to each other. This means, that for sum-frequency generation in an uniaxial crystal, one fundamental mode features ordinary and the other extraordinary polarization. For second-harmonic generation, we have to fulfill the relations

$$n_e(2\omega_1, \Theta_p) = \frac{1}{2} (n_o(\omega_1) + n_e(\omega_1, \Theta_p)) \quad \text{negative-uniaxial, } [oe \rightarrow e] \quad (3.69)$$

$$n_o(2\omega_1) = \frac{1}{2} (n_o(\omega_1) + n_e(\omega_1, \Theta_p)) \quad \text{positive-uniaxial, } [oe \rightarrow o] \quad (3.70)$$

The corresponding dispersion diagrams are illustrated in Fig.3.25. Type-II phase matching is used when the birefringence is relatively strong compared to the phase velocity mismatch, hence overcompensating the dispersion in a type-I scheme.

The concept can be generalized to the case of sum-frequency generation, where the relations

$$\omega_3 n_e(\omega_3, \Theta_p) = \omega_1 n_o(\omega_1) + \omega_2 n_e(\omega_2, \Theta_p) \quad \text{negative-uniaxial, } [oe \rightarrow e] \quad (3.71)$$

$$\omega_3 n_o(\omega_3) = \omega_1 n_o(\omega_1) + \omega_2 n_e(\omega_2, \Theta_p) \quad \text{positive-uniaxial, } [oe \rightarrow o]. \quad (3.72)$$

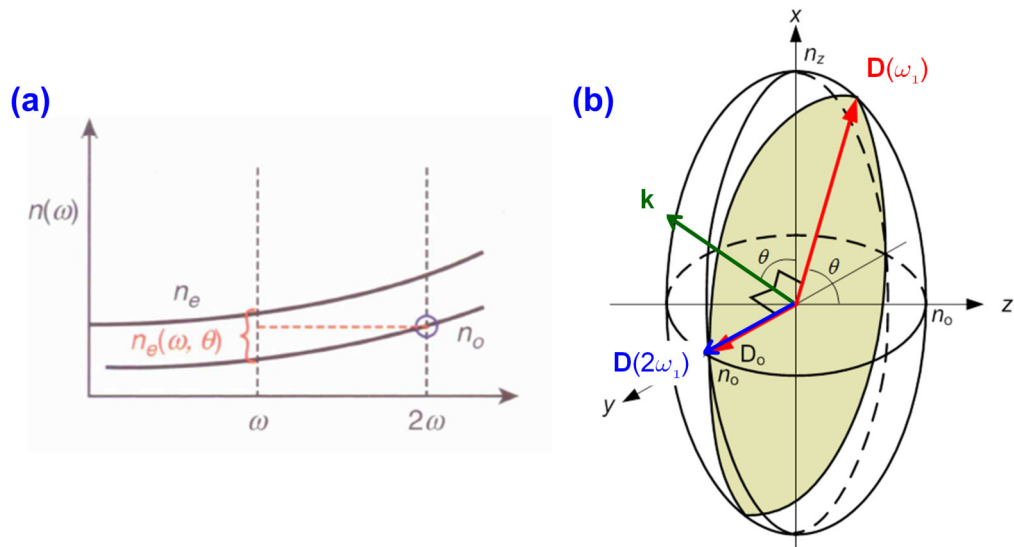


Figure 3.23: Type-1 phase matching and angle tuning in a positive-uniaxial crystal ($n_e(\omega) > n_o(\omega)$) exhibiting normal phase velocity dispersion ($dn_{e,o}/d\omega > 0$). (a) Frequency dependence of the refractive indices and phase matching concept: Phase matching is achieved by adjusting the propagation angle θ with respect to the crystal axis such that angle-dependent extraordinary refractive index $n_{e'}(\omega_1, \theta_p)$ for the fundamental is equal to the angle-independent ordinary polarization for the second harmonic ($[ee \rightarrow o]$). (b) The direction of propagation is defined by the angle θ between the \mathbf{k} -vector and the optical axis of the crystal. The fundamental wave (illustrated in red) propagates as an ordinary mode under influence of a refractive index $n_o(\omega_1)$, whereas the second harmonic (illustrated in blue) experiences an angle-dependent extraordinary refractive index $n_{e'}(2\omega_1, \theta)$. The technique is referred to as “critical phase matching” since the conversion efficiency is more sensitive to angular misalignment of the beams than for the case where all waves propagate as normal modes of the anisotropic crystal. (Figure adapted from [29, 26])

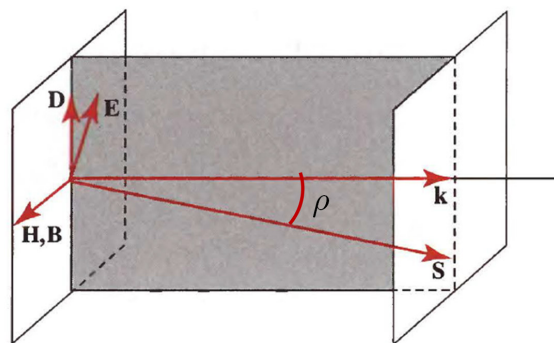


Figure 3.24: Walk-off between ordinary and extraordinary ray for the case of angle tuning. For the extraordinary wave, the Poynting vector and the wave vector are not parallel. As a consequence, there is a divergence ρ between the ordinary and extraordinary ray even though the wave vectors are parallel. This limits the spatial overlap of the beams and decreases the efficiency of nonlinear interaction. (Figure adapted from [26])

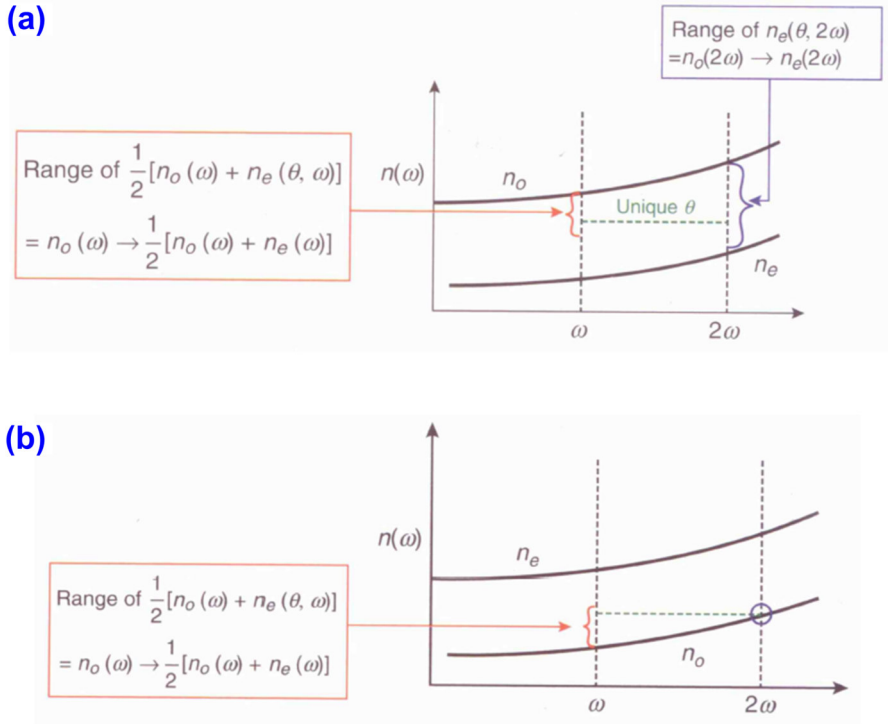


Figure 3.25: Concept of type-2 phase matching for second-harmonic generation. (a) Negative-uniaxial crystal ($[oe \rightarrow e]$): The fundamental is launched in both ordinary and extraordinary polarization, experiencing the refractive indices $n_o(\omega_1)$ and $n_e(\omega_1, \theta)$, respectively. The second harmonic propagates in extraordinary polarization and experiences the refractive index $n_e(2\omega_1, \theta_p)$, which must correspond to the mean of the indices at the fundamental, Eq. 3.69. (b) Positive-uniaxial crystal ($[oe \rightarrow o]$): The fundamental is again launched in both ordinary and extraordinary polarization, experiencing the refractive indices $n_o(\omega_1)$ and $n_e(\omega_1, \theta)$, respectively. The second harmonic now propagates in ordinary polarization and experiences the refractive index $n_o(2\omega_1)$, which must correspond to the mean of the indices at the fundamental, Eq. 3.70. (Figure adapted from [29])

have to be fulfilled.

3.3.3 Quasi-phase-matching (QPM)

Principle of quasi-phase matching

In the last section, we have discussed techniques to exploit the birefringence of an optical material for achieving phase-matching. However, there are circumstances under which these techniques can not be applied: Some second-order nonlinear materials do not exhibit birefringence. Gallium arsenide, e.g., is noncentrosymmetric, but possesses a cubic lattice, and birefringence hence vanishes. Similarly, at high frequencies that approach a resonance of the medium, the refractive index tends to increase rapidly with frequency whereas the birefringence tends to be nearly constant, see Fig. 3.26. This makes type-1 and type-2 phase matching impossible. Moreover, we also might want to exploit the d_{33} coefficient of the nonlinear tensor, which is particularly strong in some materials. This, however, requires a set of waves that are polarized in the same direction. Birefringence cannot be used to compensate for dispersion in this case.

In these cases, we may use quasi-phase-matching, which relies on a position-dependent periodic nonlinearity. To understand the concept of quasi-phase-matching (QPM), let us consider the

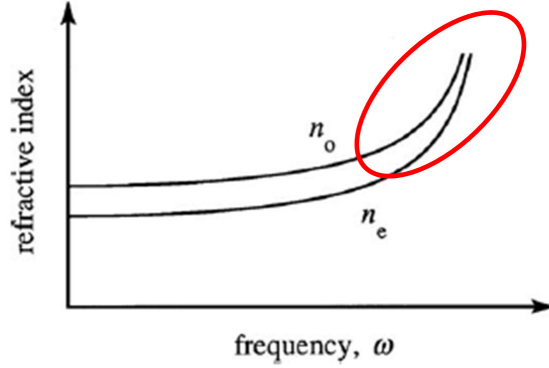


Figure 3.26: When approaching an electronic resonance at high frequencies, the refractive index of a medium increases strongly. For a given birefringence, it is then not any more possible to achieve phase matching over large frequency ranges as would be required for, e.g., SHG or SFG. In this case, quasi phase matching can be exploited to increase nonlinear interaction.

differential equation that governs sum-frequency generation,

$$\frac{\partial \underline{E}(z, t, \omega_3)}{\partial z} = -j \frac{\omega_3}{cn(\omega_3)} d_{\text{eff}} \underline{E}(z, t, \omega_1) \underline{E}(z, t, \omega_2) e^{-j\Delta k z}. \quad (3.73)$$

For zero wave vector mismatch, $\Delta k = 0$, the converted wave amplitude increases linearly with z . This effects can be visualized by sketching the phasor elements that are associated with the contributions $\Delta \underline{E}(z, t, \omega_3) = \frac{\partial \underline{E}(z, t, \omega_3)}{\partial z} \Delta z$ from different positions along z , see Fig. 3.27 (a). A nonzero wave vector mismatch $\Delta k \neq 0$ leads to a constant phase change of the contribution on the right-hand side of Eq. (3.73). Hence, when starting with $\underline{E}(0, t, \omega_3) = 0$ at $z = 0$, we will first observe build-up of the converted wave, until a phase shift of $\Delta k z = \pi$ is reached. From this point onwards, newly generated contributions on the right-hand side will interfere destructively with the existing wave, and power will be converted back from the sum frequency to the fundamental waves. This leads to a circular trace of the converted wave amplitude in the complex plane, Fig. 3.27 (b), and hence to an oscillatory behavior as we have already observed in Section 3.3.1. After complete depletion of the sum frequency for $\Delta k z = 2\pi$, the process repeats. The basic idea of quasi-phase-matching is now to reverse the sign of the nonlinearity, whenever a phase shift of π is accumulated, see Fig. 3.27 (c). This requires a material, for which the orientation of the susceptibility tensor is switched after regular intervals of $\pi/\Delta k$, see Fig. 3.27 (d).

The z -dependent evolution of the intensity $I(z, t, \omega_3) = |\underline{E}(z, t, \omega_3)|^2$ of the converted wave is sketched in Fig. 3.28. For phase matching, $\Delta k = 0$, the wave amplitude increases linearly and the intensity increases quadratically with z , and phase mismatch leads to a periodic $\sin^2(\Delta k z/2)$ -oscillation. For quasi-phase-matching, we observe a wave-like, but steady increase of $I(z, t, \omega_3)$ with z .

Mathematical analysis of quasi-phase matching

For a mathematical analysis of quasi-phase-matching, let us start from Eq. (3.73) and introduce a periodic effective second-order nonlinearity $d_{\text{eff}}(z + \Lambda) = d_{\text{eff}}(z)$. We expand $d_{\text{eff}}(z)$ in a Fourier series,

$$d_{\text{eff}}(z) = \sum_m d_m e^{jm \frac{2\pi}{\Lambda} z}, \quad (3.74)$$

where d_m are the Fourier coefficients. This transforms Eq. (3.73) into

$$\frac{\partial \underline{E}(z, t, \omega_3)}{\partial z} = -j \frac{\omega_3}{cn(\omega_3)} \sum_m d_m \underline{E}(z, t, \omega_1) \underline{E}(z, t, \omega_2) e^{-j(\Delta k - m \frac{2\pi}{\Lambda})z}, \quad (3.75)$$

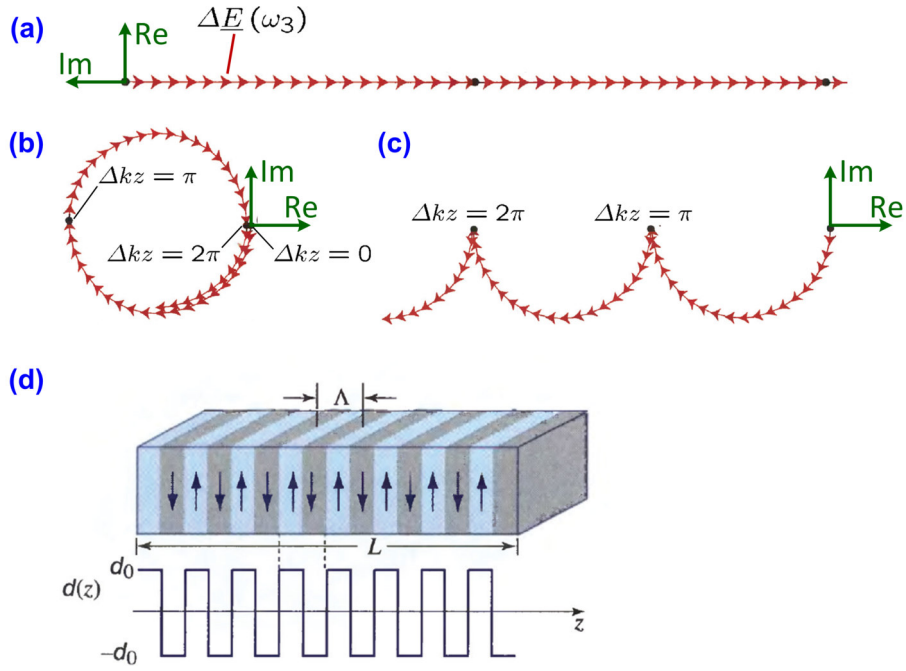


Figure 3.27: The principles of quasi-phase-matching. (a) For the case of phase matching, $\Delta k = 0$, and the contributions $\Delta \underline{E}(z, t, \omega_3) = \frac{\partial \underline{E}(z, t, \omega_3)}{\partial z} \Delta z$ to the converted wave amplitude $\underline{E}(z, t, \omega_3)$ do not change phase along z . In the complex plane, this leads to a continuous build-up of the converted wave amplitude. Re and Im denote the directions associated with the real and the imaginary part of the complex plane in the respective sketch. Note that, due to the forefactor $-j$ in Eq. (3.73), the converted amplitude $\underline{E}(z, t, \omega_3)$ features a phase shift of $-\frac{\pi}{2}$ relative to the product $\underline{E}(z, t, \omega_1) \underline{E}(z, t, \omega_2)$, which is associated negative imaginary part (horizontal direction in this plot). (b) For nonzero phase mismatch, $\Delta k \neq 0$, the contributions $\Delta \underline{E}(z, t, \omega_3)$ to the converted wave amplitude $\underline{E}(z, t, \omega_3)$ decrease linearly in phase along z . In the complex plane, this leads to circular trace and hence to an oscillation of the complex wave amplitude, i.e., power is continuously converted back and forth between the fundamental and the converted wave. (c) In the case of quasi-phase-matching, the sign of the nonlinearity is reversed whenever a phase shift of π is accumulated. (d) Quasi-phase-matching requires a material for which the orientation of the susceptibility tensor is switched after regular intervals of $\pi/\Delta k$. (Figures adapted from [26])

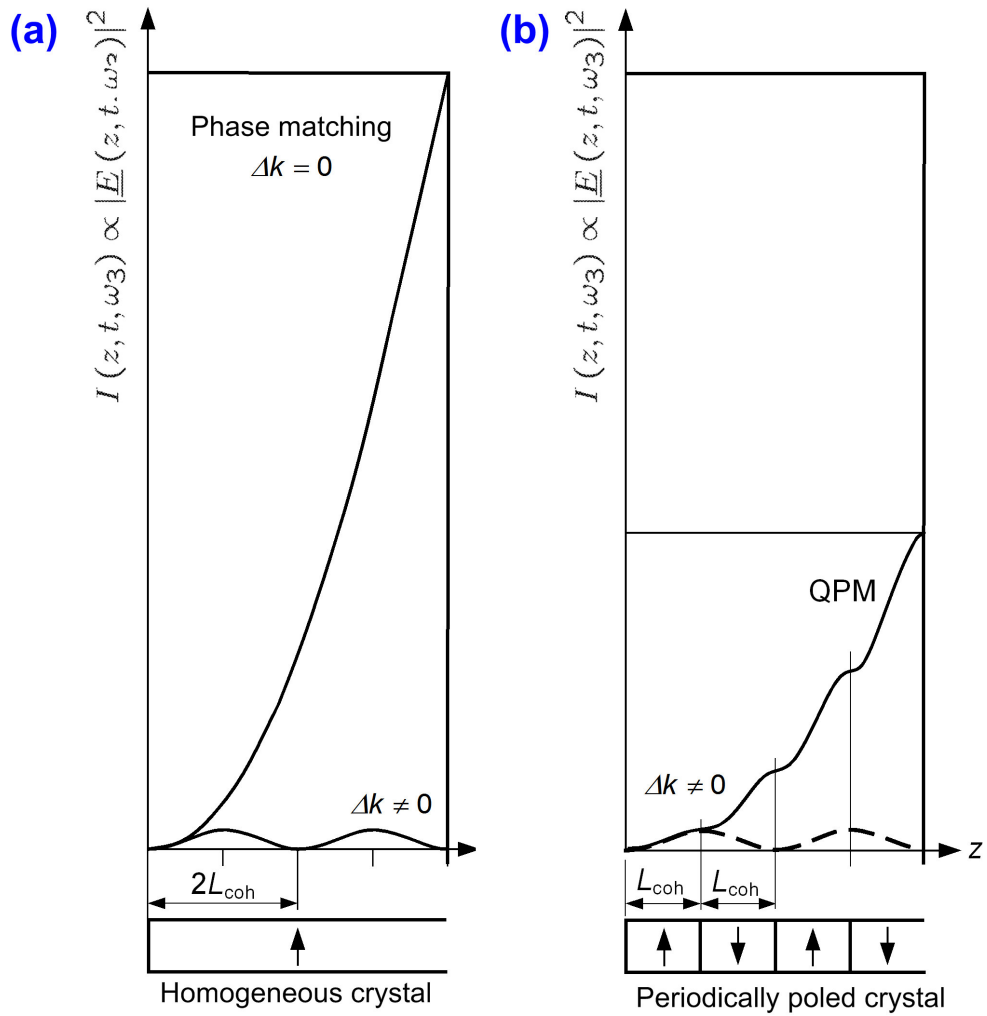


Figure 3.28: Evolution of the intensity $I(z, t, \omega_3) = |\underline{E}(z, t, \omega_3)|^2$ of the converted wave along z . (a) For phase matching, $\Delta k = 0$, the wave amplitude increases linearly and the intensity increases quadratically with z , whereas, for the case of phase mismatch, a periodic $\sin^2(\Delta k z/2)$ -oscillation is observed. (b) For quasi-phase-matching (QPM), the sign of the optical nonlinearity is reversed after $L_{\text{coh}} = \frac{\pi}{\Delta k}$. This leads to a wave-like steady increase of $I(z, t, \omega_3)$ with z .

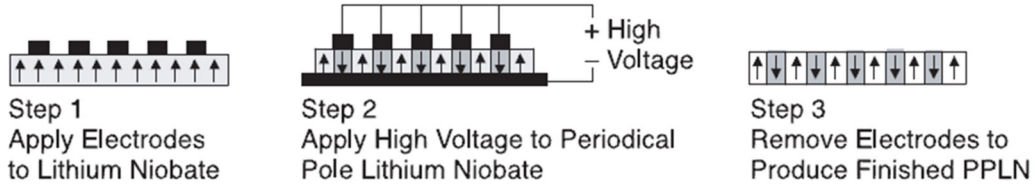


Figure 3.29: Fabrication of periodically poled lithium niobate. An intense electric field (approx. 22 kV/mm) can invert the crystal structure and, as a result, flip the orientation of the electric dipole moment and of the second-order nonlinear susceptibility tensor. To this end, a periodic electrode structure is temporarily deposited on the front side of the lithium niobate wafer to apply the poling field. (Figure adapted from [2])

Quasi-phase-matching can be achieved through an interaction with the m -th order Fourier coefficient of the periodic nonlinearity, for which $\Delta k - m\frac{2\pi}{\Lambda} = 0$. Since the Fourier coefficients tend to decrease with increasing order m , it is most desirable to achieve quasi-phase-matching through a first-order ($m = 1$) interaction. The period of the quasi-phase-matching grating is then given by

$$\Lambda = \frac{2\pi}{\Delta k}, \quad (3.76)$$

which is consistent with the idea of reversing the sign of the second-order nonlinearity after distances of $\frac{\pi}{\Delta k} = \frac{\Lambda}{2}$.

Technology and applications of quasi-phase-matching

Technologically, quasi-phase matching can be realized by, e.g., lithographical definition of periodic electrodes which are used to apply a strong periodic electric field that inscribes the direction of the crystal's permanent electric polarization, a technique called poling. This approach has been applied to ferroelectric crystals such as LiTaO_3 , KTP, and LiNbO_3 .

The fabrication of periodically poled lithium niobate (PPLN) is illustrated in Fig. 3.29. Lithium Niobate is a ferroelectric crystal, i.e., each unit cell in the crystal has a small electric dipole moment, the orientation of which is dependent on the positions of the niobium and lithium atoms in the unit cell. An intense electric field can invert the crystal structure and, as a result, flip the orientation of the electric dipole moment and of the second-order nonlinear susceptibility tensor. The electric field needed to invert the crystal is very large (approx. 22 kV/mm) and is applied for a few milliseconds only. The inverted sections of the crystal are then permanently imprinted into the crystal structure. To produce PPLN, a periodic electrode structure is deposited on the front side of the lithium niobate wafer, whereas the back side is completely covered with a large-area electrode, see Fig. 3.29. A voltage is then applied to invert the crystal underneath the electrodes. To create the poled regions with the desired shape and to produce a short periodicity, the design of the electrodes and the exact control of the applied voltage are very important. PPLN waveguides are used for sum- and difference-frequency generation, and allow, e.g., generation of entangled photon pairs by frequency downconversion.

3.4 Difference-frequency generation and parametric amplification

In the last section, we have discussed frequency upconversion by sum-frequency generation along with techniques associated to achieve phase matching for these processes. These phase matching techniques can be readily transferred to the complementary processes of difference-frequency

generation. Difference-frequency generation leads to simultaneous annihilation of a high-energy photon and creation of two low-energy photons. This process can be stimulated by the presence of at least one low-energy photon and can hence be used for so-called parametric amplification of optical signals. In this section, we will investigate difference frequency generation and parametric amplification in more detail.

3.4.1 The Manley-Rowe relations

We will start by investigating the power transfer between three waves oscillating at frequencies ω_1 , ω_2 , and $\omega_3 = \omega_1 + \omega_2$. The interaction between the respective wave amplitudes is given by Eqs. (3.50), (3.52), and (3.53)

$$\frac{\partial \underline{E}(z, t, \omega_3)}{\partial z} = -j \frac{\omega_3}{cn(\omega_3)} d_{\text{eff}} \underline{E}(z, t, \omega_1) \underline{E}(z, t, \omega_2) e^{-j\Delta kz}, \quad (3.77)$$

$$\frac{\partial \underline{E}(z, t, \omega_1)}{\partial z} = -j \frac{\omega_1}{cn(\omega_1)} d_{\text{eff}} \underline{E}(z, t, \omega_3) \underline{E}^*(z, t, \omega_2) e^{j\Delta kz}, \quad (3.78)$$

$$\frac{\partial \underline{E}(z, t, \omega_2)}{\partial z} = -j \frac{\omega_2}{cn(\omega_2)} d_{\text{eff}} \underline{E}(z, t, \omega_3) \underline{E}^*(z, t, \omega_1) e^{j\Delta kz}. \quad (3.79)$$

To understand power transfer between the three waves let us study the evolution of the respective intensities rather than the wave amplitudes,

$$I(z, t, \omega_i) = \frac{1}{2} \epsilon_0 cn(\omega_i) |\underline{E}(z, t, \omega_i)|^2. \quad (3.80)$$

The evolution of the intensities is given by

$$\frac{\partial I(z, t, \omega_i)}{\partial z} = \frac{1}{2} \epsilon_0 cn(\omega_i) \left(\underline{E}(z, t, \omega_i) \frac{\partial \underline{E}^*(z, t, \omega_i)}{\partial z} + \underline{E}^*(z, t, \omega_i) \frac{\partial \underline{E}(z, t, \omega_i)}{\partial z} \right). \quad (3.81)$$

Inserting Eqs. (3.77), (3.78), and (3.79), we find

$$\frac{\partial I(z, t, \omega_3)}{\partial z} = -\epsilon_0 \omega_3 d_{\text{eff}} \text{Im} \{ \underline{E}^*(z, t, \omega_1) \underline{E}^*(z, t, \omega_2) \underline{E}(z, t, \omega_3) e^{j\Delta kz} \} \quad (3.82)$$

$$\frac{\partial I(z, t, \omega_2)}{\partial z} = \epsilon_0 \omega_2 d_{\text{eff}} \text{Im} \{ \underline{E}^*(z, t, \omega_1) \underline{E}^*(z, t, \omega_2) \underline{E}(z, t, \omega_3) e^{j\Delta kz} \} \quad (3.83)$$

$$\frac{\partial I(z, t, \omega_1)}{\partial z} = \epsilon_0 \omega_1 d_{\text{eff}} \text{Im} \{ \underline{E}^*(z, t, \omega_1) \underline{E}^*(z, t, \omega_2) \underline{E}(z, t, \omega_3) e^{j\Delta kz} \}. \quad (3.84)$$

The sign of $\partial I(z, t, \omega_1)/\partial z$ is the same as for $\partial I(z, t, \omega_2)/\partial z$ but opposite to $\partial I(z, t, \omega_3)/\partial z$. As expected for propagation in a lossless medium, we find from Eqs. (3.82), (3.83), and (3.84) that the total intensity does not change along z ,

$$\frac{\partial}{\partial z} (I(z, t, \omega_1) + I(z, t, \omega_2) + I(z, t, \omega_3)) = 0. \quad (3.85)$$

Equations (3.82), (3.83), and (3.84) further imply the relation

$$\frac{\partial}{\partial z} \left(\frac{I(z, t, \omega_1)}{\hbar \omega_1} \right) = \frac{\partial}{\partial z} \left(\frac{I(z, t, \omega_2)}{\hbar \omega_2} \right) = -\frac{\partial}{\partial z} \left(\frac{I(z, t, \omega_3)}{\hbar \omega_3} \right). \quad (3.86)$$

This equation is known as the so-called Manley-Rowe relation. The quantity $I(z, t, \omega_i)/\hbar \omega_i$ is associated with the photon flux density at frequency ω_i . Equation (3.86) hence states that generation of a photon at ω_1 is always accompanied by generation of a photon at ω_2 and annihilation of a photon at ω_3 and vice versa. This is graphically illustrated by the energy-level diagrams we have used earlier, see, e.g., Fig. 1.9.

It might be surprising that these relations lead to the notion of photons, even though the derivation appears to be entirely based on classical wave optics. However, a key assumption of our derivation was that the nonlinear susceptibility tensor features full permutation symmetry and that we hence have the identical coefficient d_{eff} in each of the nonlinear coupled-mode equations (3.77), (3.78), and (3.79). Full permutation symmetry is a consequence of a quantum-mechanical analysis, see [9] for further details.

3.4.2 Parametric amplification and parametric oscillators

In lossless second-order material, annihilation of a high-frequency photon at frequency ω_3 always implies generation of a first photon at some frequency ω_1 and a second photon at frequency $\omega_2 = \omega_3 - \omega_1$. If proper phase matching $\Delta k = k_1 + k_2 - k_3 = 0$ can be achieved, this mechanism can be used to amplify a signal at ω_1 by pumping the material with a strong wave at ω_3 . To analyze this, let us use undepleted-pump approximation, i.e., we assume that the pump signal $\underline{E}(z, t, \omega_3)$ is very strong, such that we can neglect depletion by nonlinear interaction and assume $\underline{E}(z, t, \omega_3) = \underline{E}(0, t, \omega_3)$ to be constant along z . Assuming further phase matching, the nonlinear coupled-wave equations for $\underline{E}(z, t, \omega_1)$ and $\underline{E}(z, t, \omega_2)$ can be written as

$$\frac{\partial \underline{E}(z, t, \omega_1)}{\partial z} = -j \frac{\omega_1}{cn(\omega_1)} d_{\text{eff}} \underline{E}(0, t, \omega_3) \underline{E}^*(z, t, \omega_2), \quad (3.87)$$

$$\frac{\partial \underline{E}(z, t, \omega_2)}{\partial z} = -j \frac{\omega_2}{cn(\omega_2)} d_{\text{eff}} \underline{E}(0, t, \omega_3) \underline{E}^*(z, t, \omega_1). \quad (3.88)$$

Inserting Eq. (3.88) in Eq. (3.87), we obtain a relation for $\underline{E}(z, t, \omega_1)$ only,

$$\frac{\partial^2 \underline{E}(z, t, \omega_1)}{\partial z^2} = \kappa^2 \underline{E}(z, t, \omega_1), \quad (3.89)$$

where the coupling coefficient κ is given by

$$\kappa^2 = \frac{\omega_1 \omega_2 d_{\text{eff}}^2}{c^2 n(\omega_1) n(\omega_2)} |\underline{E}(0, t, \omega_3)|^2. \quad (3.90)$$

Eq. (3.89) is solved by

$$\underline{E}(z, t, \omega_1) = \underline{E}_a \cosh(\kappa z) + \underline{E}_b \sinh(\kappa z), \quad (3.91)$$

and the corresponding solution for $\underline{E}(z, t, \omega_2)$ can be derived from Eq. (3.87)

$$\underline{E}(z, t, \omega_2) = -j \sqrt{\frac{\omega_2 n(\omega_1)}{\omega_1 n(\omega_2)}} \frac{\underline{E}(0, t, \omega_3)}{|\underline{E}(0, t, \omega_3)|} (\underline{E}_a^* \sinh(\kappa z) + \underline{E}_b^* \cosh(\kappa z)) \quad (3.92)$$

Let us assume that we only launch a signal at frequency ω_1 into the waveguide,

$$\underline{E}(0, t, \omega_1) = \underline{E}_1, \quad \underline{E}(0, t, \omega_2) = 0. \quad (3.93)$$

The solution for these boundary conditions is then given by

$$\underline{E}(z, t, \omega_1) = \underline{E}_1 \cosh(\kappa z), \quad (3.94)$$

$$\underline{E}(z, t, \omega_2) = -j \sqrt{\frac{\omega_2 n(\omega_1)}{\omega_1 n(\omega_2)}} \frac{\underline{E}(0, t, \omega_3)}{|\underline{E}(0, t, \omega_3)|} \underline{E}_1^* \sinh(\kappa z). \quad (3.95)$$

Both fields experience monotonic growth during propagation along z , and for $\kappa z \gg 1$, each of the two grows as $e^{\kappa z}$. The signal wave at ω_1 preserves its original phase and is just amplified, whereas the so-called idler wave at frequency ω_2 is generated with a phase that is given by the signal and the pump. This process is also referred to as parametric amplification of the signal

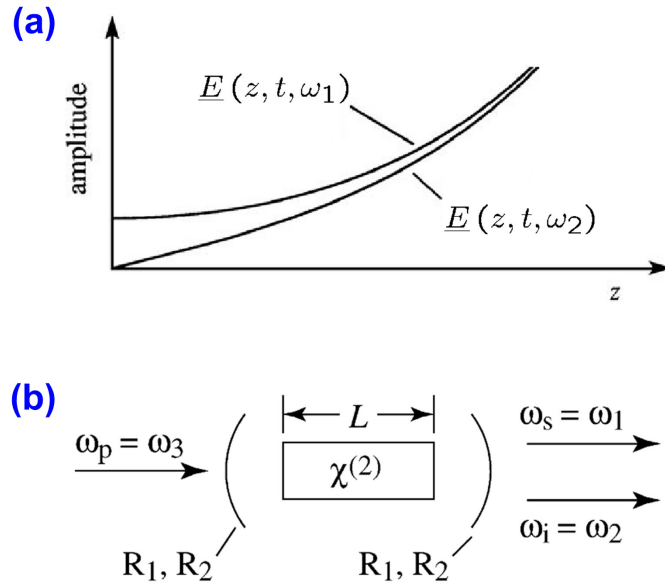


Figure 3.30: (a) Optical parametric amplifier (OPA): A strong wave at frequency ω_3 is launched into the second-order nonlinear material along with a signal at frequency ω_1 . Phase matching is established for difference frequency generation $\omega_2 = \omega_3 - \omega_1$. This leads to amplification of the signal at frequency ω_1 and to creating of a new, so-called idler wave at frequency ω_2 . (b) The OPA is turned into an optical parametric oscillator (OPO) by placing mirrors with high reflectivities R_1 and R_2 at ω_1 and/or ω_2 at both sides of the nonlinear medium. This leads to optical feedback and hence to self-sustained oscillation that starts from zero-point fluctuations. (Figures adapted from [26])

at ω_1 . The evolution of $\underline{E}(z, t, \omega_1)$ and $\underline{E}(z, t, \omega_2)$ along z is depicted in Fig. (3.30) (a). The optical parametric amplifier (OPA) can be turned into an optical parametric oscillator (OPO) by introducing a feedback mechanism, i.e., by placing mirrors with high reflectivities at ω_1 and/or ω_2 at both sides of the nonlinear medium to form an optical resonator, see Fig. 3.30 (b). The OPO starts from zero-point fluctuations; the oscillation frequencies ω_1 and ω_2 are defined by the phase matching conditions. OPO are often used as broadband tunable sources for frequencies that cannot be accessed by lasers.

Chapter 4

Acousto-optics and photon-phonon interactions

Acousto-optics is a branch of optics that studies the interactions of sound waves and light waves such as, e.g., lead to diffraction of laser light by ultrasound waves. Photon-phonon interactions can occur in both directions: The presence of phonons can influence the propagation of photons, while, at the same time, phonons can be stimulated by interaction of photons with matter. This may eventually lead to phonon-assisted nonlinear interaction of light waves, and we hence consider photon-phonon interactions as a part of nonlinear optics.

4.1 Elasto-optic effect

If strain is applied to a medium, the density of the material changes locally, and this leads to variations of the local refractive index. This effect is referred to as the elasto-optic effect. Strain of a material is related to its deformation, i.e., to the vectorial displacement $u = (u_1, u_2, u_3)$ of a volume element (dx, dy, dz) at a position $(x_1, x_2, x_3) = (x, y, z)$. This deformation is quantified by the so-called strain tensor, a symmetric tensor with elements

$$\sigma_{kl} = \frac{1}{2} \left(\frac{\partial u_k}{\partial x_l} + \frac{\partial u_l}{\partial x_k} \right) \quad (4.1)$$

The diagonal elements σ_{11} , σ_{22} , and σ_{33} denote tensile strain along the x -, y -, and z -direction, whereas the off-diagonal elements $\sigma_{23} = \sigma_{32}$, $\sigma_{13} = \sigma_{31}$, and $\sigma_{12} = \sigma_{21}$ are related to shear strain, see Fig. 4.1 for a visualization of the displacements associated with the different kinds of strain. In the presence of strain, the dielectric impermeability tensor $\boldsymbol{\eta}$ changes. To a first-order approximation, the strain-induced changes $\Delta\eta_{ij}$ of the impermeability tensor elements depend linearly on the various elements of the strain tensor,

$$\eta_{ij}(\sigma_{kl}) = \eta_{ij}(0) + \sum_{kl} p_{ijkl} \sigma_{kl}, \quad (4.2)$$

where p_{ijkl} denotes the fourth-rank elasto-optic or photo-elastic tensor. Note that both η_{ij} and σ_{kl} are symmetric tensors and that the pairs of indices (i, j) and (k, l) can be contracted to a single index in analogy to Eq. (3.22),

$$\begin{array}{cccccc} ij/kl & 11 & 22 & 33 & 23, 32 & 13, 31 & 12, 21 \\ I/K & 1 & 2 & 3 & 4 & 5 & 6 \end{array} \quad (4.3)$$

The elasto-optic tensor can be written as 6×6 -matrix p_{IK} ,

$$\Delta\eta_I = p_{IK} \sigma_K \quad (4.4)$$

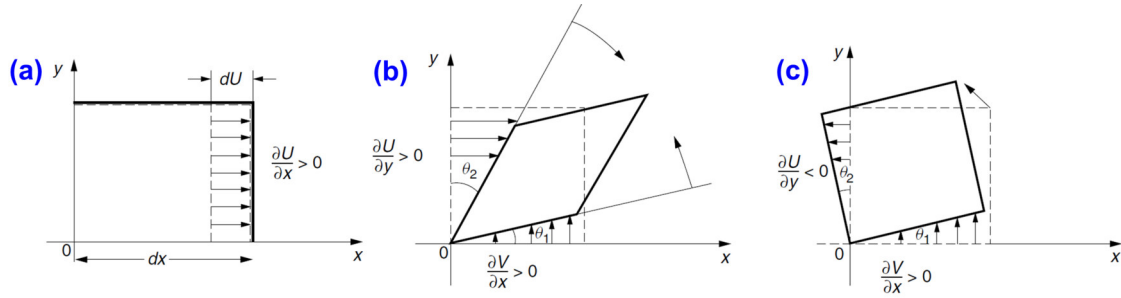


Figure 4.1: Illustration of strain in solid-state medium (U and V correspond to u_1 and u_2 , respectively). (a) Tensile strain ($\sigma_{11} > 0$) corresponds to a displacement $u_1 = U$ that increases with the corresponding spatial coordinate x_1 . (b) Shear strain ($\sigma_{12} > 0$) is described by a steadily increasing lateral displacement perpendicular to a coordinate axis. Note that for the case of shear strain, the lateral displacements $u_1 = U$ and $u_2 = V$ have different signs. (c) The case where the lateral displacements $u_1 = U$ and $u_2 = V$ have different signs corresponds to a simple rotation of the body and does not lead to strain. (Figures adapted from [17])

Similarly to the case of the electric susceptibility tensor, crystal symmetry requires that some of the coefficients p_{IK} vanish and that others are related. Elasto-optic tensors of commonly used materials are shown in Fig. 4.2 and can, e.g., be found in [17].

4.2 Acousto-optics

The elasto-optic effect describes the change of the refractive index as a consequence of local mechanical strain. If the strain is generated by an acoustic wave, the interaction is often referred to as the acousto-optic effect. The refractive index then experiences a spatial modulation which propagates with the acoustic wave. The period of the modulation is defined by the frequency Ω of the sound wave,

$$\Lambda = \frac{2\pi v_s}{\Omega}, \quad (4.5)$$

where v_s denotes the speed of sound in the respective material.

4.2.1 Acousto-optic light deflector

A simple example of an acousto-optic modulator is sketched in Fig. 4.3 (a). The device is based on y -cut tellurium dioxide (TeO_2). This material does not only exhibit elasto-optic properties, but is also piezoelectric, i.e., the acoustic wave is generated by interdigital electrodes which are driven by an electrical AC signal. The acoustic wave is launched on the surface of the crystal; these devices are therefore also called surface acoustic wave (SAW) light deflectors. The incident light is diffracted by the strain-induced periodic index variation, where the direction of diffraction depends on the wavelength (frequency) of the acoustic wave. Such a light deflector is called an acousto-optic light deflector.

For a simple analysis, let us assume that the optical wave and the acoustic wave are launched in (x,z) -plane. If TeO_2 is used as a base material for an acousto-optic device, it is advantageous to exploit the large p_{13} coefficient of the elasto-optic tensor, see Fig. 4.2. This requires application of tensile strain along the z -direction ($\sigma_3 \neq 0$) in combination with an optical wave which is polarized along the x - or the y -direction. In the absence of any strain, TeO_2 is an isotropic medium with refractive index n_0 for all polarizations. If tensile strain is applied along the z -direction, the material becomes uniaxial with the optical axis oriented along the z -direction and the refractive

Name of Substance	Chemical Symbol	Photoelastic Constant	Index of Refraction	Wavelength (μm)	Crystal Symmetry	Elasto-optic Tensor
Fused silica	SiO_2	$p_{11} = 0.121$ $p_{12} = 0.270$ $p_{44} = p_{55} = p_{66}$ $= \frac{1}{2}(p_{11} - p_{12})$	$n = 1.457$	0.63	Isotropic	$\begin{bmatrix} p_{11} & p_{12} & p_{12} & 0 & 0 & 0 \\ p_{12} & p_{11} & p_{12} & 0 & 0 & 0 \\ p_{12} & p_{12} & p_{11} & 0 & 0 & 0 \\ 0 & 0 & 0 & p_{44} & 0 & 0 \\ 0 & 0 & 0 & 0 & p_{55} & 0 \\ 0 & 0 & 0 & 0 & 0 & p_{66} \end{bmatrix}$
Water	H_2O	$p_{11} = 0.31$ $p_{12} = 0.31$ $p_{44} = p_{55} = p_{66}$ $= \frac{1}{2}(p_{11} - p_{12})$	$n = 1.33$	0.63	Isotropic	$\begin{bmatrix} p_{11} & p_{12} & p_{12} & 0 & 0 & 0 \\ p_{12} & p_{11} & p_{12} & 0 & 0 & 0 \\ p_{12} & p_{12} & p_{11} & 0 & 0 & 0 \\ 0 & 0 & 0 & p_{44} & 0 & 0 \\ 0 & 0 & 0 & 0 & p_{55} & 0 \\ 0 & 0 & 0 & 0 & 0 & p_{66} \end{bmatrix}$
Gallium arsenide	GaAs	$p_{11} = -0.165$ $p_{12} = -0.140$ $p_{44} = -0.061$	$n_x = n_y = n_z = 3.42$	1.15	$\bar{4}3m$	$\begin{bmatrix} p_{11} & p_{12} & p_{12} & 0 & 0 & 0 \\ p_{12} & p_{11} & p_{12} & 0 & 0 & 0 \\ p_{12} & p_{12} & p_{11} & 0 & 0 & 0 \\ 0 & 0 & 0 & p_{44} & 0 & 0 \\ 0 & 0 & 0 & 0 & p_{44} & 0 \\ 0 & 0 & 0 & 0 & 0 & p_{44} \end{bmatrix}$
Zinc sulfide	$\beta\text{-ZnS}$	$p_{11} = 0.091$ $p_{12} = -0.01$ $p_{44} = 0.075$	$n_x = n_y = n_z = 2.352$	0.63		$\begin{bmatrix} p_{11} & p_{12} & p_{12} & 0 & 0 & 0 \\ p_{12} & p_{11} & p_{12} & 0 & 0 & 0 \\ p_{12} & p_{12} & p_{11} & 0 & 0 & 0 \\ 0 & 0 & 0 & p_{44} & 0 & 0 \\ 0 & 0 & 0 & 0 & p_{44} & 0 \\ 0 & 0 & 0 & 0 & 0 & p_{44} \end{bmatrix}$
Lithium niobate	LiNbO_3	$p_{11} = -0.02$ $p_{12} = 0.08$ $p_{13} = 0.13$ $p_{14} = -0.08$ $p_{31} = 0.17$ $p_{33} = 0.07$ $p_{41} = -0.15$ $p_{44} = 0.12$ $p_{66} = \frac{1}{2}(p_{11} - p_{12})$	$n_x = n_y = 2.286$ $n_z = 2.20$	0.63	$3m$	$\begin{bmatrix} p_{11} & p_{12} & p_{13} & p_{14} & 0 & 0 \\ p_{12} & p_{11} & p_{13} & -p_{14} & 0 & 0 \\ p_{13} & p_{13} & p_{33} & 0 & 0 & 0 \\ p_{41} & -p_{41} & 0 & p_{44} & 0 & 0 \\ 0 & 0 & 0 & 0 & p_{44} & p_{41} \\ 0 & 0 & 0 & 0 & p_{14} & p_{66} \end{bmatrix}$
Lithium tantalate	LiTaO_3	$p_{11} = -0.08$ $p_{12} = -0.08$ $p_{13} = 0.09$ $p_{14} = -0.03$ $p_{31} = 0.09$ $p_{33} = -0.044$ $p_{41} = -0.085$ $p_{44} = 0.02$ $p_{66} = \frac{1}{2}(p_{11} - p_{12})$	$n_x = n_y = 2.176$ $n_z = 2.180$	0.63	$3m$	
Rutile	TiO_2	$p_{11} = -0.011$ $p_{12} = 0.172$ $p_{13} = -0.168$ $p_{31} = -0.096$ $p_{33} = -0.058$ $p_{44} = 0.0095$ $p_{66} = \pm 0.072$	$n_x = n_y = 2.585$ $n_z = 2.875$	0.63	$\bar{4}2m$	
Potassium dihydrogen phosphate (KDP)	KH_2PO_4	$p_{11} = 0.251$ $p_{12} = 0.249$ $p_{13} = 0.246$ $p_{31} = 0.225$ $p_{33} = 0.221$ $p_{44} = -0.019$ $p_{66} = -0.058$	$n_x = n_y = 1.51$ $n_z = 1.47$	0.63	$\bar{4}2m$	$\begin{bmatrix} p_{11} & p_{12} & p_{13} & 0 & 0 & 0 \\ p_{12} & p_{11} & p_{13} & 0 & 0 & 0 \\ p_{13} & p_{13} & p_{33} & 0 & 0 & 0 \\ 0 & 0 & 0 & p_{44} & 0 & 0 \\ 0 & 0 & 0 & 0 & p_{44} & 0 \\ 0 & 0 & 0 & 0 & 0 & p_{66} \end{bmatrix}$
Ammonium dihydrogen phosphate (ADP)	$\text{NH}_4\text{H}_2\text{PO}_4$ or ADP	$p_{11} = 0.302$ $p_{12} = 0.246$ $p_{13} = 0.236$ $p_{31} = 0.195$ $p_{33} = 0.263$ $p_{44} = -0.058$ $p_{66} = -0.075$	$n_x = n_y = 1.52$ $n_z = 1.48$	0.63	$\bar{4}2m$	
Tellurium dioxide	TeO_2	$p_{11} = 0.0074$ $p_{12} = 0.187$ $p_{13} = 0.340$ $p_{31} = 0.090$ $p_{33} = 0.240$ $p_{44} = -0.17$ $p_{66} = -0.046$	$n_x = n_y = n_z = 2.35$	0.63	$\bar{4}2m$	$\begin{bmatrix} p_{11} & p_{12} & p_{13} & 0 & 0 & 0 \\ p_{12} & p_{11} & p_{13} & 0 & 0 & 0 \\ p_{13} & p_{13} & p_{33} & 0 & 0 & 0 \\ 0 & 0 & 0 & p_{44} & 0 & 0 \\ 0 & 0 & 0 & 0 & p_{44} & 0 \\ 0 & 0 & 0 & 0 & 0 & p_{66} \end{bmatrix}$

Figure 4.2: Elasto-optic tensors of different materials. Crystal symmetry requires that some of the coefficients p_{IK} vanish and that others are related. (Table adapted from [17])

indices

$$n_x = n_y = n_0 - \frac{1}{2}n_0^3 p_{13} \sigma_3, \quad (4.6)$$

$$n_z = n_0 - \frac{1}{2}n_0^3 p_{33} \sigma_3. \quad (4.7)$$

The index ellipsoid is depicted in Fig. 4.3 (b).

4.2.2 Coupled-wave analysis

In the following, we will analyze the diffraction of light waves at the grating that is produced by the sound wave in an acousto-optic modulator, Fig. 4.3. For TeO_2 , the elasto-optic tensor element $p_{13} = 0.340$. Since the strain tensor element is much smaller than unity, $\sigma_3 \ll 1$, we may assume that the relative refractive index change is also small $\Delta n_y \ll n_y$. In the following, we will assume a wave polarized along the y -direction and omit the subscript y for the sake of readability.

Wave equation

For a basic analysis, let us decompose the time- and space-dependent refractive index change into a constant background index n_0 and a weak variation Δn that is generated by the plane sound wave,

$$n(\mathbf{r}, t) = n_0 + \Delta n(\mathbf{r}, t), \quad (4.8)$$

$$\Delta n(\mathbf{r}, t) = \Delta n_0 \cos(\Omega t - \mathbf{q}\mathbf{r}). \quad (4.9)$$

Here, Ω denotes the acoustic frequency and \mathbf{q} is the wave vector defining the propagating direction of the acoustic wave,

$$|\mathbf{q}| = \frac{\Omega}{v_s}, \quad (4.10)$$

where v_s is the phase velocity of the sound wave within the medium. To derive the wave equation for the acousto-optic interaction, we first use Eqs. (4.8) and (4.9) to write the electric displacement as

$$\underline{\mathbf{D}}(\mathbf{r}, t) \approx \epsilon_0 (n_0^2 \underline{\mathbf{E}}(\mathbf{r}, t) + 2n_0 \Delta n(\mathbf{r}, t) \underline{\mathbf{E}}(\mathbf{r}, t)). \quad (4.11)$$

Inserting this relation into Maxwell's equations (1.2) and (1.4) and following a derivation similar to that of Eq. (1.80), we obtain the wave equation for acousto-optic interaction,

$$\nabla^2 \underline{\mathbf{E}}(\mathbf{r}, t) - \frac{n_0^2}{c^2} \frac{\partial^2 \underline{\mathbf{E}}(\mathbf{r}, t)}{\partial t^2} = \frac{2n_0}{c^2} \frac{\partial^2 (\Delta n(\mathbf{r}, t) \underline{\mathbf{E}}(\mathbf{r}, t))}{\partial t^2}. \quad (4.12)$$

The left-hand side of Eq. (4.12) corresponds to the wave equation for a homogeneous medium. The source term on the right-hand side leads to generation of waves at new frequencies that arise from temporal modulation of the electric field $\underline{\mathbf{E}}(\mathbf{r}, t)$ with the time-dependent refractive index perturbation $\Delta n(\mathbf{r}, t)$ according to Eq. (4.9). As a consequence, a solution of Eq. (4.12) cannot consist of a single plane wave but has to comprise a superposition of plane waves at different frequencies.

Slowly-varying envelope approximation (SVEA)

To solve Eq. (4.12), we use an ansatz that comprises a superposition of several monochromatic plane waves, oscillating at frequencies ω_l ,

$$\underline{\mathbf{E}}(\mathbf{r}, t) = \sum_l \underline{E}(\mathbf{r}, \omega_l) \mathbf{e}_l e^{j(\omega_l t - \mathbf{k}_l \mathbf{r})}. \quad (4.13)$$

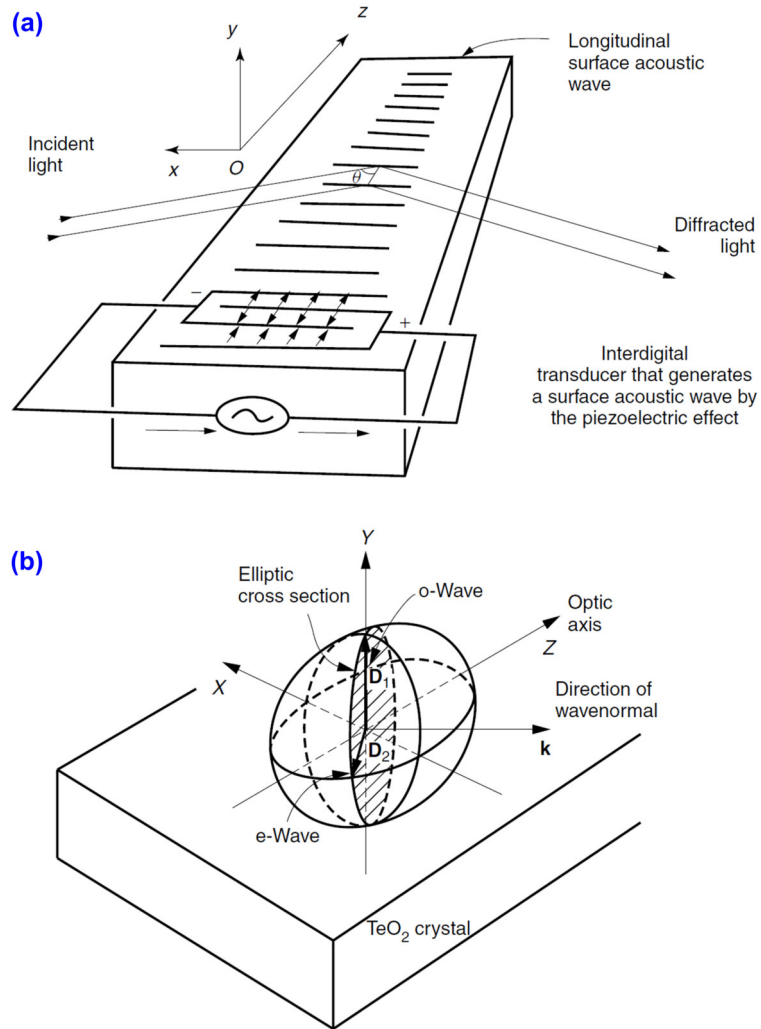


Figure 4.3: Acousto-optic modulator based on y-cut tellurium dioxide (TeO_2). (a) Device concept: The material is piezo-electric, and a surface acoustic wave can easily be generated by interdigital electrodes which are driven by an electrical AC signal. The incident light is diffracted by the strain-induced periodic index variation. Such a light deflector is called an acousto-optic light deflector or an surface acoustic wave (SAW) light deflector. (b) Analysis: In the absence of any strain, TeO_2 is an isotropic medium with refractive index n_0 for all polarizations. If tensile strain is applied along the z -direction, the material becomes uniaxial with the optical axis oriented along the z -direction. Due to the large value of $p_{13} = p_{23}$, this leads to strong changes in refractive index for an optical wave polarized along the y -direction and hence to efficient diffraction in the backward direction. (Figures adapted from [17])

In this relation, the unit vector \mathbf{e}_l defines the polarization of the plane wave oscillating at frequency ω_l . The dominating space dependence of the plane waves is contained in the complex propagator $\exp(j(\omega_l t - \mathbf{k}_l \mathbf{r}))$, whereas the weakly space-dependent scalar amplitudes $\underline{E}(\mathbf{r}, \omega_l)$ account for coupling of the plane waves by the space-dependent index variation $\Delta n(\mathbf{r}, t)$. The magnitude of the wave vector is related to the frequency by $|\mathbf{k}_l| = \frac{\omega_l n_0}{c}$. Note that the time dependence of the index variation is already covered by the fact that we assume a superposition of various carrier frequencies ω_l . An explicit time-dependence of the amplitude \underline{E} is hence not required.

We insert Eq. (4.13) into Eq. (4.12), use the product rule for the Laplace operator, $\nabla^2(\Phi\Psi) = \Phi\nabla^2\Psi + 2\nabla\Phi \cdot \nabla\Psi + \Psi\nabla^2\Phi$, and make use of the slowly-varying envelope approximation, i.e., the fact that $\underline{E}(\mathbf{r}, \omega_l)$ varies only weakly with space,

$$|\nabla^2 \underline{E}(\mathbf{r}, \omega_l)| \ll |\mathbf{k}_l \cdot \nabla \underline{E}(\mathbf{r}, \omega_l)|.$$

This leads to the coupled-wave equation for the space-dependent wave amplitudes $\underline{E}(\mathbf{r}, \omega_l)$,

$$\sum_l [-2j\mathbf{k}_l \cdot \nabla \underline{E}(\mathbf{r}, \omega_l)] \mathbf{e}_l e^{j(\omega_l t - \mathbf{k}_l \mathbf{r})} = \frac{2n_0}{c^2} \sum_l \frac{\partial^2}{\partial t^2} \left(\Delta n(\mathbf{r}, t) \underline{E}(\mathbf{r}, \omega_l) \mathbf{e}_l e^{j(\omega_l t - \mathbf{k}_l \mathbf{r})} \right). \quad (4.14)$$

Let us assume that we launch a single optical wave at frequency ω_0 . Spatio-temporal modulation of the refractive index profile according to Eq. (4.9) leads to generation of new frequencies $\omega_{\pm 1} = \omega_0 \pm \Omega$. For simplicity, let us only consider the evolution of the complex amplitude $\underline{E}(\mathbf{r}, \omega_1)$ at frequency ω_1 ,

$$\mathbf{k}_1 \cdot \nabla \underline{E}(\mathbf{r}, \omega_1) = -j \frac{1}{2} (\mathbf{e}_1 \cdot \mathbf{e}_0) \frac{\omega_1^2}{c^2} n_0 \Delta n_0 \underline{E}(\mathbf{r}, \omega_0) e^{-j(\mathbf{k}_0 + \mathbf{q} - \mathbf{k}_1) \mathbf{r}}. \quad (4.15)$$

Oscillation of the acoustic wave at frequency Ω hence leads to coupling of the optical waves at frequency ω_0 and $\omega_1 = \omega_0 + \Omega$. In this case, the frequency is up-shifted. In other configurations, the acoustic wave can also lead to a downshift of frequency from ω_0 to $\omega_{-1} = \omega_0 - \Omega$. The efficiency with which these processes occur is again given by the corresponding phase matching condition on the right-hand side of Eq. (4.15).

Phase matching and Bragg condition

Efficient interaction between the waves can only occur if the spatially quickly varying exponential on the right-hand side of Eq. (4.15) vanishes. For the case of up-shifted frequencies, this leads to the phase matching condition

$$\mathbf{k}_1 = \mathbf{k}_0 + \mathbf{q}. \quad (4.16)$$

The corresponding wave vector diagrams are sketched in Fig. 4.4. The solution of the phase matching condition can be simplified by exploiting the fact that the relative change in frequency Ω/ω_0 is much smaller than the relative change of the wavevector

$$\frac{|\mathbf{q}|}{|\mathbf{k}_0|} = \frac{c}{v_s} \frac{\Omega}{\omega}. \quad (4.17)$$

As a consequence we may neglect the change in optical frequency and hence the energy transfer between the optical and the acoustic wave and assume that the magnitude of the wavenumber remains unchanged,

$$|\mathbf{k}_0| \approx |\mathbf{k}_1|, \quad (4.18)$$

see Fig. 4.4 (a). The deflection angle $2\Theta_B$ of the optical wave can then be obtained from

$$\sin \Theta_B = \frac{|\mathbf{q}|}{2|\mathbf{k}_0|} = \frac{\lambda/n_0}{2\Lambda}. \quad (4.19)$$

The quantity Θ_B is also referred to as the Bragg¹ angle: At this angle, incremental optical reflections from neighboring wavefronts of the acoustic wave experience a relative phase delay of 2π and hence interfere constructively in the backward direction. This angle is observed for both frequency upconversion and downconversion - depending on the propagation direction of the sound wave, see Figs. 4.4 (a) and (b).

In many cases of practical interest, the interacting optical and acoustic beams do not have plane phase fronts, see Fig. 4.5. If a converging optical beam interacts with a plane sound wave, only one plane-wave component of the optical beam satisfies the Bragg condition, and the diffracted light hence represents a plane wave, Fig. 4.5 (a). In contrast to that, for sufficiently large divergence angles $\delta\Theta$ of the acoustic beam, every plane-wave component of the converging optical beam finds an acoustic plane-wave counterpart that satisfies the Bragg condition. The diffracted beam hence represents a diverging beam, Fig. 4.5 (b).

Quantum interpretation

In a quantum picture, light of angular frequency ω and wavevector \mathbf{k} , where $|\mathbf{k}| = \omega/c$, is represented by a stream of photons of energy $\hbar\omega$ and momentum $\hbar\mathbf{k}$. Likewise, an acoustic wave of angular frequency Ω and wavenumber \mathbf{q} , where $|\mathbf{q}| = \Omega/v_s$ and where v_s denotes the speed of sound in the respective material, can be regarded as a stream of phonons of energy $\hbar\Omega$ and momentum $\hbar\mathbf{q}$. Acousto-optic effects correspond to interaction of photons with phonons, whereby new photons with frequency ω_s and wavevectors \mathbf{k}_s can be generated, where energy and momentum conservation require

$$\omega_s = \omega + \Omega, \tag{4.20}$$

$$\mathbf{k}_s = \mathbf{k} + \mathbf{q}. \tag{4.21}$$

For so-called acoustic phonons, we have $\Omega \ll \omega$, which leads again to the illustrations sketched in Fig. 4.4. Further insight into interactions of photons with different kinds of phonons will be given in Section 4.3.

4.2.3 Acousto-optic devices

Acousto-optic effects are used in various applications, a few of which will be discussed in the following.

Acousto-optic modulators If the sound wave is sufficiently weak, the intensity of the refracted light is proportional to the intensity of the acoustic wave. The device can then be used as an analogue modulator that translates the envelope of the sound wave to the envelope of the optical wave, see Fig. 4.6 (a). At high acoustic intensities, however, the light beam is completely reflected, and the intensity of the optical wave is not any more proportional to that of the sound wave. The device can then be used as an optical switch, which turns the reflected light on and off by switching the sound wave on and off, Fig. 4.6 (b). For a broadband acoustic modulation signal, each frequency component of the sound wave must find a suitable optical plane wave component that has a suitable propagation direction to fulfill the Bragg condition. The acousto-optic modulation bandwidth is therefore connected to the angular divergence of the optical beam, see, e.g., [26] for more details.

Beam scanners Acousto-optic scanners rely on the relation between the angle $2\Theta_B$ of deflection and the sound frequency Ω , see Eq. (4.19). For small deflection angles, we can approximate this relationship by

$$2\Theta_B = \frac{c}{v_s} \frac{\omega}{\Omega}. \tag{4.22}$$

¹Bragg observed similar effects when sending coherent X-ray beams through a crystalline solid: For suitable combinations of propagation direction, lattice constant, and frequency, the scattered waves interfere constructively and form ring- and point-like diffraction patterns.

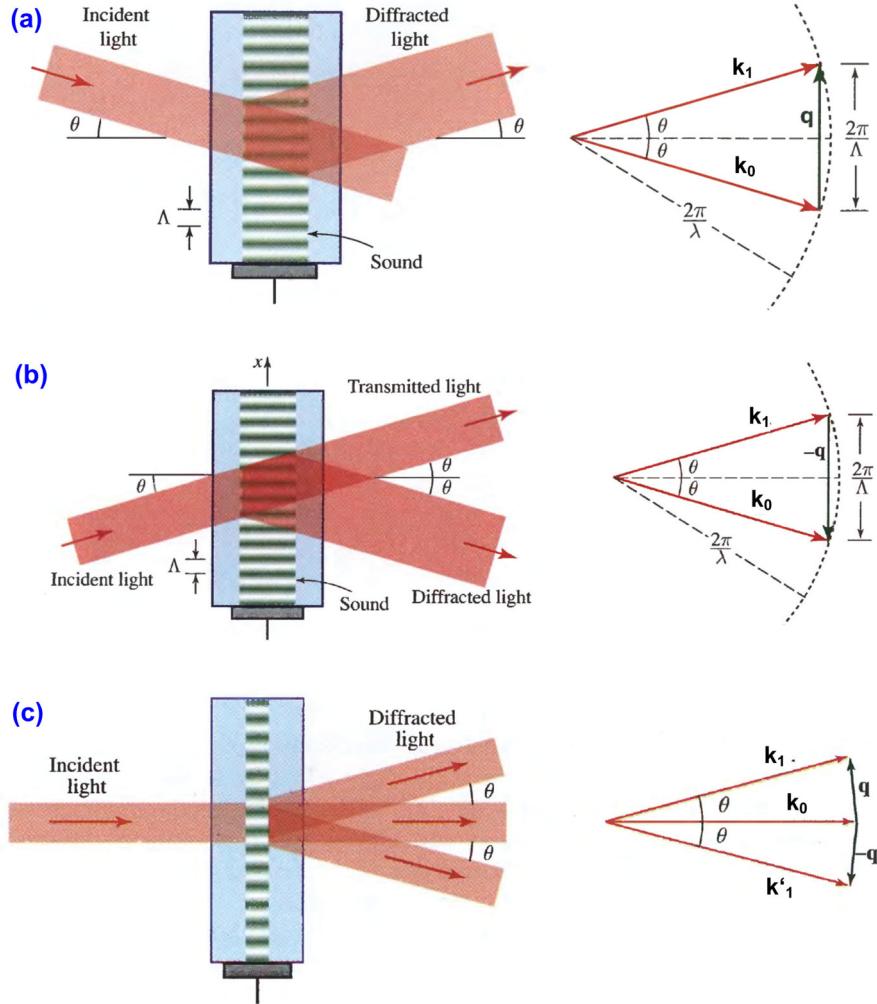


Figure 4.4: Diffraction of beams in acousto-optic modulators. Momentum conservation requires $\mathbf{k}_1 = \mathbf{k}_0 + \mathbf{q}$, whereas for interaction with acoustic phonons we may assume that $\Omega \ll \omega$ and hence $|\mathbf{k}_0| \approx |\mathbf{k}_1|$. (a) Upconversion of the optical frequency: The optical beam is diffracted by a counter-propagating optical beam, which leads to an increased frequency $\omega_1 = \omega + \Omega$ of the diffracted light by the Doppler effect. The vector wave equation $\mathbf{k}_1 = \mathbf{k}_0 + \mathbf{q}$ is equivalent to the Bragg condition $\sin \theta_B = |\mathbf{q}| / (2|\mathbf{k}_0|)$. (b) Downconversion of the optical frequency: The optical beam is diffracted from a co-propagating optical beam, which leads to a decreased frequency of the diffracted light, $\omega_1 = \omega - \Omega$. Again, the vector wave equation $\mathbf{k}_1 = \mathbf{k}_0 + \mathbf{q}$ is equivalent to the Bragg condition $\sin \theta_B = |\mathbf{q}| / (2|\mathbf{k}_0|)$. (c) A standing acoustic wave leads to a diffraction of the optical wave in two directions. Both outgoing optical waves contain an up-shifted frequency component $\omega + \Omega$ and a down-shifted frequency component $\omega - \Omega$. (Figures adapted from [26])

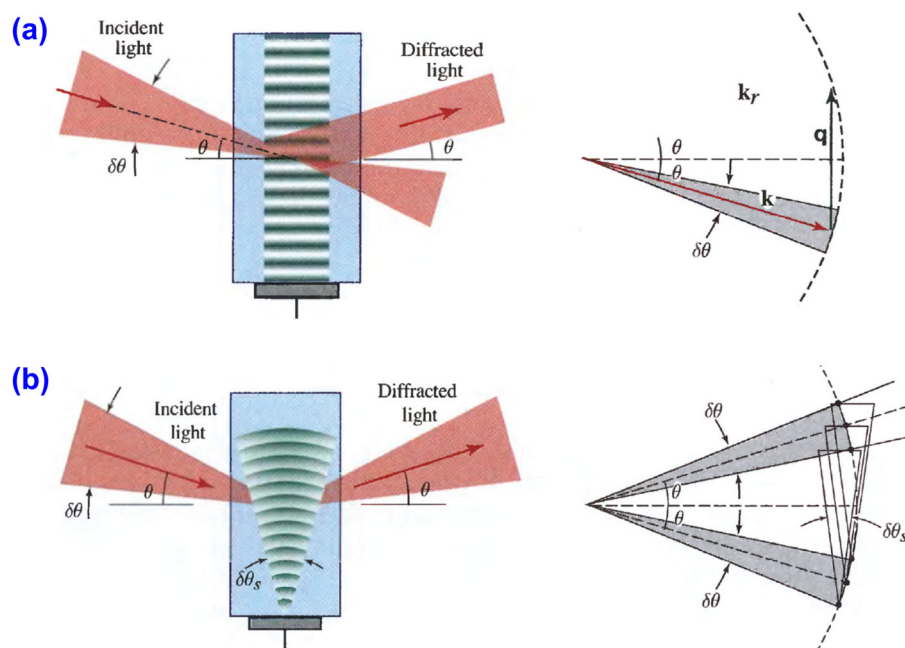


Figure 4.5: Interaction of optical and acoustic beams that do not have plane phase fronts. (a) If a converging optical beam interacts with a plane sound wave, only one plane-wave component of the optical beam satisfies the Bragg condition. The diffracted light hence represents a plane wave. (b) For sufficiently large divergence angles $\delta\theta$ of the acoustic beam, every plane-wave component of the optical beam finds an acoustic plane-wave counterpart that satisfies the Bragg condition. (Figures adapted from [26])

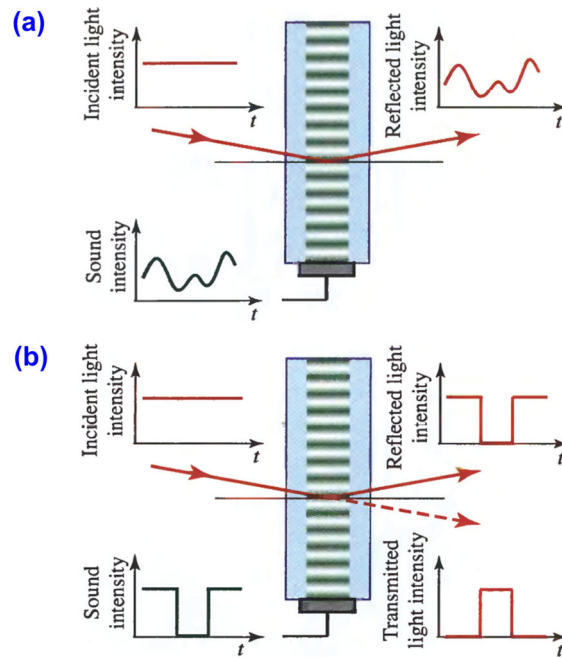


Figure 4.6: Acousto-optic modulators. (a) Analogue modulator: For weak acoustic waves, the intensity of the refracted light is proportional to the intensity of the acoustic wave. (b) Acousto-optic switch: At high acoustic intensities, the light beam is completely reflected. The reflected beam can be turned on and off by switching the sound wave on and off. (Figures adapted from [26])

Hence, by changing the modulation frequency, the beam can be scanned in the lateral direction. Phase matching can be maintained by varying both the angle of incidence and the acoustic frequency simultaneously. This can be accomplished by using, e.g., a phased array of acoustic transducers which are driven with a phase delay as to generate the required phase shift, see Fig. 4.7 (a). Alternatively, a diverging sound beam can be used rather than a plane sound wave such that the incoming light wave always finds an acoustic plane-wave component with the matching propagation direction, see Fig. 4.7 (b).

Space switches Acousto-optic beam scanners can also be used to realize space switches, see Fig. 4.8 (a). By using acoustic drive signals that comprise various frequency components, it is possible to split the incident optical beam to various different directions, where the intensity coupled to a certain direction is proportional to the power of the respective sound-frequency component, Fig. 4.8 (b).

Frequency shifters In an acousto-optic cell, the Bragg-reflected light is shifted up or down by the frequency of the sound wave, Fig. 4.9 (a). The devices can hence be used as a tunable frequency shifter. Such devices are, e.g., used for highly sensitive heterodyne detection, where a received signal is superimposed with a frequency-shifted copy of the transmitted signal to measure amplitude and phase changes simultaneously. The example of a vibrometer is illustrated in Fig. 4.9 (b). More information on the principles of vibrometry can be found in [1].

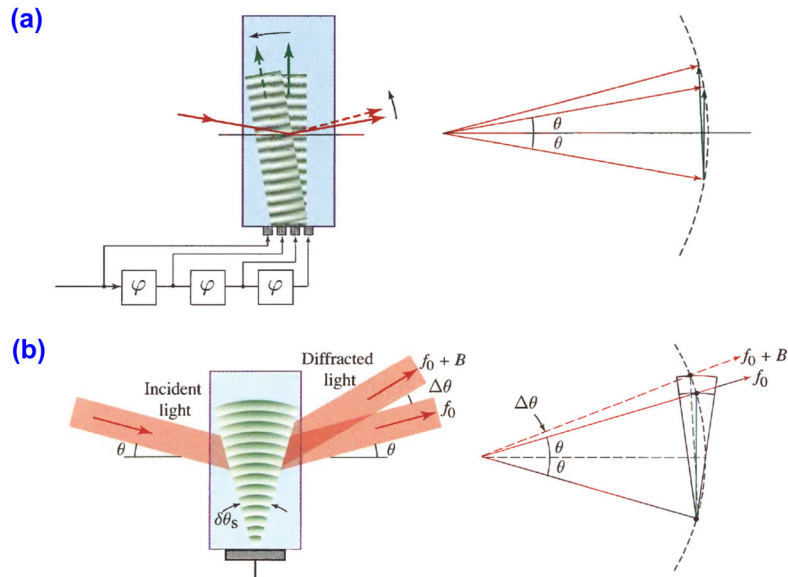


Figure 4.7: Acousto-optic beam scanners. (a) Phased array of acoustic transducers: Simultaneous variation of the angle of incidence and the acoustic frequency is necessary to maintain phase matching. (b) Diverging sound beam: Incoming light wave always finds an acoustic plane-wave component that fulfills the Bragg condition. (Figures adapted from [26])

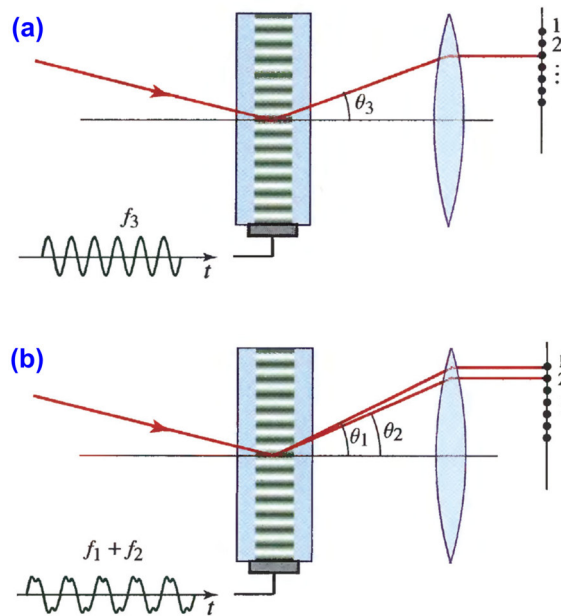


Figure 4.8: Acousto-optic space switches (a) By changing the modulation frequency, the beam can be switched from one port to another. (b) Using acoustic drive signals that comprise various frequency components, it is possible to split the incident optical beam to various different directions, where the intensity coupled to a certain direction is proportional to the power of the respective acoustic frequency component. The Bragg condition is disregarded in these sketches for simplicity. (Figures adapted from [26])

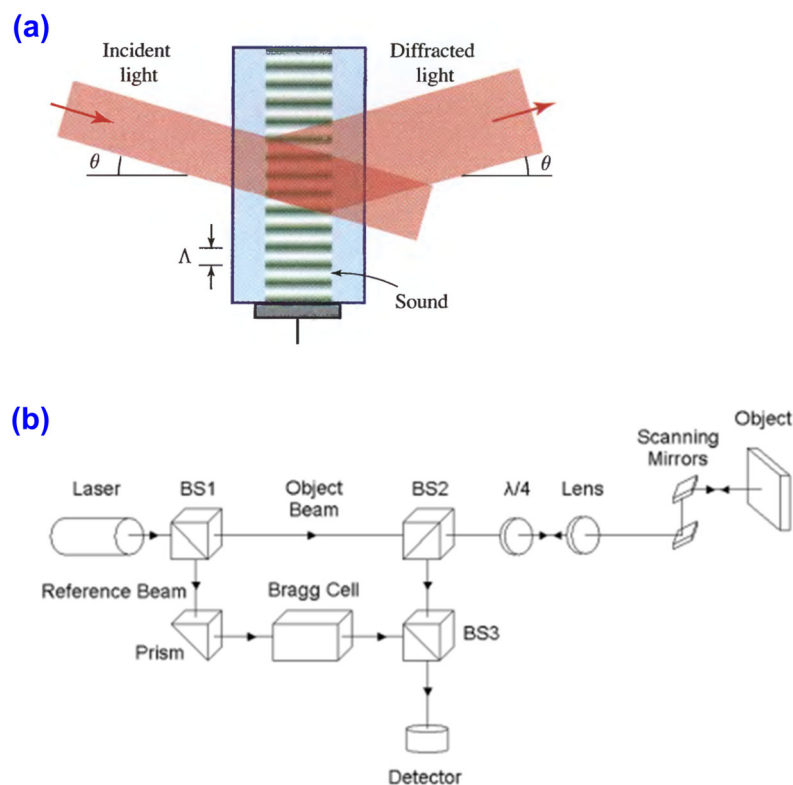


Figure 4.9: Acousto-optic space frequency shifter. (a) In the case of counter-propagating sound and light waves, the Doppler effect leads to an up-shift in frequency of the the diffracted light by the frequency of the sound wave. For co-propagating waves, the frequency would have been down-shifted. (b) Basic principle of optical vibrometry: Light reflected from an object is superimposed with a frequency-shifted copy of itself and detected. If the object does not move, this leads to a narrowband beatnote in the photodetector current. Vibration of the object leads to a spectral broadening of this beatnote. Spectral analysis of the photocurrent allows to derive the mechanical vibration spectrum of the object. (Figures adapted from [26, 1])

4.3 Interaction of photons and phonons

The acousto-optic interactions considered in the last section can be interpreted as a special case of interaction of photons and phonons. Such interactions, however, are not restricted to the case where traveling sound waves are launched into the material. In this section we will consider two more interaction mechanisms of photons and phonons: Brillouin scattering, which is associated with interaction of photons with propagating sound waves, so-called acoustic phonons, and Raman scattering, which originates from interaction of photons with vibrational normal modes of molecules, so-called optic phonons. Simplified dispersion relations and motion patterns of acoustic and optical phonons in a linear diatomic chain are illustrated in Fig. 4.10. The term “acoustic phonon” refers to a lattice vibration pattern in which neighboring atoms move in phase. In this case, the phonon energy is much smaller than that of optical phonons and increases linearly with momentum. For optical phonons, neighbouring atoms move out of phase. The energy of optical phonons is much larger than that of acoustic phonons and is largely independent of momentum. Note that in an optical fiber Brillouin scattering can only occur in backward direction, whereas Raman scattering can occur in both backward and forward direction.

An overview of different photon-phonon-interactions by means of elastic and inelastic light scattering is illustrated in Fig. 4.11. For completeness, Rayleigh scattering is also illustrated, even though no energy transfer between photons and phonons is involved in this case. Rayleigh scattering is caused by elastic scattering of photons from tiny inhomogeneities in the medium that are much smaller than the wavelength. Energy conserved in this process and the frequency of the light does hence not change. Brillouin and Raman scattering, in contrast, lead to transfer of energy between the incident photons and phonons. This can lead to a loss of photon energy and creation of a new phonon, or to an increase of photon energy by absorption of a phonon. The case where the photon loses energy is also referred to as the Stokes process, whereas the an increase of photon energy corresponds to the Anti-Stokes process. Brillouin and Raman scattering can occur in both the Stokes and the Anti-Stokes case. Since the energy of optical phonons is much larger than that of acoustic phonons, the Raman frequency shift is much larger than the Brillouin shift.

In the following, we will restrict ourselves to a brief phenomenological description of Brillouin and Raman scattering. A more in-depth discussion of Brillouin and Raman scattering in optical fibers can be found in [5].

4.3.1 Brillouin scattering

Spontaneous Brillouin scattering can be viewed as scattering of pump-wave photons from an acoustic wave. For a rough estimate of the associated frequency shift, let us consider the case of an optical wave at a wavelength of $\lambda = 1.55 \mu\text{m}$, propagating along a silica fiber of refractive index 1.45. When considering Brillouin scattering in an optical fiber, we observe inelastic scattering of light in the backward direction only. As both energy and momentum have to be conserved during the scattering event, Eqs. (4.20) and (4.21), we find that the Brillouin shift of the backscattered light is given by

$$f_B = \frac{\Omega_B}{2\pi} = 2n \frac{v_s}{c} f, \quad (4.23)$$

where f is the optical frequency, and where v_s is the speed of sound within the silica material of the fiber. Using $v_s = 5.96 \text{ km/s}$ for sound waves in silica, we find the Brillouin shift of a silica fiber to be approximately 11 GHz. For backward scattering, the momentum of the phonon corresponds to twice the momentum of the incident photon. At the same time, since $f_B \ll f$, i.e., the energy of the scattered photon is practically identical to that of the incident photon, even though twice the photon momentum is transferred to the phonon. For forward scattering, the momentum transfer to the acoustic phonon would be close to zero, and hence no energy would be transferred. Forward scattering is therefore indistinguishable from elastic Rayleigh scattering, which does not

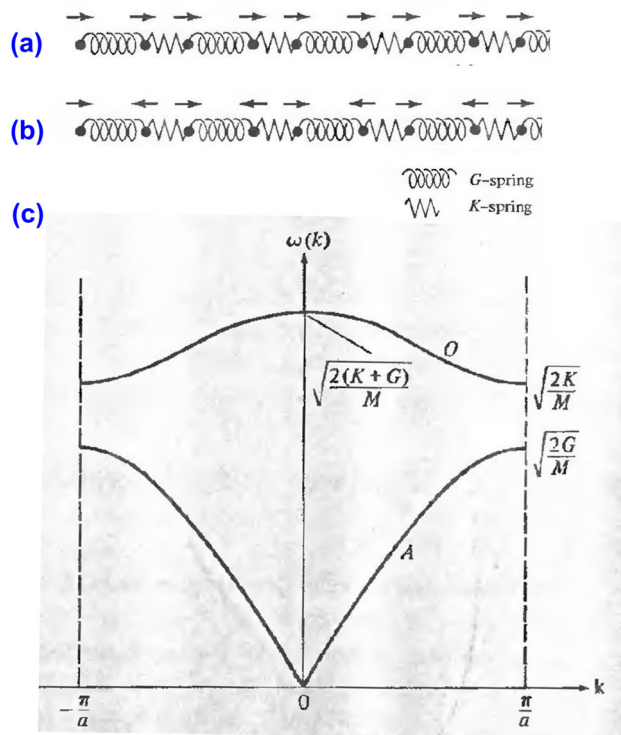


Figure 4.10: Acoustic and optical phonons along with the corresponding dispersion relations. (a) Illustration of an acoustic phonon using a simplified diatomic linear-chain model medium: The crystal is assumed to consist of a linear chain of identical atoms, which are connected by springs of alternating strengths (“G-spring” and “K-spring”). For long-wavelength acoustic phonons, the local ensemble of atoms moves in the same direction. The K-vector is associated with the wavelength of the long-range oscillation. Acoustic phonons can be thought of as sound waves that propagate through the medium. (b) Illustration of an optical phonon, for which neighboring atoms move 180° out of phase. The wave vector is now associated with a long-range envelope of the oscillation of neighboring atoms with respect to each other. This leads to a higher oscillation frequency and hence a higher energy. Optical phonons can be thought of as vibrational modes of molecules and chains of atoms. (c) Dispersion relation of the acoustic (A) and the optical (O) phonons of the diatomic linear chain. Optical phonons have nonzero energy even though the K-vector (momentum) is equal to zero. (Figures adapted from [6])

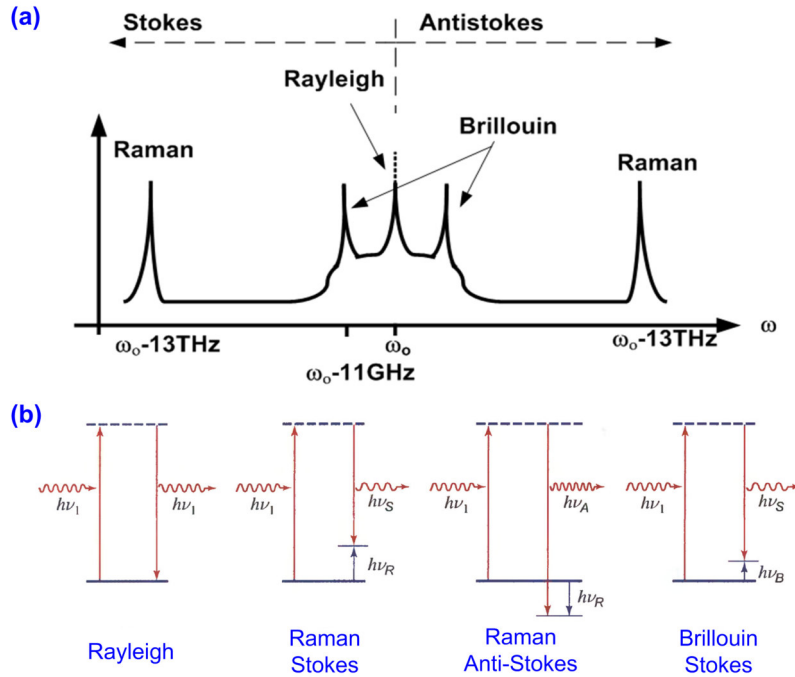


Figure 4.11: Interaction of photons and phonons by elastic and inelastic light scattering. (a) Spectral distribution of scattered light. The incident light beam oscillates at frequency ω_0 . Elastic Rayleigh scattering is caused by inhomogeneities in the medium that are much smaller than the wavelength. Energy is conserved in this process and the frequency of the light does hence not change. Brillouin scattering leads to transfer of energy between the incident photons and acoustic phonons. This can lead to a loss of photon energy and creation of a new phonon, or to an increase of photon energy by absorption of a phonon. The case where the photon loses energy is also referred to as the Stokes process, whereas the an increase of photon energy corresponds to the Anti-Stokes process. Raman scattering can also occur in both the Stokes and the Anti-Stokes case, but the frequency shift is much larger than for Brillouin scattering due to interaction with high-energy optical phonons. (b) Energy-level illustrations of various light scattering processes. The dashed horizontal lines indicate virtual energy states. For Brillouin scattering, only the Stokes case is illustrated, even though scattering may occur in both Stokes and Anti-Stokes configuration. (Figures adapted from [26])

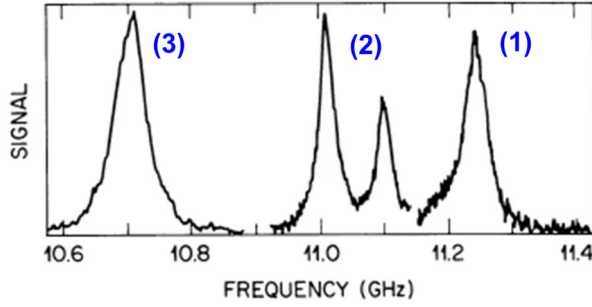


Figure 4.12: Gain spectra of stimulated Brillouin scattering in different optical fibers for a pump wavelength of 1525 nm. The gain spectrum is influenced by both the guided nature of the optical modes and by the presence of dopants in the core. (1) Silica-core fiber; (2) Depressed-cladding fiber; (3) Dispersion-shifted fiber (Figures adapted from [5])

change photon energy. For optical phonons, however, the dispersion relation does not go through the origin, see Fig. 4.10. As a consequence, a measurable amount of energy can be transferred from the incident photon to an optical phonon even for the case of forward scattering, where the momentum of the scattered photon changes only slightly. Raman scattering can therefore occur both in the forward and in the backward direction, see Section 4.3.2.

Once the scattered lightwave is generated by spontaneous Brillouin scattering, it interferes with the pump wave, leading to a beat signal at exactly the frequency Ω_B . The beating leads to formation of new phonons, e.g., via the process of electrostriction², and hence acts as a source for the sound wave, which in turn increases the amplitude of the scattered wave, see [9] for a more detailed analysis. The positive feedback leads to stimulated Brillouin scattering (SBS), which can be described by the relations

$$\frac{dI_p}{dz} = -g_B I_p I_s - \alpha I_p, \quad (4.24)$$

$$\frac{dI_s}{dz} = g_B I_p I_s - \alpha I_s, \quad (4.25)$$

where I_s and I_p denote the Stokes and the pump intensity, respectively, $g_B(\Omega) = g_B(\omega_p - \omega_s)$ is the frequency-dependent Brillouin gain, and α accounts for fiber loss. Measured Brillouin gain spectra for different optical fibers are depicted in Fig. 4.12. The three fibers have different structures and different doping levels of germania (GeO_2) in their core, leading to slight deviations from the estimated Brillouin shift of 11 GHz. In addition, the gain spectrum has a certain width which is associated with the phonon lifetime within the respective optical fiber. Depending on the type of optical fiber, the SBS gain bandwidth can vary significantly. Typical values are around 50 MHz, but gain bandwidths beyond 100 MHz are also possible.

SBS can lead to significant transfer from the pump power to the scattered wave. Once the optical power launched into a fiber exceeds a certain threshold, most of the light is reflected back by SBS. This ultimately limits the power of a narrowband source that can be transmitted through an optical fiber. SBS thresholds can be as low as a few milliwatts for a fiber length of several kilometers, see [4] for more details.

4.3.2 Raman scattering

Similarly to the case of Brillouin scattering, spontaneous Raman scattering can be viewed as scattering of the pump by interaction with vibrational states of the material molecules or atoms. The two phenomena differ, however, by the fact that for Raman scattering, the photons interact with an optical phonons instead of propagating acoustic waves, and that energy transfer between

²Electrostriction is a process in which dielectrics change their shape under the application of an electric field.

the photons and the phonons is hence largely independent from the momentum transfer. As a consequence, spontaneous Raman scattering in an optical fiber occurs both in forward and backward direction, or isotropically in all direction if no fiber is involved. As indicated by the dispersion relation in Fig. 4.10, optical phonons carry much more power than acoustic phonons. The frequency shift associated with Raman scattering is hence much larger than the Brillouin shift.

Just like stimulated Brillouin scattering, stimulated Raman scattering (SRS) can occur due to a positive feedback: The scattered wave interferes with the incoming wave, generating a beat signal at the Raman frequency. This leads to the creation of new phonons, e.g., by electrostriction, which further enhance Raman scattering. SRS is governed by the relations,

$$\frac{d I_s}{d z} = g_R I_p I_s - \alpha_s I_s, \quad (4.26)$$

$$\frac{d I_p}{d z} = -\frac{\omega_p}{\omega_s} g_R I_p I_s - \alpha_p I_p, \quad (4.27)$$

where I_s and I_p denote the Stokes and the pump intensity, respectively, $g_R(\Omega) = g_R(\omega_p - \omega_s)$ is the frequency-dependent Raman gain, and α_s and α_p account for fiber losses at the Stokes and pump frequencies, respectively. In silica fibers, the maximum Raman gain occurs at a frequency shift of 13 THz from the pump wave. The factor ω_p/ω_s on the left-hand side of Eq. (4.27) takes into account the different photon energies.

Since silica is an amorphous material, it contains microscopic inhomogeneities, i.e., each silica molecule experiences a slightly different environment and the frequencies of the vibrational eigenstates hence differ slightly. This leads to inhomogeneous broadening of the Raman gain spectrum - the Raman gain bandwidth in optical fibers can easily exceed 10 THz, see Fig. 4.13. In contrast to that, the Raman gain spectra of crystalline materials such as silicon are much more narrowband.

Similar to the case of SBS, SRS can also limit the power that can be transmitted through an optical fiber. For SRS, the threshold power levels are much larger than in the case of SBS, but the large gain bandwidth may still lead to SRS-induced impairments in wavelength-division multiplexing (WDM) systems with large numbers of optical channels, see [4] and the references therein for more details.

Raman amplifiers and Raman lasers

If the pump and the signal wavelengths are chosen accordingly, SRS can be used for amplification of signals, thereby making use of the extremely large gain bandwidth, see [4] and the references therein for more details. A forward-pumped Raman amplifier is depicted in Fig. 4.14. We can calculate the Raman gain of a fiber of length L by using Eqs. (4.26) and (4.27). If the signal is much weaker than the pump, we may neglect pump depletion due to Raman scattering. We can readily integrate Eq. (4.27) to obtain the evolution of the pump intensity along the fiber,

$$I_p(z) = I_p(0) e^{-\alpha_p z}. \quad (4.28)$$

This relation can be used to solve Eq. (4.26), leading to

$$I_s(L) = I_s(0) e^{-\alpha_s L} G_R, \quad (4.29)$$

where the Raman gain G_R is given by

$$G_R = e^{g_R I_p(0) L_{\text{eff}}}. \quad (4.30)$$

The effective length L_{eff} is slightly shorter than the geometrical length L of the fiber due to attenuation of the pump,

$$L_{\text{eff}} = \frac{1 - e^{-\alpha_p L}}{\alpha_p}. \quad (4.31)$$

When used within an optical cavity, SRS can serve as an amplification mechanism for laser emission. This principle has, e.g., been exploited to realize one of the first integrated all-silicon light sources [25].

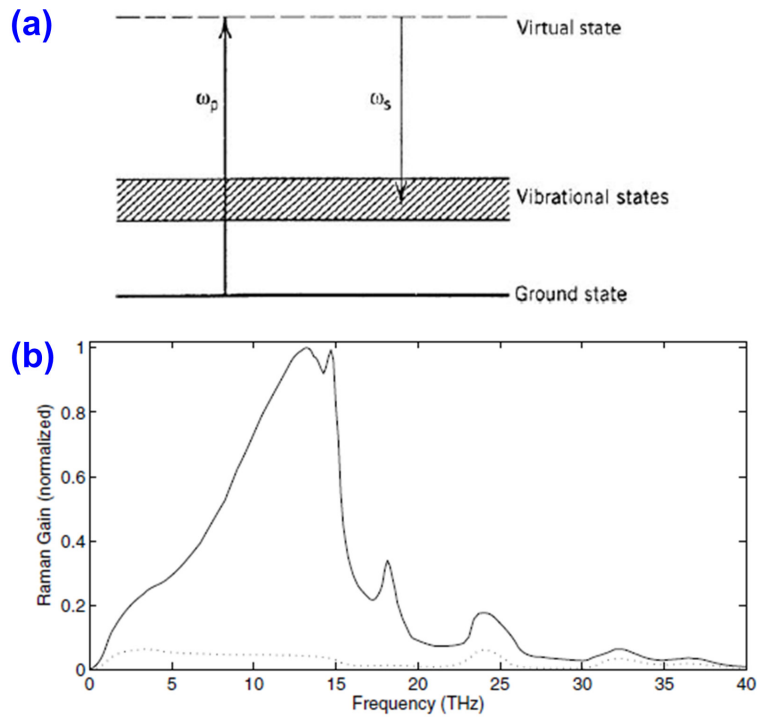


Figure 4.13: Raman scattering. (a) Energy-level representation of Raman scattering in a silica fiber. Silica is an amorphous material, and each silica molecule hence experiences a slightly different environment. As a consequence, the frequencies of the vibrational eigenstates differ slightly, which leads to inhomogeneous broadening of the Raman gain spectrum. (b) Raman gain spectrum in a silica fiber. The gain bandwidth can easily exceed 10 THz. (Figures adapted from [4])

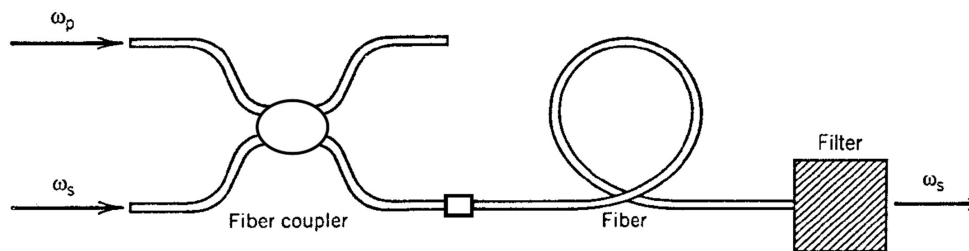


Figure 4.14: Fiber-based Raman amplifier in forward-pumping configuration. A strong pump wave at frequency ω_p is launched into the fiber along with the signal centered at $\omega_s < \omega_p$. The frequency difference $\omega_p - \omega_s$ is chosen such that the signal experiences amplification by stimulated Raman scattering (SRS). A filter at the end of the fiber blocks residual pump light. In an alternative configuration, the pump light can also be launched from the end of the fiber (backward pumping), thereby exploiting backward scattering for signal amplification. (Figure adapted from [4])

Chapter 5

Third-order nonlinear effects

In many materials, second-order nonlinearities are absent, and third-order nonlinear interactions are dominant. Even though they might be weak, third-order nonlinearities can lead to significant effects if high intensities are involved and if the interaction length is large. This is, e.g., true in optical fibers, where light waves can copropagate over many kilometers while being confined to a tiny micrometer-scale cross section in the core. If optical waves with similar frequencies interact with a third-order nonlinear material, they can generate new frequency components that are identical or similar to the initial frequencies, where phase matching is inherently fulfilled for some effects (e.g., SPM and XPM). We have already given an overview on various third-order nonlinear effects in Section 1.5.2 using the simplistic examples of plane waves. In this chapter, we focus on third-order nonlinear effects in waveguides and study various effects that can lead to interaction of co-propagating signals.

5.1 Signal propagation in linear waveguides

5.1.1 Waveguide modes for monochromatic waves

A homogeneous optical waveguide in general is a dielectric structure which is invariant along the propagation direction of the optical power, which is usually associated with the positive z -direction, see Fig. 5.1. The refractive index profile can then be written as

$$n(\mathbf{r}) = n(x, y). \quad (5.1)$$

It can be shown that a lossless homogeneous waveguide possesses a set of eigenmodes, i.e., electromagnetic wave patterns which do not change their transverse shapes during propagation [22]. For a monochromatic wave oscillating at frequency ω , the total field associated with a specific eigenmode can be written as

$$\underline{\mathbf{E}}(\mathbf{r}, t) = \underline{\mathcal{E}}(x, y, \omega) e^{j(\omega t - \beta(\omega)z)}, \quad (5.2)$$

$$\underline{\mathbf{H}}(\mathbf{r}, t) = \underline{\mathcal{H}}(x, y, \omega) e^{j(\omega t - \beta(\omega)z)}. \quad (5.3)$$

The mode fields $\underline{\mathcal{E}}(x, y, \omega)$ and $\underline{\mathcal{H}}(x, y, \omega)$ and the dispersion relation $\beta(\omega)$ are calculated by inserting Eqs. (5.2) and (5.3) into Maxwell's equations. Using the identity $\nabla \times (\Phi \mathbf{F}) = \Phi (\nabla \times \mathbf{F}) + (\nabla \Phi \times \mathbf{F})$, Eq. (1.2) leads to a relation of the form

$$(\nabla \times \underline{\mathcal{E}}(x, y, \omega)) - j\beta(\omega) \mathbf{e}_z \times \underline{\mathcal{E}}(x, y, \omega) = -j\omega\mu_0 \underline{\mathcal{H}}(x, y, \omega). \quad (5.4)$$

A similar relation can be obtained from Eq. (1.4),

$$(\nabla \times \underline{\mathcal{H}}(x, y, \omega)) - j\beta(\omega) \mathbf{e}_z \times \underline{\mathcal{H}}(x, y, \omega) = j\omega\epsilon_0 n^2 \underline{\mathcal{E}}(x, y, \omega). \quad (5.5)$$

Solving these relations leads to an eigenvalue problem: Nontrivial solutions $\underline{\mathcal{E}}(x, y, \omega) \neq 0$ and $\underline{\mathcal{H}}(x, y, \omega) \neq 0$ are only obtained for certain values of $\beta = \beta(\omega)$. For most waveguide structures of practical interest, numerical methods are needed to calculate the mode fields and the dispersion relation.

An arbitrary field pattern propagating along a waveguide can be expressed as a superposition of eigenmodes,

$$\underline{\mathbf{E}}(\mathbf{r}, t) = \sum_{\mu} \underline{A}_{\mu} \underline{\mathcal{E}}_{\mu}(x, y, \omega) e^{j(\omega t - \beta_{\mu}(\omega)z)}, \quad (5.6)$$

$$\underline{\mathbf{H}}(\mathbf{r}, t) = \sum_{\mu} \underline{A}_{\mu} \underline{\mathcal{H}}_{\mu}(x, y, \omega) e^{j(\omega t - \beta_{\mu}(\omega)z)}, \quad (5.7)$$

where $\beta_{\mu}(\omega)$ is the propagation constant of mode μ and where dimensionless complex quantities¹ \underline{A}_{μ} describe the magnitude and phase with which mode μ contributes to the total field². For given field patterns $\underline{\mathbf{E}}(\mathbf{r}, t)$ and $\underline{\mathbf{H}}(\mathbf{r}, t)$, the mode amplitudes can be calculated by using the orthogonality relation for guided modes,

$$\frac{1}{4} \iint_{-\infty}^{\infty} (\underline{\mathcal{E}}_{\mu}(x, y) \times \underline{\mathcal{H}}_{\nu}^*(x, y) + \underline{\mathcal{E}}_{\nu}^*(x, y) \times \underline{\mathcal{H}}_{\mu}(x, y)) \cdot \mathbf{e}_z \, dx \, dy = \mathcal{P}_{\mu} \delta_{\nu\mu}, \quad (5.8)$$

where $\delta_{\nu\mu}$ denotes the Kronecker delta, and where \mathcal{P}_{μ} represents the power that is associated with the mode field,

$$\mathcal{P}_{\mu} = \frac{1}{2} \iint_{-\infty}^{\infty} \text{Re} \{ \underline{\mathcal{E}}_{\mu}(x, y) \times \underline{\mathcal{H}}_{\mu}^*(x, y) \} \cdot \mathbf{e}_z \, dx \, dy. \quad (5.9)$$

More information on waveguide theory can be found in the lecture Optical Waveguides and Fibers and in the corresponding lecture notes [22].

5.1.2 Propagation of time-dependent signals in linear dispersive waveguides

In the last section, we have considered optical waveguide modes for monochromatic signals, i.e. signals that have a constant wave amplitude. The spectrum consists of a discrete spectral peak at frequency ω . Any time-dependent signal can be represented as a superposition of monochromatic waves, the amplitudes of which are obtained by means of a Fourier transform. Each of these frequency components travels with a specific propagation constant $\beta(\omega)$. In general, the frequency dependence of the propagation constant leads to a frequency-dependent delay of the various components and hence to deformation of the signal shape during propagation. This effect is referred to as dispersion. In linear optics, signal propagation in a dispersive waveguide is most easily described in the frequency domain.

In nonlinear optics, however, it is advantageous to use a time-domain description of signal propagation, since multiplications of electric fields in the time domain would correspond to convolutions of the corresponding spectra in the frequency domain, which are usually difficult to handle. For this reason, we introduce a slowly varying complex envelope $\underline{A}(z, t)$ in the time domain and

¹Note that we will later introduce an alternative definition of the complex time-domain amplitude, where $|\underline{A}_{\mu}|^2$ denotes the power (in Watts) carried by the waveguide mode, and where \underline{A}_{μ} hence has the unit $\sqrt{\text{W}}$.

²Note that in Eqs. (5.6) and (5.7), we have used a discrete set of eigenmodes, i.e., the superposition is represented by a discrete sum of field patterns, each of which propagates with a distinct wavenumber along the z -direction. This is valid as long as only guided modes are involved, i.e., as long as the field pattern does not lose energy by radiation. If the field pattern loses energy, we also need to consider radiation modes, which can assume any propagation constant β and hence form a continuous set. The discrete sum must then be replaced by a continuous integral. Nevertheless, the basic conclusion of the presented analysis remains valid. More information on mode expansions can be found in the lecture Optical Waveguides and Fibers and in the corresponding lecture notes [22].

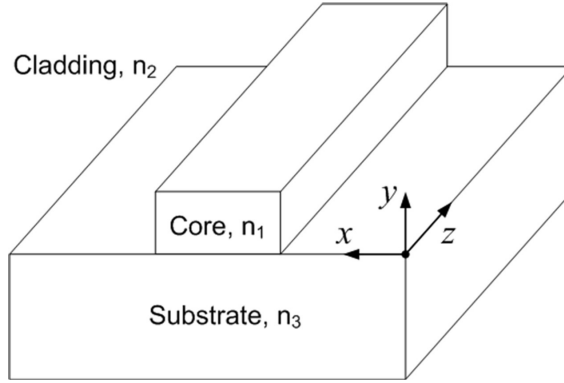


Figure 5.1: Homogeneous waveguide: The structure is invariant along the propagation direction of the optical power, which is usually associated with the z -direction. A lossless homogeneous waveguide features a set of electromagnetic wave patterns which do not change their transverse shapes during propagation along z , so-called eigenmodes.

try to derive an equation that describes the deformation of the signal envelope during propagation along z .

Let us first consider the simplified case where the waveguide is still linear, but dispersive. In a linear medium, the propagating fields do not influence each other, and we can consider the waveguide modes individually. For a single waveguide mode, the slowly varying envelope ansatzes for the electric and the magnetic field can be written as

$$\underline{\mathbf{E}}(\mathbf{r}, t) = \underline{A}(z, t) \underline{\mathcal{E}}(x, y, \omega_c) e^{j(\omega_c t - \beta(\omega_c)z)}, \quad (5.10)$$

$$\underline{\mathbf{H}}(\mathbf{r}, t) = \underline{A}(z, t) \underline{\mathcal{H}}(x, y, \omega_c) e^{j(\omega_c t - \beta(\omega_c)z)}, \quad (5.11)$$

where ω_c denotes the carrier frequency of the signal, $\beta(\omega_c)$ is the corresponding modal propagation constant, and $\underline{A}(z, t)$ is the complex wave amplitude. We take the Fourier transforms of Eqs. (5.10) and (5.11) and insert them into the corresponding Maxwell's equations (1.15) and (1.17). Using again the identity $\nabla \times (\Phi \mathbf{F}) = \Phi (\nabla \times \mathbf{F}) + (\nabla \Phi \times \mathbf{F})$, we obtain a relation of the form

$$\begin{aligned} & \tilde{\underline{A}}(z, \omega - \omega_c) (\nabla \times \underline{\mathcal{E}}(x, y, \omega_c)) \\ & + \left(\frac{\partial \tilde{\underline{A}}(z, \omega - \omega_c)}{\partial z} - j\beta(\omega_c) \tilde{\underline{A}}(z, \omega - \omega_c) \right) \mathbf{e}_z \times \underline{\mathcal{E}}(x, y, \omega_c) \\ & = -j\omega\mu_0 \underline{\mathcal{H}}(x, y, \omega_c). \end{aligned} \quad (5.12)$$

We now multiply Eq. (5.4) with $\tilde{\underline{A}}(z, \omega - \omega_c)$ and subtract the result from Eq. (5.12). Since we consider a narrowband signal $\tilde{\underline{A}}(z, \omega - \omega_c)$ which has nonzero frequency components only for frequencies ω that are close to the carrier frequency ω_c , we can assume the modal fields do not depend on frequency, i.e., $\underline{\mathcal{E}}(x, y, \omega) \approx \underline{\mathcal{E}}(x, y, \omega_c)$ and $\underline{\mathcal{H}}(x, y, \omega) \approx \underline{\mathcal{H}}(x, y, \omega_c)$. We hence obtain a simple frequency-domain relation for the evolution of $\underline{A}(z, t)$ during propagation along z ,

$$\frac{\partial \tilde{\underline{A}}(z, \omega - \omega_c)}{\partial z} + j(\beta(\omega) - \beta(\omega_c)) \tilde{\underline{A}}(z, \omega - \omega_c) = 0 \quad (5.13)$$

The exact dispersion relation $\beta(\omega)$ is usually unknown. As an approximation, it is useful to expand $\beta(\omega)$ in a Taylor series about the carrier frequency ω_c ,

$$\beta(\omega) \approx \beta_c^{(0)} + (\omega - \omega_c)\beta_c^{(1)} + \frac{(\omega - \omega_c)^2}{2!} \beta_c^{(2)} + \frac{(\omega - \omega_c)^3}{3!} \beta_c^{(3)} + \dots, \quad (5.14)$$

where

$$\beta_c^{(i)} = \left. \frac{d^i \beta(\omega)}{d\omega^i} \right|_{\omega=\omega_c}. \quad (5.15)$$

Eq. (5.13) can then be rewritten as

$$\frac{\partial \tilde{\underline{A}}(z, \omega - \omega_c)}{\partial z} + j \left(\beta_c^{(1)} (\omega - \omega_c) + \frac{1}{2} \beta_c^{(2)} (\omega - \omega_c)^2 + \dots \right) \tilde{\underline{A}}(z, \omega - \omega_c) = 0, \quad (5.16)$$

where the dots ... denote higher-order Taylor expressions. Translating this equation back into the time domain, we obtain a partial differential equation for the time-domain evolution of the signal envelope,

$$\frac{\partial \underline{A}(z, t)}{\partial z} + \beta_c^{(1)} \frac{\partial \underline{A}(z, t)}{\partial t} - j \frac{1}{2} \beta_c^{(2)} \frac{\partial^2 \underline{A}(z, t)}{\partial t^2} + \dots = 0. \quad (5.17)$$

In this equation, the expression $\beta_c^{(1)} \frac{\partial \underline{A}(z, t)}{\partial t}$ on the left-hand side leads to time shift of the optical signal by the so-called group delay

$$\tau = \beta_c^{(1)} z. \quad (5.18)$$

This can be verified by introducing a retarded time frame similarly to Eqs. (1.96) - (1.98),

$$t' = t - \beta_c^{(1)} z, \quad (5.19)$$

$$z' = z, \quad (5.20)$$

$$\underline{A}(z, t) = \underline{A}'(z, t - \beta_c^{(1)} z). \quad (5.21)$$

Eq. (5.17) can then be rewritten as

$$\frac{\partial \underline{A}'(z', t')}{\partial z'} - j \frac{1}{2} \beta_c^{(2)} \frac{\partial^2 \underline{A}'(z', t')}{\partial t'^2} + \dots = 0. \quad (5.22)$$

In the following, we will omit the primes keeping in mind that the time dependence refers to a retarded reference frame.

Example: Propagation of a Gaussian pulse through a dispersive waveguide Transforming Eq. (5.22) back into the frequency domain, we obtain the relation

$$\tilde{\underline{A}}(z, \omega) = \tilde{\underline{A}}(0, \omega) e^{-j \frac{1}{2} \beta_c^{(2)} \omega^2 z}. \quad (5.23)$$

If a Gaussian pulse is launched at the fiber input,

$$\underline{A}(0, t) = \underline{A}_0 e^{-\frac{t^2}{2\sigma_t^2}}, \quad (5.24)$$

we obtain a so-called chirped Gaussian pulse at the output,

$$\underline{A}(z, t) = \underline{A}_0 \sqrt{\frac{2\pi\sigma_t^2}{2\pi(\sigma_t^2 - j\beta_c^{(2)}z)}} e^{-\frac{t^2}{2(\sigma_t^2 + j\beta_c^{(2)}z)}}. \quad (5.25)$$

A “chirped” Gaussian impulse is a waveform with a Gaussian envelope and a time-dependent frequency³. The instantaneous frequency of the complete signal $\underline{a}(0, t) = \underline{A}(0, t) \exp(j\omega_c t)$ can be defined by the rate at which the phase of the complex signal changes,

$$\omega(t) = \frac{d}{dt} \arg \{ \underline{A}(z, t) \} = \omega_c + \frac{\beta_c^{(2)} z}{\sigma_t^4 + (\beta_c^{(2)} z)^2} t \quad (5.26)$$

³to chirp = zirpen, zwitschern

For $\beta_c^{(2)} > 0$, the leading edge of the signal has a lower frequency (“red shift”) than the trailing edge (“blue shift”); for $\beta_c^{(2)} < 0$, the situation is reversed. This is consistent with the picture that $\beta_c^{(2)}$ gives the frequency dependence of the group delay $\beta_c^{(1)}z$: For $\beta_c^{(2)} > 0$, the group delay increases with frequency, i.e., “blue” frequency components experience a bigger delay than “red” components, and the leading edge is hence red-shifted. Likewise, for $\beta_c^{(2)} < 0$, the leading edge is blue-shifted. These principles are illustrated on the lecture slides. The case of $\beta_c^{(2)} > 0$ is also referred to as normal group velocity dispersion, (GVD), whereas $\beta_c^{(2)} < 0$, corresponds to so-called anomalous GVD.

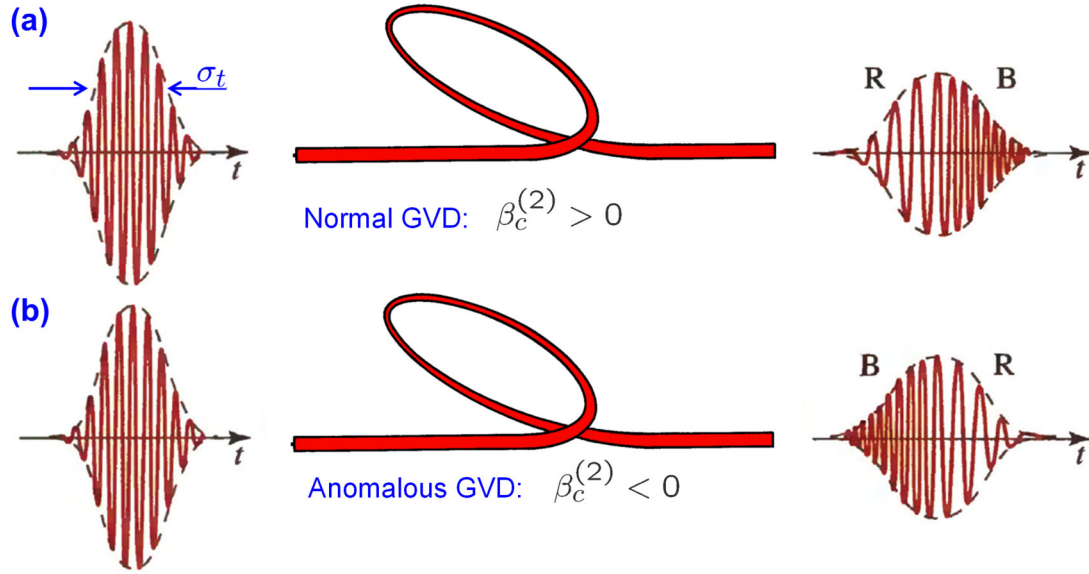


Figure 5.2: Propagation of a Gaussian pulse through a dispersive waveguide. (a) For normal group velocity dispersion (GVD), $\beta_c^{(2)} > 0$ and the group delay $\beta_c^{(1)}z$ increases with frequency, i.e., “blue” frequency components (B) experience a bigger delay than “red” components (R). (b) For anomalous GVD, $\beta_c^{(2)} < 0$ and the group delay $\beta_c^{(1)}z$ decreases with frequency, i.e., “blue” frequency components (B) experience a smaller delay than “red” components (R). (Figures adapted from [26])

5.2 Signal propagation in third-order nonlinear waveguides

5.2.1 Maxwell’s equations and mode expansion for nonlinear propagation

Let us now consider the case where an optical signal propagates along a Kerr-nonlinear waveguide. The propagation is governed by Maxwell’s equations, Eqs. (1.1) to (1.4). Separating the linear from the nonlinear polarization according to Eq. (1.77), the curl equations can be written as

$$\nabla \times \mathbf{H}(\mathbf{r}, t) = \epsilon_0 n^2 \frac{\partial}{\partial t} \mathbf{E}(\mathbf{r}, t) + \frac{\partial}{\partial t} \mathbf{P}_{\text{NL}}(\mathbf{r}, t), \quad (5.27)$$

$$\nabla \times \mathbf{E}(\mathbf{r}, t) = -\mu_0 \frac{\partial}{\partial t} \mathbf{H}(\mathbf{r}, t). \quad (5.28)$$

In contrast to the linear waveguide considered in Section 5.1.2, where only a single guided mode was analyzed, the various modes of the waveguide might now be coupled by nonlinear effects. We

therefore need to consider the complete expansion, comprising all waveguide modes and carrier frequencies. Moreover, in the mode expansion defined in Eqs. (5.6) and (5.7), dimensionless complex wave amplitudes \underline{A}_μ are used to describe the contribution of mode μ to the total field. In this representation, the physical power carried by mode μ cannot be directly derived from the mode amplitude \underline{A}_μ , since it depends on the normalization of the mode fields $\underline{\mathcal{E}}_\mu(x, y, \omega)$ and $\underline{\mathcal{H}}_\mu(x, y, \omega)$. In nonlinear optics, we therefore introduce an explicit power normalization of the mode fields $\underline{\mathcal{E}}_\mu(x, y, \omega)$ and $\underline{\mathcal{H}}_\mu(x, y, \omega)$ to the associated power \mathcal{P}_μ according to Eq. (5.9). The mode expansion can then be written as

$$\mathbf{E}(\mathbf{r}, t) = \frac{1}{2} (\underline{\mathbf{E}}(\mathbf{r}, t) + cc) = \frac{1}{2} \sum_{m=-M}^M \sum_{\mu} \underline{A}_\mu(z, t, \omega_m) \frac{\underline{\mathcal{E}}_\mu(x, y, \omega_m)}{\sqrt{\mathcal{P}_\mu}} e^{j(\omega_m t - \beta_\mu(\omega_m)z)}, \quad (5.29)$$

$$\mathbf{H}(\mathbf{r}, t) = \frac{1}{2} (\underline{\mathbf{H}}(\mathbf{r}, t) + cc) = \frac{1}{2} \sum_{m=-M}^M \sum_{\mu} \underline{A}_\mu(z, t, \omega_m) \frac{\underline{\mathcal{H}}_\mu(x, y, \omega_m)}{\sqrt{\mathcal{P}_\mu}} e^{j(\omega_m t - \beta_\mu(\omega_m)z)}, \quad (5.30)$$

where $\omega_m = -\omega_{-m}$ denote the various positive and negative frequencies that are needed to represent real field quantities $\mathbf{E}(\mathbf{r}, t)$ and $\mathbf{H}(\mathbf{r}, t)$. In this representation, the nonlinear polarization is given by

$$\mathbf{P}_{\text{NL}}(\mathbf{r}, t) = \frac{1}{2} \sum_{m=-M}^{+M} \underline{\mathbf{P}}_{\text{NL}}(\mathbf{r}, t, \omega_m) e^{j\omega_m t}, \quad (5.31)$$

where the complex amplitudes $\underline{\mathbf{P}}_{\text{NL}}(\mathbf{r}, t, \omega_m)$ can be derived by inserting Eq. (5.29) in Eq. (2.22).

To analyze nonlinear propagation, we first insert the mode expansion, Eqs. (5.29) and (5.30), into Eqs. (5.27) and (5.28). Considering only the terms that belong to a specific carrier frequency ω_m , making use of the identity $\nabla \times (\Phi \mathbf{F}) = \Phi (\nabla \times \mathbf{F}) + (\nabla \Phi \times \mathbf{F})$, and transforming the resulting relations to the frequency domain, we obtain

$$\begin{aligned} & \sum_{\mu} \tilde{\underline{A}}_\mu(z, \omega - \omega_m, \omega_m) e^{-j\beta_\mu(\omega_m)z} \left[\nabla \times \frac{\underline{\mathcal{H}}_\mu(x, y, \omega_m)}{\sqrt{\mathcal{P}_\mu}} \right] \\ & + \frac{\partial}{\partial z} \left[\tilde{\underline{A}}_\mu(z, \omega - \omega_m, \omega_m) e^{-j\beta_\mu(\omega_m)z} \right] \mathbf{e}_z \times \frac{\underline{\mathcal{H}}_\mu(x, y, \omega_m)}{\sqrt{\mathcal{P}_\mu}} \\ & - j\omega \epsilon_0 n^2 \tilde{\underline{A}}_\mu(z, \omega - \omega_m, \omega_m) \frac{\underline{\mathcal{E}}_\mu(x, y, \omega_m)}{\sqrt{\mathcal{P}_\mu}} e^{-j\beta_\mu(\omega_m)z} = j\omega \tilde{\underline{\mathbf{P}}}_{\text{NL}}(\mathbf{r}, \omega - \omega_m, \omega_m) \end{aligned} \quad (5.32)$$

and

$$\begin{aligned} & \sum_{\mu} \tilde{\underline{A}}_\mu(z, \omega - \omega_m, \omega_m) e^{-j\beta_\mu(\omega_m)z} \left[\nabla \times \frac{\underline{\mathcal{E}}_\mu(x, y, \omega_m)}{\sqrt{\mathcal{P}_\mu}} \right] \\ & + \frac{\partial}{\partial z} \left[\tilde{\underline{A}}_\mu(z, \omega - \omega_m, \omega_m) e^{-j\beta_\mu(\omega_m)z} \right] \mathbf{e}_z \times \frac{\underline{\mathcal{E}}_\mu(x, y, \omega_m)}{\sqrt{\mathcal{P}_\mu}} \\ & + j\omega \mu_0 \tilde{\underline{A}}_\mu(z, \omega - \omega_m, \omega_m) \frac{\underline{\mathcal{H}}_\mu(x, y, \omega_m)}{\sqrt{\mathcal{P}_\mu}} e^{-j\beta_\mu(\omega_m)z} = 0. \end{aligned} \quad (5.33)$$

In these relations, $\tilde{\underline{A}}_\mu(z, \omega - \omega_m, \omega_m)$ and $\tilde{\underline{\mathbf{P}}}_{\text{NL}}(\mathbf{r}, \omega - \omega_m, \omega_m)$ denote the Fourier transforms of the associated time-domain quantities $\underline{A}_\mu(z, t, \omega_m)$ and $\underline{\mathbf{P}}_{\text{NL}}(\mathbf{r}, t, \omega_m)$ with respect to t . We now use the fact that $\underline{\mathcal{E}}_\mu(x, y, \omega_m)$ and $\underline{\mathcal{H}}_\mu(x, y, \omega_m)$ represent guided mode fields that fulfill Eqs. (5.4)

and (5.5), i.e.,

$$\left(\nabla \times \frac{\underline{\mathcal{E}}_\mu(x, y, \omega)}{\sqrt{\mathcal{P}_\mu}} \right) = j\beta_\mu(\omega) \mathbf{e}_z \times \frac{\underline{\mathcal{E}}_\mu(x, y, \omega)}{\sqrt{\mathcal{P}_\mu}} - j\omega\mu_0 \frac{\underline{\mathcal{H}}_\mu(x, y, \omega)}{\sqrt{\mathcal{P}_\mu}}, \quad (5.34)$$

$$\left(\nabla \times \frac{\underline{\mathcal{H}}_\mu(x, y, \omega)}{\sqrt{\mathcal{P}_\mu}} \right) = j\beta_\mu(\omega) \mathbf{e}_z \times \frac{\underline{\mathcal{H}}_\mu(x, y, \omega)}{\sqrt{\mathcal{P}_\mu}} + j\omega\epsilon_0 n^2 \frac{\underline{\mathcal{E}}_\mu(x, y, \omega)}{\sqrt{\mathcal{P}_\mu}}. \quad (5.35)$$

We insert Eqs. (5.34) and (5.35) in Eqs. (5.33) and (5.32) and use the fact that $\tilde{\underline{A}}_\mu(z, \omega - \omega_m, \omega_m)$ is a narrow-band signal which has nonzero frequency components only for frequencies ω that are close to the carrier frequency ω_m . We may therefore assume that the modal fields do not depend on frequency, i.e., $\underline{\mathcal{E}}_\mu(x, y, \omega) \approx \underline{\mathcal{E}}_\mu(x, y, \omega_m)$ and $\underline{\mathcal{H}}_\mu(x, y, \omega) \approx \underline{\mathcal{H}}_\mu(x, y, \omega_m)$. This leads to the relations

$$\sum_\mu \left[\frac{\partial \tilde{\underline{A}}_\mu(z, \omega - \omega_m, \omega_m)}{\partial z} + j(\beta_\mu(\omega) - \beta_\mu(\omega_m)) \tilde{\underline{A}}_\mu(z, \omega - \omega_m, \omega_m) \right] \mathbf{e}_z \times \frac{\underline{\mathcal{H}}_\mu(x, y, \omega_m)}{\sqrt{\mathcal{P}_\mu}} e^{-j\beta_\mu(\omega_m)z} = j\omega \tilde{\underline{\mathbf{P}}}_{\text{NL}}(\mathbf{r}, \omega - \omega_m, \omega_m) \quad (5.36)$$

$$\sum_\mu \left[\frac{\partial \tilde{\underline{A}}_\mu(z, \omega - \omega_m, \omega_m)}{\partial z} + j(\beta_\mu(\omega) - \beta_\mu(\omega_m)) \tilde{\underline{A}}_\mu(z, \omega - \omega_m, \omega_m) \right] \mathbf{e}_z \times \frac{\underline{\mathcal{E}}_\mu(x, y, \omega_m)}{\sqrt{\mathcal{P}_\mu}} e^{-j\beta_\mu(\omega_m)z} = 0 \quad (5.37)$$

The left-hand sides of Eqs. (5.36) and (5.37) still comprise a superposition of many waveguide modes. Since we are interested only in the evolution of a single waveguide mode ν , we make use of the orthogonality relation, Eq. (5.8), to project out the corresponding amplitude. Dot-multiplying Eq. (5.36) with $[-\underline{\mathcal{E}}_\nu^*(x, y, \omega_m)]$ and Eq. (5.37) with $\underline{\mathcal{H}}_\nu^*(x, y, \omega_m)$ and adding the resulting relations, we obtain

$$\sum_\mu \left[\frac{\partial \tilde{\underline{A}}_\mu(z, \omega - \omega_m, \omega_m)}{\partial z} + j(\beta_\mu(\omega) - \beta_\mu(\omega_m)) \tilde{\underline{A}}_\mu(z, \omega - \omega_m, \omega_m) \right] \left[\frac{\underline{\mathcal{E}}_\mu(x, y, \omega_m) \times \underline{\mathcal{H}}_\nu^*(x, y, \omega_m) + \underline{\mathcal{E}}_\nu^*(x, y, \omega_m) \times \underline{\mathcal{H}}_\mu(x, y, \omega_m)}{\sqrt{\mathcal{P}_\mu}} \right] \mathbf{e}_z e^{-j\beta_\mu(\omega_m)z} = -j\omega \tilde{\underline{\mathbf{P}}}_{\text{NL}}(\mathbf{r}, \omega - \omega_m, \omega_m) \cdot \underline{\mathcal{E}}_\nu^*(x, y, \omega_m) \quad (5.38)$$

We now integrate over the entire (x,y)-plane and make use of Eq. (5.8).

$$\left[\frac{\partial \tilde{\underline{A}}_\nu(z, \omega - \omega_m, \omega_m)}{\partial z} + j(\beta_\nu(\omega) - \beta_\nu(\omega_m)) \tilde{\underline{A}}_\nu(z, \omega - \omega_m, \omega_m) \right] e^{-j\beta_\nu(\omega_m)z} = -\frac{j\omega}{4\sqrt{\mathcal{P}_\nu}} \iint_{-\infty}^{\infty} \tilde{\underline{\mathbf{P}}}_{\text{NL}}(\mathbf{r}, \omega - \omega_m, \omega_m) \cdot \underline{\mathcal{E}}_\nu^*(x, y, \omega_m) dx dy \quad (5.39)$$

Using a Taylor expansion of the propagation constant $\beta_\nu(\omega)$ series about the carrier frequency ω_m , Eqs. (5.14) and (5.15), we can transform Eq. (5.39) back to the time domain,

$$\left[\frac{\partial \underline{A}_\nu(z, t, \omega_m)}{\partial z} + \beta_c^{(1)} \frac{\partial \underline{A}_\nu(z, t, \omega_m)}{\partial t} - j\frac{1}{2} \beta_c^{(2)} \frac{\partial^2 \underline{A}_\nu(z, t, \omega_m)}{\partial t^2} \right] e^{j(\omega_m t - \beta_\nu(\omega_m)z)} = -\frac{1}{4\sqrt{\mathcal{P}_\nu}} \frac{\partial}{\partial t} \left(\iint_{-\infty}^{\infty} \underline{\mathbf{P}}_{\text{NL}}(\mathbf{r}, t, \omega_m) \cdot \underline{\mathcal{E}}_\nu^*(x, y, \omega_m) dx dy e^{j\omega_m t} \right) \quad (5.40)$$

We introduce again a retarded time frame defined in Eqs. (5.19) to (5.21) and make further use of the fact that $\underline{\mathbf{P}}_{\text{NL}}(\mathbf{r}, t, \omega_m)$ is only weakly time-dependent such that the time-derivative on the right-hand side of Eq. (5.40) is dominated by the expression $e^{j\omega_m t}$. This leads to

$$\begin{aligned} & \left[\frac{\partial \underline{A}_\nu(z, t, \omega_m)}{\partial z} - j \frac{1}{2} \beta_c^{(2)} \frac{\partial^2 \underline{A}_\nu(z, t, \omega_m)}{\partial t^2} \right] e^{-j\beta_\nu(\omega_m)z} \\ &= - \frac{j\omega_m}{4\sqrt{\mathcal{P}_\nu}} \iint_{-\infty}^{\infty} \underline{\mathbf{P}}_{\text{NL}}(\mathbf{r}, t, \omega_m) \cdot \underline{\mathcal{E}}_\nu^*(x, y, \omega_m) dx dy. \end{aligned} \quad (5.41)$$

This relation describes the spatio-temporal evolution of the mode amplitude $\underline{A}_\nu(z, t, \omega_m)$ under the influence of dispersion and nonlinearities. For further analysis, we need to investigate how $\underline{\mathbf{P}}_{\text{NL}}(\mathbf{r}, t, \omega_m)$ depends on the electric fields and hence on the mode amplitudes $\underline{A}_\nu(z, t, \omega_m)$.

5.2.2 The nonlinear Schrödinger equation (NLSE)

Let us now consider the most simple case where power is propagating in one waveguide mode ν only, and where only a single carrier frequency is involved. Following Eq. (2.22) and using Eq. (5.29), the complex amplitude of the nonlinear polarization can be written as

$$\begin{aligned} \underline{\mathbf{P}}_{\text{NL}}(\mathbf{r}, t, \omega_m) &= \frac{3}{4} \epsilon_0 \left(\underline{\chi}^{(3)}(\omega_m : \omega_m, -\omega_m, \omega_m) : \underline{\mathcal{E}}_\nu(x, y, \omega_m) \underline{\mathcal{E}}_\nu^*(x, y, \omega_m) \underline{\mathcal{E}}_\nu(x, y, \omega_m) \right) \\ & \quad \frac{\underline{A}_\nu(z, t, \omega_m)}{\sqrt{\mathcal{P}_\nu}} \frac{\underline{A}_\nu^*(z, t, \omega_m)}{\sqrt{\mathcal{P}_\nu}} \frac{\underline{A}_\nu(z, t, \omega_m)}{\sqrt{\mathcal{P}_\nu}} e^{-j\beta_\nu(\omega_m)z} \end{aligned} \quad (5.42)$$

Inserting Eq. (5.42) in Eq. (5.41), we obtain the so-called nonlinear Schrödinger equation (NLSE)⁴,

$$\frac{\partial \underline{A}_\nu(z, t, \omega_m)}{\partial z} - j \frac{1}{2} \beta_c^{(2)} \frac{\partial^2 \underline{A}_\nu(z, t, \omega_m)}{\partial t^2} = -j\gamma |\underline{A}_\nu(z, t, \omega_m)|^2 \underline{A}_\nu(z, t, \omega_m), \quad (5.43)$$

where the nonlinearity parameter γ is given by

$$\gamma_\nu(\omega_m) = \frac{3\omega_m \epsilon_0}{16} \frac{\iint_{-\infty}^{\infty} \left[\underline{\chi}^{(3)} : \underline{\mathcal{E}}_\nu(x, y, \omega_m) \underline{\mathcal{E}}_\nu^*(x, y, \omega_m) \underline{\mathcal{E}}_\nu(x, y, \omega_m) \right] \cdot \underline{\mathcal{E}}_\nu^*(x, y, \omega_m) dx dy}{\mathcal{P}_\nu^2}, \quad (5.44)$$

In this relation, the argument $(\omega_m : \omega_m, -\omega_m, \omega_m)$ of the nonlinear susceptibility has been dropped for the sake of readability. The numerator of this relation corresponds roughly to the spatial overlap between the fourth power of the electric mode field and the Kerr-nonlinearity of the waveguide, whereas the denominator is used for power normalization of the mode fields $\underline{\mathcal{E}}_\nu(x, y, \omega_m)$. Strong nonlinearities can hence be achieved by confining the electric field of a waveguide mode to a small region that consists of a highly nonlinear optical material, see examples on slide.

The preceding analysis was based on the assumption of a lossless waveguide. Waveguide losses corresponding to a power attenuation constant α can be taken into account by an additional expression of the form $-\frac{\alpha}{2} \underline{A}_\nu(z, t, \omega_m)$ on the right-hand side of Eq. (5.43),

$$\frac{\partial \underline{A}_\nu(z, t, \omega_m)}{\partial z} - j \frac{1}{2} \beta_c^{(2)} \frac{\partial^2 \underline{A}_\nu(z, t, \omega_m)}{\partial t^2} = -\frac{\alpha}{2} \underline{A}_\nu(z, t, \omega_m) - j\gamma |\underline{A}_\nu(z, t, \omega_m)|^2 \underline{A}_\nu(z, t, \omega_m), \quad (5.45)$$

⁴The term ‘‘nonlinear Schrödinger equation’’ originates from the fact that, when exchanging the space and the time coordinates, Eq. (5.43) resembles the Schrödinger equation with a nonlinear potential term, i.e., a potential that depends on the wave function.

Using Eq. (5.9) for the mode field power, we can rewrite Eq. (5.44) as

$$\gamma_\nu(\omega_m) = \frac{3\omega_m\epsilon_0}{4} \frac{\iint_{-\infty}^{\infty} \left[\underline{\chi}^{(3)} : \underline{\mathcal{E}}_\nu(x, y, \omega_m) \underline{\mathcal{E}}_\nu^*(x, y, \omega_m) \underline{\mathcal{E}}_\nu(x, y, \omega_m) \right] \cdot \underline{\mathcal{E}}_\nu^*(x, y, \omega_m) dx dy}{\iint_{-\infty}^{\infty} \text{Re} \{ \underline{\mathcal{E}}_\nu(x, y, \omega_m) \times \underline{\mathcal{H}}_\nu^*(x, y, \omega_m) \} \cdot \mathbf{e}_z dx dy}. \quad (5.46)$$

Note that the analysis presented here is valid for all waveguide types. In fiber optics, the refractive index n_{core} of the waveguide core and the index n_{clad} of the cladding are usually very similar, $n \approx n_{\text{core}} \approx n_{\text{clad}}$. The transverse components of the mode fields $\underline{\mathcal{E}}_\nu(x, y, \omega_m)$ and $\underline{\mathcal{H}}_\nu(x, y, \omega_m)$ may then be approximated by a scalar function $F(x, y)$,

$$\underline{\mathcal{E}}_\nu(x, y, \omega_m) \approx F_\nu(x, y, \omega_m) \mathbf{e}_x, \quad (5.47)$$

$$\underline{\mathcal{H}}_\nu(x, y, \omega_m) \approx \frac{n}{Z_0} F_\nu(x, y, \omega_m) \mathbf{e}_y. \quad (5.48)$$

If we further assume a homogeneous nonlinearity $\underline{\chi}^{(3)}$ which does not change over the cross section, then Eq. (5.46) can be simplified to

$$\gamma_\nu(\omega_m) \approx \frac{\omega_m n_2}{c A_{\text{eff}}}, \quad (5.49)$$

where n_2 denotes the Kerr coefficient, see Eq. (1.122),

$$n_2 = \frac{3Z_0}{4n^2} \chi^{(3)}, \quad (5.50)$$

and where the effective cross section of the waveguide A_{eff} is given by

$$A_{\text{eff}} \approx \frac{\left(\iint_{-\infty}^{\infty} |F_\nu(x, y, \omega_m)|^2 dx dy \right)^2}{\iint_{-\infty}^{\infty} |F_\nu(x, y, \omega_m)|^4 dx dy}. \quad (5.51)$$

5.3 Applications and phenomena related to third-order nonlinear waveguides

5.3.1 Nonlinear phase shift and spectral broadening

The nonlinear Schrödinger equation describes the evolution of the complex optical mode amplitude $\underline{A}(z, t)$ under the influence of dispersion and self-phase modulation (SPM). To understand the impact of SPM, let us consider the case of a lossy waveguide, for which dispersion can be neglected. The NLSE is then given by

$$\frac{\partial \underline{A}(z, t)}{\partial z} = -j\gamma |\underline{A}(z, t)|^2 \underline{A}(z, t) - \frac{\alpha}{2} \underline{A}(z, t), \quad (5.52)$$

As a solution ansatz, we use the expression

$$\underline{A}(z, t) = \underline{A}_0(t) e^{j\Phi_{NL}(z, t)} e^{-\frac{\alpha}{2}z}, \quad (5.53)$$

where the phase $\Phi_{NL}(z, t)$ accounts for the nonlinear phase shift due to SPM. Inserting Eq. (5.53) into Eq. (5.52), we find an expression for the nonlinear phase shift that is accumulated along a propagation distance L ,

$$\Phi_{NL}(L, t) = -\gamma |\underline{A}_0(t)|^2 L_{\text{eff}}, \quad (5.54)$$

where the effective length L_{eff} is given by

$$L_{\text{eff}} = \frac{1 - e^{-\alpha L}}{\alpha}. \quad (5.55)$$

We hence find that SPM in a lossy fiber is not governed by the geometrical length L , but by the effective length L_{eff} that is smaller than L because of fiber loss.

The nonlinear phase shift according to Eq. (5.54) leaves the temporal shape of the pulse unchanged, but leads to broadening of the pulse spectrum. This can be understood when considering the instantaneous frequency shift $\Omega = \frac{\partial \Phi_{NL}}{\partial t}$ that is associated with the nonlinear phase shift: Ω is negative near the leading edge of the pulse and hence leads to a red-shift, whereas it is positive near the trailing edge of the pulse and causes a blue-shift there. Note that this is just the opposite of anomalous group-velocity dispersion, which delays long wavelengths and hence leads to a red-shifted trailing and a blue-shifted leading edge. The interplay of self-phase modulation and anomalous group velocity dispersion can lead to pulse forms that do not change their envelope during propagation, so-called solitons, see Section 5.3.2.

In the absence of dispersion, spectral broadening increases with fiber length and launch power. For small fiber cross sections and large input powers, broadband so-called “supercontinuum” spectra can be generated from a train of short input pulses, see Fig. 5.3.

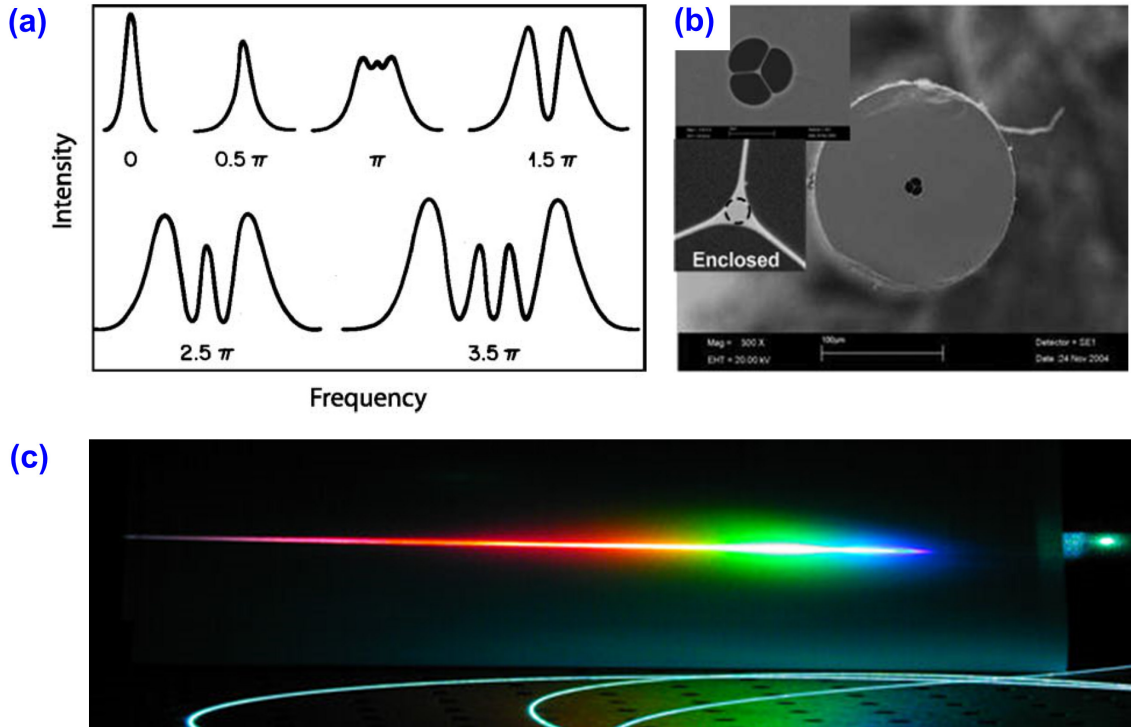


Figure 5.3: (a) Spectral broadening of an “unchirped” Gaussian pulse for different SPM-induced nonlinear phase shifts Φ_{NL} , measured at the maximum of the pulse power. (b) Cross section of a highly nonlinear fiber with ultra-small mode-field diameter. The fiber is made of highly Kerr-nonlinear lead-silicate glass. Strong light confinement is achieved by using a fiber core suspended in air by three lead silicate membranes, see inset on the lower left-hand side. (c) Octave-spanning supercontinuum generated by launching femtosecond laser pulses into a highly nonlinear fiber. (Figures adapted from [26, 5, 23])

5.3.2 Optical solitons

For anomalous group velocity dispersion ($\beta_c^{(2)} < 0$) self-phase modulation and dispersion are counteracting, see discussion in Section 5.3.1. It turns out that for certain pulse shapes, the two effects cancel each other exactly such that the pulse propagates without changing its shape. Such pulses are called solitons. Solitary wave patterns that maintain their shape while traveling at a constant speed do not only occur in nonlinear optics, but arise as solutions of a widespread class of nonlinear dispersive partial differential equations, see [5] for a description of the first observation of a solitary wave in water.

For a mathematical derivation let us start from the nonlinear Schrödinger equation, Eq. (5.45) and neglect fiber loss ($\alpha = 0$). For simplicity, we consider a signal propagating only in a single waveguide mode at a distinct carrier frequency. Omitting the mode index ν and the carrier frequency argument ω_m , Eq. (5.45) can be written as

$$\frac{\partial \underline{A}(z, t)}{\partial z} - j \frac{1}{2} \beta_c^{(2)} \frac{\partial^2 \underline{A}(z, t)}{\partial t^2} = -j \gamma |\underline{A}(z, t)|^2 \underline{A}(z, t). \quad (5.56)$$

For a solitary wave, we require the magnitude of the complex envelope $\underline{A}(z, t)$ to be independent of z , but still allow for a z -dependent global phase shift $\Phi(z)$. This leads to an ansatz of the form

$$\underline{A}(z, t) = A_0(t) e^{j\Phi(z)}, \quad (5.57)$$

where we have additionally assumed that $A_0(t) \in \mathbb{R}$, i.e., that the phase of the signal does not change for the duration of the pulse (chirp-free signal). Inserting this ansatz into Eq. (5.56), we can separate variables into groups of purely z - and purely t -dependent terms, both of which have to be constant. Assuming zero initial phase, $\Phi(0) = 0$, we obtain two relations of the form,

$$\Phi(z) = -Kz, \quad (5.58)$$

$$\frac{\partial^2 A_0(t)}{\partial t^2} = \frac{2}{\beta_c^{(2)}} (-K + \gamma A_0^2(t)) A_0(t), \quad (5.59)$$

where K denotes a real-value separation variable. Eq. (5.59) has solutions of the form

$$A_0(t) = A_1 \operatorname{sech}\left(\frac{t}{T}\right), \quad (5.60)$$

where $\operatorname{sech}(x) = 1/\cosh(x)$ denotes the hyperbolic-secant function, see [18] for a rigorous solution of Eq. (5.59). Here we simply use Eq. (5.60) as an ansatz and insert it into Eq. (5.59). This leads to two relations, linking the pulse peak power A_1^2 , the duration T , and the phase-delay parameter K ,

$$A_1^2 = \frac{-\beta_c^{(2)}}{\gamma T^2}, \quad (5.61)$$

$$K = \frac{1}{2} \gamma A_1^2. \quad (5.62)$$

From these relations, it is immediately clear that solitons can only occur for anomalous group velocity dispersion ($\beta_c^{(2)} < 0$) since the peak power A_1^2 must always be a positive number.

The total solution for the soliton can then be written as

$$\underline{A}(z, t) = A_1 \operatorname{sech}\left(\frac{t}{T}\right) e^{-jKz},$$

where the parameters A_1 , T , and K are linked by Eqs. (5.61) and (5.62). Eq. (5.61) states that, if the dispersion $|\beta_c^{(2)}|$ is increased, the pulse peak power A_1^2 must be increased as well, since stronger SPM is needed to compensate for the dispersion. Similarly, if the pulse duration T is increased,

the effects of dispersion will decrease, since the pulse spectrum narrows, resulting in less delay between the various spectral components. As a consequence, we may also reduce the pulse peak power A_1^2 , since “less” SPM is needed to compensate for the dispersion. The parameter K in Eq. (5.62) quantifies the phase delay caused by SPM, which simply increases as the pulse peak power increases. Soliton formation resulting from an interplay of anomalous group-velocity dispersion (GVD) and self-phase modulation (SPM) is illustrated in Fig. 5.4.

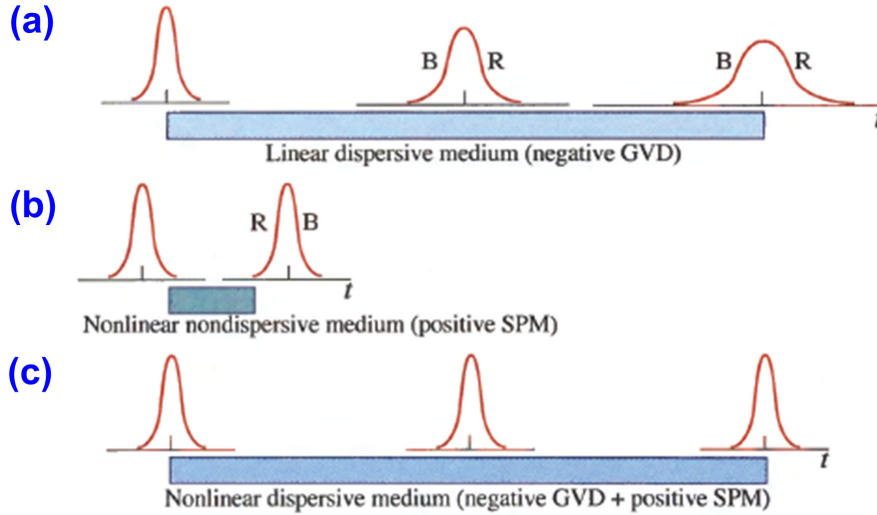


Figure 5.4: Formation of a soliton by an interplay of anomalous group-velocity dispersion (GVD) and self-phase modulation (SPM). (a) In a linear medium with negative GVD, the high-frequency spectral components (“blue”, B) experience a smaller group delay than the low-frequency components (“red”, R). This results in spectral broadening of the pulse. (b) In a nondispersive Kerr-nonlinear medium, self-phase modulation (SPM) leads to a red-shift of the leading edge of the pulse and to a blue-shift of the trailing edge. The envelope of the pulse remains unchanged, but the pulse experiences a chirp. (c) If a Kerr-nonlinear medium features negative GVD, the effects of SPM and dispersion-induced broadening can cancel each other, leading to formation of an optical soliton. Exact balance between negative GVD and SPM links the pulse duration to its power. (Figures adapted from [26])

A sech-pulse is sketched in Fig. 5.5 (a) along with a Gaussian function of the same height and width (full width at half the maximum, FWHM). Note that apart from the family of fundamental solitons with real, z -invariant envelopes, Eq. (5.56) also possesses solutions with complex envelopes that reproduce themselves periodically during propagation. A so-called $N = 2$ soliton is depicted in Fig. 5.5 (c). A more detailed discussion of higher-order solitons can be found in the literature [26, 5].

5.3.3 Modulation instability

Stability analysis

In nonlinear optics, modulation instability is a phenomenon whereby a nonlinear interaction of a strong continuous-wave (cw) signal and quantum noise leads to amplification of the noise, generation of spectral sidebands and eventually to the break-up of the cw signal into a train of pulses. Let us assume a monochromatic continuous-wave signal with carrier frequency ω_c , amplitude A_0 and power $P_0 = A_0^2$ propagating along an optical waveguide,

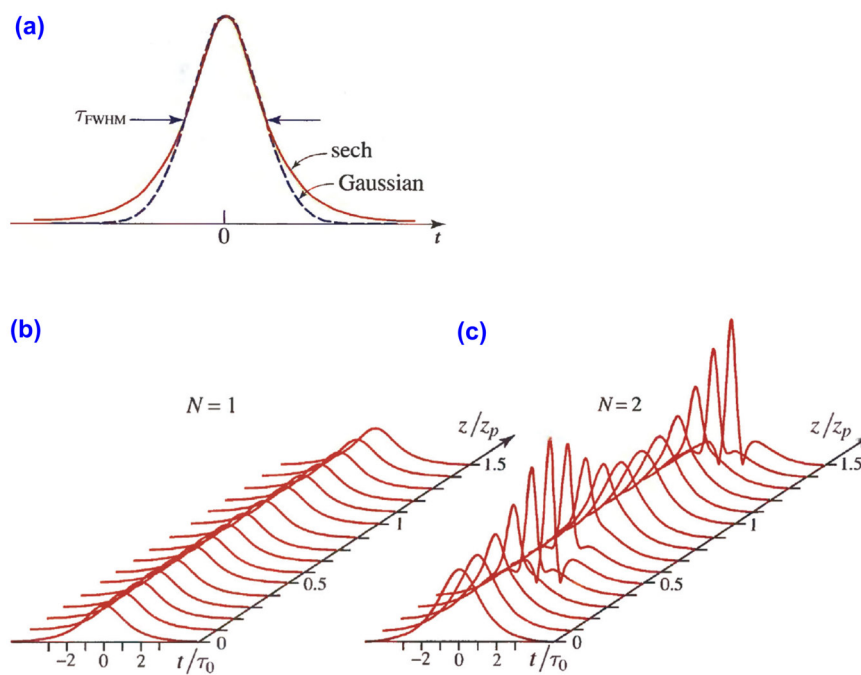


Figure 5.5: Fundamental and higher-order solitons. (a) Sech-shape soliton pulse, combined a Gaussian pulse of the same height and width (full width at half the maximum, FWHM) (b) Fundamental soliton, maintaining its amplitude during propagation. (c) Higher-order soliton, featuring a complex envelope that reproduces itself periodically during propagation. (Figures adapted from [26])

$$\mathbf{E}(\mathbf{r}, t) = \frac{1}{2} A_0 e^{j\Phi_{NL}(z)} \frac{\underline{\mathcal{E}}(x, y, \omega_c)}{\mathcal{P}(\omega_c)} e^{j(\omega_c t - \beta_c z)}. \quad (5.63)$$

Note that in this relation, phase factors can be transferred at will between A_0 and $\underline{\mathcal{E}}(x, y, \omega_c)$. We may hence assume without loss of generality that $A_0 \in \mathbb{R}$, which is used later to simplify the derivation. The expression $\Phi_{NL}(z)$ accounts for the power-dependent nonlinear phase shift that the wave experiences due to self-phase modulation. This phase shift can be calculated by inserting the corresponding slowly varying envelope,

$$\underline{A}(z, t) = A_0 e^{j\Phi_{NL}(z)}, \quad (5.64)$$

into the nonlinear Schrödinger Equation, Eq. (5.43). This leads to

$$\Phi_{NL}(z) = -\gamma |A_0|^2 z, \quad (5.65)$$

i.e., the monochromatic wave experiences a phase delay which is proportional to the launched power $|A_0|^2$ and increases linearly with distance z . This is consistent with the observation that the Kerr effect leads to an increase of the refractive index and hence to an increase of the modal propagation constant by $\Delta\beta = \gamma |A_0|^2$, which is proportional to the signal power, see Eq. (1.123) and the discussion thereof.

However, the fact that the ansatz according to Eq. (5.63) yields a physically meaningful solution of Eq. (5.43) does not yet imply stability of this solution. In this context, stability is related to the question whether or not a small deviation from the solution $\underline{A}(z, t) = A_0 e^{-j\gamma |A_0|^2 z}$ will decay and eventually vanish or grow to infinity. This question is of particular relevance in nonlinear optics - in linear optics, a small perturbation of a known solution will just evolve in the very same way as the solution itself.

To analyze the stability of the monochromatic wave in the presence of third-order nonlinearity let us assume that the cw solution $A_0 e^{-j\gamma |A_0|^2 z}$ is perturbed by a small amplitude deviation $\Delta\underline{A}(z, t)$. The ansatz can then be written as

$$\underline{A}(z, t) = (A_0 + \Delta\underline{A}(z, t)) e^{-j\gamma |A_0|^2 z}. \quad (5.66)$$

We may think of $\Delta\underline{A}(z, t)$ as the optical amplitude that is associated with an additional noise photon that is emitted into the waveguide mode at position z and time t . Note that in principle we are free to incorporate the perturbation $\Delta\underline{A}(z, t)$ into the bracket on the right-hand side of Eq. (5.66) or not. We have decided to do it in order to simplify the subsequent analysis.

We insert Eq. (5.66) into Eq. (5.43). Since the perturbation is much weaker than the amplitude of the cw signal, $|\Delta\underline{A}(z, t)| \ll |A_0|$, we may linearize the resulting equation about A_0 by neglecting all second-order products of small perturbation terms. Using again $\Phi_{NL}(z) = -\gamma |A_0|^2 z$, we obtain a differential equation that describes the evolution of $\Delta\underline{A}(z, t)$,

$$\frac{\partial \Delta\underline{A}(z, t)}{\partial z} = j \frac{1}{2} \beta_c^{(2)} \frac{\partial^2 \Delta\underline{A}(z, t)}{\partial t^2} - j\gamma |A_0|^2 (\Delta\underline{A}(z, t) + \Delta\underline{A}^*(z, t)), \quad (5.67)$$

where $\Delta\underline{A}^*(z, t)$ denotes the complex conjugate of $\Delta\underline{A}(z, t)$.

The spatial evolution of $\Delta\underline{A}(z, t)$ depends on both its temporal change and the cw power. To understand this better, let us try a time- and space-harmonic ansatz $\Delta\underline{A}(z, t)$ for a wave propagating in positive z -direction. Due to the complex conjugate on the right-hand side of Eq. (5.67), the amplitudes at frequencies Ω and $-\Omega$ are coupled, and we hence need to incorporate both of them into the ansatz,

$$\Delta\underline{A}(z, t) = C_1 e^{j(\Omega t - Kz)} + C_2 e^{-j(\Omega t - Kz)}, \quad (5.68)$$

where the wave amplitudes C_1 and C_2 are complex numbers. Note that, since $\Delta\underline{A}(z, t)$ is a perturbation of the slowly varying envelope $\underline{A}(z, t)$, the frequencies $\pm\Omega$ and the wave numbers

$\pm K$ denote only the offset from the modal frequency ω_c and the corresponding wave number β_c . Inserting Eq. (5.68) into Eq. (5.67), we can derive two linear equations for the wave amplitudes C_1 and C_2 ,

$$\begin{pmatrix} -K + \frac{1}{2}\Omega^2\beta_c^{(2)} + \gamma|\underline{A}_0|^2 & \gamma|\underline{A}_0|^2 \\ \gamma|\underline{A}_0|^2 & K + \frac{1}{2}\Omega^2\beta_c^{(2)} + \gamma|\underline{A}_0|^2 \end{pmatrix} \begin{pmatrix} C_1 \\ C_2 \end{pmatrix} = \begin{pmatrix} 0 \\ 0 \end{pmatrix}. \quad (5.69)$$

Nontrivial solutions of this equation exist only if the determinant of the 2×2 -matrix on the left-hand side vanishes. This leads to the dispersion relation of the perturbation, i.e., to a relationship between the offset frequency Ω and the corresponding wave number change K ,

$$K = \pm \sqrt{\left(\frac{1}{2}\Omega^2\beta_c^{(2)}\right)^2 + \Omega^2\beta_c^{(2)}\gamma|\underline{A}_0|^2}. \quad (5.70)$$

From this relation, we can already infer that for the case of normal group-velocity dispersion, $\beta_c^{(2)} > 0$, we will always find a real wave number $K \in \mathbb{R}$, no matter what the frequency offset Ω and power $|\underline{A}_0|^2$ of the cw pump wave are. A perturbation launched into the waveguide mode will hence propagate along with the cw pump and the propagation constant is influenced by nonlinear interaction, but the amplitude of the perturbation will not increase to infinity. For real fibers with nonzero propagation loss, the perturbation will even decrease during propagation and eventually vanish along with the cw wave. The system is hence stable in this case.

For anomalous group velocity dispersion, $\beta_c^{(2)} < 0$, things are different. In this case, K becomes purely imaginary for a certain range of frequency offsets,

$$|\Omega| < \Omega_g = \sqrt{\frac{4\gamma|\underline{A}_0|^2}{\beta_c^{(2)}}}. \quad (5.71)$$

In this case, the wavenumber is purely imaginary,

$$K = \pm j \frac{1}{2}\beta_c^{(2)}\Omega \sqrt{\Omega_g^2 - \Omega^2}. \quad (5.72)$$

As a consequence, the amplitude of the perturbation increases or decreases exponentially with z . The situation of an exponentially increasing perturbation can be interpreted as an energy transfer from the cw pump wave to two sidebands that emerge at distance $\pm\Omega$ from the pump, see Fig. 5.6 (a). This energy transfer can be triggered by an infinitesimally small perturbation, which then increases exponentially, thereby depleting the strong cw pump. The system is hence unstable, and the cw pump breaks up into a train of pulses. This phenomenon is referred to as modulation instability. The measured gain spectrum of modulation instability in an optical fiber is depicted in Fig. 5.6 (b). Modulation instability can be induced by launching a weak cw probe wave along with the pump. The repetition frequency of the generated pulse train is given by the spectral distance of the probe wave from the pump, see Fig. 5.6 (c).

Gain spectrum

For the case of modulation instability, we may calculate the associated gain with which the sidebands are amplified. Let us consider the upper sideband, which, according to Eq. (5.68) propagates as $\exp(j(\Omega t - Kz))$. The power gain is related to the imaginary part of the wavenumber by $g(\Omega) = 2\text{Im}\{K\}$. Similarly, the lower sideband propagates as $\exp(-j(\Omega t - Kz))$, and the associated power gain is given by $g(\Omega) = -2\text{Im}\{K\}$. The frequency dependence of the gain can be directly inferred from Eq. (5.72),

$$g(\Omega) = \left|\beta_c^{(2)}\right| \Omega \sqrt{\Omega_g^2 - \Omega^2}, \quad (5.73)$$

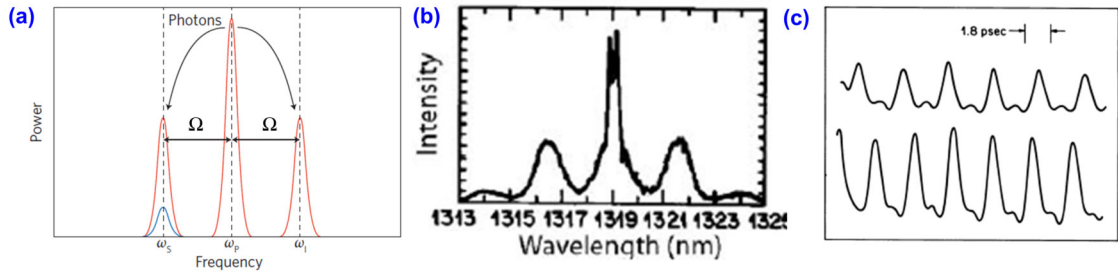


Figure 5.6: Modulation instability (a) Nonlinear interaction transfers power from a strong continuous-wave (cw) signal to spectral sidebands. This may lead to the break-up of the cw signal into a train of pulses. (b) Measured gain spectrum of modulation instability in an optical fiber. (c) Autocorrelation traces of time-domain signals that are subject to modulation instability. Within the gain region according to Eq. 5.71, modulation instability can be induced by launching a weak cw probe wave along with the pump. The repetition frequency of the generated impulses is given by the spectral distance of the probe wave from the pump. The figure depicts two pulse trains, generated by different probe waves. (Figures adapted from [16, 5])

The theoretically calculated gain spectrum of an optical fiber is sketched in Fig. 5.7. The gain spectrum is perfectly symmetric with respect to the strong cw signal. Asymmetry can arise from higher-order dispersion and different initial conditions that are related to the population of the waveguide mode with random noise photons. According to Eq. (5.73), modulation instability gain should always occur close to the optical carrier. Note, however, that real fibers have propagation loss, which was not included in the preceding analysis, and modulation instability only plays an important role once the associated gain is larger than the fiber loss.

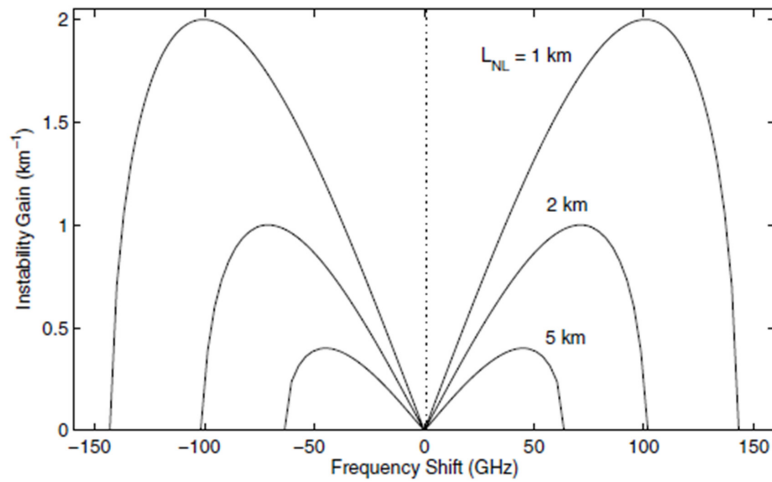


Figure 5.7: Calculated gain spectrum of modulation instability. In a simplified consideration, the gain spectrum is perfectly symmetric with respect to the strong CW signal. Asymmetry can arise from higher-order dispersion and different initial conditions that are related to the population of the waveguide mode with random noise photons. (Figures adapted from [5])

Kerr frequency comb generation

When combined with a high-Q optical resonator that “stores” the sideband photons, modulation instability can be exploited to generate broadband frequency combs [20, 12, 21, 16]. The corresponding experimental setup is illustrated in Fig. 5.8 (a). A high-Q Kerr-nonlinear microresonator is pumped by a cw laser which is tuned to one of the resonance frequencies. The output power of the pump laser is amplified to overcome the pump threshold power, for which the gain due to modulation instability overcomes the cavity losses. Given the right dispersion profile, this leads to the formation of broadband so-called Kerr frequency combs, where the line spacing is dictated by the local free-spectral range (FSR) of the microresonator. The principle of Kerr frequency comb generation is illustrated in Fig. 5.8 (b). Power is transferred from the pump to the sidebands by degenerate and nondegenerate four-wave mixing (FWM). Fig. 5.8 (c) illustrates a couple resonator implementations, including silica and silicon nitride waveguide-based resonators, silica toroid resonators, and crystalline resonators that are fabricated by ultra-precision turning and polishing of the surface. Octave-spanning frequency combs can be obtained from silica toroid resonators, which exploit low-loss whispering-gallery mode propagation to achieve particularly high Q-factors, see Fig. 5.9.

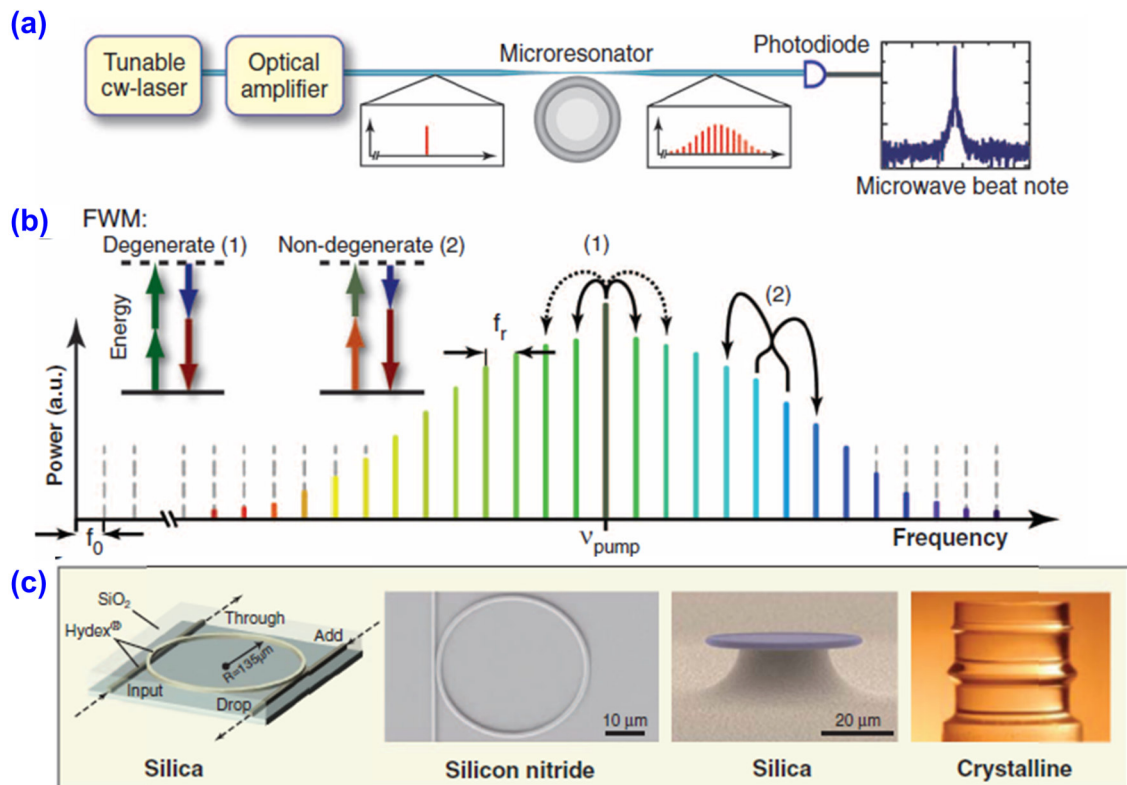


Figure 5.8: Kerr frequency comb generation, exploiting modulation instabilities in high-Q Kerr-nonlinear resonator. (a) Setup used for Kerr comb generation: A high-Q Kerr-nonlinear microresonator is pumped by a cw laser which is tuned to one of the resonance frequencies. Above a certain pump threshold, the gain due to modulation instability overcomes the cavity losses. (b) Principle of Kerr frequency comb generation: Power is transferred from the pump to the sidebands by degenerate and nondegenerate four-wave mixing (FWM). This leads to a broadband so-called Kerr frequency comb, where the line spacing is dictated by the local free spectral range (FSR) of the microresonator. (c) Different resonator implementations, including silica and silicon nitride waveguide-based resonators, silica toroid devices, and crystalline resonators that are fabricated by ultra-precision turning. (Figures adapted from [16])

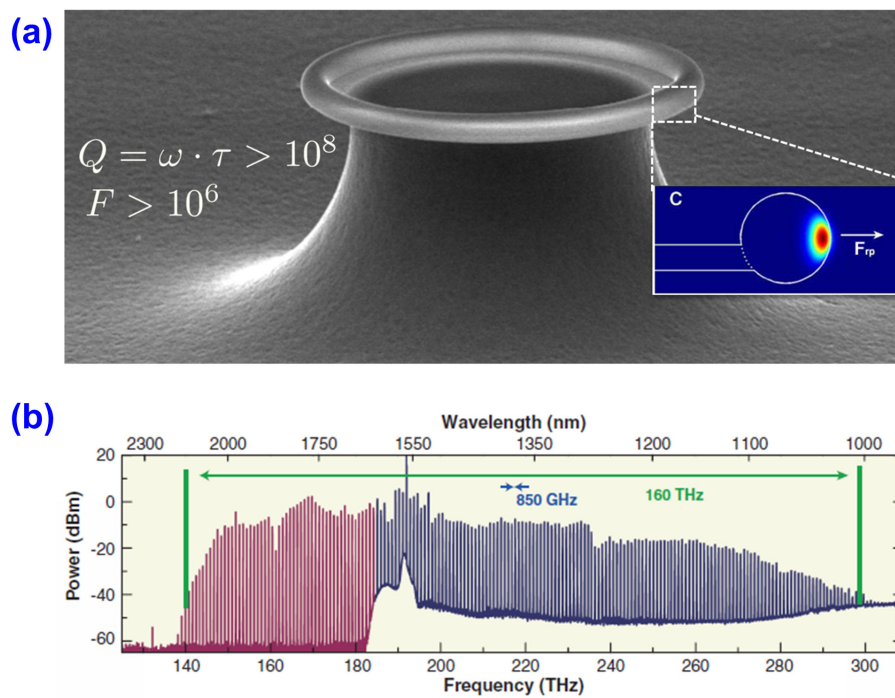


Figure 5.9: Generation of octave-spanning Kerr frequency combs in a toroidal whispering-gallery mode resonator. (a) Scanning electron microscope (SEM) picture of the device along with a calculated whispering-gallery mode field. The resonators are fabricated by laser-induced reflow of silica disc resonator. (b) Recorded comb spectrum, spanning more than an octave of optical frequencies. (Figures adapted from [16])

Appendix A

Mathematical Definitions and Conventions

A.1 Time- and Frequency-Domain Quantities

If not otherwise stated, t is the independent time domain variable, and ω denotes the corresponding frequency domain variable. The quantities $u(t)$, $v(t)$, and $h(t)$ are functions in the time domain, and $\tilde{u}(\omega)$, $\tilde{v}(\omega)$, and $\tilde{h}(\omega)$ are the corresponding frequency domain spectra.

A.1.1 Fourier Transformation

The Fourier transform of a function $u(t)$ with respect to the independent variable t is denoted as $\mathfrak{F}_t \{u(t)\}$. Accordingly, $\mathfrak{F}_\omega^{-1} \{\tilde{u}(\omega)\}$ refers to the inverse Fourier transform of a function $\tilde{u}(\omega)$ with respect to the independent variable ω ,

$$\mathfrak{F}_t \{u(t)\} = \tilde{u}(\omega) = \int_{-\infty}^{+\infty} u(t) e^{-j\omega t} dt, \quad (\text{A.1})$$

$$\mathfrak{F}_\omega^{-1} \{\tilde{u}(\omega)\} = u(t) = \frac{1}{2\pi} \int_{-\infty}^{+\infty} \tilde{u}(\omega) e^{j\omega t} d\omega. \quad (\text{A.2})$$

The independent variable t usually represents the time, and ω is angular frequency.

A.2 Vector calculus

A.2.1 The Nabla operator

Gradient

$$\nabla\psi = \text{grad } \psi = \begin{pmatrix} \partial_x \\ \partial_y \\ \partial_z \end{pmatrix} \psi = \begin{pmatrix} \partial_x \psi \\ \partial_y \psi \\ \partial_z \psi \end{pmatrix} \quad (\text{A.3})$$

Example: $\nabla e^{-j\mathbf{k}\cdot\mathbf{r}} = -j\mathbf{k}e^{-j\mathbf{k}\cdot\mathbf{r}}$

Curl

$$\nabla \times \mathbf{A} = \text{rot } \mathbf{A} = \begin{pmatrix} \partial_x \\ \partial_y \\ \partial_z \end{pmatrix} \times \begin{pmatrix} A_x \\ A_y \\ A_z \end{pmatrix} = \begin{pmatrix} \partial_y A_z - \partial_z A_y \\ \partial_z A_x - \partial_x A_z \\ \partial_x A_y - \partial_y A_x \end{pmatrix} \quad (\text{A.4})$$

Example: $\nabla \times \mathbf{A}_0 e^{-j\mathbf{k}\cdot\mathbf{r}} = -j\mathbf{k} \times \mathbf{A}_0 e^{-j\mathbf{k}\cdot\mathbf{r}}$

Divergence

$$\nabla \cdot \mathbf{A} = \text{div } \mathbf{A} = \begin{pmatrix} \partial_x \\ \partial_y \\ \partial_z \end{pmatrix} \cdot \begin{pmatrix} A_x \\ A_y \\ A_z \end{pmatrix} = \partial_x A_x + \partial_y A_y + \partial_z A_z \quad (\text{A.5})$$

Example: $\nabla \cdot \mathbf{A}_0 e^{-j\mathbf{k}\cdot\mathbf{r}} = -j\mathbf{k} \cdot \mathbf{A}_0 e^{-j\mathbf{k}\cdot\mathbf{r}}$

Laplacian

$$\nabla^2 \mathbf{A} = \Delta \mathbf{A} = (\partial_x^2 + \partial_y^2 + \partial_z^2) \begin{pmatrix} A_x \\ A_y \\ A_z \end{pmatrix} = \begin{pmatrix} (\partial_x^2 + \partial_y^2 + \partial_z^2) A_x \\ (\partial_x^2 + \partial_y^2 + \partial_z^2) A_y \\ (\partial_x^2 + \partial_y^2 + \partial_z^2) A_z \end{pmatrix} \quad (\text{A.6})$$

Example: $\nabla^2 \mathbf{A}_0 e^{-j\mathbf{k}\cdot\mathbf{r}} = (-j)^2 (\mathbf{k} \cdot \mathbf{k}) \mathbf{A}_0 e^{-j\mathbf{k}\cdot\mathbf{r}}$

A.2.2 Basic formulae of vector differential operators

A short summary of basic relations from vector differential calculus is given in Fig. A.1.

<p>Linearität</p> <ol style="list-style-type: none"> $\nabla(\alpha\Phi + \beta\Psi) = \alpha \nabla\Phi + \beta \nabla\Psi$ $\nabla \cdot (\alpha \mathbf{F} + \beta \mathbf{G}) = \alpha \nabla \cdot \mathbf{F} + \beta \nabla \cdot \mathbf{G}$ $\nabla \times (\alpha \mathbf{F} + \beta \mathbf{G}) = \alpha \nabla \times \mathbf{F} + \beta \nabla \times \mathbf{G}$ <p>Operation auf Produkten</p> <ol style="list-style-type: none"> $\nabla(\Phi\Psi) = \Phi \nabla\Psi + \Psi \nabla\Phi$ $\nabla(\mathbf{F} \cdot \mathbf{G}) = (\mathbf{F} \cdot \nabla)\mathbf{G} + (\mathbf{G} \cdot \nabla)\mathbf{F} + \mathbf{F} \times (\nabla \times \mathbf{G}) + \mathbf{G} \times (\nabla \times \mathbf{F})$ $\nabla \cdot (\Phi \mathbf{F}) = \Phi \nabla \cdot \mathbf{F} + (\nabla\Phi) \cdot \mathbf{F}$ $\nabla \cdot (\mathbf{F} \times \mathbf{G}) = \mathbf{G} \cdot \nabla \times \mathbf{F} - \mathbf{F} \cdot \nabla \times \mathbf{G}$ $\nabla \times (\Phi \mathbf{F}) = \Phi \nabla \times \mathbf{F} + (\nabla\Phi) \times \mathbf{F}$ $\nabla \times (\mathbf{F} \times \mathbf{G}) = (\mathbf{G} \cdot \nabla)\mathbf{F} - (\mathbf{F} \cdot \nabla)\mathbf{G} + \mathbf{F}(\nabla \cdot \mathbf{G}) - \mathbf{G}(\nabla \cdot \mathbf{F})$ <p>Zweifache Anwendung von ∇</p> <ol style="list-style-type: none"> $\nabla \cdot (\nabla \times \mathbf{F}) = 0$ $\nabla \times (\nabla\Phi) = \mathbf{0}$ $\nabla \times (\nabla \times \mathbf{F}) = \nabla(\nabla \cdot \mathbf{F}) - \nabla^2 \mathbf{F}$ 	$\text{grad}(\alpha\Phi + \beta\Psi) = \alpha \text{grad } \Phi + \beta \text{grad } \Psi$ $\text{div}(\alpha \mathbf{F} + \beta \mathbf{G}) = \alpha \text{div } \mathbf{F} + \beta \text{div } \mathbf{G}$ $\text{rot}(\alpha \mathbf{F} + \beta \mathbf{G}) = \alpha \text{rot } \mathbf{F} + \beta \text{rot } \mathbf{G}$ $\text{grad}(\Phi\Psi) = \Phi \text{grad } \Psi + \Psi \text{grad } \Phi$ $\text{grad}(\mathbf{F} \cdot \mathbf{G}) = (\mathbf{F} \cdot \text{grad})\mathbf{G} + (\mathbf{G} \cdot \text{grad})\mathbf{F} + \mathbf{F} \times \text{rot } \mathbf{G} + \mathbf{G} \times \text{rot } \mathbf{F}$ $\text{div}(\Phi \mathbf{F}) = \Phi \text{div } \mathbf{F} + \mathbf{F} \cdot \text{grad } \Phi$ $\text{div}(\mathbf{F} \times \mathbf{G}) = \mathbf{G} \cdot \text{rot } \mathbf{F} - \mathbf{F} \cdot \text{rot } \mathbf{G}$ $\text{rot}(\Phi \mathbf{F}) = \Phi \text{rot } \mathbf{F} + (\text{grad } \Phi) \times \mathbf{F}$ $\text{rot}(\mathbf{F} \times \mathbf{G}) = (\mathbf{G} \cdot \text{grad})\mathbf{F} - (\mathbf{F} \cdot \text{grad})\mathbf{G} + \mathbf{F} \text{div } \mathbf{G} - \mathbf{G} \text{div } \mathbf{F}$ $\text{div rot } \mathbf{F} = 0$ $\text{rot grad } \Phi = \mathbf{0}$ $\text{rot rot } \mathbf{F} = \text{grad div } \mathbf{F} - \Delta \mathbf{F}$
--	--

Figure A.1: Basic relations of vector differential operators (Adapted from [24])

Bibliography

- [1] Polytec online tutorials.
- [2] Tutorial on periodically poled lithium niobate (ppln).
- [3] G. P. Agrawal. *Nonlinear Fiber Optics*. Academic Press, San Diego, third edition, 2001.
- [4] Govind P. Agrawal. *Fiber-optic communications systems*. John Wiley & Sons, 2002.
- [5] Govind P. Agrawal. *Nonlinear Fiber Optics*. Academic Press, 2013.
- [6] N. W. Ashcroft and N. D. Mermin. *Solid State Physics*. Thomson Learning, Inc., 1976.
- [7] N. Bloembergen. *Nonlinear Optics*. Originally pub. Reading Mass.: W.A. Benjamin, (1965), Reprint: Addison and Wesley, Redwood City, 1992.
- [8] M. Born and E. Wolf. *Principles of Optics*. Pergamon Press, 6 edition, 1993.
- [9] R. W. Boyd. *Nonlinear Optics*. Academic Press, San Diego, 2003.
- [10] R.W. Boyd. *Nonlinear Optics*. Academic Press, New York, 1992.
- [11] P.N. Butcher and D. Cotter. *The Elements of Nonlinear Optics*. Cambridge University Press, New York, 1990.
- [12] P. Del’Haye, A. Schliesser, O. Arcizet, T. Wilken, R. Holzwarth, and T. J. Kippenberg. Optical frequency comb generation from a monolithic microresonator. *Nature*, 450(7173):1214–1217, December 2007.
- [13] V.G. Dmitriev, G.G. Gurzadyan, and D.N. Nikogosyan. *Handbook of Nonlinear Optical Crystals*. Springer, Berlin, 3 edition, 1999.
- [14] G. Grau and W. Freude. *Optische Nachrichtentechnik*. Springer, 1991.
- [15] Alex Hayat, Pavel Ginzburg, and Meir Orenstein. Observation of two-photon emission from semiconductors. *Nat Photon*, 2(4):238–241, April 2008.
- [16] T. Herr, K. Hartinger, J. Y. Riemensberger, C. Wang, E. Gavartin, R. L. Holzwarth, M. J. Gorodetsky, and T. Kippenberg. Universal formation dynamics and noise of kerr-frequency combs in microresonators. *Nat Photon*, 6(7):480–487, July 2012.
- [17] K. Iizuka. *Elements of Photonics*, volume 1. John Wiley & Sons, 1 edition, 2002.
- [18] K. Iizuka. *Elements of Photonics*, volume 2. John Wiley & Sons, 1 edition, 2002.
- [19] J. D. Jackson. *Classical Electrodynamics*. John Wiley and Sons, New York, 1998.
- [20] T. J. Kippenberg, R. Holzwarth, and S. A. Diddams. Microresonator-based optical frequency combs. *Science*, 332(6029):555–559, 2011.

- [21] T. J. Kippenberg, S. M. Spillane, and K. J. Vahala. Kerr-nonlinearity optical parametric oscillation in an ultrahigh- q toroid microcavity. *Phys. Rev. Lett.*, 93:083904, Aug 2004.
- [22] C. Koos. *Optical Waveguides and Fibers*. Karlsruhe Institute of Technology (KIT), Institute of Photonics and Quantum Electronics (IPQ), 2012. Lecture Notes, available at .
- [23] J. Y. Y. Leong, P. Petropoulos, S. Asimakis, H. Ebendorff-Heideprim, R. C. Moore, Ken. Frampton, V. Finazzi, X. Feng, J. H. V. Price, T. M. Monro, and D. J. Richardson. A lead silicate holey fiber with $\gamma = 1860 \text{ (Wkm)}^{-1}$ at 1550 nm. In *Optical Fiber Communication (OFC) Conference*, Anaheim (CA), USA, March 2005. PDP22.
- [24] L. Rade and B. Westergren. *Mathematische Formeln*. Springer, 1997.
- [25] Haisheng Rong, Shengbo Xu, Ying-Hao Kuo, Vanessa Sih, Oded Cohen, Omri Raday, and Mario Paniccia. Low-threshold continuous-wave raman silicon laser. *Nat Photon*, 1(4):232–237, April 2007.
- [26] B. E. A. Saleh and M. C. Teich. *Fundamentals of Photonics*. John Wiley and Sons, 2007.
- [27] E. G. Sauter. *Nonlinear Optics*. John Wiley and Sons, New York, 1996.
- [28] Y. R. Shen. *Nonlinear Optics*. John Wiley and Sons, New York, 1984.
- [29] George I. Stegeman and Robert A. Stegeman. *Nonlinear Optics: Phenomena, Materials and Devices*. Wiley, 2012.
- [30] Optoelectronic Business Division Sumitomo Osaka Cement Co. Ltd. Application note for In modulators, 2002.
- [31] E. Voges and K. Petermann. *Optische Kommunikationstechnik*. Springer, 2002.
- [32] Amnon Yariv. *Quantum Electronics*. John Wiley & Sons, 1989.
- [33] David E. Zelmon, David L. Small, and Dieter Jundt. Infrared corrected sellmeier coefficients for congruently grown lithium niobate and 5 mol.% magnesium oxide –doped lithium niobate. *J. Opt. Soc. Am. B*, 14(12):3319–3322, Dec 1997.